Cover Photo

The sky, the stars and the Milky Way visible from a crossroad, from which a path that leads to the Sanctuary of the Holy Bed (Holy Cross) begins. The Sanctuary is located on the peak (882 m above the sea level) of one of the Nebrodi Mountains, in the territory of S.Stefano di Camastra, a small town in the northern coast of Sicily. The light by which the sky is enlightened, comes from the little church and it seems like it form a cross there, where it is stronger.

Photographer: *Alberto Cosenza*

Università degli Studi di Milano
Dipartimento di Chimica

Doctorate School in Chemical Sciences and Technologies
Doctorate in Chemical Sciences
XXVIII cycle

THE HETEROARYLETHENES: SYNTHESIS, ELECTROCHEMISTRY AND INVESTIGATION ON THE AGGREGATION-INDUCED EMISSION OF A PROMISING CLASS OF MOLECULES WITH LUMINESCENT PROPERTIES

LUCIA VIGLIANTI
R10028

Supervisor: Prof. Emanuela Licandro

Co-supervisor: Prof. Patrizia Romana Mussini

School director: Prof. Emanuela Licandro

Academic Year 2014/2015

I am the light of the world.
Whoever follows me will never walk in darkness,
but will have the light of the life.
John 8,12

Greater love has no one than this:
to lay down one's life for one's friends
John 15,13

To You light of the world, who led me so far,

To my mother and my father

Index

1

Introduction

1.1 How Light can be generated

Light is a form of energy. To create light another form of energy must be provided. Depending on the source of supply and on the phenomena that occur, light can be generated by two different processes: incandescence and luminescence [1].
Incandescence occurs when light is produced using heat energy. If you heat a body to a high enough temperature, at a certain point it will begin to glow, so you generate light by heating. This occurs because when a body is heated, it emits electromagnetic waves due to the conversion of the thermic energy into radiant one. In this case the light emitted is produced in thermodynamic equilibrium conditions (in this case thermic equilibrium) and the irradiation provided is called "thermic radiation" [2]. This is the phenomenon according to which both the stars and the sun glow.

Luminescence is a general term applied to all forms of cool light generated in absence of thermic equilibrium as defined by Eilhard Wiedemann in 1888[2,3] according to whom, luminescence is a term referred to a phenomenon belonging to a material/physical substance whether pure or complex which, after absorbing or developing a certain amount of energy, (due to the interaction with an external system), emits luminescent radiation due to the lack of thermic equilibrium conditions. It is a spontaneous emission of UV, visible or infrared photons from an excited state that relaxes to the fundamental state by a radiative channel, thus providing light emission. The phenomenon can be schematized according to the equation 1.

$$M^* \rightarrow M + nhv' \quad (1)$$

Where *M**is the excited state of the system *M,* while nhv' is the number of the emitted photons.
According to the type of energy source responsible for the formation of the excited state, different kinds of luminescence processes have been recognised.
Bioluminescence is the spontaneous emission of visible light due to the chemical reactions that occur in living organism and in which are involved enzymes or photoproteins. This luminescence process occurs in several organisms, both marine and terrestrial (*e.g.* plankton, fishes, bacteria, insects).
Chemiluminescence occurs when the electrons can reach their excited state thanks to the energy generated from an exoergonic chemical reaction. This allows the formation of a product in its excited state able to emit light. In this case there is the conversion from chemical energy to light.
Electrochemiluminescence is produced during electrochemical reactions whose intermediates can undergo a highly exoergonic reaction which can be a redox reaction and which allows to generate an electronically excited state that will relax to the ground state, by emitting light.
Electroluminescence is the luminescent radiation produced by an electric field or an electrical discharge that have acted on the radiant system. It can also happen because of the radiative recombination of electrons and holes previously generated by the effect of an electric field or electric current, as it occurs in OLED devices.
Photoluminescence is the luminescence provided by the absorption of optical photons.
Radioluminescence is produced when specific substances are hit by X, γ rays or particles emitted during the radioactive decay.

Sonoluminescence is the luminescence produced by the sonorous waves.
Triboluminescence is produced from an excited state formed by the rubbing mechanic energy.

1.1.1 The Photoluminescence Process

In molecules constituted by light atoms (namely with a low atomic number), the spin-orbit coupling is weak, in this case the photoluminescence is divided in two categories: fluorescence and phosphorescence. For those systems which contain elements with a high atomic number the spin-orbit coupling is stronger (the higher is the atomic number, the stronger is the spin-orbit interaction indeed it varies as Z^4 [4] where Z is the atomic number); in this case some authors prefer to define the phenomenon just as luminescence.[2]
Fluorescence is the electromagnetic radiation emitted between electronic states that have the same spin multiplicity. It is an allowed transition according to the selection rule concerning the electronic spin that should keep the same multiplicity during the transition (ΔSpin = 0), an example of a fluorescence transition is reported in the equation 2:

$$S_1 \rightarrow S_0 + h\nu_f \quad (2)$$

Where S_1 is the first excited singlet state and S_0 is the fundamental state of the molecule. In this case the transition is singlet-singlet.
Phosphorescence is the electromagnetic radiation emitted between electronic states with the same spin multiplicity. According to the selection rule for the spin number this transition is forbidden, as there is a variation of the multiplicity during the transition (ΔSpin ≠ 0); in this case the transition is triplet-singlet. As an example, the process is schematized in the equation 3:

$$T_1 \rightarrow S_0 + h\nu_p \quad (3)$$

Where T_1 is the first excited triplet state of the molecule and S_0 is the fundamental one.
Fluorescence and Phosphorescence are monomolecular radiative relaxation processes by which the excited state of the molecule can be deactivated, they are *intra*molecular processes. Other *intra* molecular processes which are monomolecular as well, can be those in which the light emission is not involved: the "internal conversion" *ic*, and the "intersystem crossing" *isc*; they are defined non-radiative processes. The first one is due to the vibronic coupling between electronic states that have the same spin multiplicity; the second one is caused by the spin-orbit interaction between electronic states with different spin multiplicity. As a consequence of these phenomena, the population of the excited molecules is diminished, the excited state is deactivated without light emission and the excitation energy is converted in heating. The process for a generic system M is summarized in the equation 4.

$$M^* \rightarrow M + heating \quad (4)$$

Radiative and non-radiative intramolecular interactions are summerized in Jablonski diagram shown in Figure 1.1. The order of magnitude of the kinetic constants of the several photophisycal monomolecular processes is summarized in Table 1[2].

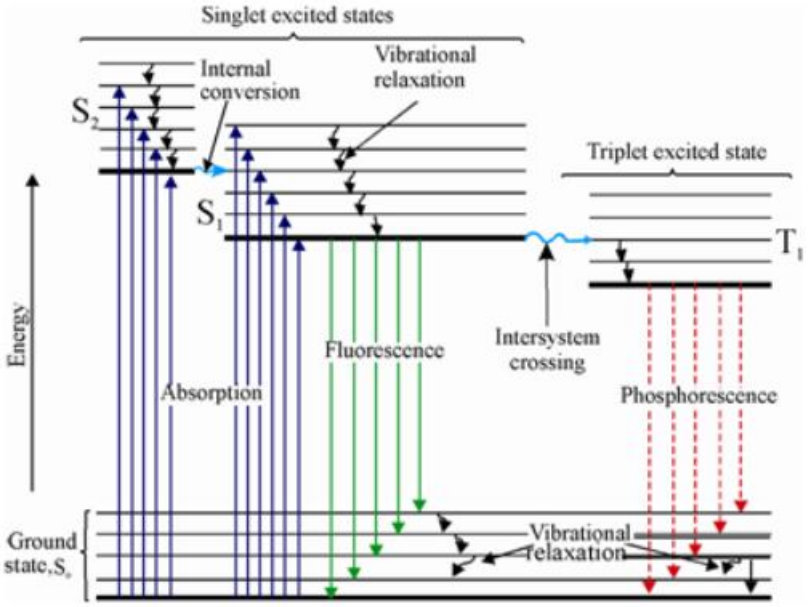

Figure 1.1

Table 1 Order of magnitude of the kinetic constants of the several photophisycal monomolecular processes

Photophisycal Phenomenon	**Kinetic Constant *k* / s^{-1}**
Absorption	10^{15}
Fluorescence $S_1 \longrightarrow S_0$	10^{9}-10^{6}
Phosphorescence $T_1 \longrightarrow S_0$	10^{3}-10^{-2}
Vibrational Relaxation S_1	10^{12}
Internal Conversion and Vibrational Relaxation S_n ----▶ S_1 e T_n ----▶ T_1	10^{12}
Intersystem Crossing S_1 ----▶ T_n	10^{6}-10^{11}
Intersystem Crossing T_1 ----▶ S_0	10^{4}-10^{-2}

Straight line and dots-based narrows indicate radiative and non-radiative processes respectively.

1.2 Use of the fluorescence as powerful techniques in bio-tech applications in the last decades.

Fluorescence is a powerful technique that offers high sensitivity, low background noise and a broad dynamic range. [5] It has been used in many fields, one of the most important is biotechnology, in

order to visualize cellular environment at many levels, from molecules to complete organisms. [5,6] Initially fluorescence was observed from small organic molecules that were incorporated into biological systems as labels via chemical attachment or probes via physical mixing. [5,6] The fluorophores used for these aims were able to directly recognize cellular organelles but at the same time they were featured by low brightness and mediocre photostability. A competitive substitute for bio-applications were inorganic nanocrystals better known as quantum dots (QDs) [6] but their employment was limited due to their difficult synthesis and inherently cytotoxicity caused by the presence of heavy metals such as: Cd, Zn, Pd, Hg [5,6,8]. The use of organic-based fluorophores remained the best perspective. The only limit to overcome was the low brightness, low photostability, and the impossibility of using fluorophore at high concentration in the biological environment. Indeed while at the beginning most of the label probes are dissolved and hence emissive (emission on), they become non-emissive (emission off) when an aggregation condition is induced by changes in the analytes or in the medium in which they are dissolved [5,8]. This aggregation effect is responsible for their emission quenching and has forced researchers to make use of the fluorophores as isolated single species in very dilute solutions. But in dilute solutions, the emission is often quite weak (low brightness) and leads to poor sensitivity especially in bioassay of trace amounts of biomolecules; furthermore the small number of the dyes can be quickly photobleached when a harsh laser beam is used as the excitation light source. [8] The emission quenching phenomenon in organic systems is something which has affected not only the application of organic fluorophores in biotechnology field, but also the development of efficient organic molecules-based luminescent devices (e.g. OLEDs), for which, molecules are generally used in solid state. This phenomenon has also precluded the possibility of understanding the photophysics of organic luminescence correctly, as both studies on luminescent behaviour and determination of physical parameters (rate decay, lifetimes, luminescence efficiency) have been conducted in dilute solutions. In this environment, the luminophoric molecules can be approximated as isolated species for which it is not possible to evaluate the effect depending on the *intra* and *inter* molecular chromophoric interactions that significantly affect the luminescence phenomenon. So the conclusion drawn from the dilute solution data cannot explain what happens in concentrated solutions or solid state. [9]

1.3 Aggregation-Induced Emission AIE: a phenomenon that revolutionized application and fundamental understanding of the science of the light

The emission quenching effect in aggregate conditions, mentioned in the previous paragraph, is a phenomenon well known for more than half century, since Förster and Kasper focused their attention on the pyrene molecule discovering that its fluorescence was weakened with an increase of its concentration.[8,10a] The same effect was observed in other aromatic derivatives so that the phenomenon was generalized and defined by Birks in his classic book “Photopysics of Aromatic Molecule” edited in 1970 [8,10b] “to be common to most aromatic hydrocarbons and their derivatives”.

This phenomenon is manifested in aggregation conditions and in solid state. When the solubility of the solute in the medium in which it is dissolved begins to become poor, the molecules come to be located very close to each other and the formation of aggregates occurs. In this framework

molecules experience strong intermolecular interactions especially those with a disk-like shape (Figure 1.2), between which the π-π stacking interaction can be exerted. In this context, upon absorption of UV-vis light, the excited state of the aggregates can be deactivated just through the π-π stacking interactions, and the light emission is quenched due to the realization of a non-radiative relaxation pathway. This is why this effect has been called "Aggregation-Caused Quenching" ACQ. [8,9] Therefore until the molecule is well solvated by the solvent and it is possible to consider it as an isolated specie, the emission occurs, as any non-radiative pathway is available. With the increase of the concentration, the solubility becomes poor and molecules begin to aggregate. The disk-like shape owned thanks to their planar structure helps them to pile-up and to experience strong π-π stacking interaction that will constitute the non-radiative pathway responsible of the emission quenching. Since this occurs upon aggregation formation, the phenomenon has been called ACQ, but it also occurs in solid state, where the absence of the solvent lets molecules experience stronger intermolecular interactions.

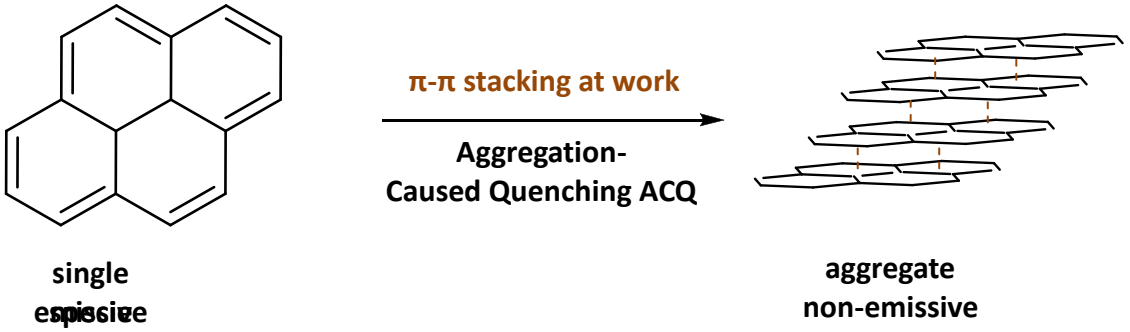

Figure 1.2 Exemplification of the Aggregation-Quenching Effect, ACQ in planar, polynuclear systems such as Pyrene molecule.

For many years scientists all over the world have done many efforts to try to overcome this thorny obstacle which has not allowed to employ organic luminophores in advanced applications descending from photophysics. Attempts to mitigate the ACQ effect have been done both by chemical and physical methods. To prevent the detrimental packing in aggregation condition, branched chains or bulky cyclic groups have been covalently linked to the aromatic cores. But this attempt revealed to be passive and sometimes even destructive. For example, attaching sterically bulky pendant group twisted the conformation of the luminogens, jeopardizing the π-electron conjugation. Physical processes were constituted by the use of non-conjugated encapsulants and the transparent matrices which were non-emissive and insulating so being dilutants and barriers for luminogen density and charge transport, respectively.[8] Although several approaches have been taken to tackle the problem of luminogen aggregation, the results obtained at that period were characterized by limited success as in most cases the aggregation was impeded partially or temporarily.

The difficulty lay in the fact that the ACQ was an intrinsic feature of organic polynuclear hydrocarbons, which emerged when molecules came to be in close vicinity such as in condensed (aggregation or solid) phase. Since ACQ phenomenon is a natural process, it is very hard to work against it in order to solve the emission quenching effect, without altering at the same time the molecular features of the luminogen. Therefore it would have been nice to discover a system or

molecular class, for which the emission in aggregation condition would have been enhanced rather than quenched.
The turning point arrived in 2001 thanks to an accidental discover occurred at the Hong Kong University of Science and Technology, in Professor Ben Zhong Tang's group. [11]

The group of Professor Tang had been investigating incessantly in alkyne chemistry employing acetylenic triple bonds as building block to synthesize new molecules with advanced properties [12]
In this context they had synthesized a new molecule belonging to the molecular class of the siloles which are accessible by silylation of metallated alkynes. In particular they had synthesized the Hexaphenylsylole (HPS) shown in chart 1.

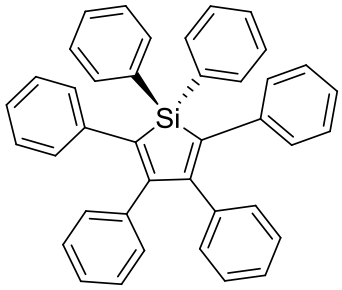

Chart 1.1 Chemical structure of the HexaPhenylSylole (HPS). The First AIE luminogen.

Before running column chromatography in order to purify the reaction product, a routine TLC test was done. After taking out the TLC plate from the development tank, they were amazed to observe that not even one spot was visible on the wet plate but a green-light emitting one appeared after the evaporation of the solvent.[8] This amazing result spurred the Chinese researcher to further investigate the phenomenon. The HPS resulted soluble in the most common organic solvents but not in water, so a series of solutions in ACN as main solvent and water as co-solvent were prepared. The solutions in pure ACN and the ones with low water content, in which HPS was well dissolved, resulted non-emissive; while the ones with a high amount of water were emissive, as it is possible to see in Figure 1.3. [8]

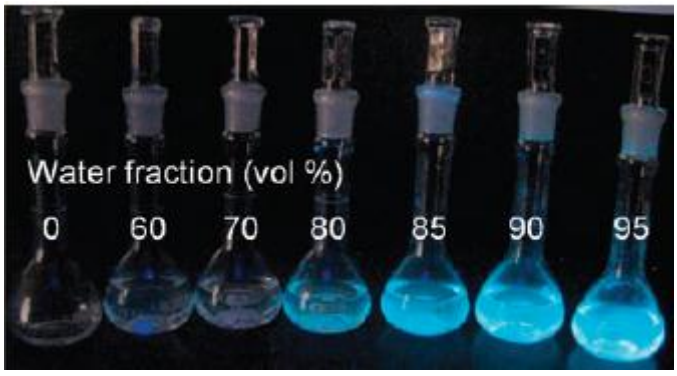

Figura 1.3 [8] Photographs taken under the illumination of UV-lamp of the HPS solutions in pure ACN and in ACN with increasing water content.

This confirmed the qualitative observation of the TLC test. Until HPS is dissolved in a good solvent, solution does not emit, with the increasing of the co-solvent the solubility of the molecule

becomes poorer and poorer, it begins to aggregate and the emission is turned on. This phenomenon has been defined by Professor Tang and co-workers with the term of "Aggregation-Induced Emission" AIE. To quantitatively confirm the AIE phenomenon of HPS, spectroscopic analyses were carried on, recording the PL spectrum and measuring the quantum yield. Figure 1.4 [8,13].

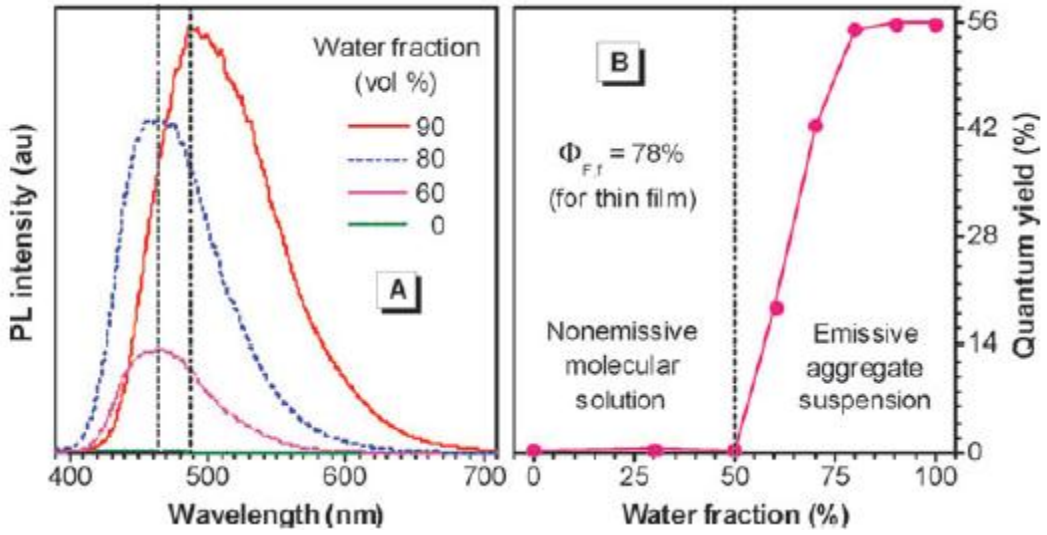

Figure 1.4 [8,13] (A) PL spectra of HPS solution in pure ACN and in ACN-water mixtures. (B) Fluorescence quantum yield (Φ_F) of HPS versus solvent composition of the ACN-water mixture. Data for a thin film of HPS are also given for comparison.

As it is possible to see in Figure 1.4, the PL spectrum of HPS in pure ACN is nearly a flat line parallel to the abscissa, HPS is not emissive and the corresponding quantum yield is 0.22% [8,13], this value remains unchanged until 50% in volume of water is added. Afterwards the emission is turned on and increases together with the increasing of water content; the quantum yield also increases and reaches the maximum value of 56% when the water content is equal to 99%. HPS also emits as a thin film, for which the quantum yield is even higher and equal to 78%.

1.3.1 AIE a special case for HPS molecule?

At this point Professor Tang and co-workers wondered if this phenomenon was an isolated case for HPS or if it generically belonged to the silole molecular class. This is why they synthesized other silole derivatives, which are shown in Chart 1.2. [8] All the derivatives showed the same behavior of HPS: they are non-emissive in a good solvent or in solutions with water content less than 50%, in solvent-mixtures with "medium" water content their emission progressively increases with the increasing of water; in solutions with high water content >80% the emission has a small bathochromic and significant iperchromic shift. For example for the derivative nr 2 the emission in aggregation condition is boosted up to 1417 times respect to the solution state. [8]

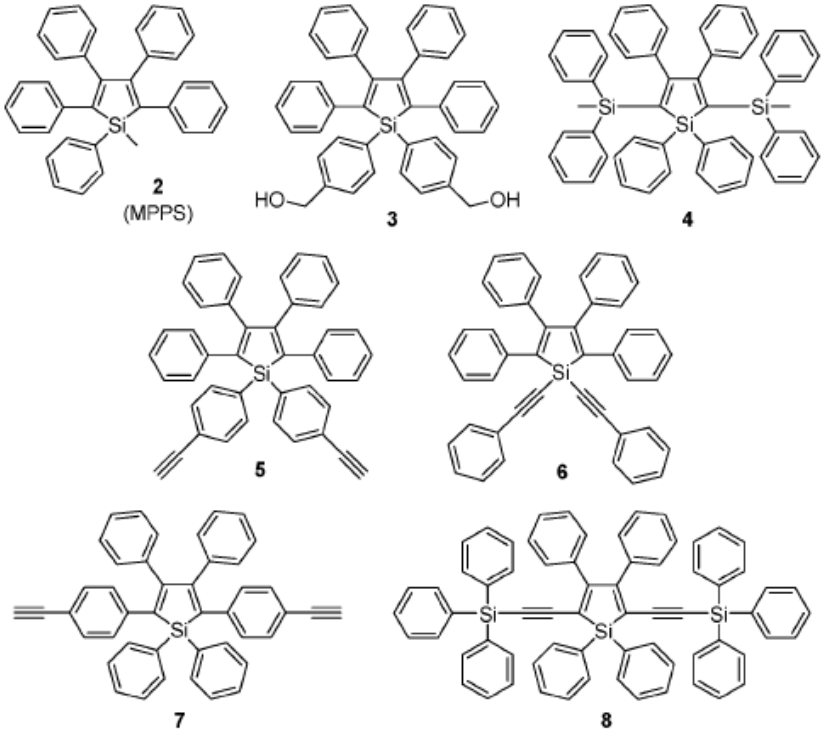

Chart 1.2[8] Some of the silole derivatives synthesized in Prof. Tang's group.

1.3.2 Mechanism of the AIE phenomenon

While the ACQ effect had been studied for more than half a century [8,10] and matured theories existed on the argument, for the AIE one, unearthed models were needed in order to decipher its working mechanism. Several hypotheses were done before fully comprehending the phenomenon. In particular: conformational planarization, *J*-aggregate formation, and twisted intramolecular charge transfer, TICT. All these hypotheses did not find any confirmation in the experimental data.

If the emission had been turned on, due to the planarization of the structure as a consequence of the aggregation formation, both emission and absorption spectra would have been red-shifted but only a small change occurs in PL spectrum case, Figure 1.5(A) and none in absorption spectrum of solutions with different water content, Figure 1.5.[8,13]

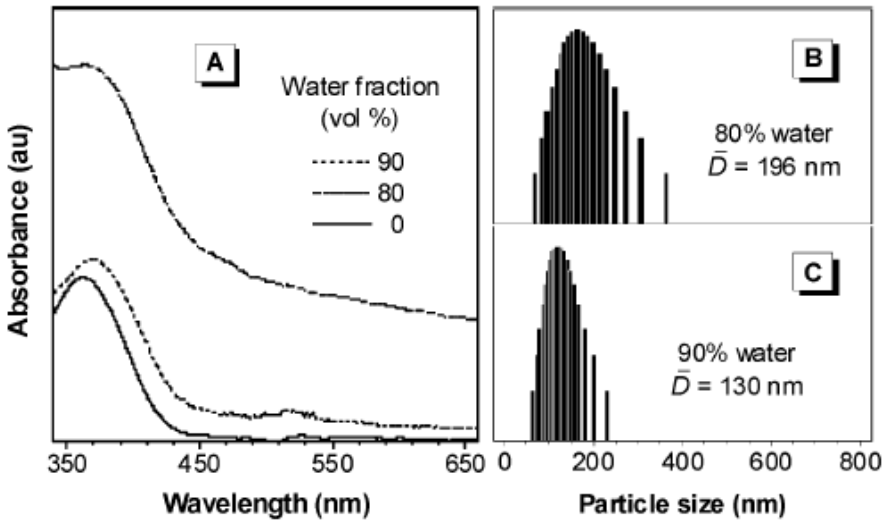

Figure 1.5 [8,13] (A) absorption spectrum of HPS in pure ACN and in ACN-water mixtures; (B) and (C) size distribution of HPS nanoparticles in solutions with 80% and 90% of water fraction respectively. The existence of nanoparticles proves the existence of the aggregate state.

Furthermore the planarization hypothesis did not find foundation in the crystal structure either. Even if it is not possible to know exactly how molecules are oriented when they form nanoparticles and then aggregate, the crystal structure, which allows to know what happens in the solid state, can provide an accurate picture of what happens in the aggregation condition. As shown in Figure 1.6 [8,14] the HPS molecule is not a planar system, as the phenyl rings are twisted out respect to the molecular plane constituted by the cyclopentasylole core; especially the ones directly linked to the Silicium atom which, due to its sp3 hibrydization, imposes a tetrahedric geometry causing a twisting angle of ~70° *versus* 30° of the other phenyl rings.

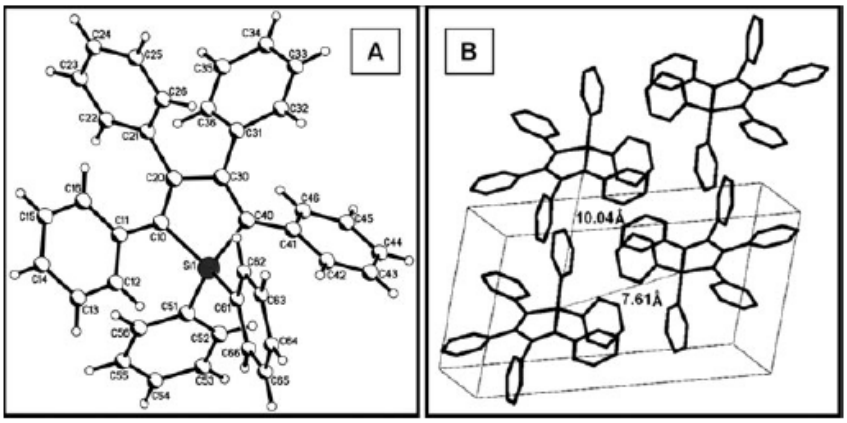

Figure 1.6 [8,14] (A) ORTEP picture of HPS; (B) packing of HPS crystal structure. Intermolecular distance inside the unit cell and interplanar distance are also shown.

Unlike the classic luminophore which shows a typical ACQ behavior, HPS is not planar, but its structure is similar to a propeller-shape one. *J*-aggregate formation and TICT mechanism have been also excluded as working mechanism. To realize these mechanisms the molecular structure of the dye of interest, should contain a donor D and acceptor A units, and this was not the case neither for

HPS nor for its derivatives (Chart 1.2). A *J*-aggregate is a system whose absorption spectrum bathochromic shift when the dye aggregates under the influence of a solvent or additive, as a result of supramolecular self-organization. If this mechanism had occurred as a consequence of the increasing of water content and then if the aggregates of HPS had been *J*-aggregates, a bathochromic shift of the absorption spectrum would have been verified, but this was not the case, as mentioned above (Figure 1.5). As the molecule have not D-A moieties, it cannot undergo TICT effect, because it only occurs on a polar systems and it provides a red-shift of the emission peak.

As fundamental physics teaches, any molecular motion can consume energy. Looking at Chart 1.1, it is possible to observe that the HPS structure is constituted by 6 phenyl rings, that are linked to the sylole core via covalent single bond. The phenyl rings can be considered as *rotors* that can rotate by the single bond against the sylole-core that is possible to consider as the *stator*. These intramolecular rotations can easily occur in the solution state thus they constitute a non-radiative relaxation channel by which the excited state is deactivated. In the aggregate and solid state the rotations are deactivated due to the physical constraint that blocks the non-radiative pathway. Due to the molecular structure that is propeller-like and not a planar one, molecules are not piled up like the ACQ dye do, so that an efficient π-π stacking does not occur and the only available channel is the radiative one. The restriction of intramolecular rotation occurring in solid state and abbreviate in RIR, has been considered as the working mechanism of the AIE phenomenon. To prove this hypothesis, several experiments have been done both by external and internal controls. The first ones have been conducted changing external parameters such as: viscosity, temperature and pressure. [8] All the experiments led to the same results: an increase of the viscosity and pressure and a decreasing of the temperature externally activate the RIR process.
The internal control has been realized intervening at molecular level and covalently linking bulky groups such as isopropyl one, to some of the phenyl rings of HPS, so making steric hindrance between some of the rotors and preventing the intramolecular rotations. The structure of this derivative is shown in Figure 1.7[8].

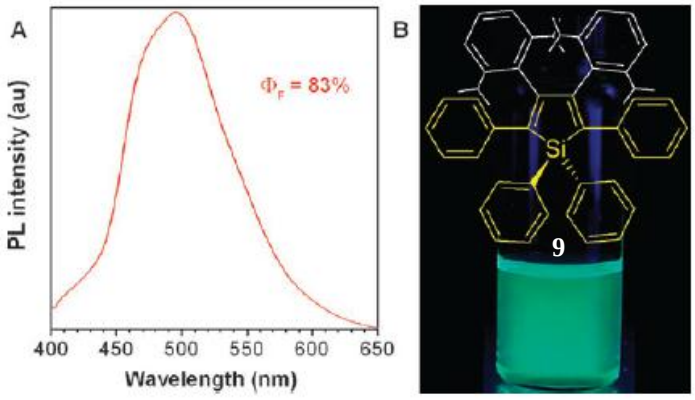

Figure 1.7 [8] (A) Photoluminescence spectrum in Acetone of the sterically hindered HPS; (B) Molecular structure and photograph of the acetone solution taken under the UV lamp.

Contrarily to the parent compound, the unfunctionalized HPS, the hindered derivative 9, shown in Figure 1.7 is emissive in solution. As a proof of this, the lifetime of excited state and quantum yield of the two molecules have been compared. For derivative number 9, lifetime is equal to 6.18 ns *vs* 0.40 ps of HPS and quantum yield in solution is 83% for 9 against 0.031-0.05 % of HPS. Thus the

bulky groups prevented the intramolecular rotations so activating at molecular level the RIR mechanism due to (in this case) not to a physical constraint but to the structural chemical features. This experiment proved that the PL behaviour of silole-based molecules can be tuned by structural tailoring and proper molecular design.[8]

1.3.3 AIE phenomenon for other molecular class

The mechanistic picture about AIE allowed to extend the investigation to other molecules. The RIR mechanism was not supposed to be a special feature only for the silole molecules but an intrinsic characteristic for all the molecules with the same molecular structure: *rotors* which can rotate via single bond against a *stator*. This insight spurred the Chinese researcher on to investigate other molecules whose structure is shown in Chart 1.3.[8]

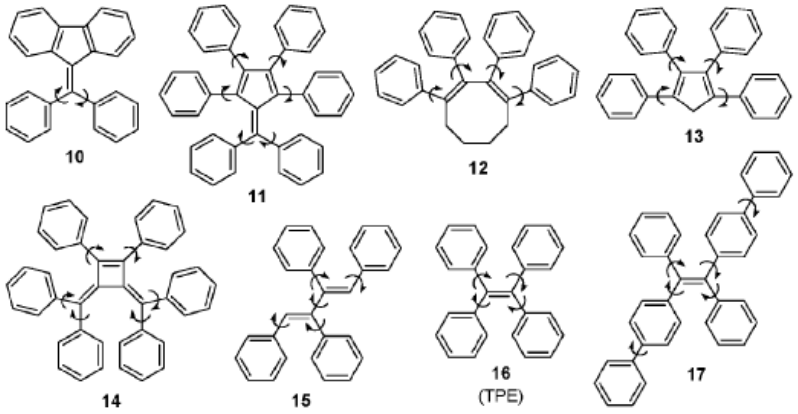

Chart 1.3[8] Molecular structure of other AIE luminogens

All the systems have the same construction of HPS, because there are aryl blades that can rotate against a stator, a ring or a double bond. All the molecules show AIE behaviour, and none of them owns heteroatom or polar groups. This feature allowed to unambiguously exclude a possible involvement of *J/H* aggregate formation and TICT effect in the PL process. Therefore the study on the series shown in Chart 1.3, allowed to definitively confirm that the AIE process occurs in all systems that contain rotatable moieties whose movements are: permitted in solution, thus being responsible for the deactivation of the excited state by a non-radiative channel, and prevented in aggregate or solid state so favouring the radiative pathway through that the system can emits light.

The AIE study proceeded by synthesizing other AIE gen containing various heteroatoms and polar groups, in order to enrich the colour emission palette. [8,15] An example is shown in Figure 1.8, the emission colour of the butterfly-shaped dye, changes according to the amount of water, namely depending on the solvent polarity [15a].

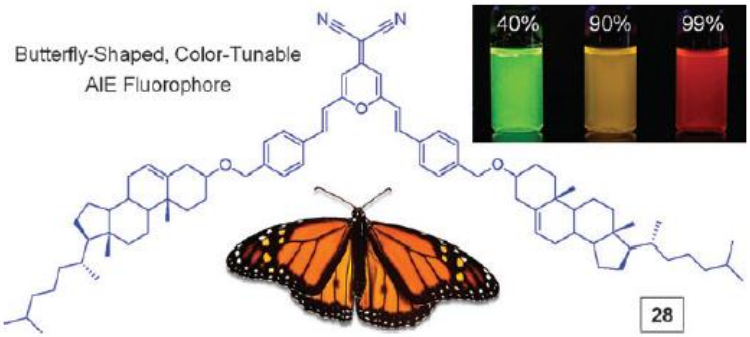

Figure 1.8 [15a] Molecular structure of the molecule 28, and emission color of the solutions with different water content

1.3.4 Restriction of Intramolecular Motion

Many other systems were developed over the years and new insight into working mechanism of AIE phenomenon have been obtained. Although for many AIE systems the phenomenon can be explained by the RIR mechanism, there are some molecules which despite they do not contain rotor moieties, they are AIE active, an example is shown in Chart 1.4.[16]

Chart 1.4 [16] structure of 10,10',11,11'- tetrahydro- 5,5'- bidibenzo [*a*,*d*] [7] annulenylidene THBA

Even if THBA does not carry any rotors, it shows AIE behaviour. This evidence can be explained thinking to this system as constituted by two flexible parts linked by a double bond. In each of them the phenyl rings are connected by a bendable flexure that is in this case a cicloheptane. The two parts are no-coplanar and the whole molecule adopts an *anti*-conformation. The flexibility of the two flexures allows the phenyl rings of THBA to dynamically bend or vibrate in the solution state. These intramolecular movements, similarly to what happens in rotors-based AIE gen, constitute a non-radiative relaxation channel, by which the excited state can be deactivated. Therefore for this kind of structure, the dynamic vibrations is responsible for the occurring of the non-radiative pathway.

These movements can easily occur in solution, while in aggregate or solid state, the physical constraint associated with the space limitation make them not realizable. For this reason, the only accessible relaxation channel remains the radiative one and light emission is observed. Similarly to the restriction of intramolecular rotation, the phenomenon just described can be defined "Restriction of Intramolecular Vibrations" RIV. Therefore the AIE mechanism of propeller-shape and shell-like molecules have been explained by Restriction of Intramolecular Rotations RIR and Restriction of Intramolecular Vibrations RIV, respectively. These two concepts can be unified providing a general

picture that the restriction of Intramolecular Motion RIM processes mechanistically account the AIE systems developed so far.[16] This concept is exemplified in Figure 1.9.[16]

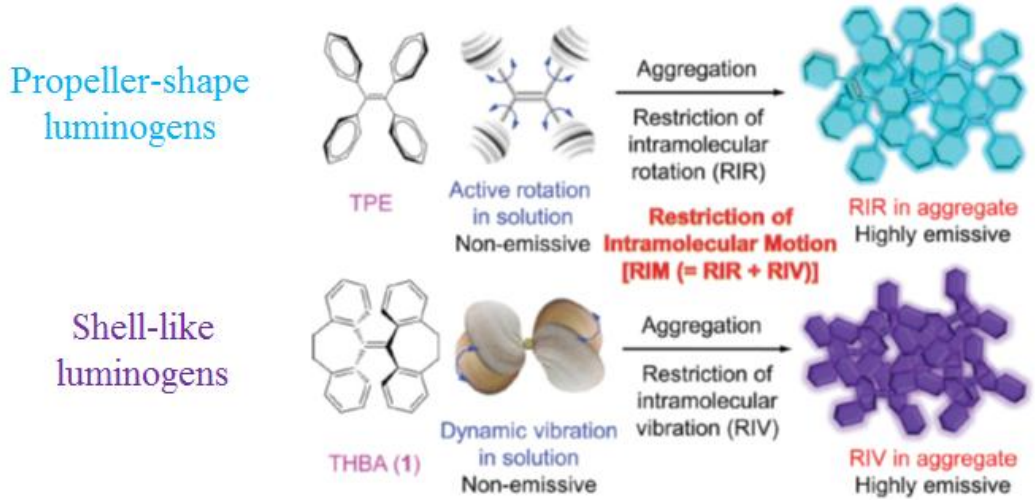

Figure 1.9 [16] Sketch of the working mechanism of the AIE phenomenon.

The discovery of the AIE phenomenon indelibly marked a turning point in Photophysics understanding and in the applications directly deriving from it. Until its unearthing there was the common belief that the emission quenching was a phenomenon belonging to most of the aromatic hydrocarbons and their derivatives. [8,10b] This limited the employment of these systems in Hi-Tech applications and when used, their employment had been distinguished by mediocre results. AIE discovery allowed to prove that the emission quenching in aggregate or solid conditions cannot be generalized to all aromatic hydrocarbons because it is actually true only for the molecules which have a disk-like shape, as their flat structure allows them to pile-up and intermolecularly interact thanks to their effective π-conjugation. Propeller-shape systems have shown a different behavior from the disk-like ones as described above; they have probably been eliminated in the early stages of the screening process for candidate emitters for the fabrication of OLEDs, because the photophysical properties evaluation have traditionally been done in dilute solutions in which these molecules are not emissive as explained before. According to the common belief by which a poor emitter in solutions will also be a mediocre luminophore in aggregate or solid state, these molecules have not been taken into account and as a consequence neither deeply investigated from the photophysical mechanistic point of view.[8]
AIE studies proved that it is not correct to prematurely discard a molecule non-emissive in the solution state or to generalize and extend what happens to one molecular class to another one because, as it can be seen, the behavior could be totally different.

Over the years, plenty of AIE active molecules have been synthesized over the world, for each of them Restriction of Intramolecular Motions RIM accounted for the working mechanism.
In organic luminophores, luminescence can also be enhanced due to other phenomena such as: *J*-Aggregate Formation, *JAF*, Excited State Intramolecular Proton Transfer, *ESIPT* and Twisted Intramolecular Charge Transfer, *TICT*. Looking for the synthesis of new and efficient luminogenes, plenty of molecules with different structures have been synthesized all over the world. In some cases, due to the presence of heteroatoms or polar moieties, some of the above mentioned effects

took place and since these dyes were emissive in aggregate and solid state as well, researchers explained the phenomenon saying that it was (depending on the structure) due to *JAF* or *TICT* or *ESIPT* processes, creating this way a general misunderstanding. In order to clarify this concept and in order to provide a clearer picture even for these systems which have a more complicated structure and which can have one of the above mentioned processes, Professor Tang and co-workers performed a very deep mechanistic study comparing the RIM process with each of the above mentioned mechanisms.[16] As a conclusion it has been possible to confirm that, if the dye shows AIE activity, namely it is luminescent in aggregate or solid state and not in solution, even if the structure consents to have one of the above mentioned process (e.g. *JAF*, *TICT* or *ESIPT)* only the RIM is the mechanism responsible for the AIE phenomenon, while the other processes, in case they occur, can also contribute to increase the luminescence that is anyway due to the restriction of intramolecular motions RIM. Indeed, those dyes which have a molecular structure that does not consent to activate a RIM mechanism in solid state, they will not be AIE active even if they show one of the aforesaid processes.[16]

1.3.5 Different classes of AIE luminogens

Under the direction of the mechanistic understanding, researchers have designed and synthesized plenty of new AIE systems over the years. The luminogens that have AIE features have been defined AIEgens, like in the case of liquid crystals where molecules showing *meso*morphism are named *meso*genes. [16] The new AIE systems have been constituted by a central stator bearing multiple rotors or vibrators that can rotate or vibrate to large extents. The wide array of new AIE gens can be grouped in different classes according to their structural features: hydrocarbon, heteroatom and organometallic systems [9,16].

1.3.5.1 Hydrocarbon-based AIE molecules

Development of pure hydrocarbons AIEgens has served, first of all to fully comprehend the AIE phenomenon, and to prove that the mechanism of RIM is responsible for the AIE luminescence, thus excluding other effects such as *JAF* and *TICT* that are involved when heteroatoms or polar moieties are present in the molecular structure. [8,9,16] So hydrocarbon-based AIEgens have been extremely important for fundamental research and mechanistic decipherment. They also have been used as building blocks for the synthesis of advanced functional materials. In most cases the hydrocarbon-based AIEgens have been molecularly designed with a central stator bearing peripheral rotors, therefore the AIE working mechanism accounted for the Restriction of Intramolecular Rotation RIR. Chart 1.5. [16]

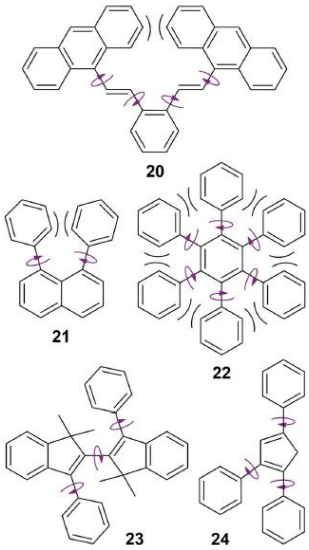

Chart 1.5 Some examples of Hydrocarbon-based AIEgens

The mechanism has been proved by obtaining the crystal structure of the above-mentioned molecules. Figure 1.10 [16]. The rotations are prevented in solid state and the propeller shape impedes to have an effective packing so preventing the π-π stacking interactions. The only accessible relaxation channel remains the radiative one.

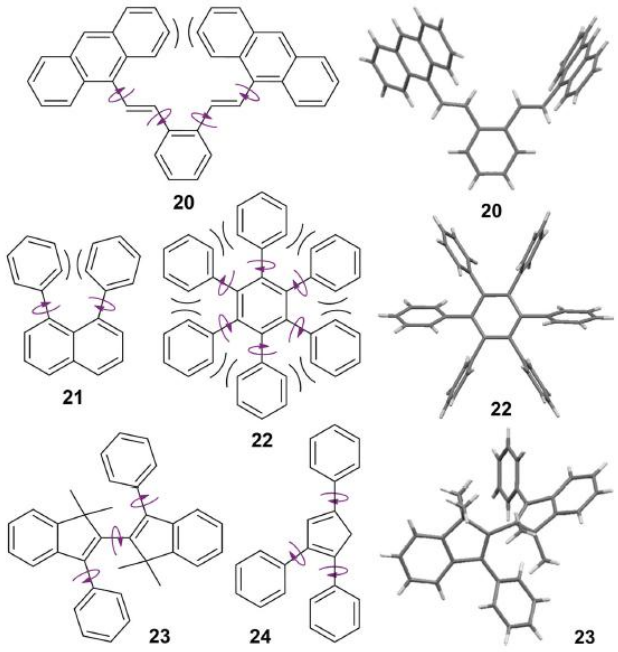

Figure 1.10 Some examples of Hydrocarbon-based AIEgens and their crystal structure.

1.3.5.2 Heteroatom-based AIE molecules

Although Hydrocarbon-based systems are indispensable both for mechanistic understanding and for being important building blocks to construct more complicated systems, their reactivity and chemical features are anyway limited for the exclusive presence of Carbons and Hydrogens. Indeed

heteroatoms, thanks to the presence of extended molecular orbitals and lone pair electron couples, render the chemical structure more reactive, contributing to extend effectively the π-conjugation efficiency as well. Plenty of heteroatom-based AIEgens have been synthesized both according to the classic design: central stator with peripheral rotors, and by linking the rotors to a condensed polynuclear core, so creating a bended and vibrating structure. The activity of these systems accounted for RIR and RIV+RIR = RIM mechanisms respectively. Figure 1.11-12.[16]

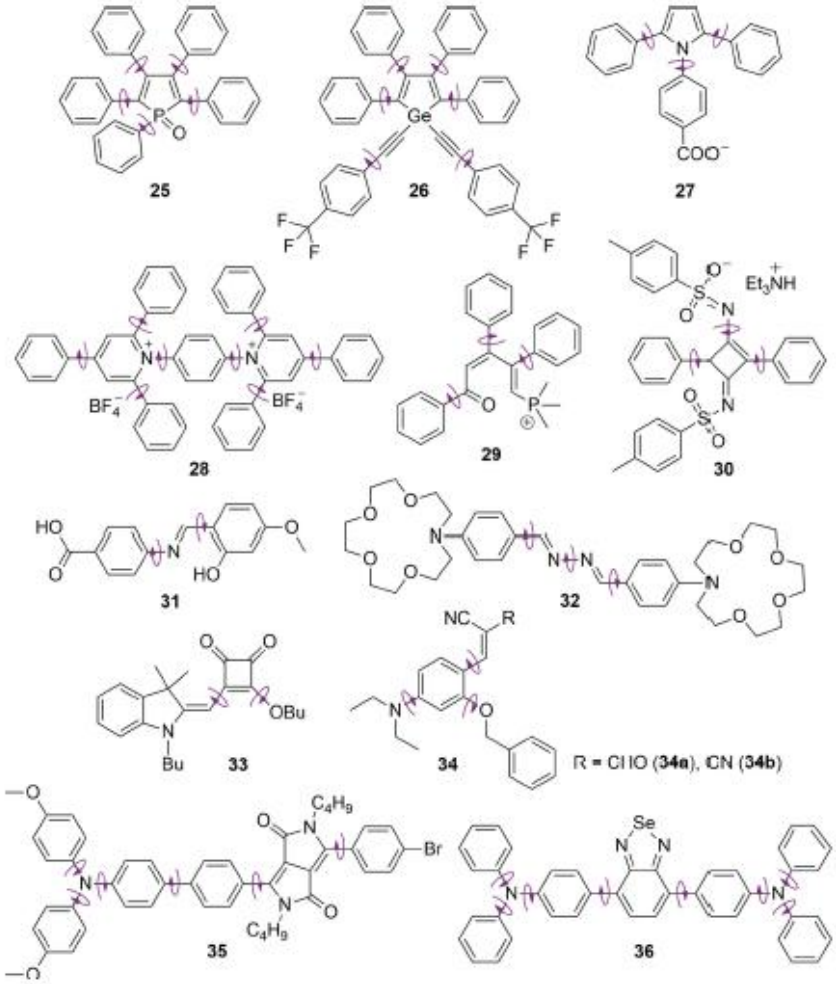

Figure 1.11 [16] Some examples of Heteroatom-based AIEgens with RIR phenomenon as working AIE mechanism.

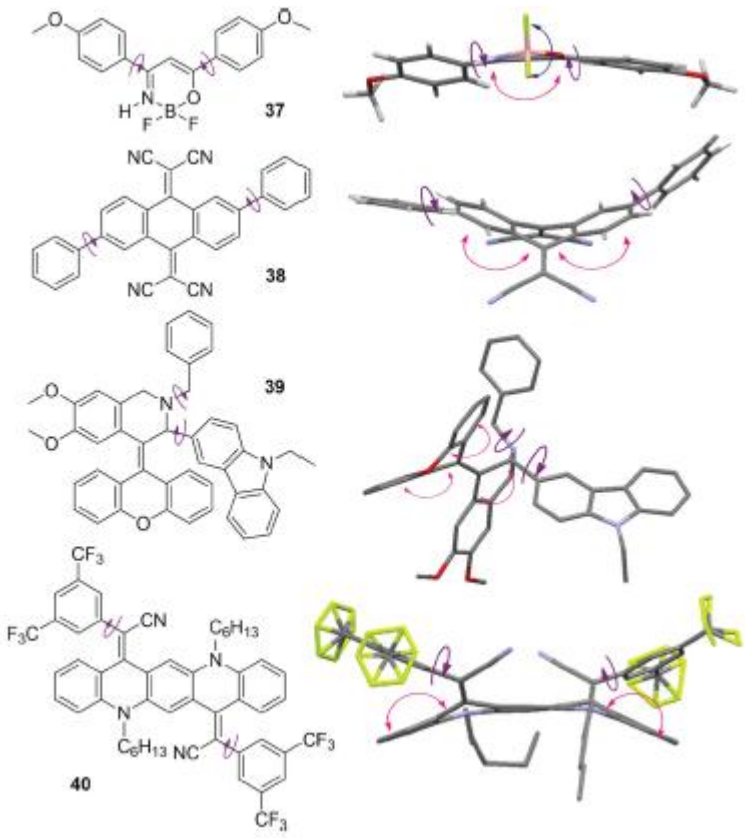

Figure 1.12 [16] Some examples of Heteroatom-based AIEgens with RIM phenomenon as working AIE mechanism.

Thanks to the multiple presence of the heteroatoms, in the crystal state many CX---H, H-bonds can exist. These interactions help to rigidify the molecular structure, locking the rotating units thus barricading the intramolecular rotations and vibrations. In some cases the formation of the intermolecular H-bonds in solid state is the main reason for the turning on of luminescence. [16]

1.3.5.3 Organometallic-based AIE molecules

The emission of the systems described so far is fluorescence because the radiative decay is associated with the transition of the singlet which excited state. In organometallic systems, the phosphorescence process is easy to achieve thanks to the presence of the heavy metallic component. Even this molecular class suffered of the ACQ effect, as phosphorescence emission has often been quenched by the increasing of concentration or aggregate formation. However, properly projecting the molecular design, even for these systems it is possible to turn on the emission behavior in solid state or upon aggregate formation.[16] Indeed for propeller shape-based dye phosphorescence in aggregate conditions has been observed, as a consequence these phenomena have been defined "Aggregation-Induced Phosphorescence AIP". Complexes based on Iridium (III) have been deeply investigated as organometallic phosphors but many of them, such as tris(2-phenylpiridine) iridium (III) complex [Ir(ppy)$_3$], showed ACQ behavior.[17] The group of Professor Su synthesized a series of AIP-active cationic Ir(III) complexes with different ligands.[18] For example functionalizing the [Ir(ppy)$_3$] complex by introducing carbazole units, an AIP luminophore is easily obtained. Figure 1.13[16,18].

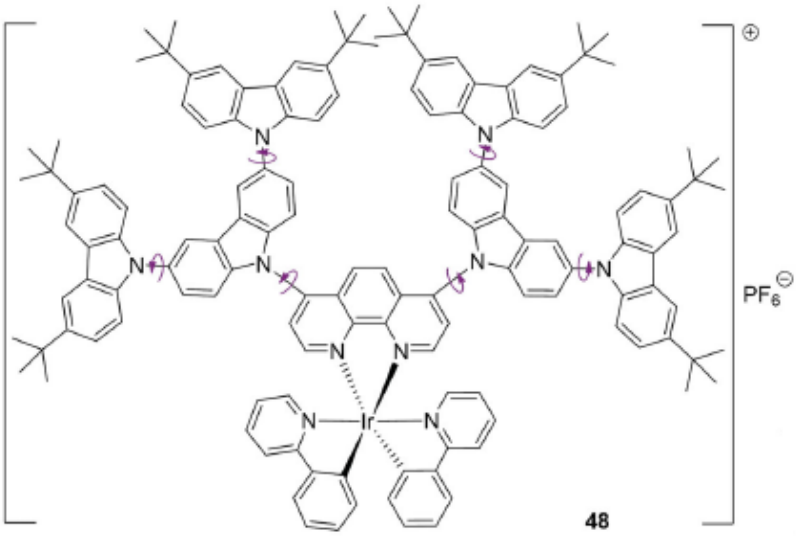

Figure 1.13[16,18] Structure of one of the AIP active Iridium (III) based complexes synthesized by Prof. Su group.

While the $[Ir(ppy)_3]$ core is not AIP active and its luminescence is quenched in aggregate or solid state, the derivative 48, is an AIP phosphor, because it is not phosphorescent in solution but only in aggregate and solid state. As schematized in the Figure 1.15, the mechanism responsible for the solid state luminescence is the RIR one, indeed in solution the excited state can be deactivated by the intramolecular rotations of the carbazole moieties. Upon aggregation these movements are inhibited due to the physical constraint and the radiative relaxation channel is thus activated.

1.3.6 Use of the AIE luminogens in Hi-Tech applications

As mentioned above, using effectively organic luminophores for advanced applications such as bioprobes, light emitting devices, chemical sensor and so on, seemed to be something not conquerable because of the thorny obstacle of ACQ effect which occurs in aggregate conditions. Thanks to the AIE discovery, it has been possible to achieve a significant turning point in the photophysical state of the art, the decipherment of the working mechanism which is behind this great phenomenon allowed first Professor Tang's group and later the rest of the scientists all over the world to produce efficient AIEgens to employ successfully in advanced applications. Indeed the generation of the AIE materials provided a new platform for technological innovations impossible up to that moment; their practical applications can be considered endless and their scope could only be limited by scientists' imagination. [16] In addition, the understanding of the AIE phenomenon has allowed not only to develop new systems belonging to a new molecular class, but also to unearth an aspect of the photophysics totally unknown or not understood until that moment.

1.3.6.1 Chemosensors

Detection of volatile organic compounds (VOCs) is very important for hygienic and environmental implications. In Figure 1.14 is shown one derivative of TetraPhenylEthene TPE, one of the most important AIE luminogen. The panel B of this figure shows the light emission from a spot of this molecule on a TLC plate, which is turned off, when the plate is put into a Petri-dish set saturated with Chloroform vapor, (panel C). The spot turns emissive again when the solvent is evaporated.

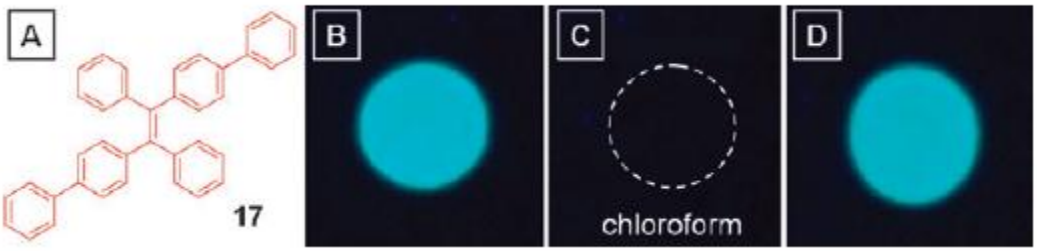

Figure 1.14 [8,19a] (A) Chemical structure of diphenylated TPE derivative 17, on TLC plate placed in Petri dish set (B-D) without and (C) saturated with Chloroform vapours.

The solvent vapors present inside the experimental set, condensing form a thin liquid layer on the TLC surface which dissolves the adsorbed luminogen molecules thus quenching its emission (Figure 1.14 B) After the evaporation of the solvent the molecules aggregate and hence emit again. This luminescence "off/on" switching is completely reversible and reliably repeatable many times, because the involved process is a non-destructive physical cycle of dissolution (deaggregation-aggregation). The same result has been obtained by using other VOCs such as: Acetone, Acetonitrile, THF, and other AIE systems as sensor, among which Hexaphenylsilole and TetraPhenylEthene TPE.

Nanostructured chemosensors for explosive detection have been also investigated. Nitroaromatics such as: 2,4,6-trinitrotoluene (TNT) and 2,4-dinitrotoluene (DNT) are warfare explosives, their detection is of value to homeland security. Since neither TNT nor DNT are commercially available, picric acid (PA) has been used as model explosive for this investigation. To serve this aim an amminated derivative of HPS has been tested as sensor, its structure is shown in Chart 1.6 [8,19b]

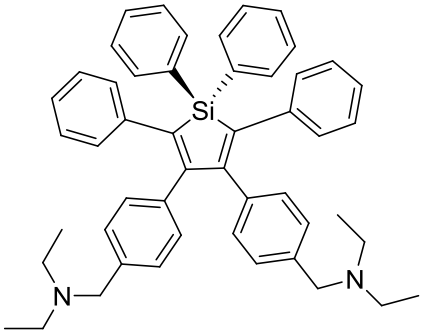

Chart 1.6 Chemical structure of Aminated HPS derivative

The nanoaggregate of the HPS derivative was prepared by admixing 1% of its THF solution with 99% of water. As a consequence of adding acid, the amino units are protonated and the molecules become soluble in water environment, thus the nanoaggregates are destroyed and the emission dramatically decreases, because in solvatating conditions the emission is turned off by the RIR mechanism that becomes active. Figure 1.15 [8,19b]

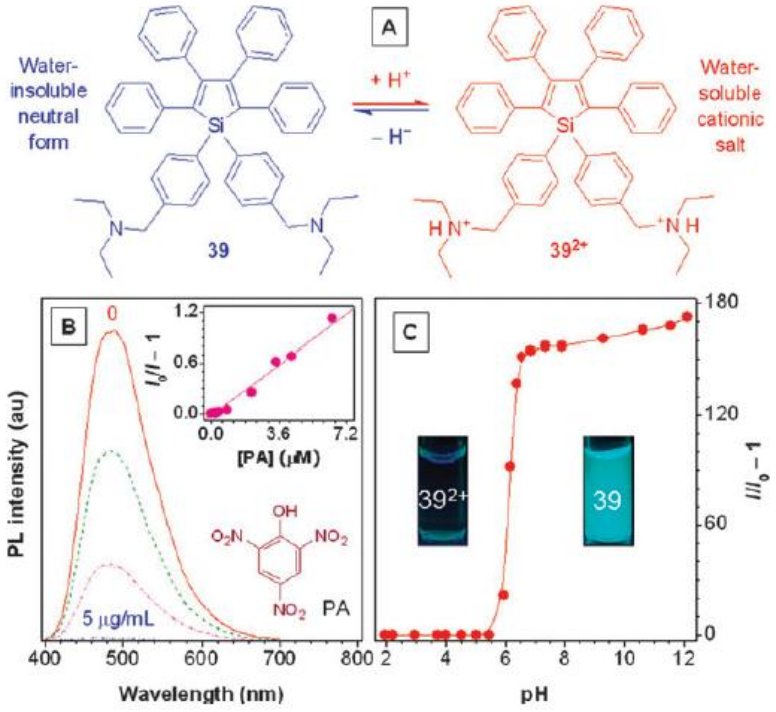

Figure 1.15 [8,19b] (A) equilibrium protonation reaction of Aminated HPS derivative 39; (B) PL spectra of 39 in THF:water mixture 1:99, containing different amount of picric acid (PA);
(C) Change of PL intensity of 39^{2+} or 39 with pH value of the acqueous mixture. I_0 is the intensity at pH 2.

Because of the presence of amino moieties which can be protonated, the solubility and the AIE behavior change depending on the pH value, thus by this experiment, the molecule 39 revealed to be a pH sensor as well. Indeed increasing pH and creating basic conditions, the protonated moieties lose their proton and the system turns to be insoluble in water environment and then emissive due to the re-formation of the nanoparticles.

1.3.6.2 Application in Light Emitting Devices

Organic Light Emitting Diodes, OLEDS, have attracted a lot of attention due to their application in full-color displays and solid state light systems. In these devices, luminophores have to be used in solid state, for example as thin film and for this reason the AIE systems have been the ideal candidate materials for the fabrication of efficient OLEDs. The AIEgens have been used as light-emitting layers, thus making possible the realization of multilayers OLEDs. [19c] In order to compare the results obtained from an OLED made by using the HPS or tetraPhenylEthene TPE AIEgens as emitting layer, a similar device in which the emitting layer was Alq_3 has been built as well. Alq_3 system whose structure is shown in Chart 1.7

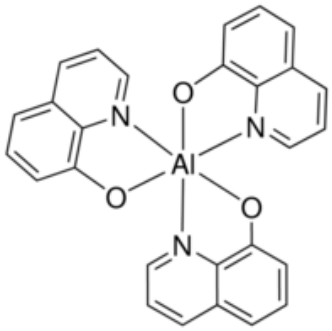

Chart 1.7 Molecular structure of Alq_3

Alq_3 has been the first organic-based luminophore which allowed to build a low-voltage, bright and efficient OLED. [19c(v)] Despite this, it is not a stable dye as its anodic oxidation is irreversible, and the cationic species produced lead to a long-term degradation. Furthermore it is an ACQ dye, because its luminescence in solid state is lower than in solution conditions. [8] The OLED built by using this molecule, provided a maximum luminance of 9234 cd m^{-2} a maximum current efficiency of 20 cd A^{-1} and a power efficiency of 14 lm W^{-1}. Its external quantum efficiency is 8% well approaching the limit of that possible in electroluminescence (EL) devices based on organic singlet emitters. [8,19c(vi)] By using HPS AIE active molecule, instead of Alq_3 as emitting layer, the maximum luminance is significantly higher, 55880 cd m^{-2} and by using TPE, the value is equal to 10680 cd m^{-2}. In particular, using TPE as building block, several derivatives with blue-emission ability have been synthesized and they allowed to reach up to 100% solid state emission efficiency. [16]

1.3.6.3 Biosensors

AIE molecules have also been used in biological applications, where ACQ dyes, as mentioned at the beginning of the introduction, have been employed with disappointing results. The AIE systems employed in this field have been the fluorogen ones, namely the molecules that don't contain metallic atoms and hence can provide fluorescence as emitting light. Depending on the bioanalyte that has to be monitored, AIE fluorogens can be used as molecule, or as aggregates. For DNA, protein and small molecules sensing, the fluorogens are used as molecules; for in vitro and in vivo cellular tracing and imaging the AIE fluorogens are used as nanoaggregates.

<u>AIEgens employed as biosensors in molecular form</u>

In order to use AIEgens as molecules for DNA, protein and small molecules sensing, it is necessary to functionalize the molecular structure with some polar groups, in order to make the luminogens soluble in water environment. This way the luminogen will be soluble and hence not emissive, according to RIM mechanism, but when the bioanalyte is added in this environment and there is an interaction between the biological system and the molecule, the interaction leads the fluorogen to be bounded to the bioprobe. This interaction will lock the fluorogen in a specific conformation, according to the occurring phenomenon, so that the intramolecular motions will be impeded and the emission will be turned on. So in this case the turning on of the emission, and hence the restriction of intramolecular motions, are not due to the formation of aggregates but to the selective interaction

with the analyte. The description of some of these applications will serve as example to better understand the concept.

When functionalizing TPE by using solfonate groups (molecular structure is shown in Figure 1.16) it is possible to detect bovine serum albumin, BSA. In a neutral buffer solution sulfaneted TPE, shown in Figure 1.16[8,15c] is not emissive, because it is water-soluble thanks to the polar moieties and its ionic form. With the increasing of BSA concentration, the emission linearly increases Figure 1.16 (A) and a linear calibration curve is obtained at BSA concentrations up to 100 mg/L. Figure 1.16 (B). The spectrum of the solfonated derivative in the presence of BSA, is identical to that of its nanoaggregates and this means that even in the biological environment, the working mechanism is the Restriction of Intramolecular Motions. However RIM mechanism is not activated by the formation of aggregates, because in this case, the molecule is soluble in the aqueous medium due to the polar and ionic units. Therefore there should be another reason why the RIM are activated. Prof. Tang and co-workers, have thought of the hydrophobic interactions between the molecule and BSA. The latter is a protein and as such, it owns hydrophobic pockets of the native folding structure. The solfonated derivative may bind to the hydrophobic regions of the BSA chains and enter into hydrophobic cavities of their native folding structures. In this limited space and due to the hydrophobic intermolecular interactions, the RIM mechanism is activated and the molecule is emissive. The sodium dodecyl sulfate, SDS, is well known to unfold protein structure effectively; adding SDS into the BSA solution containing TPE derivative as biosensor as well, the emission is dramatically decreased, Figure 1.16 C. The SDS, causing the unfolding of the protein, allows the AIEgen to be released back to the solution, in which it is soluble and hence non-emissive.

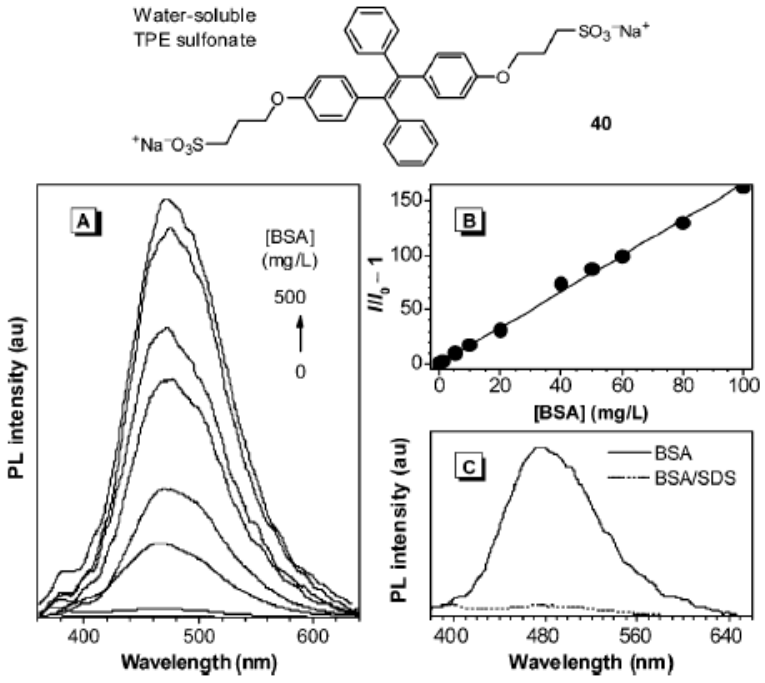

Figure 1.16[8, 15c] (A) PL spectra of TPE derivative 40, in phosphate buffer (pH = 7) containing different amount of BSA. (B) calibration curve; (B) Plot of [BSA] versus I/I_0 -1. I_0 = intensity [BSA] = 0 mg/L; (C) Effect of BSA on the PL spectrum of a buffered solution of 40 in the absence and presence of (SDS).

Similar effective results have been obtained by functionalizing TPE with cationic instead of anionic groups. The positive charge can electrostatically interact with the negative charge of nucleic acids triggering the emission of the chromophores, and selectively monitor the DNA or RNA. [5]

AIEgens employed as biosensors in aggregate form

The visualization and tracking of cellular events, have always been performed by exploiting fluorescent probes. The typical system used for this aim includes organic dyes or proteins, which unfortunately are featured by low photostability, and in some cases ACQ phenomenon. Ionic luminophore have been used as alternative systems, but their charge perturbed the membrane potential and cellular physiology. On the other hand, at low concentrations, the limited numbers of the luminophores that have entered into the cellular interiors can be easily photobleached in the imaging process. Inorganic quantum dots have not been successfully employed due to their inherently cytotoxicity. The use of more effective materials was needed even in this field. AIE systems have been the turning point even in bioapplications as they are non-ionic luminogenes that spontaneously aggregate in acqueous medium, and owing to AIE effect and electrical neutrality, the luminogens can be used in high concentration without perturbing cellular physiology. They have been able to stain HeLa cells and hold inside so robustly that they have been visible for a long period. For example, good results have been obtained by using an aminated derivative of HPS molecule shown in Chart 1.8.[20] Figure 1.17 [8,20]

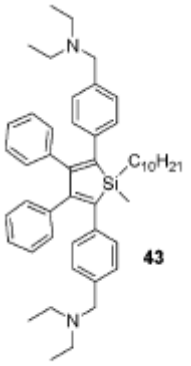

Chart 1.8 Molecular structure of an aminated derivative of HPS

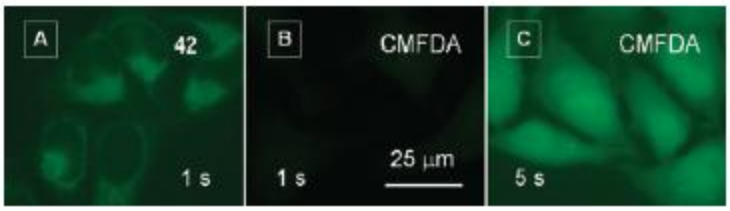

Figure 1.17[8,20] Fluorescence images of living HeLa cells stained with (A) derivative 43, and (B,C) commercial dye. Exposure time: (A, B) 1 s, (C) 5 s.

By using the AIE dye it has been possible to stain the cytoplasmatic region of the cell just after 1 s; The commercial one, CellTracker™ Green CMFDA needed 5 s as exposure time, to provide a clear picture and it did not show selectivity as it was able to stain the entire cell.[8,20]

Better performances have been obtained by encapsulating AIEgen in a silica shell, in order to make AIE nanoparticles much more resistant to the harsh laser usually used in the imaging systems. The silica nanoparticles, which are optically transparent, cytocompatible and fluorescent inactive, have been the best host candidate material, because the silica-based matrix have served as a protective shield, reducing the likelihood of penetration of oxygen or other detrimental species, which may accelerate the photobleaching processes of fluorophores. Thus fluorescent silica nanoparticles, FSNPs, have been prepared by sol-gel technique [5] employing several AIEgens among which TPE and HPS-based derivatives which have been able to stain the cytoplasm of HeLa cells. One of the challenges in this field has been to prepare nanoparticles which could have been both fluorescent and magnetic, MFSNPs. A difficult aim to achieve, as fluorescence is usually quenched by the magnetic field, especially when the fluorophores are weak emitters. AIE nanoaggregates were able to win even this challenge because the luminescence does not come from isolated molecules but from assembled aggregates that are more robust than individual molecules of the traditional luminophores and hence more resistant to magnet quenching.

1.4 TetraPhenylEthene TPE: an archetypal AIEgen

Among the AIEgens, discussed especially in the first paragraphs of this chapter, it is noteworthy the TetraPhenylEthene TPE, whose structure is shown in Chart 1.9. TPE is an aromatic hydrocarbon known since 1910. [21] Despite its old "age", only upon AIE discovery, it has been used in Photophysics and related applications. In fact before the advent of AIE, it was employed just in synthetical procedures, but the AIE discovery made swiftly grow its employment during the years. It has been one of the pure hydrocarbon AIEgens, used in order to prove the working mechanism of RIM. Thanks to the fluorescence efficiency and synthetical versatility, this scaffold has been used, not only as simple model for mechanistic studies, but also as building block for the construction of more complex structures, giving the possibility to convert classic ACQ molecules in efficient AIE dye. [16] TPE-based AIEgens found application in a lot of important fields, making possible what was inaccessible before, because of the ACQ effect. Some examples have been reported above, [8, 15c, 16, 19a] other noteworthy results have been obtained in OLED applications [22] and forensic science.[23]

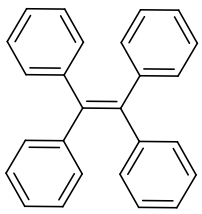

Chart 1.9 Molecular structure of TetraPhenylEthene TPE.

Bibliography chapter 1

[1] N. Thejo Kalyani, S. J. Dhoble, *Renewable and Sustainable Energy Reviews*, **2012**, *16*, 2696;
[2] I. Baraldi, *La Luminescenza, Elementi di fotofisica molecolare, Quaderni di fotochimica*, **2007**, Bononia University press;
[3] E. Wiedermann, *Ann. Phys. Chem*., **1888**, *34*, 446;
[4] P. Atkins, J. De Paula, *Chimica Fisica,* quarta edizione italiana, **2004,** Zanichelli editore;
[5] A. Qin, B. Z. Tang, *Aggregation-Induced Emission: Applications*, first edition, **2013**, Jhon Wiley & Sons Ltd.
[6] R. Y. Tsien *et al*, *Science*, **2006**, *312*, 217;
[7] S. M. Borisov, O. S. Wolfbeis, *Chem. Rev*., **2008**, *108*, 423;
[8] Y. Hong, J. W. Y. Lam and B. Z. Tang, *Chem. Commun*., **2009**, 4332;
[9] Y. Hong, J. W. Y. Lam and B. Z. Tang, *Chem. Soc. Rev.*, **2011**, *40*, 5361;
[10] (a)T. Förster and K. Kasper, *Z. Phys. Chem. (Munich)*, **1954**, *1*, 275; (b) J. B. Birks, *Photophysics of Aromatic Molecules*, **1970**, Wiley, London;
[11] J.W.Y. Lam, B.Z. Tang *et al Chem. Commun.* 2001, 1740;
[12] ref 17 and 18 da main review
[13] J. Chen, C. C. W. Law, J. W. Y. Lam, Y. Dong, S. M. F. Lo, I. D. Williams, D. Zhu, B. Z. Tang, *Chem. Mater*., **2003**, *15*, 1535;
[14] B. Z. Tang *et al*., *J. Inorg. Organomet. Polym. Mater*., **2005**, *15*, 287;
[15] (a) B. Z. Tang *et al., J. Phys. Chem. B,* **2007**, *111*, 2000; (b) B. Z. Tang *et al., J. Phys. Chem.C,* **2007**, *111*, 2287; (C) B. Z. Tang *et al., J. Phys. Chem. B*, **2007**, *111*, 11817;
[16] A. Qin, B.Z. Tang, *et al*, *Adv. Mater.*,**2014**, *26*, 5429; N. L. C. Leung, N. Xie, W. yuan, Y. Liu, Q. Wu, Q. Peng, Q. Miao, J. W. Y. lam, B. Z. Tang, *Chem. Eur. J*., 2014, **20**, 15349;
[17] C. Adachi *et al Appl. Phys. Lett.*, **2005**, *86*, 071104;
[18] riff 153-156 review advanc mater.
[19] (a) A. Qin, B. Z. Tang *et al Appl. Phys. Lett.*, **2007**, *91*, 011111; (b) A. Qin, B. Z. Tang *et al Chem. Phys. Lett.*, **2007**, *446*, 011111; (c) (i) B. Z. Tang *et al J. Mater. Chem.,* **2001**, *11*, 2974, (ii) B. Z. Tang *et al J. Am. Chem. Soc.,* **2005**, *127*, 6335; (iii) A. Qin, B. Z. Tang, H. S. Kwok, *Appl. Phys. Lett.*, **2007**, *91*, 0111111, (iv) B. Z. Tang *et al J. Phys. Chem. B,* **2005**, *109*, 17086, (v) Y. Qiu *et al*, *Adv. Mater*., **2011**, *23*, 1137; (vi) B. Z. Tang *et al Appl. Phys. Lett.*, **2002**, *81*, 574;
[20] B. Z. Tang *et al Chem. Mater.*, **2003**, *15*, 1535;
[21] M. Delacre, *Bullettin de la Societe Chimique de France*, **1910**, *5*, 1149;
[22] (a) B. Z. Tang *et al, J. Mater. Chem.*, **2012**, *22*, 4527; (b) Z. Li *et al*, *J. Mater. Chem.*, **2012**, *22*, 2478; (c) Z. Li *et al*, *J. Mater. Chem.*, **2012**, *22*, 12001; (d) Z. Li *et al*, *Adv, Funct. Mater.*, **2013**, *23*, 2329;
[23] Y. Li, L. Xu, B. Su, *Chem. Commun.*, **2012**, *48*, 4109;

2

Motivation and Aims of the Thesis

2.1 The HeteroarylEthenes

The present research has been aimed on the synthesis and to the electrochemical and photophysical investigation of the HeteroArylEthene class, focusing on the terms shown in Chart 2.1.

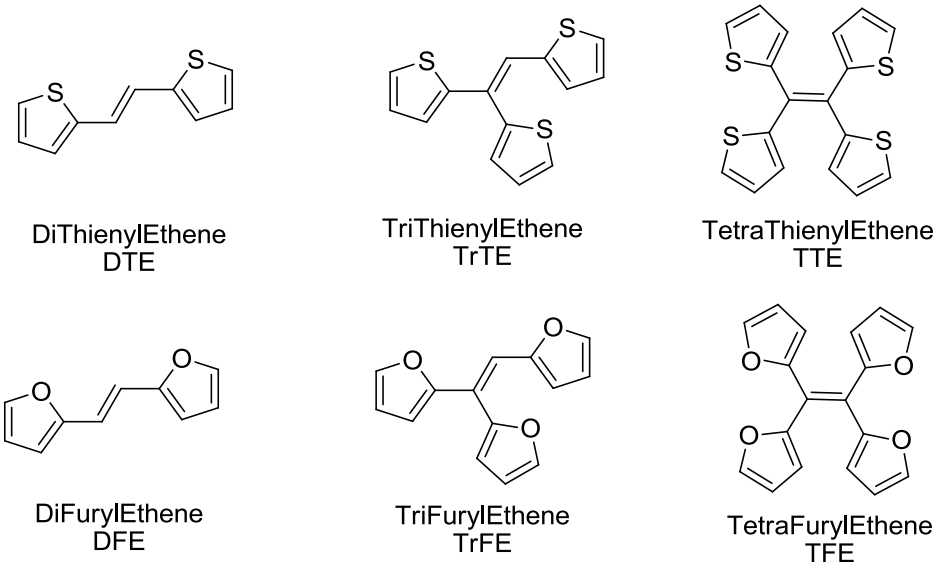

Chart 2.1 Molecular structures of the investigated HeteroArylEthenes.

The study includes as a benchmark the analogous phenyl-based series (chart 2.2), which was already well known concerning the synthesis the photophysical properties and the applications.

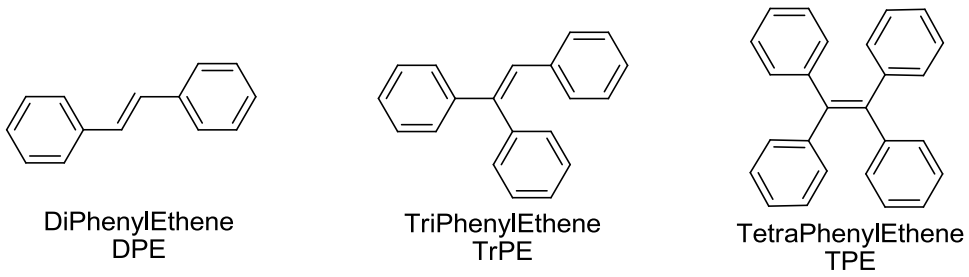

Chart 2.4 Molecular structure of the aryl aryl-substituted ethenes.

A very limited knowledge was so far available concerning the corresponding heteroaryl-based ethenes. Of the systems in Chart 2.1, TFE and TrTE are entirely new compounds and have been never investigated before; the other structures had already been reported in literature [1] but only obtained by McMurry coupling, while in this work we have proposed a convenient alternative approach (besides significantly improving the McMurry protocol). Moreover, a deep electrochemical and photophysical characterization was still lacking; as a consequence, the highly interesting electrochemical and photoluminescence properties remained concealed until the study performed in this PhD research work.

2.1.2 Why the HeteroArylEthenes ?

Our interest for this molecule class arose from the promising results obtained with one of its terms, TetraThienylEthene TTE (Chart 2.1). In 2009, looking for an efficient π-conjugated scaffold to be

employed in organic photovoltaics, we focused our attention on TTE because attracted by its molecular structure, constituted of four thiophene rings linked to a central double bond. According to our previous experience concerning thiophene-based systems for advanced applications, we expected the TTE structure to have a high π-conjugated efficiency; thus we performed a detailed pioneer study on this molecule in terms of both synthesis and characterization of electronic properties. The emerged results prompted us to extend our investigation to the lower terms of the series (DTE and TrTE) and to the analogous heteroarylethene series with furanyl substituents instead of thienyl ones.

2.1.2.1 TTE a promising molecule born in 1992

TTE has been conceived for the first time in 1992 in Japan [2] by Dr. Takanori Suzuki, who synthesized it in order to get an efficient electron-donor species. The synthetic procedure, a McMurry coupling, is reported in Scheme 2.1.

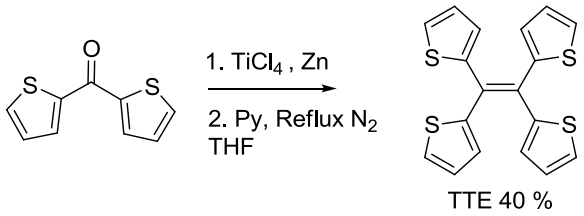

Scheme 2.1 McMurry coupling on the DiThienylKetone to synthesize TTE.

He also synthesized some of its derivatives, functionalizing the basic backbone on the α-position with methyl and thiomethyl groups, and studying their electron donating effect on the redox properties of the parent molecule. Scheme 2.2.

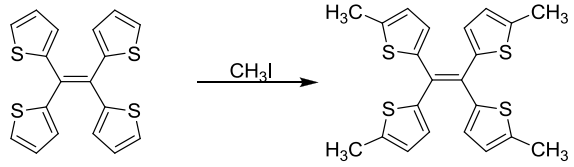

(a)

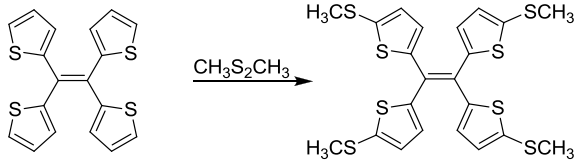

(b)

Scheme 2.2 Synthesis of (a) Methyl and (b) Thiomethyl-TTE performed by Dr. Suzuki.

No other electrochemical or physico-chemical property has been investigated for TTE or for its derivatives. Even from the synthetic point of view, no other pathways have been investigated. Despite the great potentialities of TTE, it has been slowly forgot over the years; only a few other groups have focused their attention on this scaffold,[3] synthesizing it by McMurry coupling (the only known way) and using it just as a building block to construct other systems.

In particular TTE has been used in 1996 in Professor Harrit's group in Denmark, [3a] who employed this molecule as a substrate for a photocyclization reaction, thus obtaining semi- and fully-locked structures as shown in Scheme 2.3.

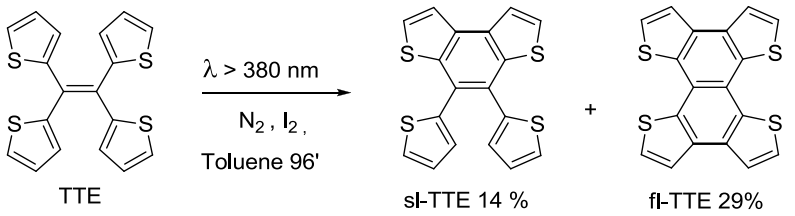

Scheme 2.3 Photoreaction perfomed on TTE in Prof. Harrit's laboratories

In 2007 [3b] Hakon Hope *et al*. synthesized the structures showed in Chart 2.2, similar but not equal to the TTE backbone, by using the McMurry coupling on the relative ketones, and rationalizing the electronic properties of the obtained molecules, by cyclic voltammetry and UV-vis spectroscopy; they got the crystal structure as well.

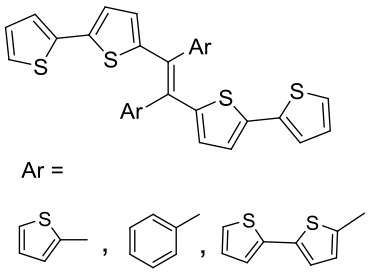

Chart 2.2 Molecular structure of some Aryl-substituted olefins

In 2013 the group of Professor Wang [3c], starting from a dithienylketone functionalized on its alpha positions with TriMethylSilane TMS groups, synthesized the derivative TTE$(TMS)_4$ coded 4T in Figure 2.1, by McMurry coupling. This scaffold have been subsequently used to get dendrimeric species containing up to 16 and 20 Thiophene rings, as shown in Figure 2.1. [3c]

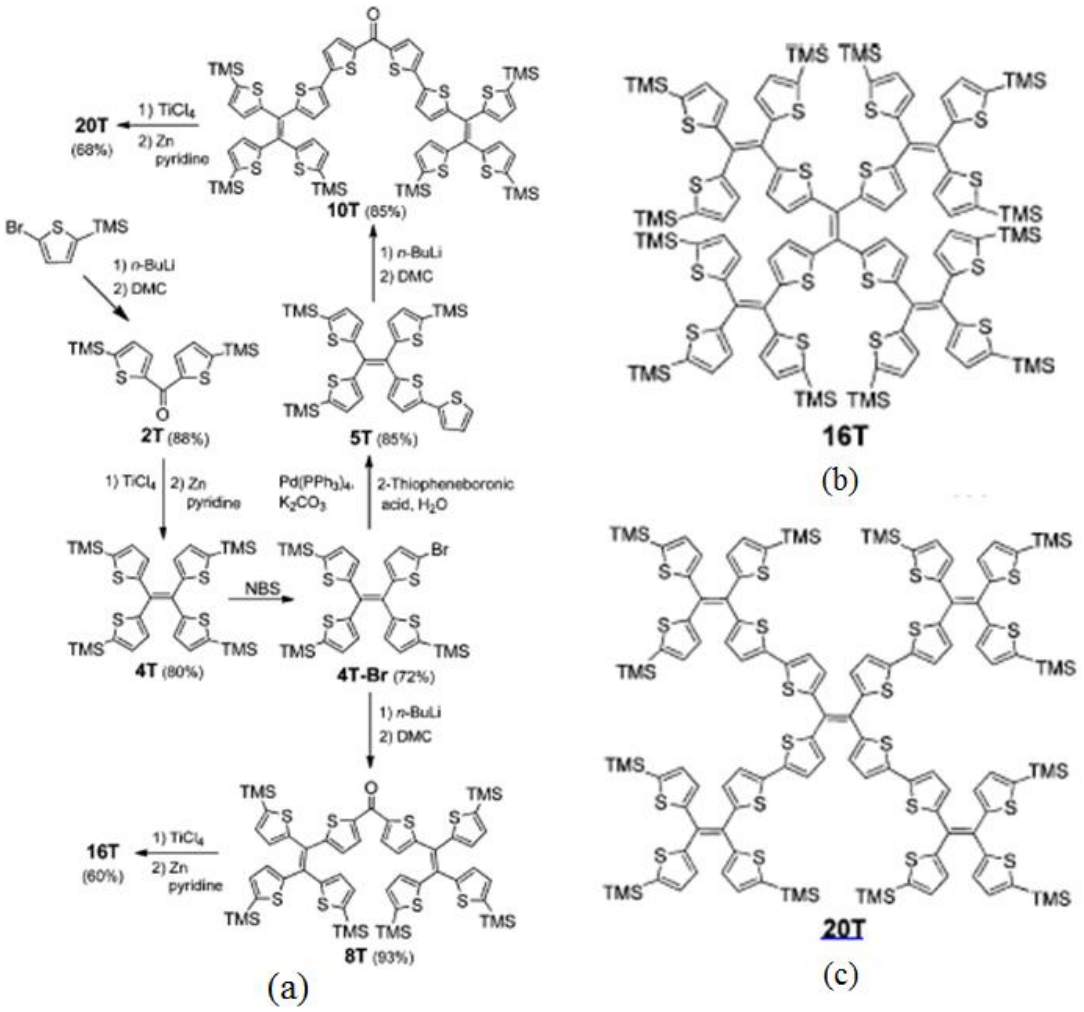

Figure 2.1 [3c] (a) synthetic strategy leading to 16T (b) and 20T (c) dendrimers, starting from TTE functionalized by TMS groups, here defined 4T derivative.

The examples just described are the only ones in which TTE has been employed since its introduction in 1992. No deep physico-chemical and synthetical investigations have been ever done over 17 years (1992 – 2009).

2.1.2.2 Our pioneering study on TTE

2.1.2.2.1 Electrochemical and Optical properties

Exploring the literature, very few information [1-3] was available about the electronic properties of the TTE scaffold. Even if, for example, the oxidation potential had already been investigated [2] no information was available about the reduction process, the optical properties and the related experimental energy gap. Thus, before undertaking a synthetic study in order to develop an alternative, more convenient pathway, we investigated the electrochemical and optical properties of TTE, comparing its features with those of two other thiophene-based scaffolds, that is *angular* and *linear* benzodithiophene (*ang*-BDT and *lin*-BDT), which had been favourite building blocks in our group for many years (Chart 2.3)

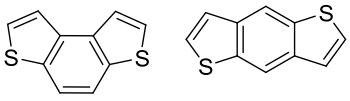

ang-BDT *lin*-BDT

Chart 2.3 Molecular structure of angular and linear benzodithiophene.

Comparing the electrochemical properties of TTE with those of *ang*- and *lin*- BDT, TTE resulted to be, as expected, the most conjugated structure.

In Figure 2.2 cyclic voltammetry characteristics are reported for the three scaffolds, performed in ACN as solvent. The BDT isomers have similar CV patterns but first oxidation and first reduction (both chemically irreversible) take place at milder potentials for linear BDT respect to the angular one. TTE, due to the presence in the same structure of four thiophene rings and the double bond, has a lower energy gap in respect to BDT systems, thus resulting the most efficient π-conjugated molecule.

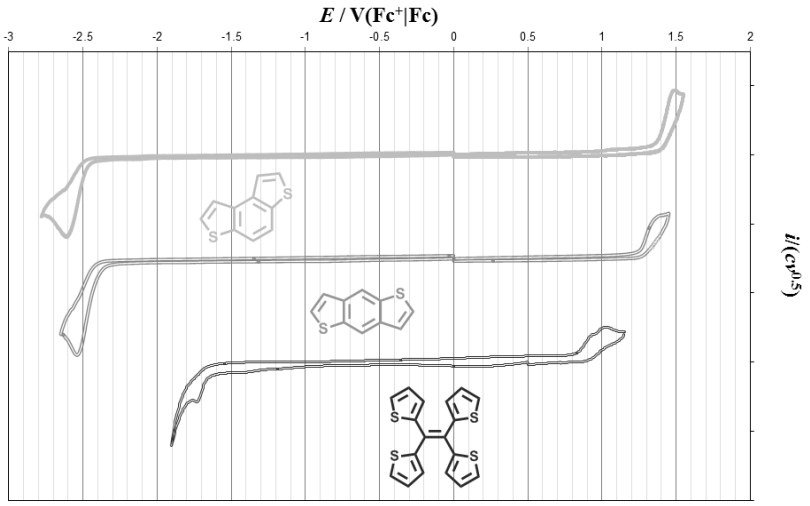

Figure 2.2 Cyclic Voltammetry of the *ang*-BDT in orange, *lin*-BDT in green, and TTE in red.

The optical data confirmed the electrochemical evidences. TTE has significantly higher effective conjugation, as it is possible to observe from the spectra comparison reported in Figure 2.3.

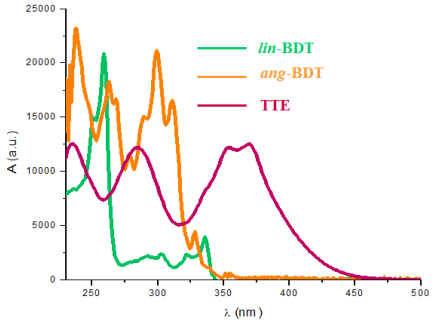

Figure 2.3 Absorption spectra of the *ang*-BDT in orange, *lin*-BDT in green, and TTE in red.

	Optical Data		***Electrochemical Data***	
spacer	E_g **(onset) /eV**	E_g **(max) /eV**	E_g **(onset) /eV**	E_g **(max) /eV**
lin-BDT	3.57[ii]	3.70[ii]	3.62[iii]	3.94[iii]
ang-BDT	3.84[ii]	3.90[ii]	3.79[iii]	4.10[iii]
TTE	2.79[ii]	3.21[ii]	2.53[iv]	2.68[iv]

[ii] CH_2Cl_2 ,[iii] ACN+0.1 M TBAP, [iv] ACN +0.1M $TBAPF_6$

Thus TTE revealed to be an even more promising thiophene-based scaffold than BDT isomers. In this context we also investigated by cyclic voltammetry the electropolymerization ability of TTE. Cycling around its first oxidation peak, it is possible to obtain an oligomeric film; the latter has electrochromic properties, evidenced employing an ITO as working electrode.

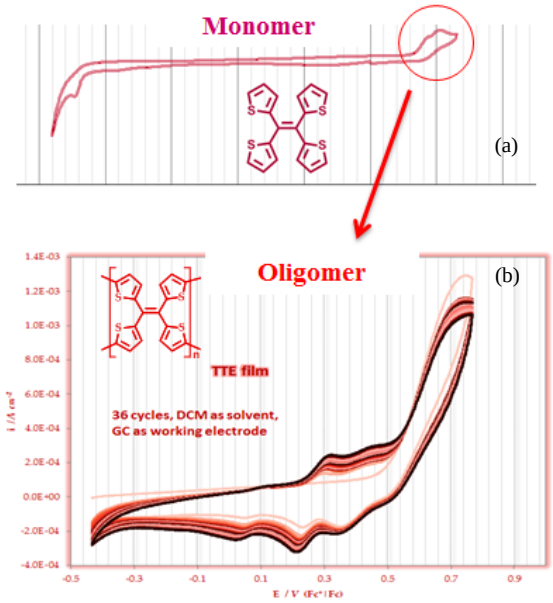

Figure 2.4 Cylcic Voltammetry of (a) TTE and (b) its oligomeric film.

2.1.2.2.2 New Synthetic Procedure and TTE derivatives

Although the McMurry coupling is a convenient method to get TTE because *(i)* it is an economic one-step synthesis which requires an easy achievable starting material,[4] *(ii)* it has a low reaction time, and *(iii)* the reaction product is easy to purify, it is unfortunately unsuitable for the synthesis of non-symmetrically substituted olefins because the coupling between two different carbonyl-based compounds would lead to a mixture of products. In addition some functional groups such as formyl or halogen one, are not compatible with the McMurry reaction conditions.

Considering the limits of the McMurry coupling, we first investigated another synthetic pathway which would allow to get both TTE in higher yield, and its derivatives regio-selectively functionalized. This method, reported in our feature paper, [5] is shown in Scheme 2.4 and it is widely described in the dedicated chapter.

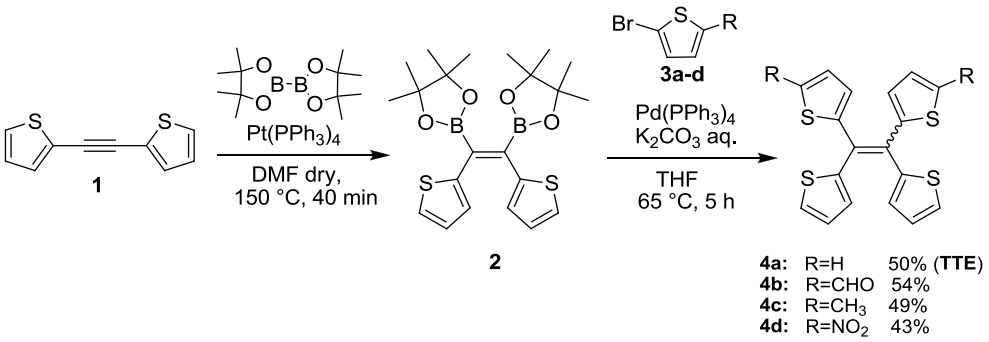

Scheme 2.4 Synthetic strategy for TTE and some of its derivatives

We also investigated the reactivity of TTE in electrophilic conditions according to the reaction shown in Scheme 2.5, which allowed us to obtain the derivatives 5.

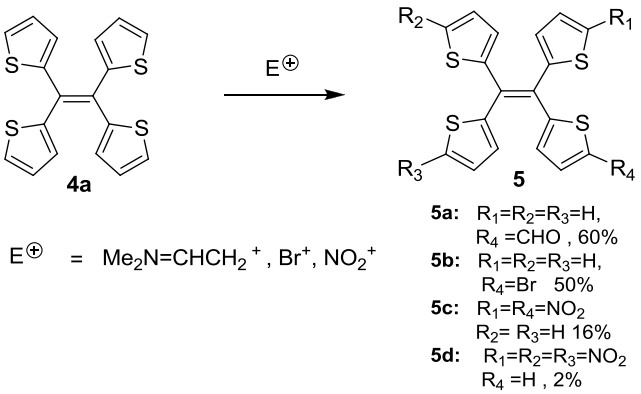

Scheme 2.5 Synthetic strategy to synthesized TTE and some of its derivatives

The electronic properties of all of these derivatives (4 and 5) have been investigated by cyclic voltammetry, by which we achieved a satisfactory rationalization of the structure *vs* electronic properties relationship, including localization of the redox centers and justification of the observed trends in HOMO and LUMO levels and gaps as a function of the substituents. The solvent effect has been investigated as well, comparing Acetonitrile and DiChloroMethane as working solvents.

2.1.2.2.3 TTE and AIE: a shiny encounter

A preliminary photophysic investigations have been also performed, and it was in this framework that we discovered the ability of TTE to be luminescent in solid state but not in solution, Figure 2.5. This observation let us consider TTE as a possible pure AIEgen (AIE luminogen); indeed it can be regarded as the thienyl counter-part of TetraPhenylEthene TPE (AIEgen par excellence) Chart 2.4, since it features four thiophene rings in place of the four phenyl ones.

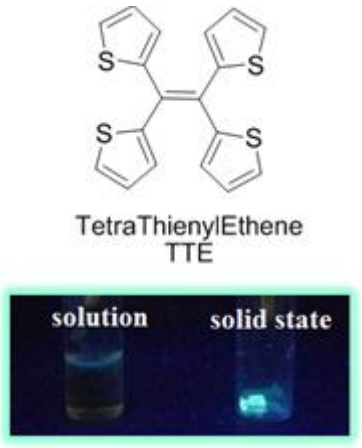

Figura 2.5 Luminescent behaviour of TTE in solution and solid state upon UV-vis light absorption.

2.1.2.2.4 Goals of the research

Heterocycle-based systems containing a double bond as spacer unit have not been sistematically investigated so far.

In the present research, considering the excellent properties of efficient π-conjugation emission, electropolymerization ability and solid state luminescence found out for TTE in our mentioned preliminary study, we have decided to perform a complete study of heteroarylethenes, extending both to the lower members of the series, DiThienylEthene DTE, and TriThienylEthene TrTE, and to the analogous furane-based series thus synthesizing the heteroaryl family molecules shown in Chart 2.1.

This prompted us both to optimize the literature McMurry synthetic protocol and to develop an alternative one, too, based on the Suzuki coupling reaction.

Besides performing a detailed electrochemical investigation of the synthesized family members in terms of redox properties and electrooligomerization ability, we particularly concentrated on their photophysical investigation in terms of Aggregation-Induced Emission features. The latter has been performed in a seven-month stage at the Hong Kong University of Science and Technology, in the laboratories of Professor Ben Zhong Tang, the discoverer of the AIE phenomenon. The results obtained are of high interest and applicative potential, and a patent is being deposited concerning a possible biotechnological application.

Thus systematic study performed in this thesis now provides a deep knowledge about the heteroarylethene properties which can allow to properly design more complex systems in which these scaffold could be used as starting block. In addition, their unique property of emitting light in solid but not in solution, renders them even more appealing, as small single molecule to be employed in hi-tech applications.

Bibliography Chapter 2

[1] (a) E. Castagnino, *Tetrahedron Lett*. **1985**, *26*, 6399; (b) G. Karminski-Zamola et al, *Heteroatom Chemistry*, **2003**, *14*, 218; (c) J. Roncali et al, *Journal of Materials Chemistry*, **1996**, *6*, 1859;
[2] T. Suzuki, H. Shiohara, M. Monobe *et al*., *Angew. Chem.*, **1992**, *104*, 454. *Angew. Chem. Int. Ed. Engl.*, **1992**, *31*, 455;
[3] (a) E. Fischer, J. Larsen, J. B. Christensen, M. Formigue, H. G. Madsen, N. Harrit, *J. Org. Chem.*, **1996**, *61*, 6997; (b) H. Halvorsen, J. Skramstad, H. Hope, *Synth. Commun*., **2007**, *37*, 1179; (c) T. Wu, J. Shi, C. Li, J. Song, L. Xu, H. Wang, *Org. Lett.*, **2013**, *15*, 354;
[4] dtih ket
[5] A. Bolzoni, L. Viglianti, P.R. Mussini, C. Baldoli, E. Licandro *et al*, *Eur. JOC.*, **2013**, *33*, 7489.

3

Synthesis of HeteroArylEthenes

The molecules synthesized in this research work are mainly poly-substituted ethenes. For our purpose they can be conveniently divided into three classes according to the number of heterocycles linked to the central double bond (Chart 3.1):

1) Disubstituted ethenes
2) Trisubstituted ethenes
3) Tetrasubstituted ethenes

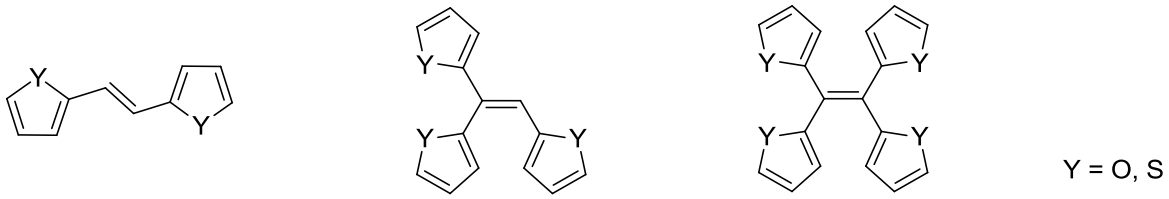

Chart 3.1

Stereocontrolled synthesis of olefins is one of the most challenging issues for organic chemists[1,2]. Indeed, even if all molecules have an ethylene backbone they cannot be always conveniently synthesized by well known, traditional synthetic procedures like Wittig, Horner-Wadsworth-Emmons or Peterson olefination[3,4,5]. Indeed the outlook here below suggests that the synthesis would not be so easy as well as the preparation of the reagents involved.

Wittig reaction[3,6-14] is the reaction of a phosphorus ylide with an aldehyde or ketone. As first described in 1953 by Wittig and Geissler[3] (Scheme 3.1), is probably the most widely recognized method for carbonyl olefination. This reaction occurs with total positional selectivity (that is, an alkene always directly replaces a carbonyl group). By comparison, a number of other carbonyl olefination reactions often occur with double-bond rearrangement. Factors that influence *E*- and *Z*-stereoselectivity are well understood and in some cases can be controlled through careful selection of the phosphorus reagent and reaction conditions. Nevertheless mixtures of *E*/*Z* isomers are often obtained with this procedure.

The stereoselectivity of the Wittig reaction is directly linked to this mechanism (Scheme 3.1).

In particular, the reaction of a carbonyl compound with an ylide produces both the cis and trans oxaphosphetanes, which undergo stereospecific syn-elimination to give the corresponding *E*- and *Z*-alkenes, respectively. The *Z*-alkene tends to predominate under kinetic conditions, indicating an intrinsic preference for the *cis*-oxaphosphetane, a preference that as yet is not fully understood. However, under thermodynamic conditions, equilibration of the two oxaphosphetanes with reactants allows predominant formation of the more stable *trans*-oxaphosphetane and hence the *E*-alkene.

A wide variety of phosphorus reagents are known to participate in Wittig reactions and the exact nature of these species is commonly used to divide the Wittig reaction into three main groups, namely the ‘‘classic’’ Wittig reaction of phosphonium ylides, the Horner–Wadsworth–Emmons reaction of phosphonate anions, and the Horner–Wittig reaction of phosphine oxide anions.

Each of these reaction types has its own distinct advantages and limitations, and these must be taken into account when selecting the appropriate method for a desired synthesis. However ylides and

phosponate normally are not commercially available. Moreover the synthesis of the halogenated compound (R_2CHX) requires additional synthetic steps and, especially for those leading to tetrasubstituted ethenes, is rather tricky. Analogous problem are encountered when Peterson[15-18] olefination is used.

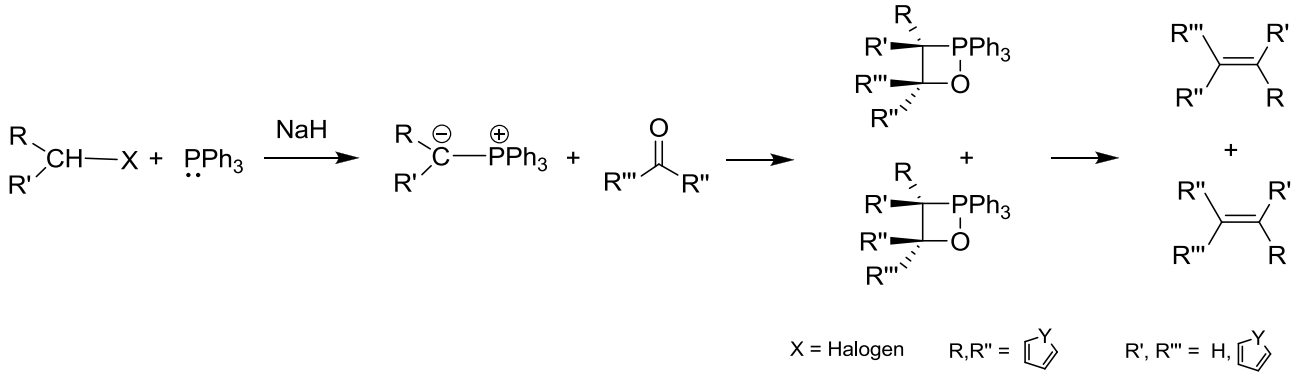

Scheme 3.1

So we faced the problem to find a straightforward methodology to synthesize the desired ethenes, requiring basic chemicals and few steps. We experienced that, depending on the class of molecules to be synthesized (i.e. according to the number of heterocycles linked to the double bond), a dedicated synthetic pathway was needed in order to get a well-defined product with a good yield.
Here below the synthetic strategies adopted in this work are discussed.

3.1 Mc Murry's coupling for disubstituted ethylenes

The synthesis of disubstituted ethenes was easily achieved by Mc Murry's coupling[19-24] (Scheme 3.2).

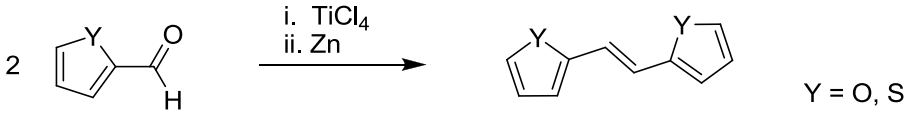

Scheme 3.2

This procedures is a one-step reaction involving cheap organic reagents and reactants. It is a reductive coupling (Scheme 3.3a) in which a low valence specie Ti(0), generated *in situ*, interacts with the oxygen atoms of the carbonyl compound affording an intermediate having a pinacolate structure. Finally TiO_2 is extruded affording the substituted olefin; a mixture of *E*/*Z* isomer is obtained. However due to steric hindrance the *E* isomer is by far the preferred one when disubstituted ethenes are to be obtained (up to 96% *E* isomer). So we decided this procedure to be the preferred one for the synthesis of *E*-diheteroaryl ethenes[24]: it is fast (since aldehydes are more reactive than ketones), cheap and affords selectively *E* isomers (which have better π-conjugation efficiency, optical and electronic properties). We also tried to extend this method to the synthesis of tri- and tetrasubstituted ethenes, since examples with heterocycles were already reported in literature[25-28].

In the latter case we performed a homocoupling between two molecules of the same ketone (Scheme 3.3a), in order to have no any problem of *E*/*Z* isomers formation and purifications. Of course no problems of regioselectivity are encounter also when two different ketones having each same substituents are coupled (Scheme 3.3b). However in this case, which is an example of Mc Murry cross coupling[29-32], not only the desired cross coupling product, but also the products coming from the homocoupling are obtained. Undesired consequences are lower reaction yields, several purification steps and increased costs.

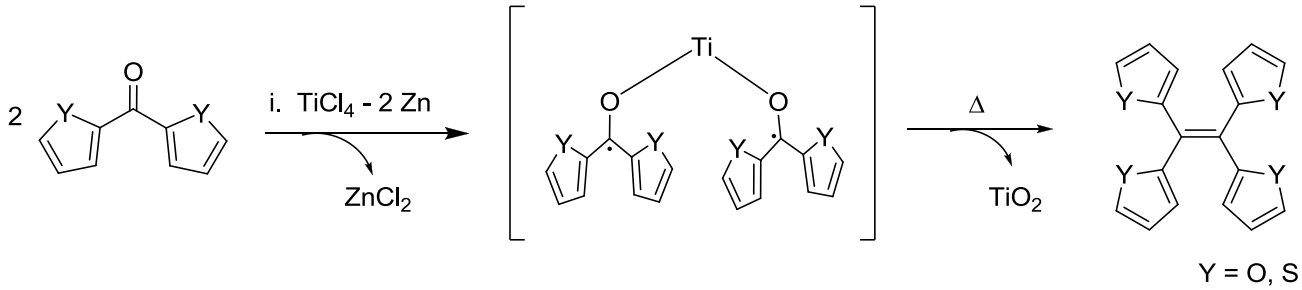

Scheme 3.3a Example of Mc Murry's homocoupling

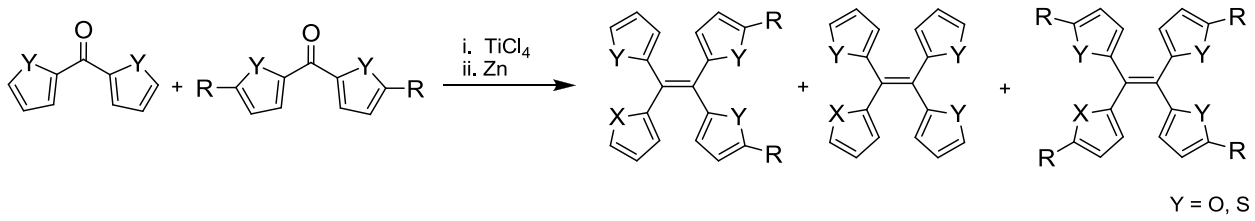

Scheme 3.3b. Example of Mc Murry's cross-coupling

At the end Mc Murry's coupling was employed for the synthesis of tetraheteroaryl ethenes only when a homocoupling was involved (though for dithiophene based ketones reaction yield are low). For the synthesis of tetrasubstituted ethenes a specific synthetic procedure was planned (see Section 3.3).

As mentioned before, we also performed a cross coupling between an aldehyde and a ketone (Scheme 3.4) in order to obtain a trisubstituted ethene. As expected also homocoupling byproducts were formed suggesting to look for more selective procedures.

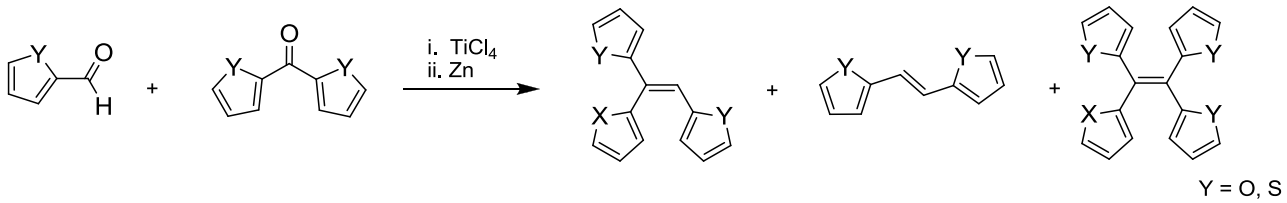

Scheme 3.4

3.2 Desei-Mc Kelvie reaction, a way to trisubstituted ethylenes

Looking for a specific synthetic process to obtain tri- and tetrasubstituted ethenes, we encountered Corey-Fuchs[33-35] type reactions.

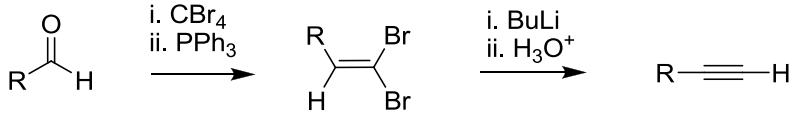

Scheme 3.5 Corey-Fuchs reaction

However our idea was to exploit the first step of this procedure (Desei, Mc Kelvie and Rodriguez reaction[36]) and react the dibromo alkene, according to traditional Suzuki coupling, to get the desired product (Scheme 3.6). This pathway was also reported by Professor Atsunori Mori and coworkers[37].

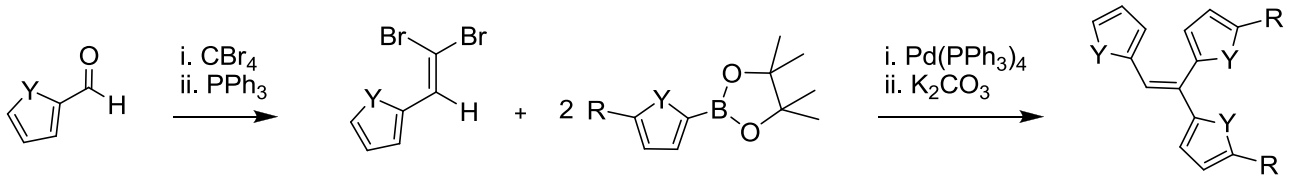

Scheme 3.6

Our procedure involves two reaction steps:

(a) Desei, Mc Kelvie and Rodriguez reaction[36]

This reaction involves the formation of a ylide (Scheme 3.7) by the use of a mole of tetrabromomethane and two moles of triphenylphosphine.

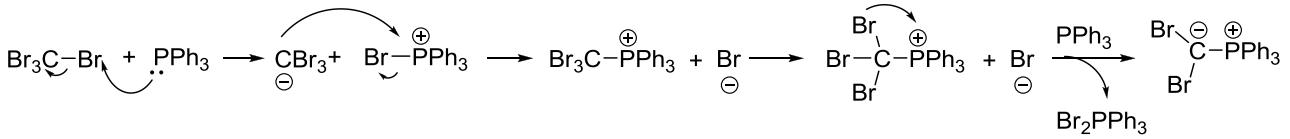

Scheme 3.7.

Then the ylide attacks the carbonyl compound with the same mechanism of the Wittig reaction (Scheme 3.8) affording the desired dibromoalkene.

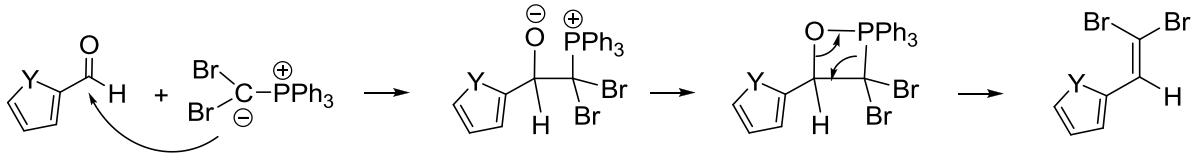

Scheme 3.8

(b) Suzuki coupling

Suzuki coupling is a reaction that allow C-C bond formation by means of the interaction between an aromatic boronic acid (or ester) and a conjugated bromide. The mechanism, shown in Scheme 3.9, proceeds by oxidative insertion of the Palladium catalyst to the halogenated aromatic/heteroaromatic compound (slow reaction steps). Halogenated molecules bearing electronwithdrowing groups favour palladium insertion since their attitude to be reduced increases.

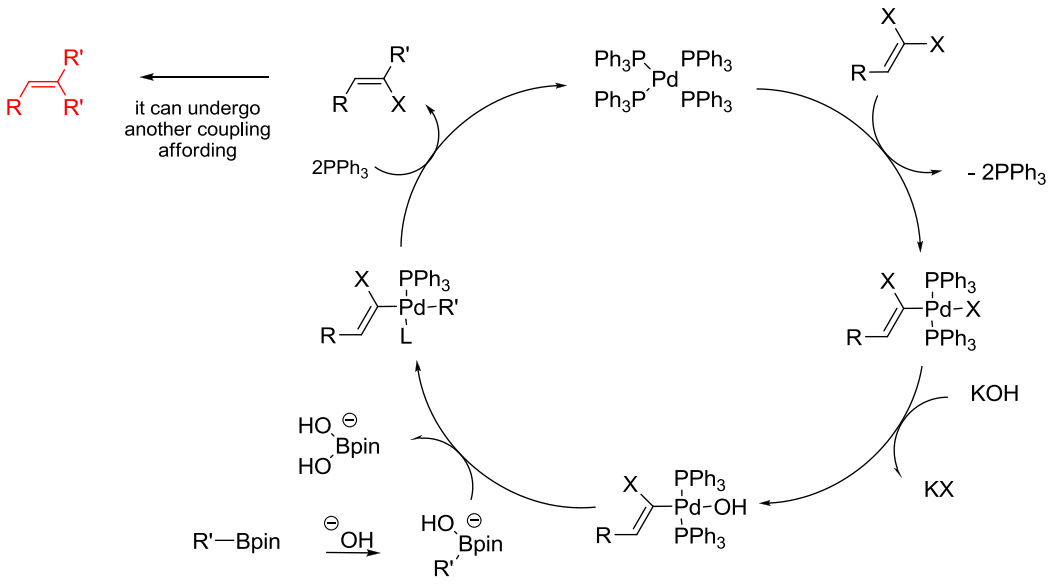

Scheme 3.9

Another important role is played by the halogenated reagent, indeed the reaction rate increases with increasing electronegativity of the halogen atom: Cl > Br > I. In the meantime activation of the boron compound by means of a base take place. Activated boronic reagent reacts with the Palladium specie by transametallation: the OH group is transferred from the soft Palladium to the hard Boron atom. Finally reductive elimination of Palladium affords the coupling product. In our case the product of the first catalytic cycle is at the same time the halo-reagent for the second catalytic cycle so that a triheteroaryl ethene is obtained.

According to Prof. Mori[36] it is also possible to synthesize selectively *E*/*Z* isomers. Indeed, using limited amount of base and one equivalent of boronic reagent, it is possible to substitute only one of the two bromine atoms and selectively the one in *trans*- position (Scheme 3.10).

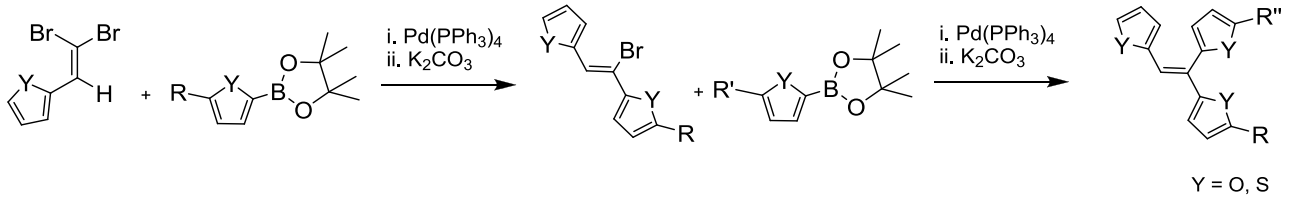

Scheme 3.10

The whole procedure is very versatile and regioselective, allowing the synthesis of a wide range of different trisubstituted ethenes.

3.3 Suzuki-Miyaura coupling[38-42], a possible solution for tetrasubstituted ethylenes

The synthesis of tetrasubstituted ethenes is one of the most challenging field in organic synthesis. Indeed not only reaction yield, but also regioselectivity, steric hindrance, byproducts, purification steps must be taken in account. Phosphorus-based olefination reactions are generally not amenable to the formation of tetrasubstituted olefins, as the ylides do not react well in sterically demanding environments.
When tetrasubstituted olefins are formed, mixtures of stereoisomers are obtained unless the starting materials are symmetrically substituted. Reports in recent years still illustrate the difficulty of preparing tetrasubstituted olefins by the Wittig reaction. [43]
As stated in Section 3.1, Mc Murry's coupling was adopted only when homocoupling was the way to the desired product. Moreover this reaction involves the use of Lewis acid ($TiCl_4$) that can promote the formation of undesired, polymeric byproducts with the substrates of our interest[44,45].
So, despite the cost of the synthesis, we researched for a highly versatile strategy in order to cover the widest range of possible products, maintaining at the same time the control over the product geometry.
In this research work a new synthetic pathway for tetraheteroaryl-ethenes was developed, previous articles refer to Mc Murry's coupling as the most viable way. Our strategy consist of a two-step procedure (Scheme 3.11), that involves a Suzuki-Miyaura diboration of alkynes[46] followed by a traditional Suzuki coupling.

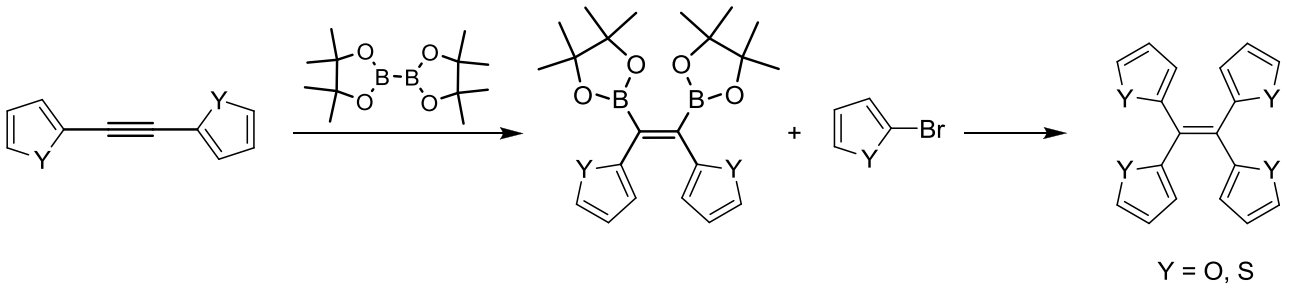

Scheme 3.11

(a) Suzuki-Miyaura diboration of alkynes

The use of boron for the carbometallation of alkynes is the first step of our synthetic pathway. It offers remarkable advantages in term of reactivity since the resulting vinyl borane is very reactive towards Palladium mediated couplings. The loss of the stereochemical information is less frequent with this kind of reaction since the diboration proceeds leading only to the *Z* isomer. One of the very first papers[46] regarding this synthetic methodology describes the diboration of aliphatic alkynes with bis-pinacolato diboron with Platinum tetrakis(triphenilphospine) to afford the corresponding *Z*-alkene (Scheme 3.12).

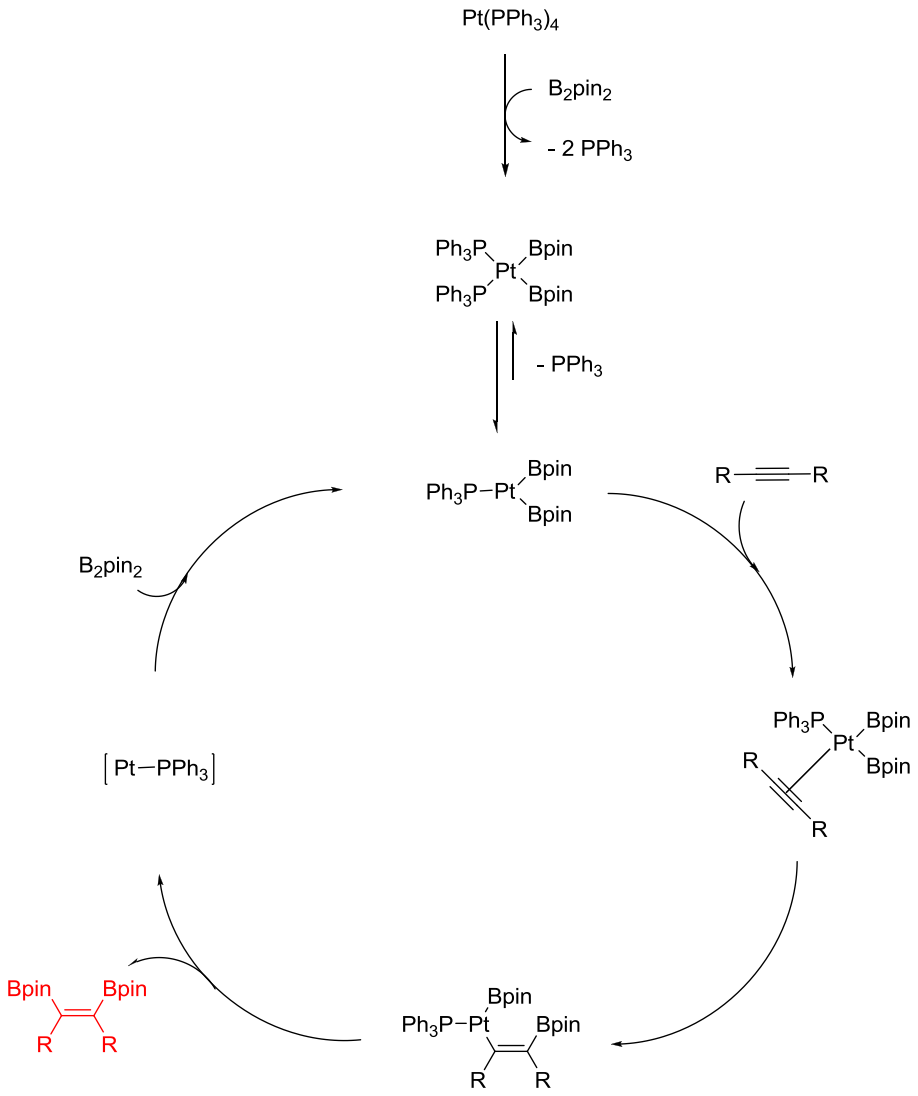

Scheme 3.12

The reaction proceeds through the *sin*-addition of the B-B bond to the alkyne triple bond. This is possible thanks to oxidative addition of the Platinum (0) complex that produces the specie bis(boryl)platinum (II). The alkyne inserts between boron and palladium with formation of a carbon-boron bond and the contemporary formation of a carbon-platinum bond on the same side. Finally the reductive elimination of platinum leads the second boronic specie onto the double bond providing the *cis*-bis(boryl)alkene.

(b) Suzuki coupling

The mechanism of Suzuki coupling is explained in Section 3.2. In this procedure (Scheme 3.11) the two boronic groups linked to the double bond are reacted with halo-heterocycles and so replaced by them. It means that selectively *cis*-addition happens through this mechanism allowing to know the exact geometry of the molecule.

Through this pathway we also synthesized some tetrasubstituted-ethenes already obtained by Mc Murry's homocoupling. We were able to get the same reaction yield of Mc Murry's coupling even

with a two-step procedure, but gaining the control over the regiochemistry. Another interesting advantage of this strategy is that it allows to employ Heterocycles bearing carbonyl groups (*see* Experimental Section) which is not possible with Mc Murry coupling. Moreover no olygomerization byproducts induced by Lewis acids are formed.

3.4 Photochemical cyclization of polysubstituded alkenes

Stilbenes can be converted to phenanthrenes by irradiation with UV light[47-50] in the presence of an oxidizing agent such as dissolved molecular oxygen, $FeCI_3$, Pd-C[51], or iodine[52]. The reaction is a photochemically allowed conrotatory[53] conversion of a 1,3,5-hexatriene to a cyclohexadiene, followed by removal of two hydrogen atoms by the oxidizing agent. The intermediate dihydrophenanthrene has been isolated[54] (Scheme 3.13). The actual reacting species must be the *cis*-stilbene like molecules, but *trans*-stilbenes one can often be used, because they undergoes isomerisation to the *cis* isomers under the reaction conditions. The isomerisation takes place because the excited states, both S_1 and T_1, of many olefins have a perpendicular instead of a planar geometry, so *cis-trans* isomerism disappears upon excitation. When the excited molecule drops back to the S_0 state, either isomer can be formed (Scheme 3.13).

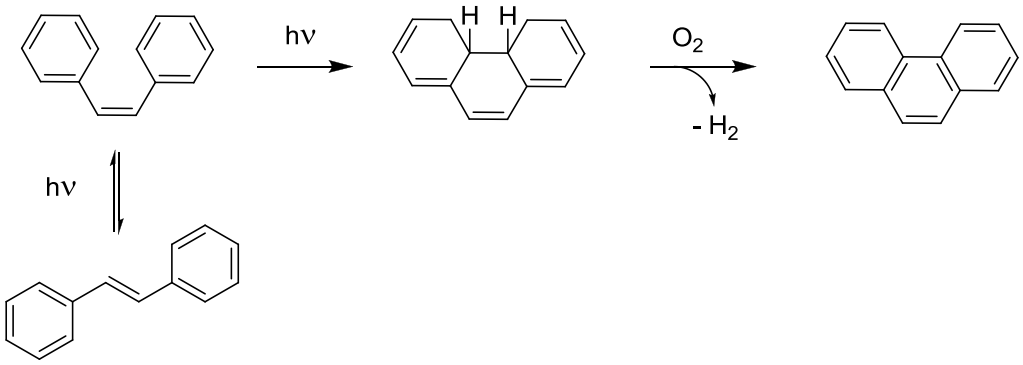

Scheme 3.13

The use of substrates containing hetero atoms (Scheme 14a) allows the formation of heterocyclic ring systems. Photocyclisation reactions can be extended to the preparation of many fused aromatic or heteroaromatic systems (Scheme 14b). An extensive investigation of this kind of reaction has been reviewed by Katz and coworkers[55,56], especially for the use of iodine as the oxidant.

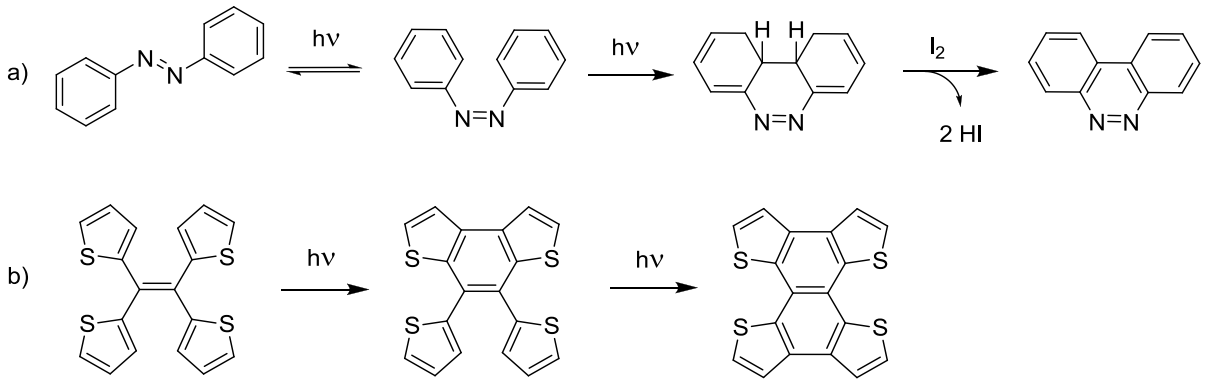

Scheme 3.14

In Scheme 3.15 are depicted the main parallel processes which could occur during the photocyclisation together with the radical processes that could also occur.

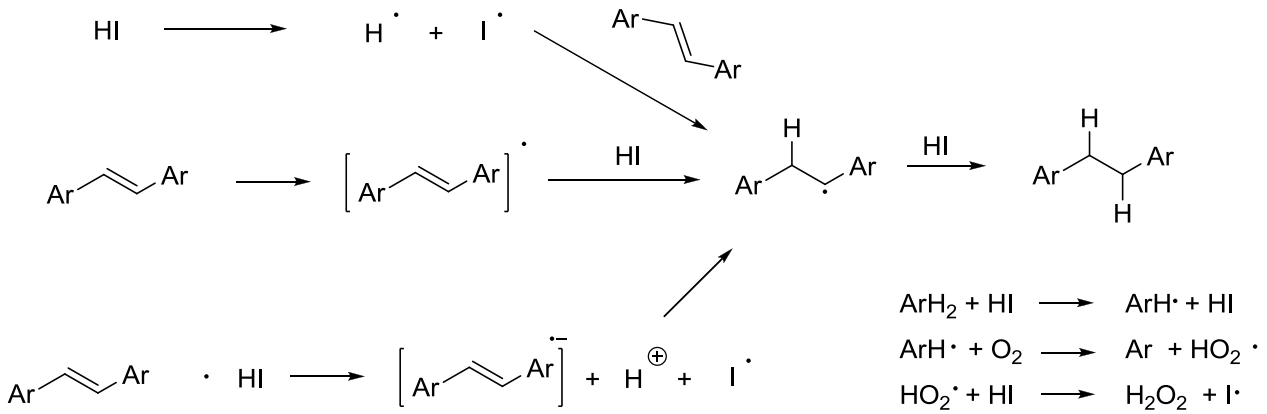

Scheme 3.15

Bibliography Chapter 3

[1] A. B. Flynn, W. W. Olgivie, *Chem. Rev.*, **2007**, 107, 4698-4745
[2] J. Gerard, L. Hevesi, *Tetrahedron*, **2001**, 107, 9109-9121
[3] G. Wittig and G. Geissler, *Justus Liebigs Annalen der Chemie*, **1953**, 580 *(1)*, 44–57
[14] Horner L., Hoffmann H., Wippel, H.G., *Chemische Berichte* , **1958**, 91, 61-63
[5] G. Wittig, W. Haag, *Chemische Berichte*, **1955**, 88 *(11)*, 1654–1666
[6] Maercker, *A. Org. React.*, **1965**, 14, 270–490
[7] W. Carruthers, *Some Modern Methods of Organic Synthesis*, Cambridge University Press, Cambridge, UK, **1971**, 81–90.
[8] R. W. Hoffmann, *Angew. Chem. Int. Ed.*, **2001**, 40 *(8)*, 1411–1416
[9] E. Vedejs and C. F. Marth, *J. Am. Chem. Soc.*, **1990**, 112 *(10)*, 3905–3909
[10] B. E. Maryanoff, A. B. Reitz, M. S. Mutter, R. R. Inners, and H. R. Almond, Jr., *J. Am. Chem. Soc.*, **1985**, 107, 1068–1070
[11] B. E. Maryanoff, A. B. Reitz, D. W. Graden, and H. R. Almond, Jr., *Tetrahedron Lett.*, **1989**, 30, 1361–1364
[12] B. E. Maryanoff, A. B. Reitz, M. S. Mutter, R. R. Inners, H. R. Almond, Jr., R. R. Whittle, and R. A. Olofson, *J. Am. Chem. Soc.*,**1986**, 108, 7664–7678
[13] E. Vedejs and C. F. Marth, *J. Am. Chem. Soc.*, **1988**, 110 *(12)*
[4] G.Wittig, U. Schöllkopf, *Chemische Berichte*, **1954**, 87 *(9)*, 1318
[15] D. J. Peterson, *J. Org. Chem*, **1968**, 33 *(2)*, 780–784
[16] Birkofer L., Stiehl O., *Top. Curr. Chem.*, **1980**, 88, 58
[17] Ager D. J., *Synthesis*, **1984**, 384–398
[18] Ager D.J., *Org. React.*, **1990**, 38, 1
[19] J. E. McMurry, M. P. Fleming, *J. Am. Chem. Soc.*, **1974**, 96 *(14)*, 4708–4709
[20] J. E. McMurry, *Accounts of Chemical Research*, **1974**, 7 *(9)*, 281-286
[21] M. Ephritikhine, *Chem. Commun.*, **1998**, 2549–2554.
[22] B. A. Furstner, B. Bogdanovic, Angew. Chem. Int. Ed., **1996**, 35, 2442.
[23] B. A. Furstner, *Transition Metals for Organic Synthesis*, **1998**, 1, 381-401
[24] J. E. McMurry, *Chem. Rev.*, **1989**, 89, 1513-1524
[25] T. Suzuki, et al., *Angew. Chem . Int. Ed. Engl.*, **1992**, 31 *(4)*, 455-458
[26] E. Fischer et al., *J. Org. Chem.*, **1996**, 61, 6997-7005
[27] L.I. Belen'kii , et al., *Russian Chem. Bull. Int. Ed.*, **2005**, 5, 1208-1213
[28] H. Halvorsen, J. Skramstad, H. Hope, *Synthetic Communications*, **2007**, 37 *(7)*, 1179-1187
[29] X-F Duan, J. Zeng, J-W. Lu, Z-B Zhang, *J. Org. Chem.*, **2006**, 71 *(26)*, 9873-9876
[30] X-F Duan, J. Zeng, J-W. Lu, Z-B Zhang, *Synthesis*, **2007**, 5, 713–718
[31] X-F Duan, J. Zeng, J-W. Lu, Z-B Zhang, *J. Org. Chem.*, **2007**, 72 *(26)*, 10283-10286
[32] M. M. Krayushkin,M.A. Kalik, V.A. Migulin, *Russian Chemical Reviews*, **2009**, 78 *(4)*, 329-336
[33] Corey, E. J., Fuchs, P. L., *Tetrahedron Lett.*, **1972**, *13*, 3769–3772
[34] Mori, M., Tonogaki, K., Kinoshita, A. *Organic Syntheses*, **2005**, 81, 1
[35] Marshall, J. A., Yanik, M. M., Adams, N. D., Ellis, K. C., Chobanian, H. R., **2005**, *Organic Syntheses*, 81,157

[36] N. B. Desai, N. McKelvie, F. Ramirez, *JACS*, **1962**, 84, 1745-1747
[37] Mori, Arai, Miyaoku, Teruya, *Tetrahedron Letters*, 49, **2008**, 1000-1003
[38] N. Miyaura, K. Yamada, A. Suzuki, *Tetrahedron Letters*, **1979**, 20 *(36)*, 3437–3440
[39] N. Miyaura A. Suzuki, *Chem. Comm.*, **1979**, 19, 866–867
[40] N. Miyaura, A.Suzuki, *Chemical Reviews*, **1995**, 95 *(7)*, 2457–2483
[41] A. Suzuki, *Pure & Appl. Chem.*, **1991**, 63 *(3)*, 419–422
[42] Suzuki, A.; *J. Organomet. Chem.*, **1991**, 576, 147
[43] Ramazani, A.; Azizian, A.; Bandpey, M.; Noshiranzadeh, N., Phosphorus, Sulfur Silicon Relat. Elem., **2006**, 2731
[44] Feng, Q., et al., *Chem. Mater.*, **1997**, 9 *(3)*, 641-643
[45] Cai, T., et al., *Solar Energy Materials & Solar Cells*, **2010**, 94, 1275–1281
[46] T. Ishiyama, N. Matsuda, N. Miyaura, A. Suzuki, *J. Am. Chem. Soc.*, **1993**,115, 11018-11019
[47] Mallory,F.B., Mallory,C.W., *Org. React*. **1984**, *30*, 1-456
[48] Blackburn, Timmons, *Q. Rev.. Chem. Soc*. **1969**, *23*, 482-503
[49] Stermitz, *Org. Photochem*. **1967**, *1*, 247-282
[50] Laarhoven Org. Photochem. **1989**, *10*, 163-308
[51] Rawal, Jones, Cava, *Tetrahedron Lett*. **1985**, *26*, 2423
[52] Liu, Yang, Katz, Poindexter, *J. Org. Chem*. **1991**, *56*, 3769
[53] Cuppen, Laarhoven, *J. Am. Chem. Soc*. **1972**, *94*, 5914
[54] Doyle, Benson, Filipescu, *J. Am. Chem. Soc*. **1976**, *98*, 3262
[55] L. Liu, B. Yang, T. J. Katz, M. K. Poindexter *J. Org. Chem*. **1991**, *56*, 3769-3775
[56] A. A. Frimer, J. D. Kinder, W. J. Y. Meador, M. A. B. Meador, *J. Org. Chem*. **1995**, *60*, 1658-1664.

4
Electrochemistry

The redox properties and electrooligomerization ability of the Heteroarylethenes (shown in Chart 4.1) have been studied by cyclic voltammetry (CV) both in ACN and in DCM as solvent, on glassy carbon (GC) for the monomer characterization, and both on GC and on ITO (indium tin oxide transparent electrode) for the electrodeposition and characterization of oligomer films, to allow observation of electrochromic features. Tetrabutylammonium Hexafluorophosphate $TBAPF_6$ has been used as supporting electrolyte. All of the potentials have been referred to the standard reference redox couple $Fc^+|Fc$ whose energetics is supposed to be invariant with the solvent. This provides a normalization for the different junction potentials arising between the reference electrode solution and the different working media; it is thus possible to correctly compare the CV patterns obtained in the two media, evaluating possible solvent effects on the process.

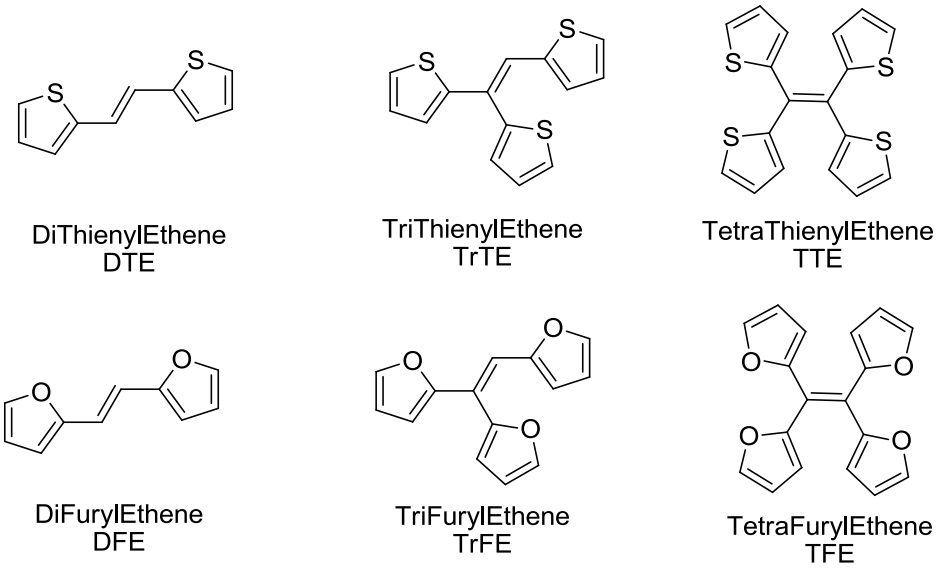

Chart 4.1 Molecular structure of the Heteroarylethenes

4.1 Cyclic Voltammetry of the Monomers

The CV features of the starting monomers are shown in Figures 4.1 (ACN) and 4.2 (DCM) sorted by kind of heterocycle, while Figure 4.3 provides a synopsis sorted by number of heterocyclic substituent rings. The CV patterns, recorded with compensation of the ohmic drop by the positive feedback method [1], consist of two half-cycles, one anodic and one cathodic, started at a potential where no electrode processes take place, in order to avoid modification of the signals of interest as a consequence of the presence of products of the opposite reaction.

The voltammograms were recorded at different scan rates, usually in a range from 0.05 V/s to 2 V/s (to achieve a comparative evaluation of chemical and electrochemical reversibility); Figures 4.1 to 4.3 report those obtained at 0.2 V/s. As the electron-transfer products tend to film the electrode surface it has been necessary to carry out a mechanical polishing procedure before each new recording.

The two chosen solvents significantly differ not only in polarity (ACN >> DCM) but also in the available potential window. In particular, DCM, being a dichloroalkane, undergoes electroreduction at a significantly less negative potential than ACN (*i.e.* -2.2 vs SCE), thus preventing the

observation of the first reduction peaks of the less conjugated molecules (*e.g.* di- and tri- substituted heteroarylethenes).

As it can be seen in the figures, nearly all of the first oxidation and reduction processes appear chemically irreversible at 0.2 V/s, pointing to an involvement of the radical-ion in a subsequent reaction process.
The values of both onset and peak potentials for first oxidations and first reductions are collected in Table 1. From them it is also possible to estimate the HOMO and LUMO values as well as the corresponding gaps, by the following equations: [2,3]

$$E_{\mathrm{LUMO}}/\mathrm{eV} \approx -1\mathrm{e} \times [\,(E_{\mathrm{p,I\,c}}/\mathrm{V}(\mathrm{Fc}^{+}|\mathrm{Fc}) + 4.8\ \mathrm{V}(\mathrm{Fc}^{+}|\mathrm{Fc\ vs\ zero})] \text{ (maxima criterion)} \quad (1)$$

$$E_{\mathrm{LUMO}}/\mathrm{eV} \approx -1\mathrm{e} \times [\,(E_{\mathrm{onset,I\,c}}/\mathrm{V}(\mathrm{Fc}^{+}|\mathrm{Fc}) + 4.8\ \mathrm{V}(\mathrm{Fc}^{+}|\mathrm{Fc\ vs\ zero})] \text{ (onset criterion)} \quad (1a)$$

$$E_{\mathrm{HOMO}}/\mathrm{eV} \approx -1\mathrm{e} \times [\,(E_{\mathrm{p,I\,a}}/\mathrm{V}(\mathrm{Fc}^{+}|\mathrm{Fc}) + 4.8\ \mathrm{V}(\mathrm{Fc}^{+}|\mathrm{Fc\ vs\ zero})] \text{ (maxima criterion)} \quad (2)$$

$$E_{\mathrm{HOMO}}/\mathrm{eV} \approx -1\mathrm{e} \times [\,(E_{\mathrm{onset,I\,a}}/\mathrm{V}(\mathrm{Fc}^{+}|\mathrm{Fc}) + 4.8\ \mathrm{V}(\mathrm{Fc}^{+}|\mathrm{Fc\ vs\ zero})] \text{ (onset criterion)} \quad (2a)$$

$$E_{\mathrm{g}}/\mathrm{eV} = 1\mathrm{e} \times (E_{\mathrm{p,I\,a}} - E_{\mathrm{p,I\,c}})\ /\ \mathrm{V} \text{ (maxima criterion)} \quad (3)$$

$$E_{\mathrm{g}}/\mathrm{eV} = 1\mathrm{e} \times (E_{\mathrm{onset,I\,a}} - E_{\mathrm{onset,I\,c}})\ /\ \mathrm{V} \text{ (onset criterion)} \quad (3a)$$

Such values are reported in Table 1, too, with the addition of the corresponding literature values for linear oligophenyls, oligothiophens and oligofurans with two to four conjugated rings (Chart 4.2; in the furan case only the oxidation potentials were available), which can be taken as benchmarks for effective conjugation. [4,5] For ease of comparison, HOMO and LUMO levels and gaps are also plotted together in Figure 4.4.

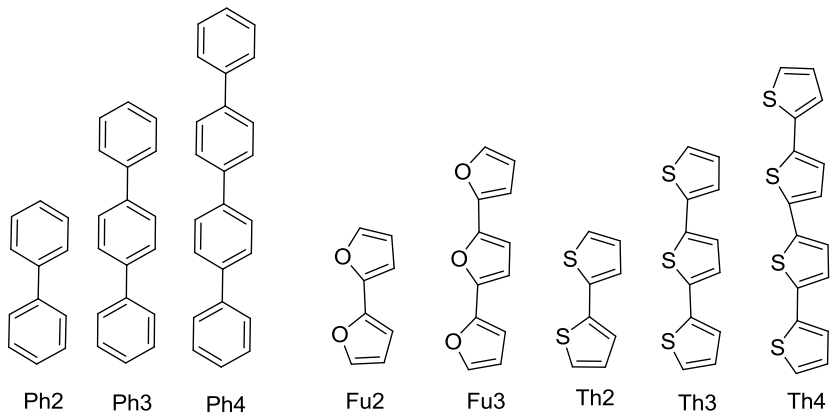

Chart 4.2 Molecular structure of the oligo arylenes and heteroarylenes used as benchmarks.

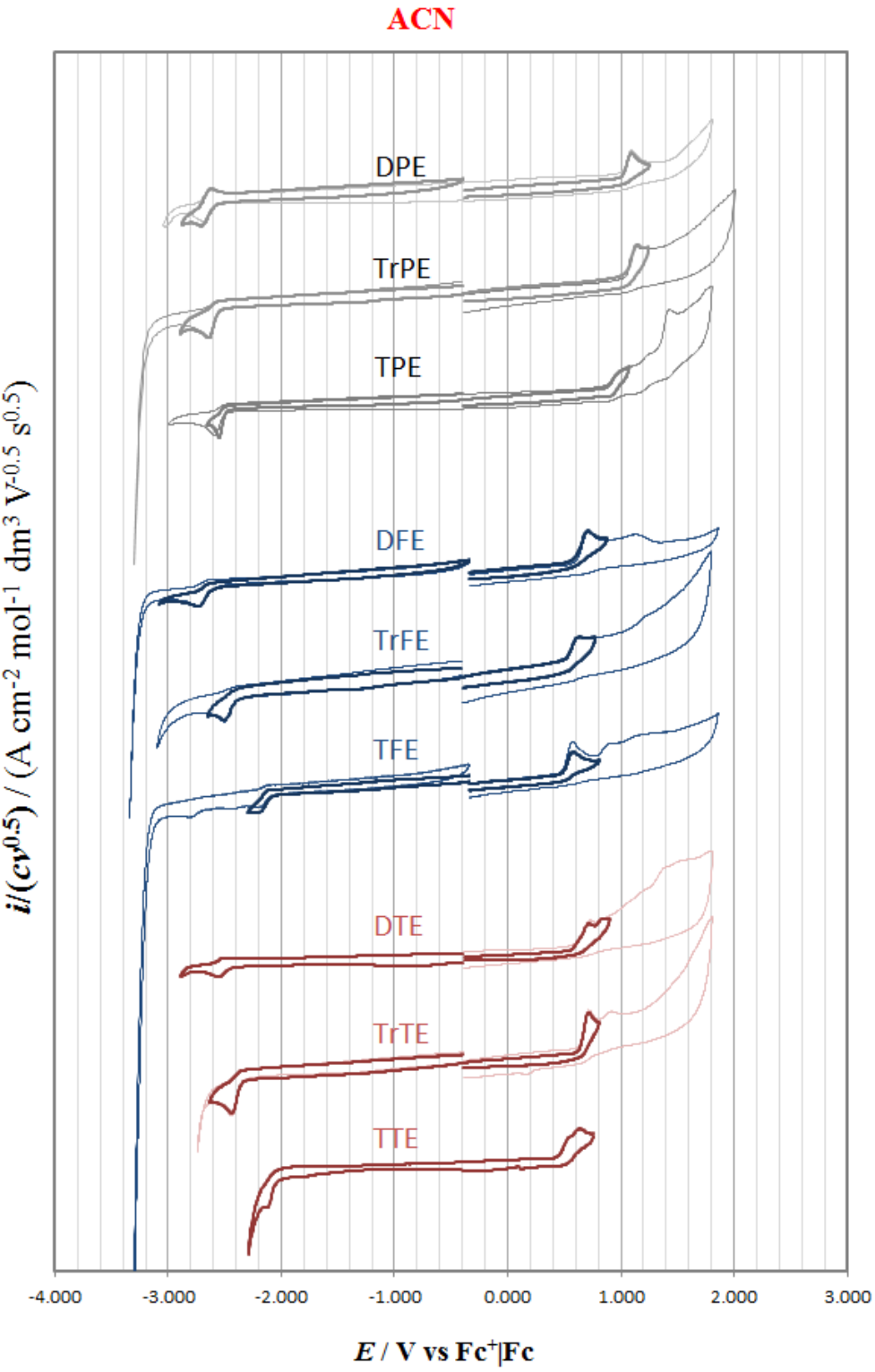

Figure 4.1 Cyclic Voltammetry of the nine investigated monomers, sorted by kind of heterocycle, in ACN, on GC electrode, at 0.2 V/s, with ohmic drop compensation.

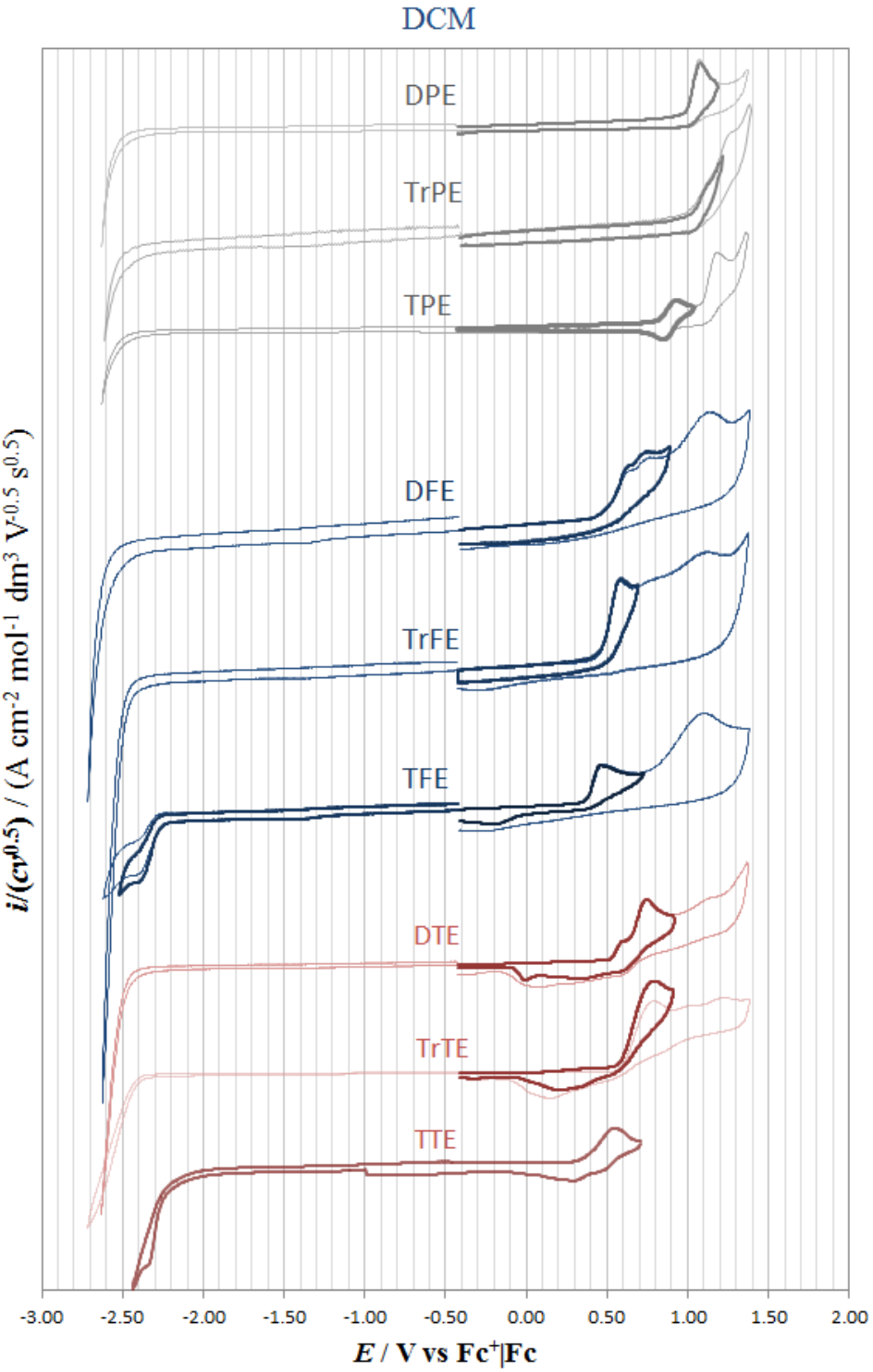

Figure 4.2 Cyclic Voltammetry of the nine investigated monomers, sorted by kind of heterocycle, in DCM, on GC electrode, at 0.2 V/s, with ohmic drop compensation.

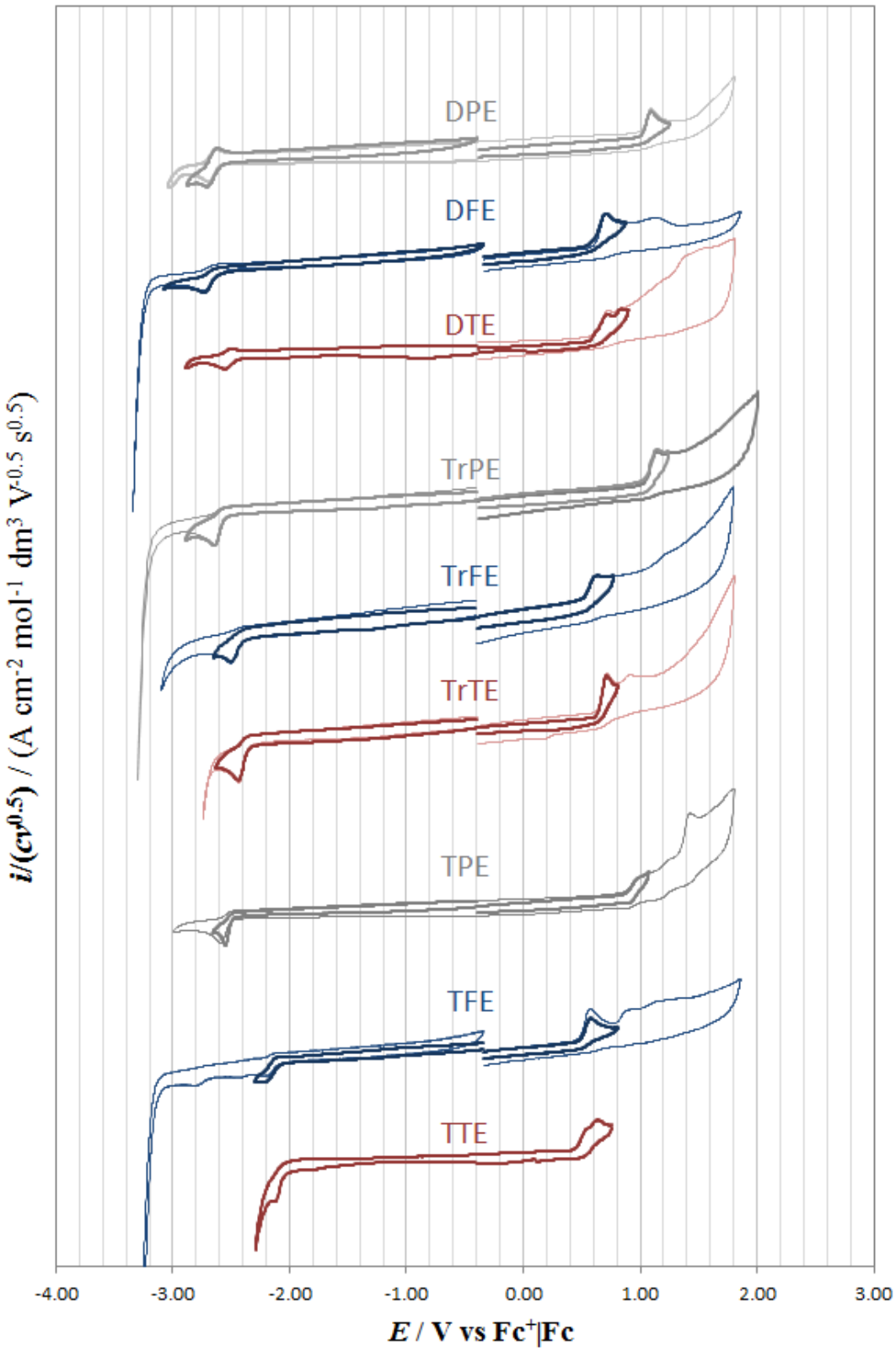

Figure 4.3 Cyclic Voltammetry of the nine investigated monomers, sorted by number of ring substituents, in ACN, on GC electrode, at 0.2 V/s, with ohmic drop compensation.

Table 1 Key electrochemical and energy parameters obtained by CV experiments for the nine investigated monomers.

	Solvente	$E_{I,c\,max}$ / V(Fc$^+$|Fc)	$E_{I,c\,onset}$ / V(Fc$^+$|Fc)	$E_{I,a\,max}$ / V(Fc$^+$|Fc)	$E_{I,a\,onset}$ / V(Fc$^+$|Fc)	$LUMO_{,max}$ / eV	$LUMO_{,onset}$ / eV	$HOMO_{,max}$ / eV	$HOMO_{,onset}$ / eV	$E_{g\,max}$ /eV	$E_{g\,onset}$ /eV
P2						**-1.71**		**-6.29**		**4.58**	
P3						**-1.96**		**-6.03**		**4.07**	
P4						**-2.09**		**-5.90**		**3.81**	
F3								**-5.37**			
F4								**-5.24**			
T2						**-1.96**		**-5.68**		**3.72**	
T3						**-2.30**		**-5.34**		**3.04**	
T4						**-2.46**		**-5.23**		**2.77**	
DPE	DCM			**1.07**	0.98			**-5.87**	-5.78		
DPE	ACN	**-2.70**	-2.57	**1.10**	1.01	**-2.10**	-2.23	**-5.90**	-5.81	**3.80**	3.58
DFE	DCM			**0.63**	0.45			**-5.43**	-5.25		
DFE	ACN	**-2.72**	-2.61	**0.71**	0.57	**-2.08**	-2.19	**-5.51**	-5.37	**3.43**	3.18
DTE	DCM			***(0.59)*** **0.75**	0.52			**-5.55**	-5.32		
DTE	ACN	**-2.54**	-2.44	***(0.61)*** **0.72**	0.61	**-2.26**	-2.36	**-5.52**	-5.41	**3.26**	3.05
TrPE	DCM			**1.13**	1.01			**-5.93**	-5.81		
TrPE	ACN	**-2.54**	-2.64	**1.14**	1.03	**-2.26**	-2.16	**-5.94**	-5.83	**3.68**	3.67
TrFE	DCM			**0.59**	0.43			**-5.39**	-5.23		
TrFE	ACN	**-2.49**	-2.40	**0.61**	0.52	**-2.31**	-2.4	**-5.41**	-5.32	**3.10**	2.92
TrTE	DCM			**0.79**	0.57			**-5.59**	-5.37		
TrTE	ACN	**-2.44**	-2.34	**0.72**	0.63	**-2.36**	-2.46	**-5.52**	-5.43	**3.16**	2.97
TPE	DCM	**-2.6**	-2.3	**0.92**	0.81	**-2.2**	-2.5	**-5.72**	-5.61	**3.52**	3.11
TPE	ACN	**-2.55**	-2.49	**0.97**	0.88	**-2.25**	-2.31	**-5.77**	-5.68	**3.52**	3.37
TFE	DCM	**-2.4**	-2.24	**0.47**	0.36	**-2.4**	-2.56	**-5.27**	-5.16	**2.87**	2.6
TFE	ACN	**-2.19**	-2.08	**0.57**	0.47	**-2.61**	-2.72	**-5.37**	-5.27	**2.76**	2.55
TTE	DCM	**-2.34**	-2.21	**0.54**	0.31	**-2.46**	-2.59	**-5.34**	-5.11	**2.88**	2.52
TTE	ACN	**-2.12**	-2.05	**0.54,0.64**	0.44	**-2.68**	-2.75	**-5.34**	-5.24	**2.66**	2.49

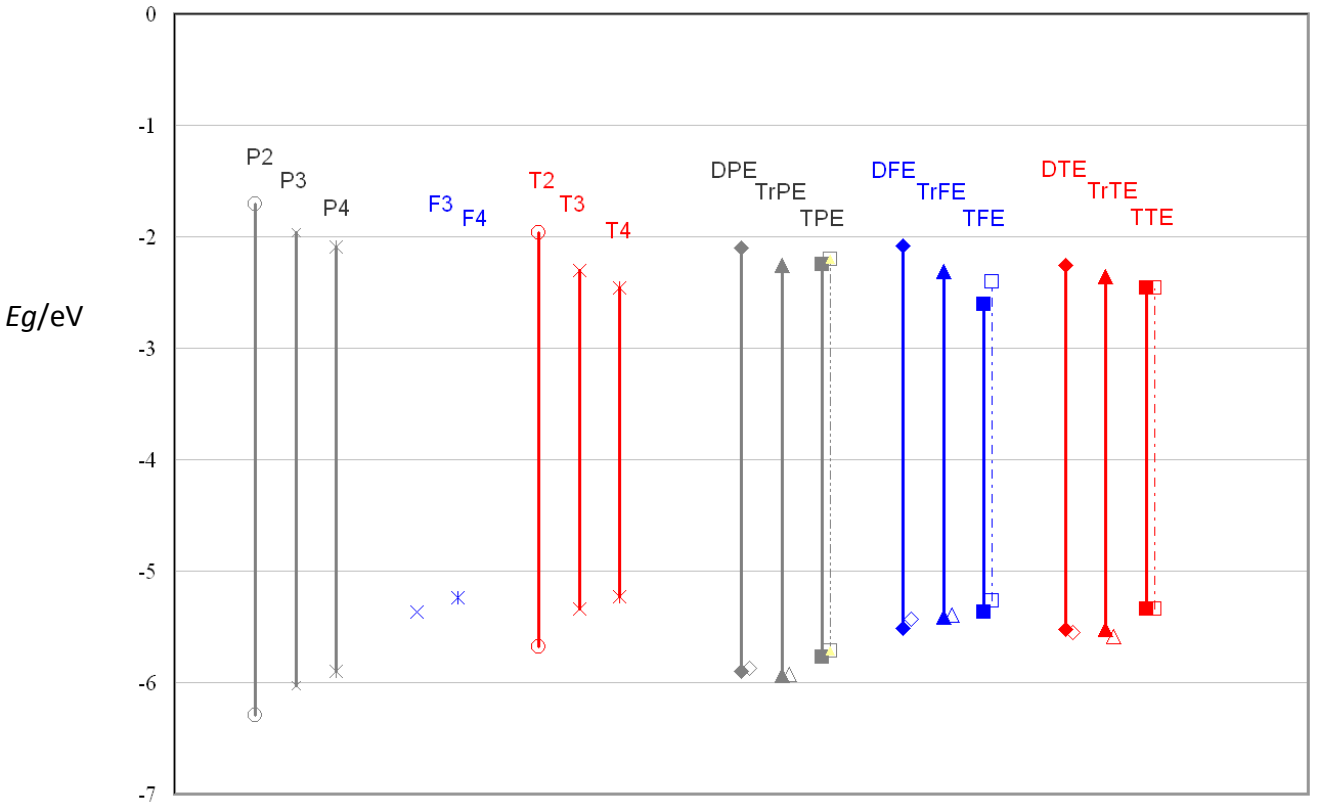

Figure 4.4 Energy Gap comparison between the linear oligoaryl/heteroarylenes and the aryl- and heteroarylethenes. The dash line, and the empty squares and triangles, indicate the gap calculated by using DCM as working solvent.

Looking at the Table 1 and Figures 4.4, the following observations can be drawn:

- Within each series, with increasing ring number both oxidation and reduction processes become easier and take place at lower (less positive) and less negative potentials respectively; as a result, the energy gaps become narrower. This is of course consistent with the increase in effective conjugation
- At constant number of aromatic rings, both thiophene- and furan-based systems have smaller gaps with respect to the corresponding phenyl-based ones, pointing to higher effective conjugation for the Heteroaryl-based systems. Moreover, they also appear much electron richer with eighbo to phenyl systems; in fact their HOMO-LUMO gaps are not only smaller but also displaced towards higher energies (favoured oxidation, unfavoured reduction, with a less positive oxidation peak and a more negative reduction one). Both effects can be justified considering that in the heterocycles the same electron density (6 π-electrons) is distributed over 5 atoms rather than 6. It is also worthwhile noticing that the electron distribution is asymmetric, with a higher localization on the heteroatom, particularly in the case of oxygen, which is harder than sulphur (Figure 4.5)

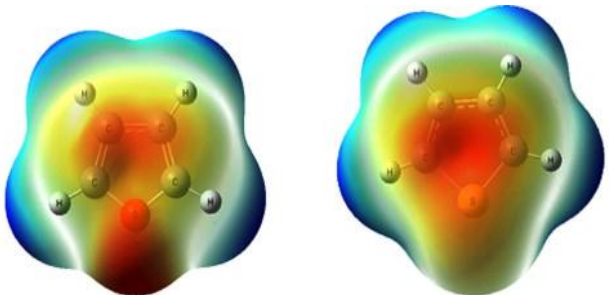

Furane *Thiophene*

Figure 4.5 Map of the electron density on the Furane and Thiophene rings

- DTE has an intermediate gap between T2 and T3; therefore the double bond contributes in increasing conjugation between the two thiophene rings;

- DPE has a gap comparable to P4, this could be possibly explained assuming the phenyl rings in P4 to be not coplanar as a consequence of the steric hindrance of the H atoms in *ortho* position with respect to the bond between adjacent rings (as in the well known case of biphenyl), thus determining a decrease in the effective conjugation;

- TrTE has a gap only slightly higher than DTE and lower than T3; accordingly the contribution of the third thiophene ring to the overall conjugation must be very low;

- TTE has a gap comparable when not inferior to T4 one (according to the working solvent); therefore also in this case the unsaturated systems present in the molecules only partially contribute to the overall conjugation;

- Furylethenes show similar features to thienylethenes at constant ring number;

- In furyl and thienyl ethene series, the LUMO decrease with increasing ring number is more remarkable than the HOMO increase, or in other words reduction is comparatively more favoured than oxidation; the effect is more evident in furylethenes;
- The solvent effect on the normalized peak potentials is significant but not remarkable. In any case the first reduction peak potentials are, for all available comparison cases, invariably more positive in ACN, while first oxidation ones are more positive in ACN for phenyl and furyl ethene series and in DCM for thienylethenes.

Scan rate effects have also been considered in the voltammetric experiments. They are summarized in Figures 4.6 (phenylethene family in DCM and ACN), 4.7 (thienylethene family in DCM and ACN) and 4.8 (furylethene family in DCM and ACN).

In the *phenyl derivative family* (Figure 4.6), both first oxidation and reduction appear rather facile, since only a slight shift is observed for the corresponding peak potentials with increasing scan rate, and they tend to chemical reversibility with increasing scan rate; in particular, with DPE this is attained by the reduction peak before the oxidation one, while the contrary holds with TPE and the TrPE case looks an intermediate one. In any case, such high reversibility degree is consistent with the family having null ability to give electrodeposited conducting films (see later on). The DCM and ACN results are similar, albeit no reduction peak can be observed in DCM on account of the narrower negative background.

In the *thienyl derivative family* (Figure 4.7) the tendency of the monomers to oligomerize by radical cation coupling (see later) results in first oxidation peaks having no symmetrical return one, while a large, irregular one can be observed at more positive potentials, corresponding to reduction of deposited electroactive products of the oxidation reaction. In the case of TTE in ACN, a second oxidation peak following the first one is perceived at low scan rate, disappearing with increasing scan rate while a beginning of symmetrical return peak appears; therefore the second oxidation peak should involve a product of the first electron transfer undergoing a rather slow reaction. First reduction peaks, corresponding to radical anion formation, are more chemically reversible, since a beginning of symmetrical return peak can always be observed with increasing scan rate; this is particularly evident in the DTE case. While in ACN all electron transfers appear rather facile, as in the former case of phenyl derivatives (slight or null shift of the peak potential with scan rate), it is significantly less so in DCM, where an intriguing prepeak can also be observed for DTE before the main first oxidation peak.

Also in the *furyl derivative family* electron transfers appear in most cases rather facile, and oxidation peaks show no symmetrical partner (excepting a slight hint with TFE at high scan rates) but rather a flat return signal pointing to formation of an electroactive layer (in fact they easily oligomerize, too, see later). Again, reduction peaks appear more chemically reversible than

oxidation ones. Similar considerations apply to both ACN and DCM (in which a reduction peak can be observed only for TFE). And, again as in the thienyl series, for the disubstituted compound a more complex first oxidation peak system is observed in DCM with respect to ACN and to higher terms in the family.

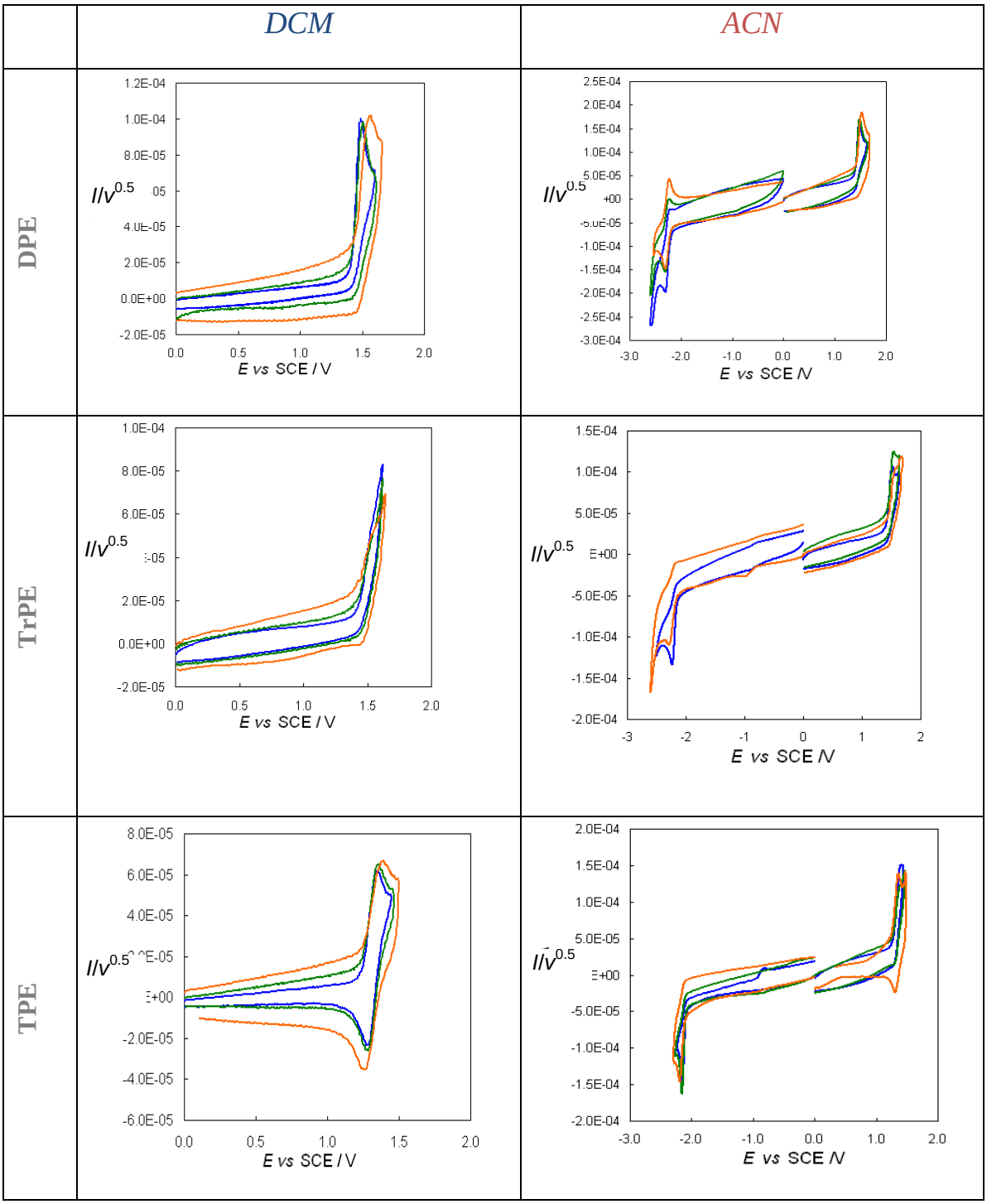

Figure 4.6. Scan rate effects on the CV patterns of the phenyl derivative family in DCM and ACN. Blue: 50 mV/s; Green: 200 mV/s; Orange: 2000 mV/s.

	DCM	*ACN*
DTE	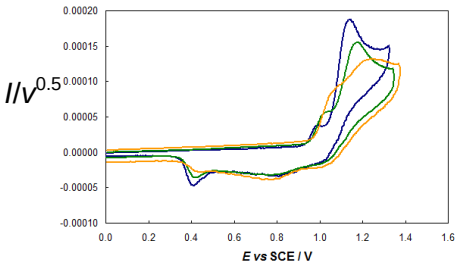	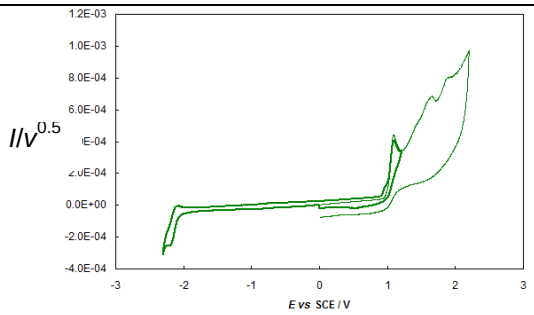
TrTE	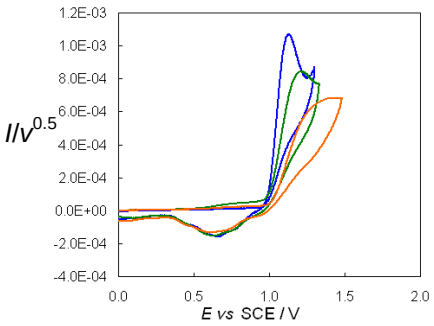	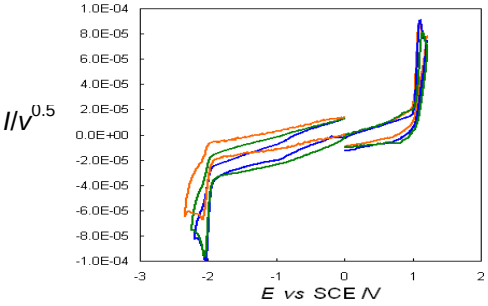
TTE	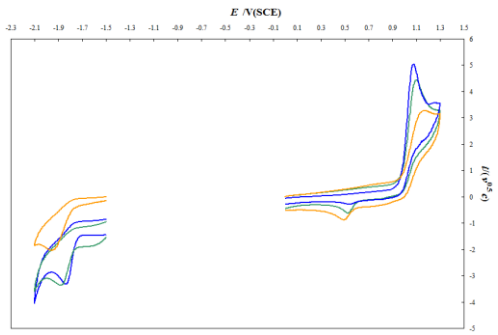 *[A. Bolzoni, degree thesis]*	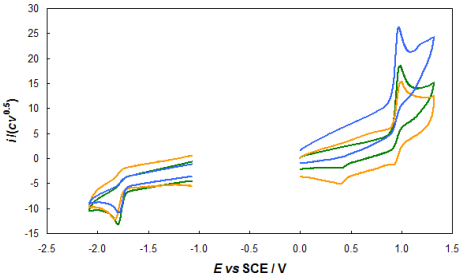 *[A. Figini, degree thesis]*

Figure 4.7. Scan rate effects on the CV patterns of the thienyl derivative family in DCM and ACN. Blue: 50 mV/s; Light Blue: 100 mV/s; Green: 200 mV/s; Orange: 2000 mV/s.

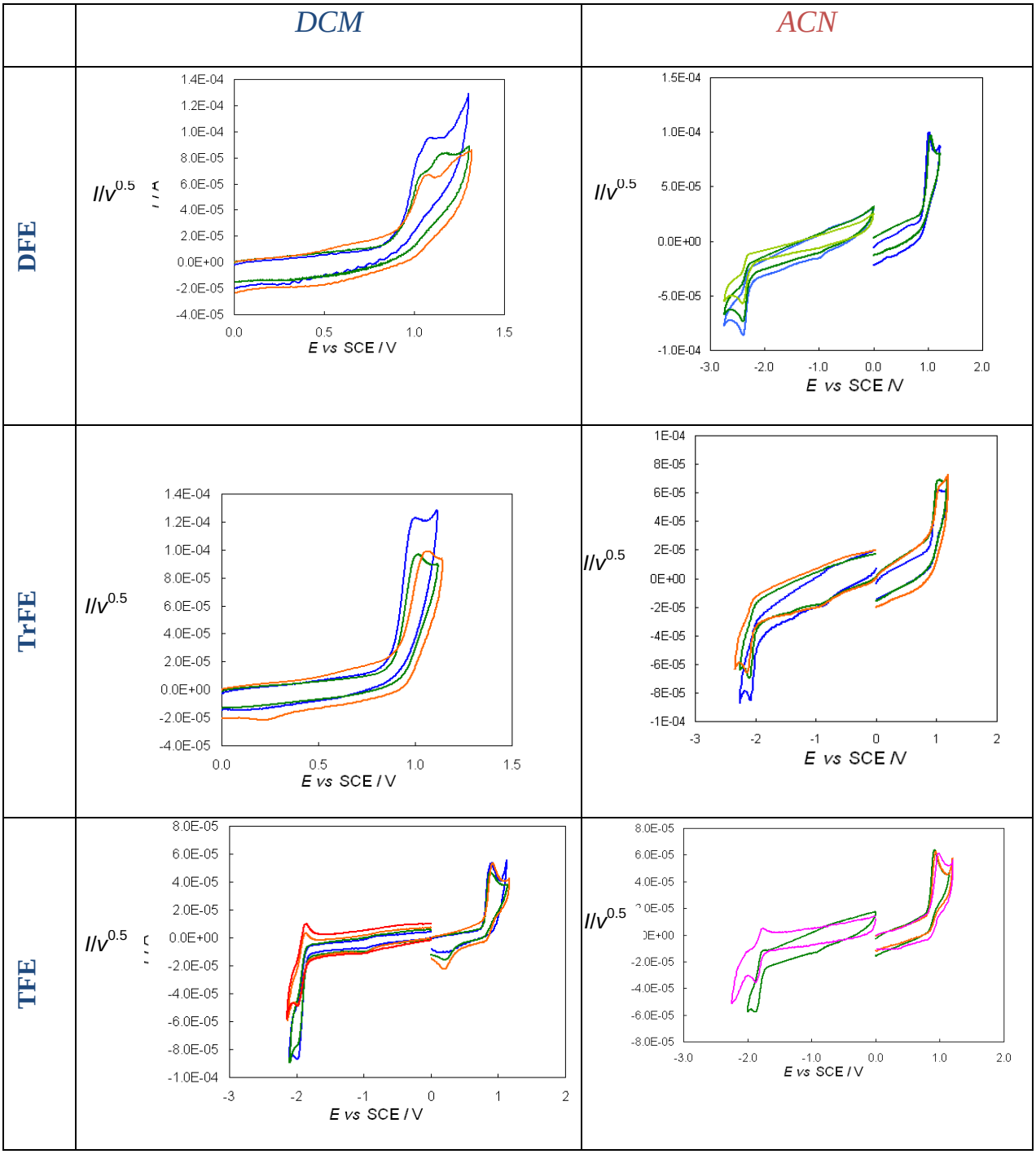

Figure 4.8. Scan rate effects on the CV patterns of the furyl derivative family in DCM and ACN. Blue: 50 mV/s; Light Blue: 100 mV/s; Green: 200 mV/s; Olive green: 1000 mV/s Orange: 2000 mV/s; Red: 5000 V/s ; Purple: 20000 V/s.

4.2 Electropolymerization Study

CV experiments also included a study of the oligomerization ability of the nine monomers by electrooxidation and subsequent radical cation coupling, according to the classical mechanism described by Heinze et al.[6] These tests consisted in performing repeated (in most cases 36) potential cycles around the first oxidation peak of each monomer; in the cases where electrodeposition was achieved, the stability of the oligomer film was checked performing further oxidative cycles in monomer free solution, at first at the same scan rate as the electrodeposition step, then at higher or lower rates, to evaluate the facility of the doping/undoping processes; finally, widening the potential cycle towards negative potentials afforded evaluation of the oligomer film reducibility and of possible charge trapping effects.

A selection of results is provided in the figures at the following pages; values of maxima potentials for first oxidation and, when available, reduction are collected in Table 2.

Phenyl derivative family
As above discussed, the CV patterns of the monomers of this family show increasing chemical reversibility with increasing scan rate, pointing to the radical anions and radical cations formed in the first oxidation and first oxidation processes being rather stable.
Consistently with this observation, practically no electrodeposition was achieved performing oxidative cycles with these monomers in our working conditions.

Thienyl derivative family
The monomers of this family, which display chemically irreversible oxidation peaks, can give by electrodeposition electroactive films of much higher effective conjugation than the starting monomers (as evident from the oxidation and reduction potentials in Table 2).
The electrooligomerization ability however remarkably decreases with increasing ring number.
In DCM the process is fast for DTE, slow for TrTE (as in ACN), and very slow but still perceivable for TTE; this trend might be a consequence of either increasing stabilization of the radical cation and/or increasing sterical hindrance due to the higher number of Thiophenes. In ACN the process is fast for DTE (even faster than in DCM), slow for TrTE (as in DCM), negligible for TTE.
In the case of DTE, as already discussed, the first oxidation peak of the monomer is preceded by a prepeak; cycling around the latter, without including the main one, also results in oligomerization of a film with similar patterns, but much slower (Figure 4.9).
With DTE, stability cycle maxima appear significantly shifting to more extreme potentials with increasing scan rate, pointing to the doping/undoping process being kinetically hindered. This effect is particularly evident working in ACN on GC, as well as working on ITO (Figure 4.10). Stability cycles on ITO afford to well observe the electrochromism of the films. Figure 4.17
With TrTE, the electrodeposition is slower working in the same conditions, as already mentioned (but can be greatly increased increasing the monomer concentration, Figure 4.11 second column), and proceeds at a similar rate in the two solvents. Stability cycles are much more symmetrical than in the DTE case, with maxima nearly constant with scan rate, pointing to a facile doping/undoping process. This could be linked to the slower, more regular electrodeposition and to the lower

thickness of the deposited film, since it does not apply to the films deposited at higher monomer concentration, on DCM or on ITO (figure 4.11). Again, stability cycles on ITO afford to well observe the electrochromism of the films. Very thin film are electrodeposited from TTE in DCM (Figure 4.13) but not in ACN. Their stability cycles appear rather symmetrical and unaffected by scan rate, as in the TrTE case and possibly for the same reasons.
Widening the potential range to study first reduction processes, the films appear easier reduced than the monomers, and able to release the negative charge at potentials only slightly more positive than the reduction peak ones.
Very slight charge trapping effects could be observed in a few cases, actually those of the thicker films, *i.e.* oligoDTE grown in ACN and DCM and oligoTrTE grown in DCM with a tenfold monomer concentration.

Furyl derivative family

Also the furyl derivative family can give electrooligomerization, but with comparatively slower rates than the thienyl one. Also in this series the same trend is observed of decreasing oligomerization ability with increasing number of heteroaromatic rings.

DFE displays a slower, more regular electrooligomerization than DTE (its behaviour appears similar to that of TrTE). The stability cycles of the film grown on GC in ACN are particularly symmetrical (like the growing part of oligomerization cycles, too) and constant with scan rate, pointing to a facile doping/undoping process. Also on ITO the oligomerization cycles appear more symmetrical than in the thienyl derivative cases, but the stability cycles are still significantly affected by the scan rate (Figure 4.14); they afford observation of the electrochromism of the film.

TrFE oligomerization is slower than the DFE one, and apparently the film lacks stability upon performing the stability cycles.

TFE oligomerization is even slower, and, again, the resulting films appear unstable upon cycling.

DTE

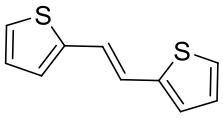

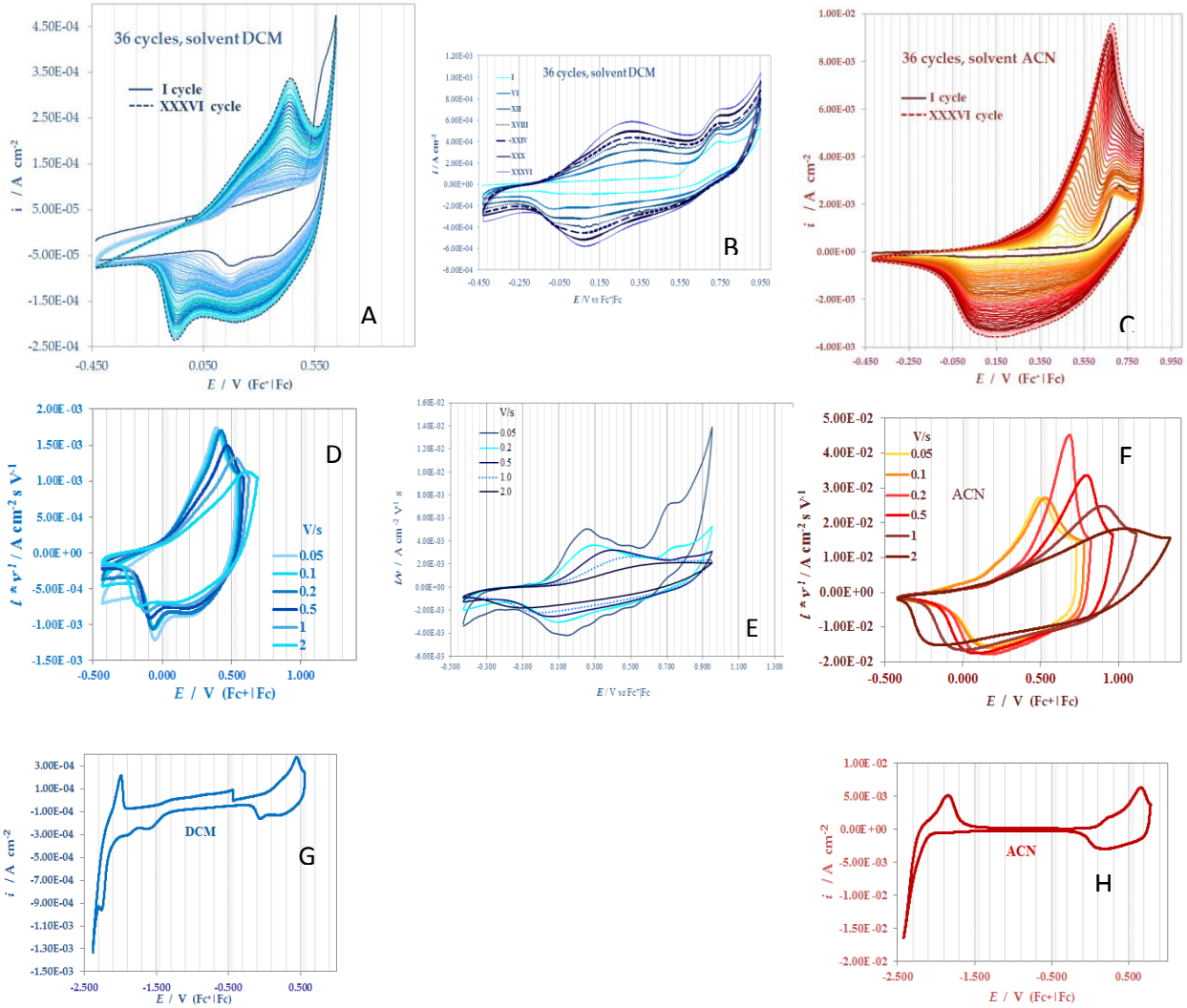

Figure 4.9 Electrooligomerization of dithienylethene at 0.2 V/s scan rate on GC electrode in (A-B) DCM cycling around the oxidation prepeak (A) or around the entire first oxidation system (B), and in ACN (C).(D-E) Oxidative stability cycles of the electrodeposited oligomer films, in (D,E) DCM and in (F) ACN, at different scan rates (the third cycle for each scan rate is plotted in the figure). Third row: entire CV patterns of the electrodeposited oligomer films, in DCM (G) and in ACN (H).

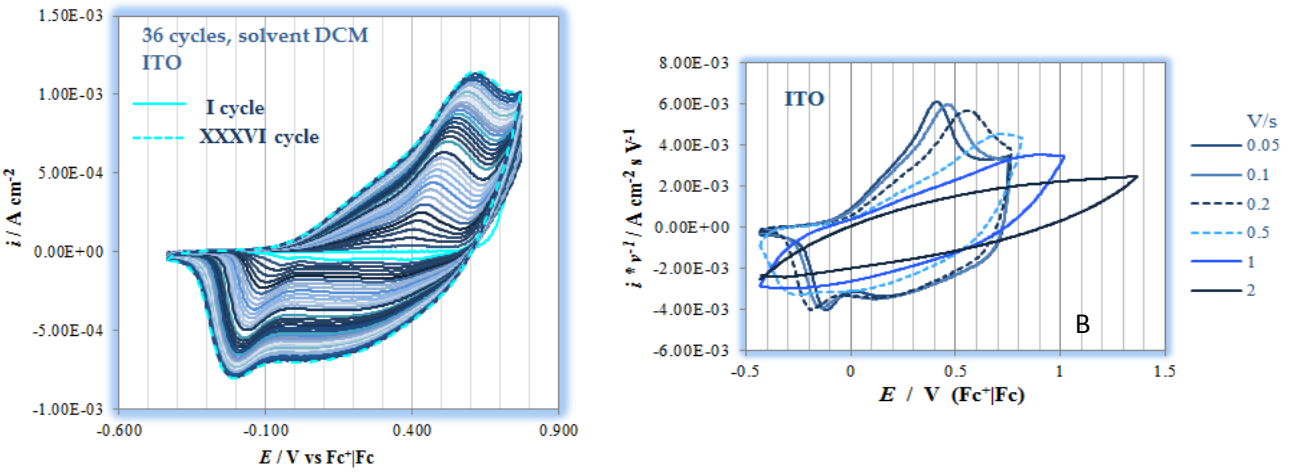

Figure 4.10. (A) Electrooligomerization of dithienylethene at 0.2 V/s scan rate in DCM on ITO electrode. (B) Oxidative stability cycles of the electrodeposited oligomer films, in the same conditions, at different scan rates (the third cycle for each scan rate is plotted in the figure).

TrTE

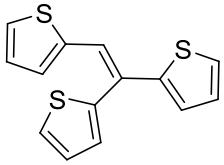

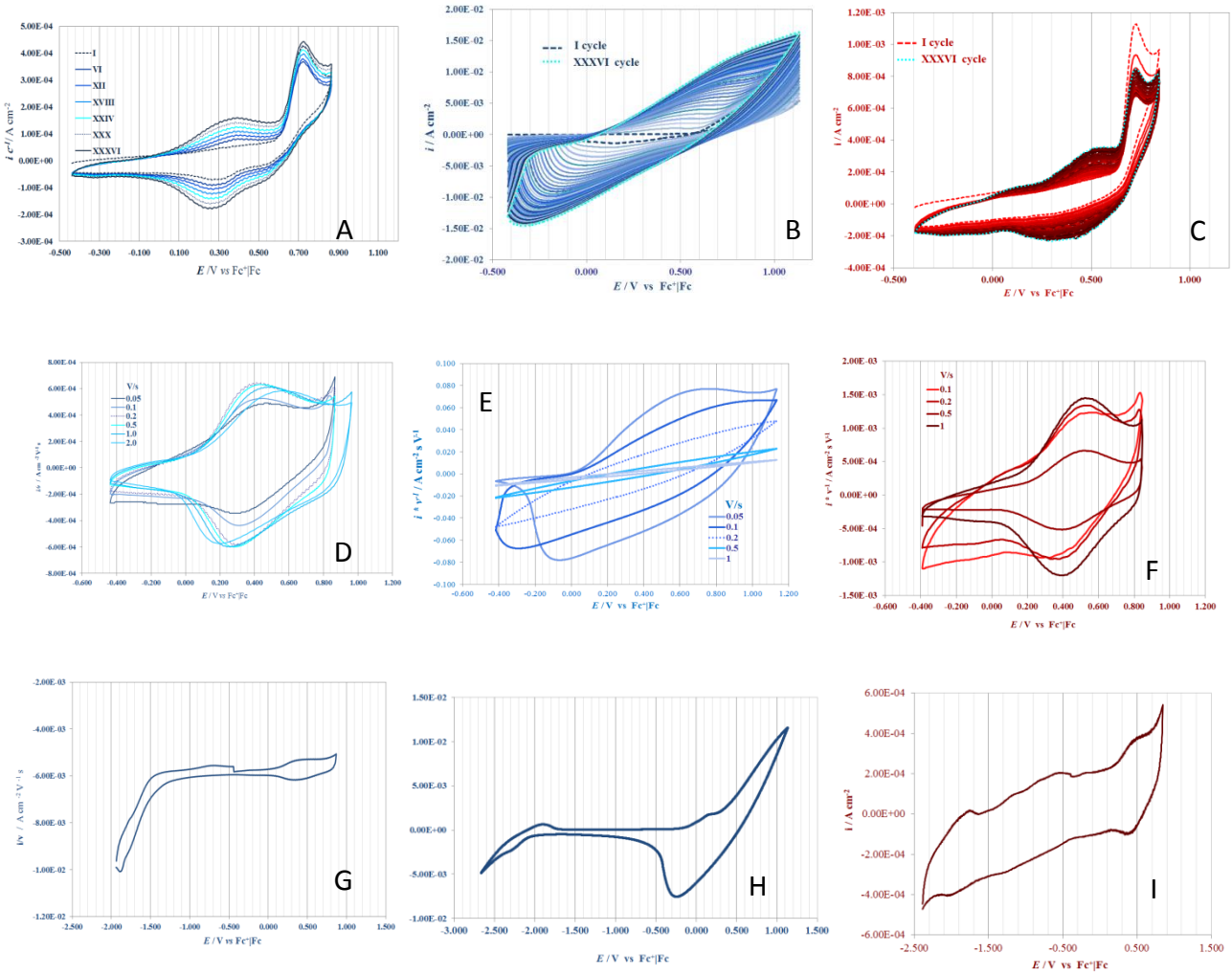

Figure 4.11 Electrooligomerization of TriThienylEthene at 0.2 V/s scan rate on GC electrode in DCM (A-B) at the usual monomer concentration (A) or at tenfold higher (B) concentration, and in ACN (C) at the usual monomer concentration. (D-F) Oxidative stability cycles of the electrodeposited oligomer films, in the DCM (D,E) and in ACN (F), at different scan rates (the third cycle for each scan rate is plotted in the figure). (G-I) Entire CV patterns of the electrodeposited oligomer films, in DCM (G,H) and in ACN (I).

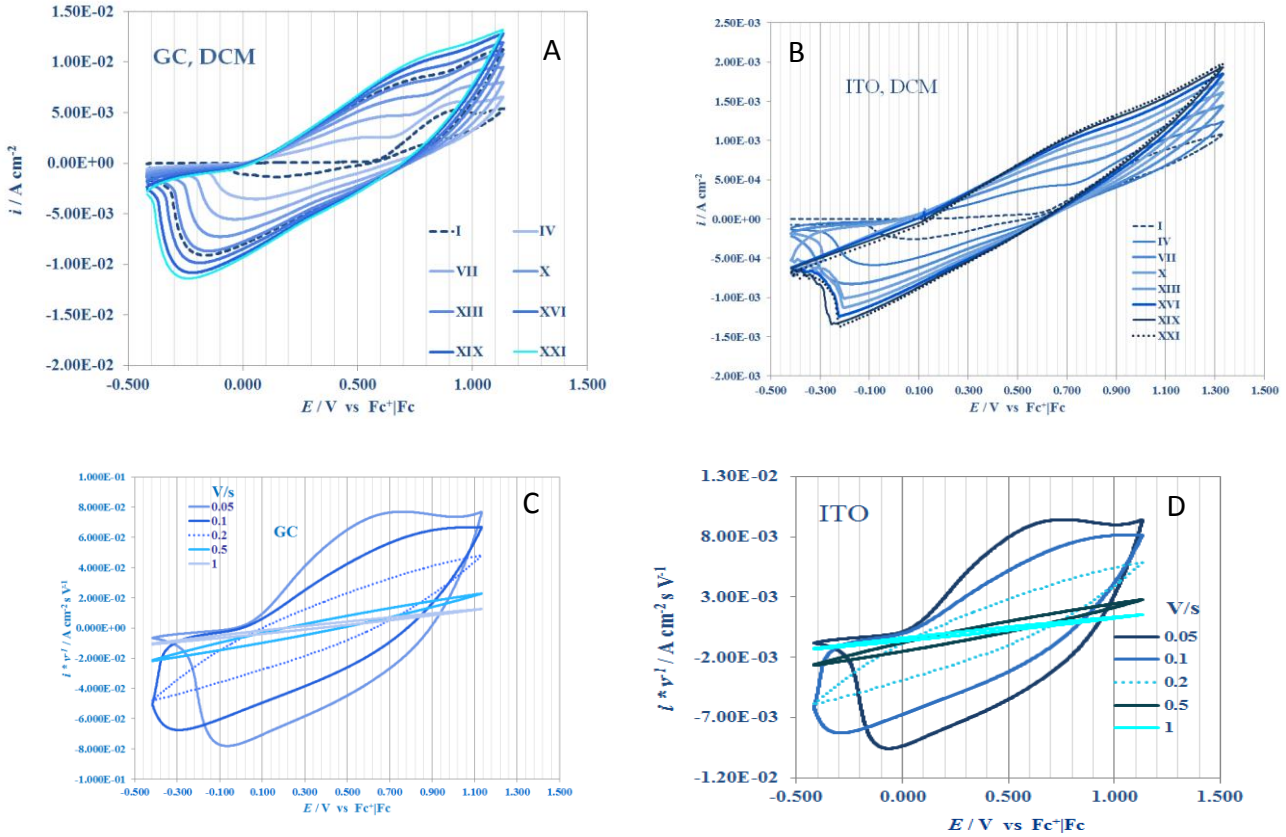

Figure 4.12. Electrooligomerization of TriThienylEthene at 0.2 V/s scan rate, in DCM, on (A) GC and (B) ITO electrode. in DCM (A-B) at the usual monomer concentration (tenfold higher than the usual one); (C) and (D) oxidative stability cycles cycles of the electrodeposited oligomer films, at different scan rates (the third cycle for each scan rate is plotted in the figure).

TTE

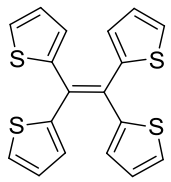

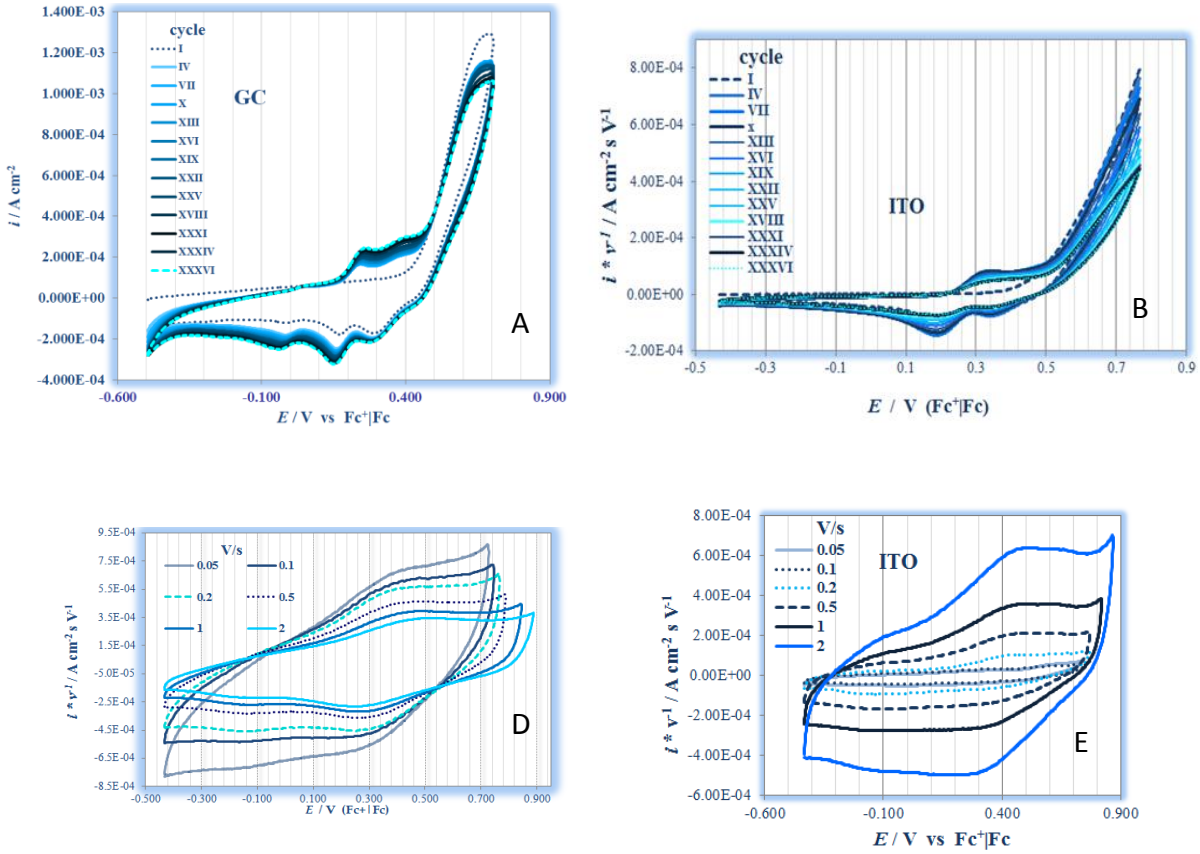

Figure 4.13. (A-B) Electrooligomerization of TetraThienylEthene TTE, at 0.2 V/s scan rate in DCM on GC electrode (A) and on ITO electrode (B). (D,E) Oxidative stability cycles of the electrodeposited oligomer films, in the same conditions, at different scan rates (the third cycle for each scan rate is plotted in the figure) (D) GC, ©ITO.

DFE

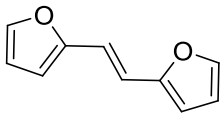

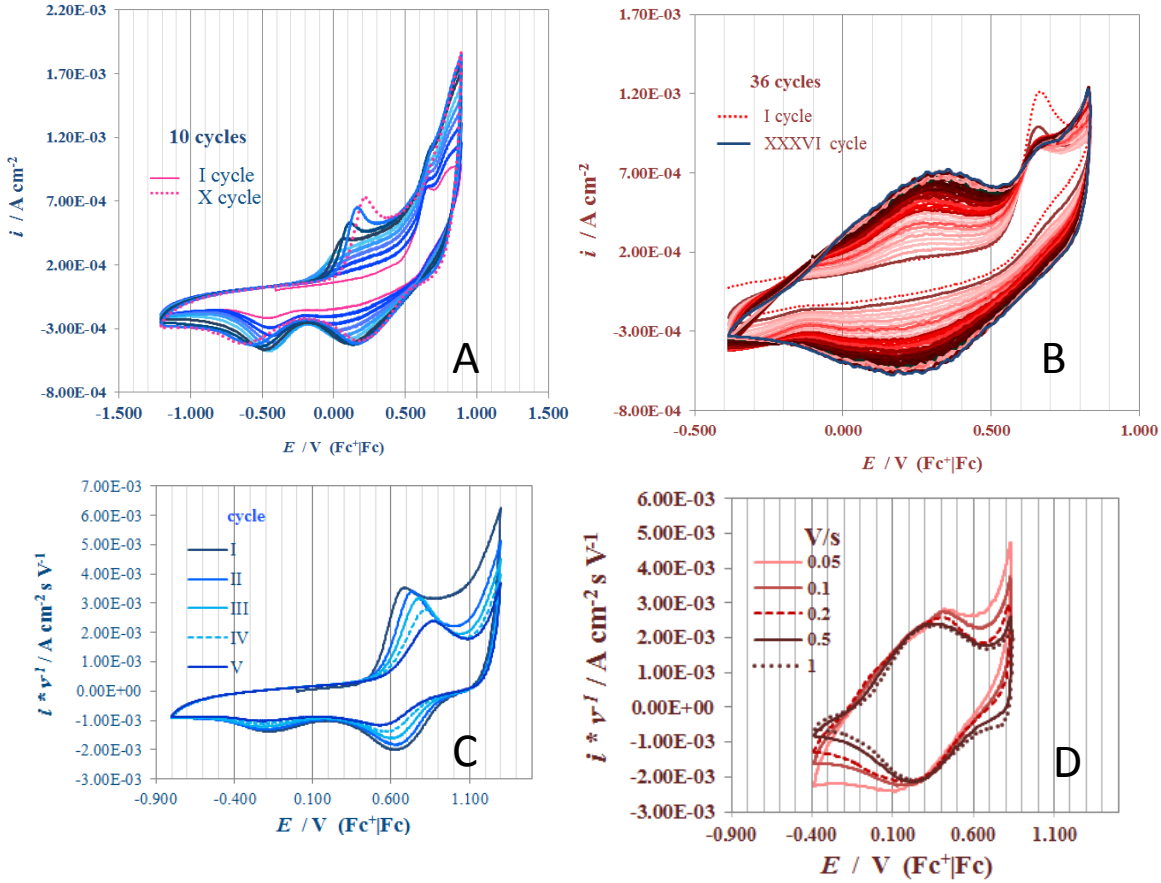

Figure 4.14. (A-B) Electrooligomerization of DiFurylEthene DFE, at 0.2 V/s scan rate on GC electrode in DCM (A) and in ACN (B). (C,D) Oxidative stability cycles of the electrodeposited oligomer films, in DCM (C) at 0.2 V/s, several cycles, and in ACN (D) at different scan rate.

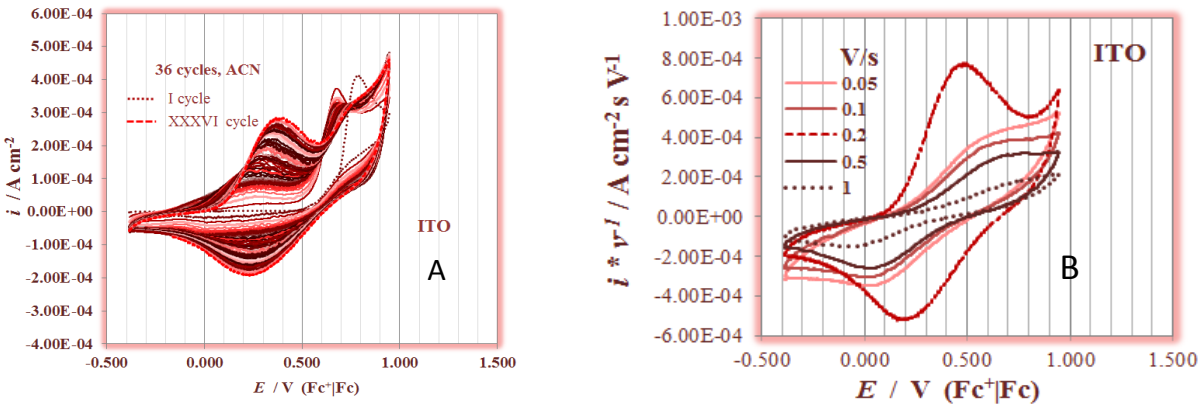

Figure 4.14. (A) Electrooligomerization of DiFurylEthene DFE, at 0.2 V/s scan rate in ACN on ITO electrode (B) Oxidative stability cycles of the electrodeposited oligomer films, in the same conditions, at different scan rates (the third cycle for each scan rate is plotted in the figure).

TrFE

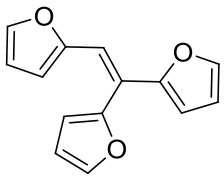

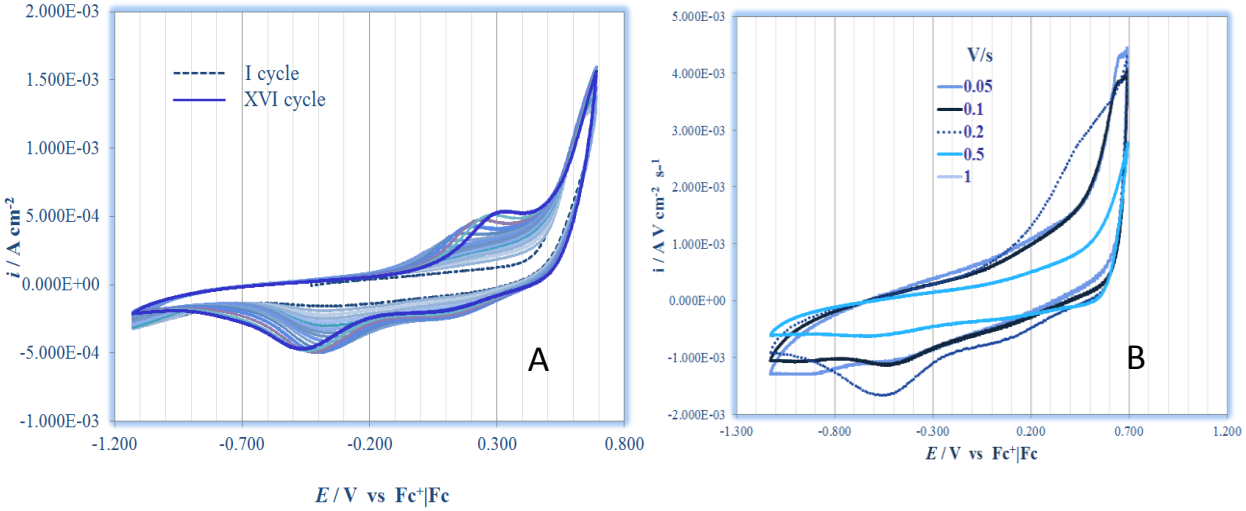

Figure 4.15. (A) Electrooligomerization of DiFurylEthene DFE, at 0.2 V/s scan rate in DCM on GC electrode (B) Oxidative stability cycles of the electrodeposited oligomer films, in the same conditions, at different scan rates (the third cycle for each scan rate is plotted in the figure).

TFE

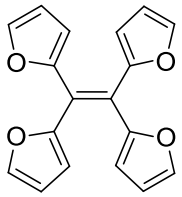

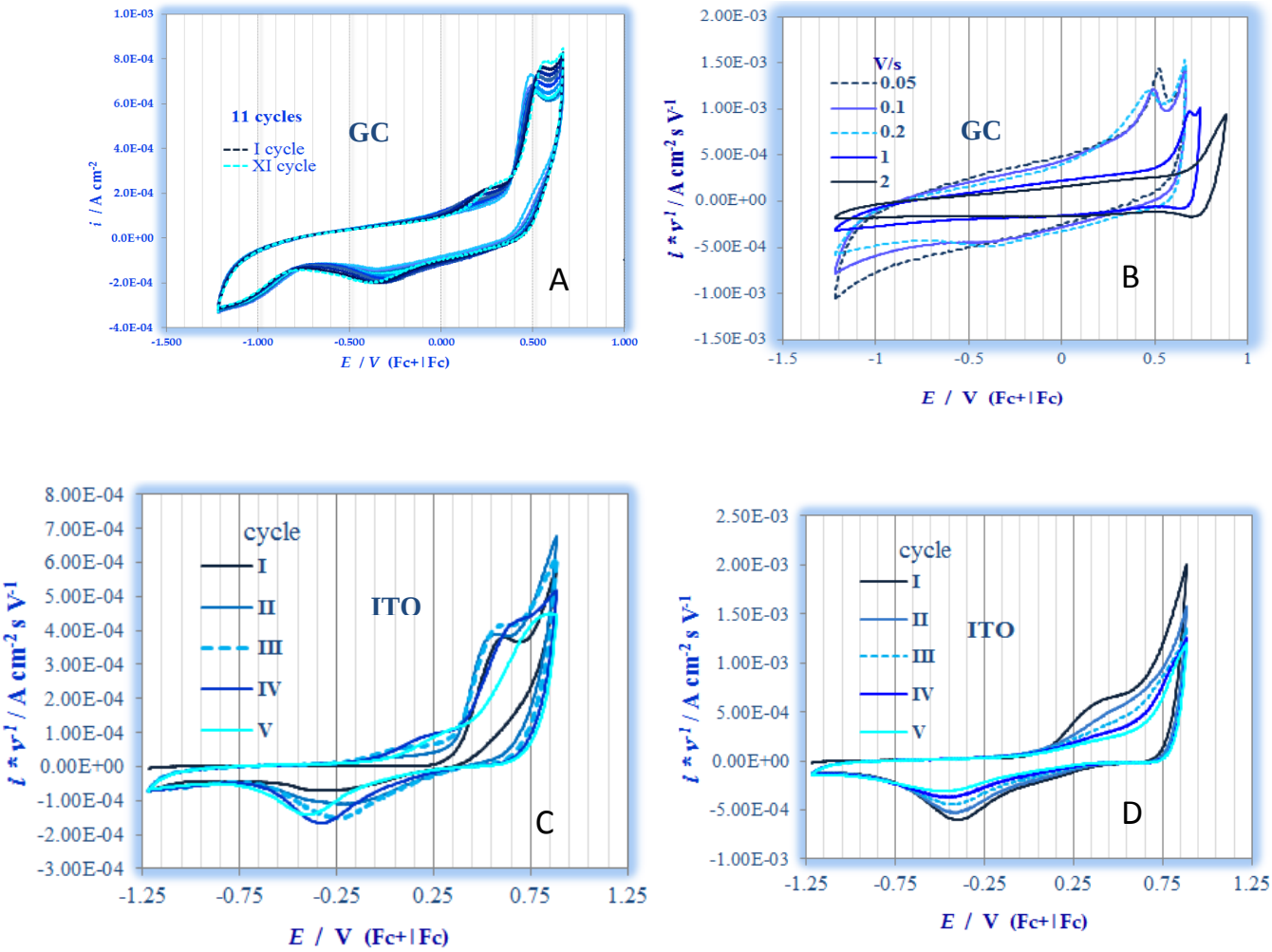

Figure 4.16. (A-B) Electrooligomerization of TetraFuryllEthene TFE, at 0.2 V/s scan rate in DCM on GC electrode (A) and on ITO electrode (B). (C,D) Oxidative stability cycles of the electrodeposited oligomer films, in the same conditions, at 0.2 V/s (severalo cycles) (C) GC, (D) ITO.

Table 2 Key oxidation potenatials of the monomer and of related films grown on GC as working electrode, in the indicated solvents.

		DCM	ACN	DCM	ACN
		Anodic peak		*Cathodic peak*	
		E /V vs Fc^+|Fc	*E* /V vs Fc^+|Fc	*E* /V vs Fc^+|Fc	*E* /V vs Fc^+|Fc
DTE	Monomer	0.75	0.72	/	-2.54
	Film	0.30	0.67	-2.24	/
TrTE	Monomer	0.79	0.72	/	-2.44
	Film	0.43	0.52	-1.86	-1.95
TTE	Monomer	0.54	0.54, 0.64	-2.34	-2.12
	Film	0.38	/	/	/
DFE	Monomer	0.63	0.71	/	-2.72
	Film	0.20	0.37	/	/
TrFE	Monomer	0.59	0.61	/	-2.49
	Film	0.40	/	/	/
TFE	Monomer	0.47	0.57	-2.4	-2.19
	Film	0.44	/	/	/

Figure 4.17 Electrochromism phenomenon of the oligomeric heteroarylethene-based inestigated films.

Bibliography Chapter 4

[1] A. J. Bard, L. R. Faulkner, in: *Electrochemical Methods. Fundamentals and Applications*, 2nd ed. Wiley, New York, **2001**, 648;
[2] W.-K Chan et al, *Nat. Mater*., **2007**, *6*, 521;
[3] M. Al-Ibrahim, S. Senfuss et al, *Macromol. Rapid Commun*. **2006**, *27*, 1454;
[4] K. Meerholz, J. Heinze, *Electrochim. Acta*, **1996**, *41*, 1839-1854;
[5] M. Bendikov, et al. *Chem. Commun*. **2013**, *49*, 6256-6258;
[6] J. Heinze *et al*., *Chem. Rev*, ***2010***, *110*, 4724.

5
Aggregation-Induced Emission

5.1 Brief introduction and motivation

As mentioned in chapter 2, the encounter between the AIE phenomenon and the HeteroArylEthenes, has occurred thanks to the TetraThienylEthene, TTE. Figure 5.1.

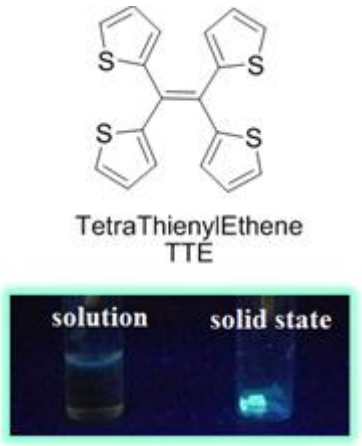

Figura 5.1 Luminescent eighbor of TTE in solution and solid state under UV-vis light illumination.

Synthesizing the other family-members, for the aim already discussed in the previous chapters, we have qualitatively noticed that this property is an intrinsic feature belonging to the other derivatives as well. Figure 5.2.

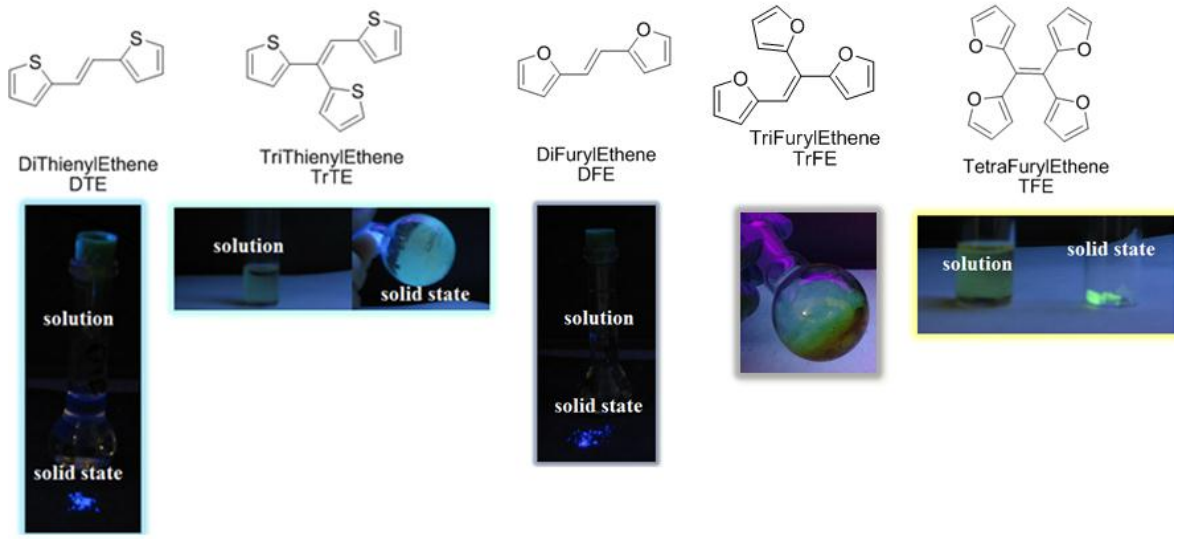

Figure 5.2 Luminescent eighbor of the indicated molecules in solution and solid state under UV-vis light illumination.

Surprisingly, not only the propeller- shape molecules (e.g. TrTE, TTE and TFE) have resulted to be emissive in solid state, but the planar system (DTE and DFE) too. This observation took us by surprise because due to the planarity (preliminary checked in literature [1] and supposed to be) and the presence of heteroaromatic rings, an emission quenching due to effective π-π stacking would have occurred.

In the figure above, it is also possible to see that TrFE derivative is the only member not showing solid-state luminescence property. This molecule has revealed to have a very particular chemical behavior: it shows a high chemical instability despite it is just a member in the middle between the di- and tetra-substituted furan-based ethenes, that are solid and stable at room temperature (see experimental section), It is a yellowish/almost colorless oil at room temperature that become very dark after being exposed to the atmosphere, for just several minutes. Therefore, despite its no-luminescence solid state property, its physical state at room temperature (oil) and the chemical instability, has made impossible to perform the photophysical study on this molecule.
The qualitative observations done on these systems have rendered all of them much more interesting than expected, but in order to confirm and to understand the phenomenon of their luminescence, a detailed study with an exact and precise experimental protocol was needed. Since the AIE phenomenon had been discovered in Prof. Ben Zhong Tang group, there would not have been a better place to deeply investigate the qualitatively observed solid state luminescence than Hong Kong. Therefore, in order to quantitatively prove the AIE effect, the photophysical characterization has been performed at *The Hong Kong University of Science and Technology HKUST*, in Prof. Ben Zhong Tang research group.

5.2 The investigated series and the experimental work-plan

The molecules investigated at HKUST, are shown in Chart 5.1, among them there is not the TrFE, a molecule on which the AIE study was not performed, for the reasons described above.

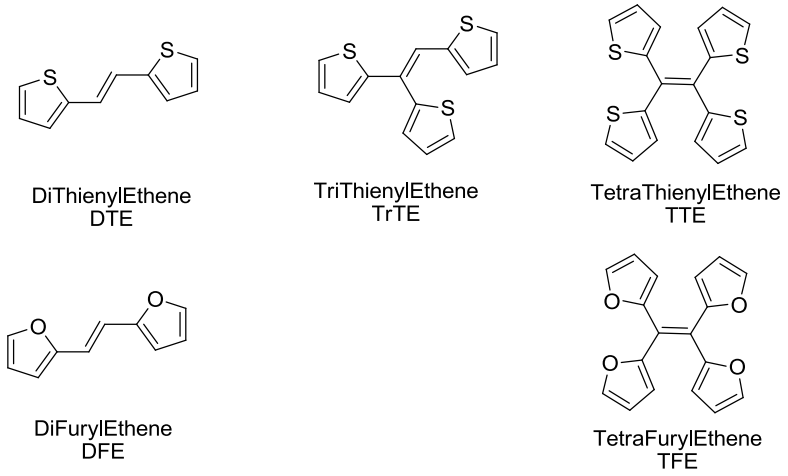

Chart 5.1 The investigated molecules at HKUST.

The study has been performed in a “vertical direction”, as shown in Figure 5.3. At first the tetra-substituted molecules have been investigated and they have been compared with TetraPhenylEthene TPE; later the planar systems have been studied and the DiPhenylEthene DPE has been used as benchmark. In the end the TriThienylEthene has been investigated.

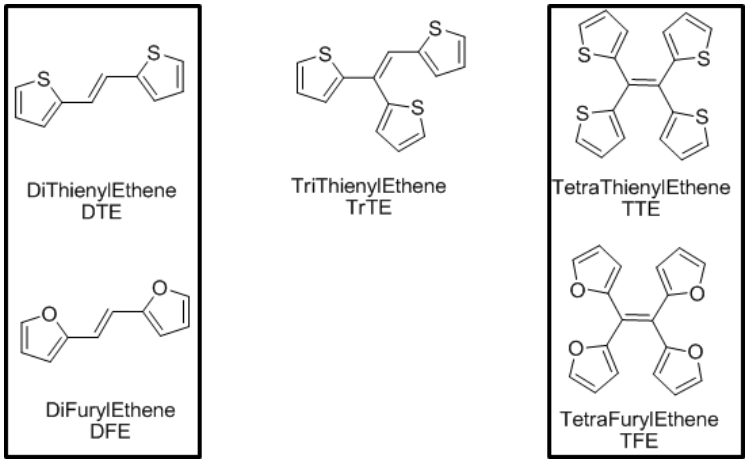

Figure 5.3 The rationalization of the work.

The AIE study has been performed following several precise steps, that can be considered to constitute the AIE experimental protocol:

- photoluminescence study on the molecules of interest, in solution, aggregation and solid state;
- investigation on the working mechanism behind the AIE effect, by performing an internal control approach[i];
- detailed investigation on the crystal structures in order to decipher the emission trend from aggregate to amorphous, to crystal state.

5.3 The study on the tetraheteroarylethenes TTE and TFE

As mentioned above the photophysical properties of the TetraThienylEthenes TTE and TetraFurylEthenes TFE have been compared with the TetraPhenylEthene TPE's. Chart 5.2

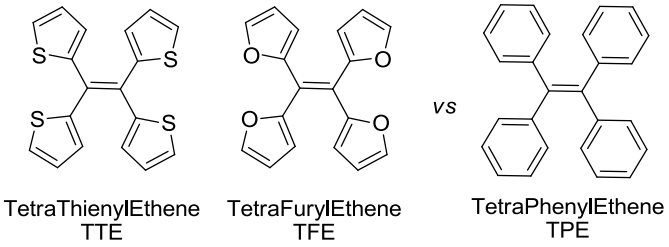

Chart 5.2 Molecular structure of the investigated Tetraheteroaryl- and phenyl- Ethenes.

It has been investigated the photoluminescence in solution, aggregation and in solid state, the single case are discussed below. The absorption spectra (several of them already reported in Literature [2]), are shown in the appendix of this chapter.

[i] As described in the introduction, the internal control is realized when the molecular moieties, supposed to be directly involved in the working mechanism responsible of the emission behavior, are modified (by covalent locking or by introducing hindered substituents) by a chemical approach.

5.3.1 TetraThienylEthene TTE

Similarly to TPE, TTE has also a good solubility in the most common organic solvents such as: THF, DCM, $CHCl_3$; while it cannot be dissolved in water, so in order to study its luminescent behavior in aggregation condition, we have chosen as solvent system the mixture THF/water. As it is described in the experimental section, we have prepared a stock solution of TTE in THF at the concentration of 10^{-4} M, from this sample we have prepared 10 more dilute solutions (10^{-5} M) with increasing water content from 0 to 99% in volume. In Figure 5.4 (A) is reported the photoluminescence spectrum of TTE in each of them, while Figure 5.4 (B) shows the trend of the photoluminescence as a function of the water content.

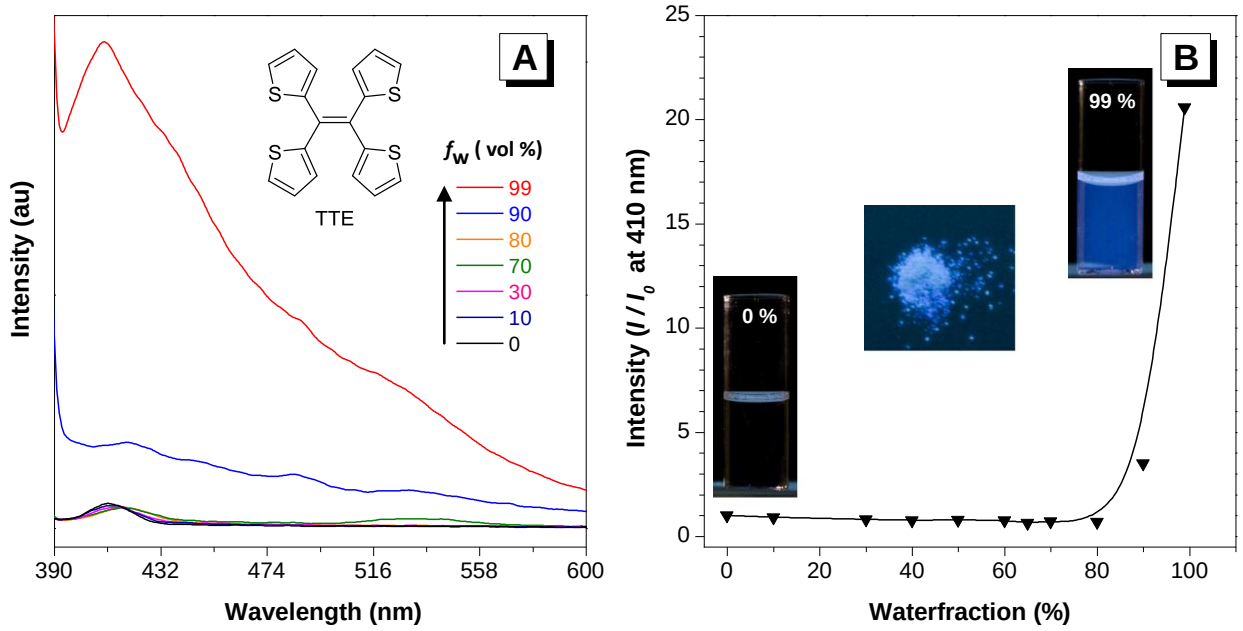

Figure 5.3 (A) The photoluminescence (PL) spectra of TTE in THF and THF/water mixtures with increasing water fractions (f_w) to 99%. (B) Change in PL intensity of TTE at 410 nm versus water fraction in THF/water mixtures. Excitation at 368 nm. Inset: photos of TTE solution at 0% *fw*, powder state and 99% *fw* respectively.

As it is possible to see in the figure above, until the TTE molecules are well solvated in the medium, no emission is observed; with the increase of the amount of water, the solubility of TTE becomes poorer and poorer, and it begins to form aggregates. When this happens (the process starts at around 90% in volume of the water content) the emission starts to increase, and the prominent enhancement of the emission intensity occurs when the amount of water reaches 99% in volume. The maximum PL intensity occurs at 410 nm as wavelength.

It is also remarkable to note that TTE starts to emit light at higher water content than TPE [3] suggesting a better solubility in aqueous medium respect to its phenyl-based counterpart; this is understandable due to the presence of Sulfur atoms that contribute to increase the polarity of the molecule so rendering it more eighbor nt. We have also investigated the emission behavior of the powder and crystal states (Figure 5.4), we have observed that as well as to be emissive even in this two different states, comparing the related PL spectra with respect to the aggregation one, there is also a red shift of the emission value going from the aggregate to the crystal state. Usually the crystallization process should induce a blue rather than red shift [4], insights about the reason of this

behavior have been provided by the crystal structure analysis and they are fully described in the related section discussed below.

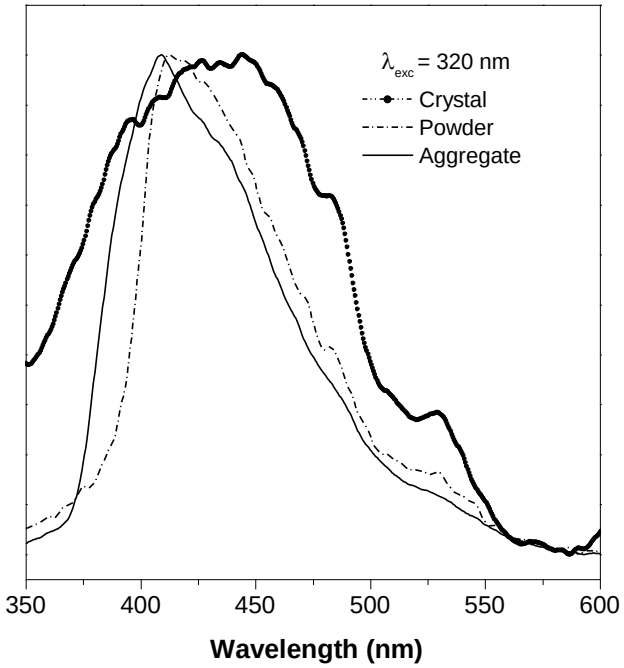

Figure 5.4 The Photoluminescence PL spectrum of TTE in aggregate, amorphous and crystal state. Excitation at 320 nm.

The experimental data just described, confirm that TTE is a AIE luminogen emissive in powder and crystal state too. The working mechanism behind the phenomenon, should be the Restriction of Intramolecular Motions RIM. In particular since TTE is a propeller-shape molecule just as TPE, the mechanism involved should be the Restriction of Intramolecular Rotations RIR[ii][4]. Indeed until the molecules are well solvated in the medium (then they are in solution state), the thienyl rings can freely rotate *via* the single bond by which they are linked to the ethene core; these movements allow to deactivate the excited state by a non-radiative relaxation channel, but upon aggregate formation, due to the physical constraint they become impeded, and since the propeller-shape does not allow a packing as effective and tight as the flat-like ones, π-π stacking interactions does not occur and the only accessible decay pathway remains the radiative one, so the emission is observed.
In order to prove the restriction of intramolecular rotations, the internal control approach has been performed, and the fully locked TTE (fl-TTE) has been synthesized by the photo-oxidation of TTE, obtaining the semi-locked derivative (sl-TTE) as well. Scheme 5.1.

[ii] As described in the introduction (page 18 Fig.1.9) the concept of RIM mechanism includes the RIR and RIV phenomenon. RIR usually occurs in propeller-shape molecules, while RIV usually accounts for the AIE effect in the shell-like systems.

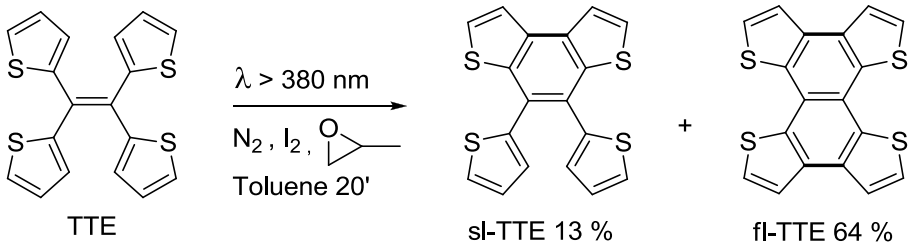

Scheme 5.1 Synthesis of fully-locked and semi-locked TTE.

If in solution the thiophene rings can freely rotate *via* the single bond so making possible the deactivation of the excited state through the non-radiative channel, once they are locked and the rotation becomes impeded, the luminescence behavior should be the opposite: light emission should be observed in solution while quenched in aggregate and solid state due to the π-π stacking interactions occurring as a consequence of the effective π-conjugation and flat molecular structure of the molecule. For this aim we investigated the PL behavior of the sl- and fl-TTE, in the same conditions performed for TTE, so preparing a solution set by using THF/water mixture with increasing amount of water, and a concentration sample of 10^{-5} M.
The PL spectra and the trend of the emission intensity (considered at the main emission peaks) as a function of the amount of water are shown in Figure 5.5 and 5.6 respectively.

Semi-locked TetraThienylEthene, sl-TTE

As shown in the previous reaction scheme, the semi-locked TTE has a very particular structure since it owns a planar moiety to which two thiophene rings are linked. Unfortunately due to the difficulty of purification of this molecule (see experimental section) only a very limited amount, nearly sufficient to perform the photophysical study has been available and no crystal structure has been possible to grow. Starting from the pure THF solution, which is 0% water fraction, two out of three emission peaks are detected in the violet region while the third one is located at 489 nm (Figure 5.5 A). With the increasing of the water fraction, both violet peaks are enhanced in terms of emission intensity, while the fluorescent emission at 489 nm dramatically decreases.
From 0% to 90% water fraction, the decrease of the emission in bluish green area (peak at 489 nm) is a fold change of 0.25 but the peaks below 400 nm get increased with a fold change of 1.47, as it can be clearly seen in Figure 5.5B. Thus the emission trend at 380 and 389 nm is typical of an AIEgen, while the one at 489 nm is typical of an ACQ dye. Considering that the molecular structure contains a planar-like part and two thiophenes supposed to be tilted also respect to the planar moiety for steric reasons, we can suppose that upon aggregation condition, the planar moiety behaves as similarly to ACQ fluorogens, and it is emissive in solution state, but not in the aggregation one due to the strong π-π stacking interactions permissible thanks to the flat geometry, so that it is able to deactivate the excited state energy going through this non-radiative relaxation channel. At the same time, the thiophene rings which were free to rotate via the single bond, in solution conditions, in aggregate state, are blocked in a specific conformation and their movements are not allowed anymore due to the physical constraint, so the RIR mechanism eighb and the eighbor nt of the emission with the increase of the water content is observed.

As a result, sl-TTE has both ACQ and AIE characteristics. It is noteworthy that the phenylbased counterpart does not have this ambivalent behavior, but it shows only one emission peak with an ACQ trend.[5]

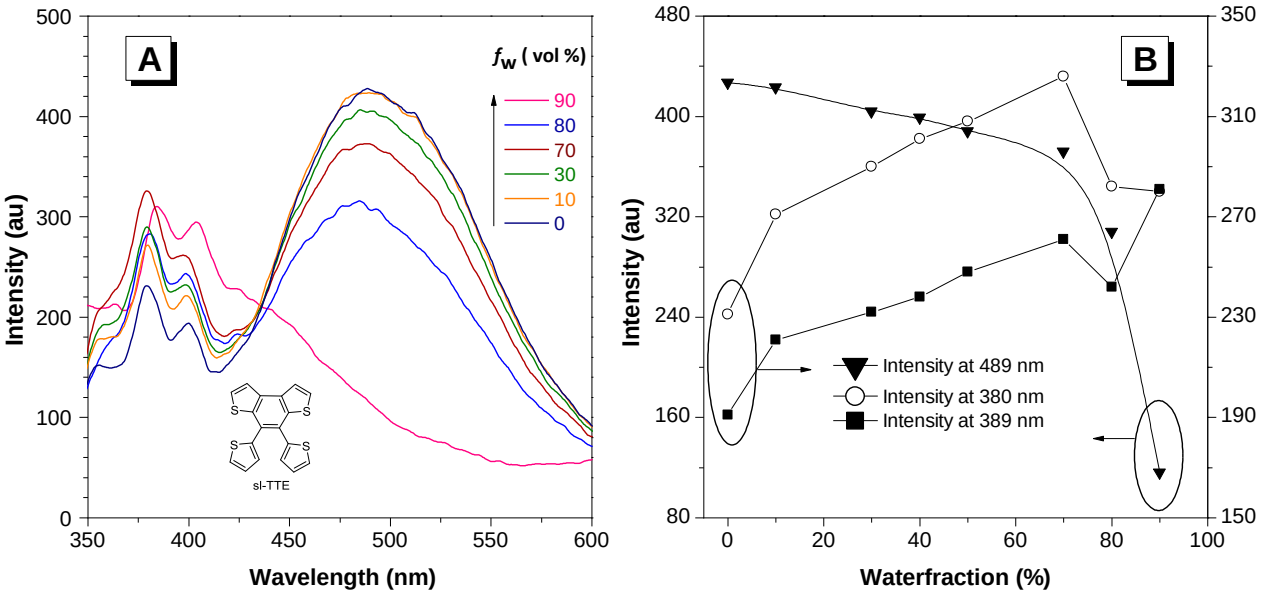

Figure 5.5 (A) The photoluminescence (PL) spectra of sl–TTE in THF and THF/water mixtures with increasing water fractions (f_w) to 90%. (B) Change in PL intensity of sl–TTE at: 489 (ACQ behavior), 389 and 380 nm (AIE behavior) versus water fraction in THF/water mixtures. Excitation at 323 nm.

Fully-locked TetraThienylEthene fl-TTE

Contrarily to TTE and sl-TTE, fl-TTE should have a full-planar structure, [4] unfortunately even in this case, despite several attempts, the crystal has not been obtained, but the insight is confirmed from the reference paper published in 1996.[6]

The study on the fully-locked derivative has been performed by using the same methodology described so far. The PL spectra and the emission trend, as a function of the water content, are reported in Figure 5.6. With the increasing of the water fraction, the emission regularly decreases and the maximum emission peak is red shifted. This behavior is a typical one of an ACQ dye; the planar structure, and the effective π-π stacking typical of condensed aromatic hydrocarbons, can induce the dimer formation, upon aggregation, so quenching the emission and at the same time shifting the emission peak at higher wavelengths (visible region of the spectrum) as a consequence of the narrower energy gap owed to the dimers formation. Thus, fl-TTE is emissive in solution state with two peaks corresponding to the fine structure but not in aggregate one, therefore it is a typical ACQ molecule.

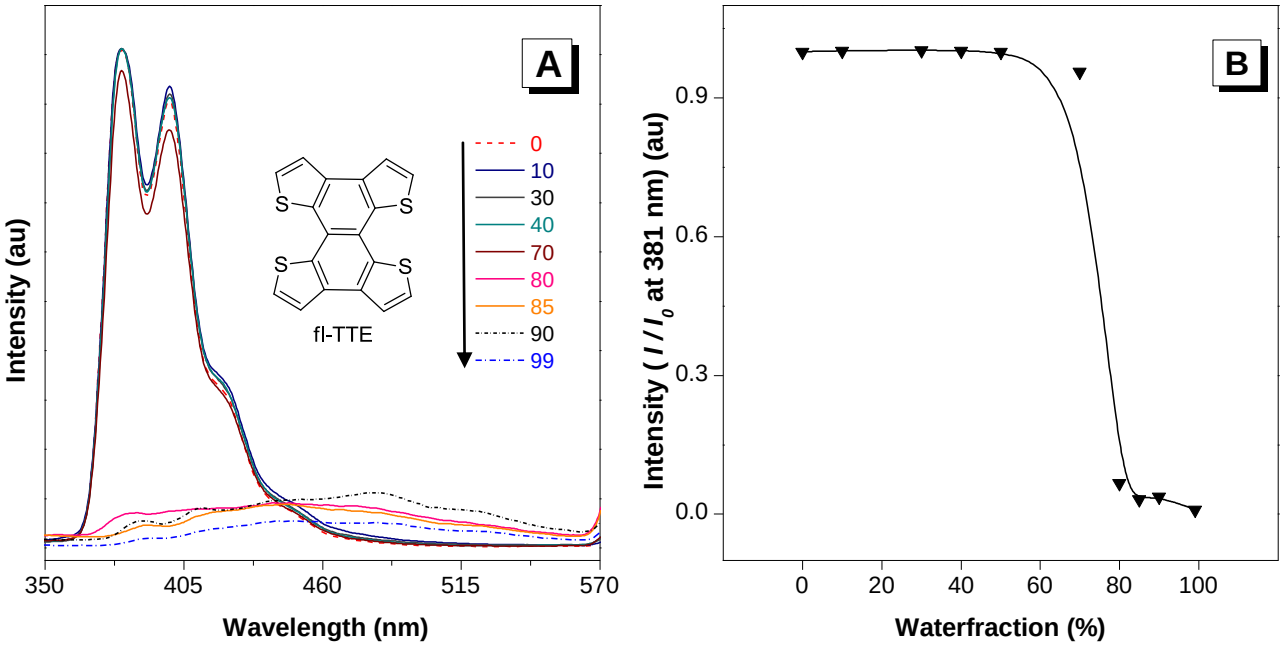

Figure 5.6 (A) The photoluminescence (PL) spectra of fl–TTE in THF and THF/water mixtures with increasing water fractions (*fw*) to 90%. (B) Change in PL intensity of fl–TTE at 381 nm versus water fraction in THF/water mixtures. Excitation at 299 nm.

The behavior in aggregation condition of TTE and its derivatives observed so far, can be summarized as shown in Figure 5.7.

Figura 5.7 Trend of the AIE phenomenon as a function of the molecular structure.

TTE is AIE, sl-TTE is AIE and ACQ while fl-TTE is only ACQ. This trend proves that the RIR phenomenon mechanistically accounts for the AIE effect observed in TTE, and it is also a function of the molecular structure since it can be modulated by internal control approach selectively locking the free rotatable rings of the molecule.

The photophysical features are summarized in Table 1 where the TPE data have been indicated as benchmark. Due to the presence of the sulphur atoms that are well known as not effective fluorescence species, the quantum yield of TTE is not as higher as the TPE one; the lifetime value confirms that the photoluminescence emission is the fluorescence. Concerning the fully-locked TTE, although it has revealed to be an ACQ dye, the lifetime value reported in Table 1, indicates that it owns a certain emission in powder, even if the corresponding quantum yield is 0.1%. This aspect will be discussed in the paragraph dedicated to the ACQ systems.

Table 1 Photophysical data of the investigated molecules and of TPE indicated as benchmark.

Luminogen	λ_{ab} * /nm	λ_{em} /nm			ΔE /eV	AIE or ACQ	**αAIE	$\Phi_{F,A}$ / %	τ / ns
		Aggregate	Powder	Crystal					
TPE	360	462	447	450	3.45	AIE	344	23[e]	1.29[e]
TTE	413	409	413	444	3.01	AIE	20	2.6[e]	0.47[e,f]
sl-TTE	359	380[a,e], 389[b,e], 489[c,g]			3.46	AIE and ACQ	1.47	n.a.	n.a.
fl-TTE	382	381[g]			3.25	ACQ	0.1	0.1	0.94

[i]Abbreviation: λ_{ab} = absorption maximum in THF; λ_{em} = emission maximum, ΔE, Energy gap calculated by UV-Vis spectrum, $\Phi_{F,A}$ = absolute fluorescent quantum yield measured by a calibrated integrating sphere; ,* onset value, **αAIE = the ratio between the emission intensity at 99% and 0% of water fraction (i_{99}/i_0),τ = lifetime, [a,b] AIE, [c]ACQ, [d]aggregation state, [e]amorphous, [f]average from two different samples, [g]solution state.

Looking at the value reported in Table 1, TTE has a maximum absorption at higher wavelength with respect to TPE, as a consequence, the optical energy gap (estimated by knowing the λ), is lower for TTE respect to TPE. This is in agreement with the presence of the thiophene rather than phenyl rings that contributes to making the system electronricher. These results match the electrochemical one from which the same observations both in terms of oxidation and reduction potentials and experimental HOMO and LUMO values, have been found out.
Considering again the emission trend of TTE going from the aggregate to the Crystal state shown in Figure 5.4, as mentioned above, it is noteworthy that the emission is red shifted going from the aggregate to the crystal, the opposite trend is observed in TPE case. The value and the relative trend is further highlighted in Table 2:

Table 2 main photophysical value of TTE and TPE (benchmark) in the three aggregation states, the blue and red arrows indicate the blue and red emission shift respectively.

Luminogen	λ_{ab} /nm	λ_{em} /nm		
		Aggregate	Powder	Crystal
TPE	308	462 →	447 →	450
TTE	364	409 →	413 →	444

Therefore two questions spontaneously arise:

1) if TTE owns a more effective conjugation and lower energy gap than TPE, why its emission value in aggregate state (as well as powder and crystal) is lower than TPE in the same conditions?
2) Why in TTE a red-shift of the emission wavelength occurs, going from the aggregate to the crystal state, while the opposite trend is observed in TPE?

The answers to these two questions have been found out through meticulous analysis of the TTE crystal structure, (and of TPE as a comparison as well), discussed in the next paragraph.

Crystal structure investigation

In Figure 5.8 are shown the ORTEP picture of TTE and TPE [7] reported as benchmark, in which is highlighted the length of the double and adjacent single bond is highlighted. Both molecules have a propeller shape and as it is understandable from the numeration of the rings and the value of the dihedral angles that exists between each ring and the double bond plane, (reported in Table 3), TTE structure is symmetric and the thiophene rings are equal two by two, while in TPE one, all rings are different and have their own orientation respect to the double bond plane. In the Figure 5.9, is represented how each dihedral angle (both in TTE and in TPE) has been calculated by owning the CIF file of the single crystal, while the Figures 5.10 and 5.11 provide a better understanding of the ring orientations respect to the double bond.

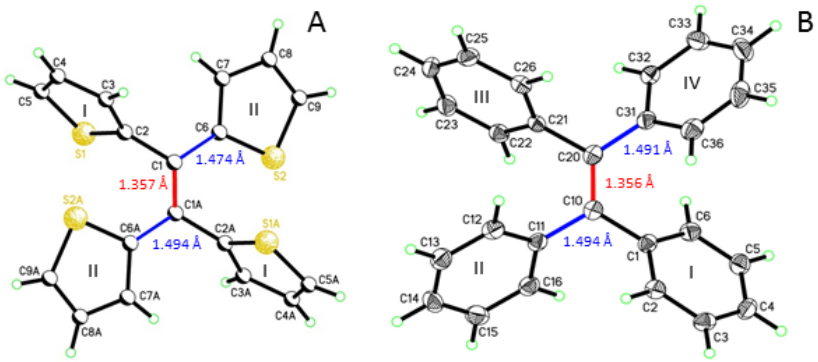

Figure 5.8 ORTEP figures of TTE and TPE, in which are highlighted the double and α–bond lengths.

Table 2 Dihedral angle of TTE and TPE

Dihedral Angle *		
Molecule / Ring	TTE	TPE
I	84.72	45.50
II	24.61	47.33
III	/	44.59
IV	/	56.37

* Angle between the plane of each ring and the one of the double bond.

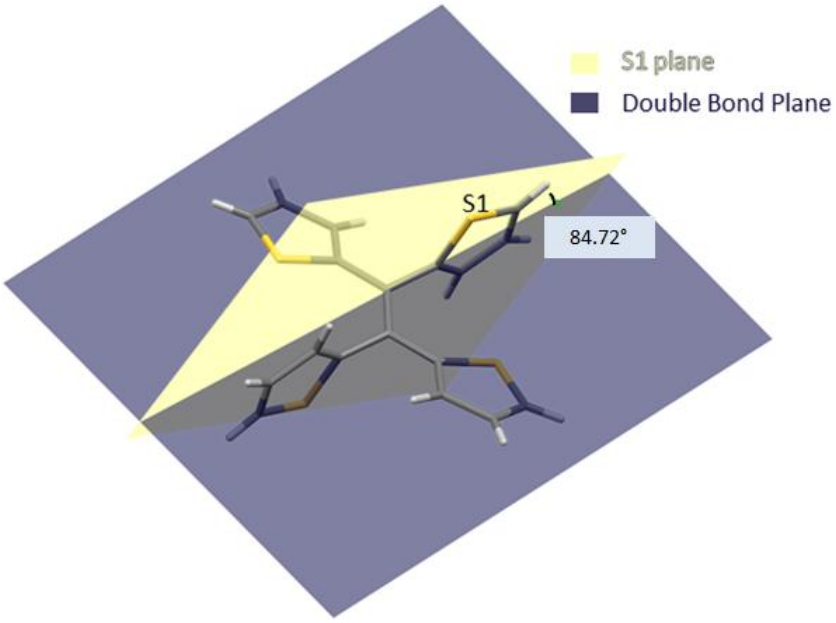

Figure 5.9 Dihedral angle between the S1 ring plane and the double bond one, in TTE single-crystal.

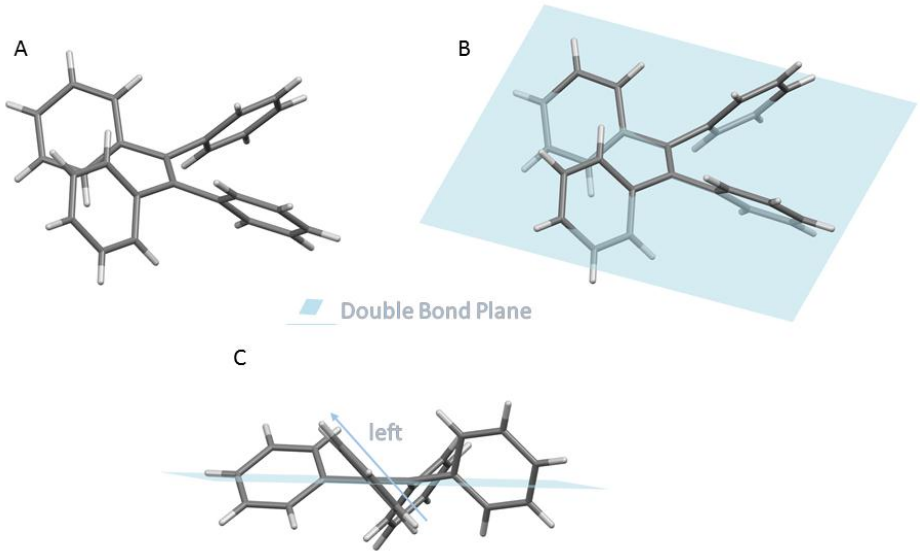

Figure 5.10 Single-crystal of TPE [7]. (A) top view. (B) top view and (C) side view of ring direction respect to the double bond plane.

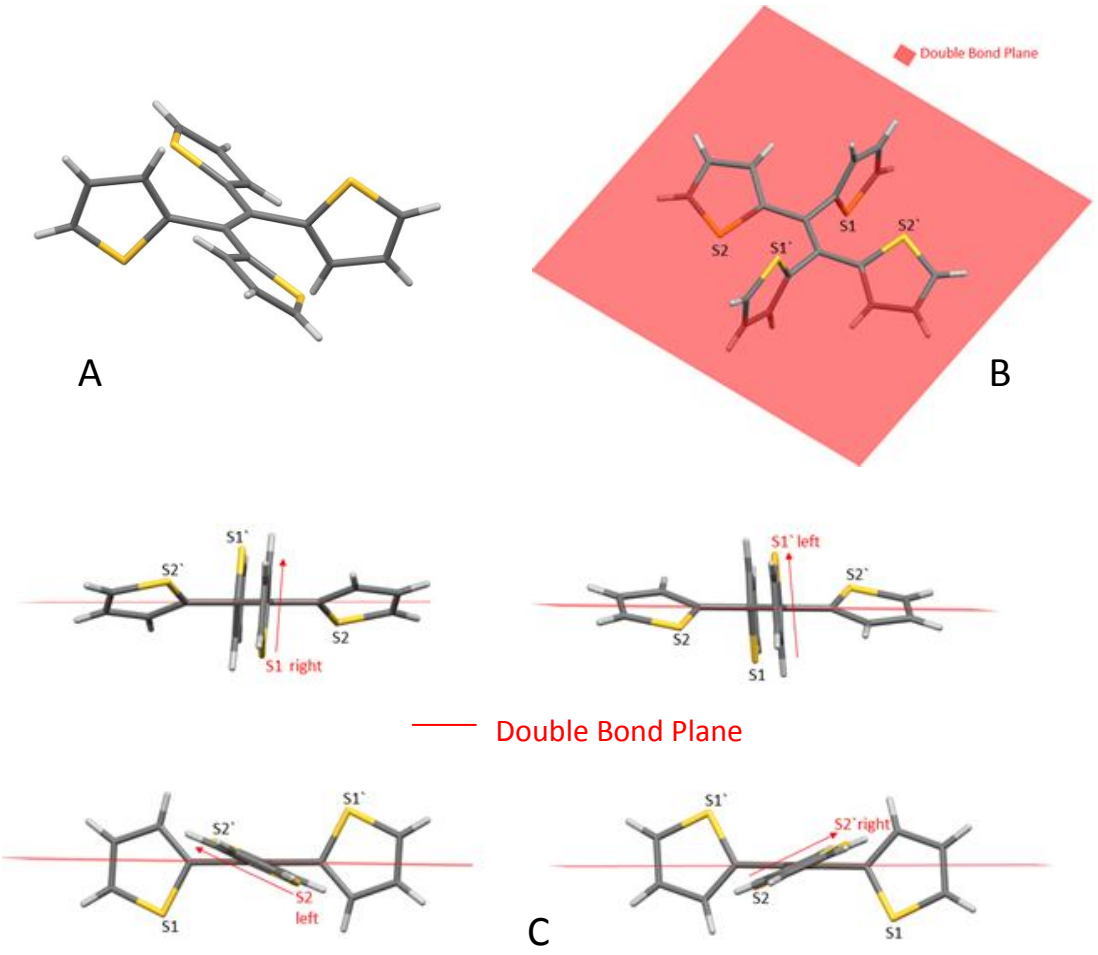

Figure 5.11 Single-crystal of TTE. (A) top view of the asymmetric unit (B) top view and (C) side views of ring direction respect to the double bond plane.

While in TPE crystal all rings are oriented[iii] towards the left (left-handed) respect to the double bond, and own an average dihedral angle of 48°, in TTE crystal, two of the thiophene rings are almost perpendicular to the ethene core (84.72°) whereas the other two, are almost coplanar (24.61°).

Respect to the double bond plane, the perpendicular rings, S1 and S1', are alternatively right-handed and left-handed individually, similarly the other two rings (the almost coplanar ones) S2 and S2' are left-handed and right handed respectively. Furthermore, considering the orientation of the single thiophene atom respect to the double bond plane, within each thiophene ring couples, it is possible to individuate a reciprocal *trans*-like orientation (*e.g.* S1 downwards *vs* S1' upwards and S2 downwards *vs* S2' upwards). As a consequence of this kind of configuration, a possible chiral property is lost within each thiophene couple and the overall structure results to be achiral.

[iii] The orientation is evaluated considering the double bond to be perpendicular respect to the reader's vision, and observing towards which side the ring is inclined.

Therefore on the contrary of TPE, in which all the rings contribute to the overall π-conjugation, in TTE crystal, only two of the four rings are conjugated with the ethene core, since the other two, due to the high dihedral angle value, are excluded from the conjugation. Even if we exactly don't know how the molecules are oriented when they form the aggregates, the crystal structure provides a very good insight about the possible arrangement of the molecules in aggregate and in general in solid state condition, thus replying to the first of the two question put at the end of the previous paragraph, it is possible to sustain that, TTE has a lower emission value respect to TPE in aggregate and solid state, because what emits, (the real chromophore) is not the whole molecular structure, but only the di-thienylethene core, constituted by the two thiophene rings (S2/S2') almost aligned, and then, conjugated with the double bond. As proof of this concept, it is noteworthy to already report in this paragraph that the emission value of DiThienylEthene DTE in aggregation condition is 402 nm. (see paraghraph 5.4.1 at page 117).
In addition the energy gap of TTE and TPE, both optical and electrochemical, and the wavelength corresponding to the maximum absorption, have been measured in solution state, where the molecule, as a consequence of its solubility, is not forced to acquire the configuration described above, because its rings are free to rotate, so that each of them can equally contribute to the overall electronic conjugation, this is what happens even for TPE, but since the thiophene rings are intrinsically electron-richer than the phenyl one (due to the heteroatom), the energy gap is higher. As further proof of concept an absorption spectrum of TTE and TPE in aggregate or solid state would have been useful. Thus we can image that if in TTE crystal the two thiophene rings S1/S1' had been less tilted out, they would have contributed as well, to the overall conjugation and the trend of the energy gap between TTE and TPE already observed and evaluated in solution, would have been the same in the crystal state too.

The evaluation of the *intra*- and *inter*- molecular interactions in the crystal structure have provided us with a highly useful tool to understand and interpret the emission trend in TTE, that occurs going from the aggregation to the crystal state, and its difference respect to TPE one. We have measured the CH---π interactions in TTE crystals and we have compared them with TPE ones [7], in addition, due to the presence of the sulphur heteroatom, it has been possible to catch CH---S interactions in TTE crystal as well. Figures 5.12-14.

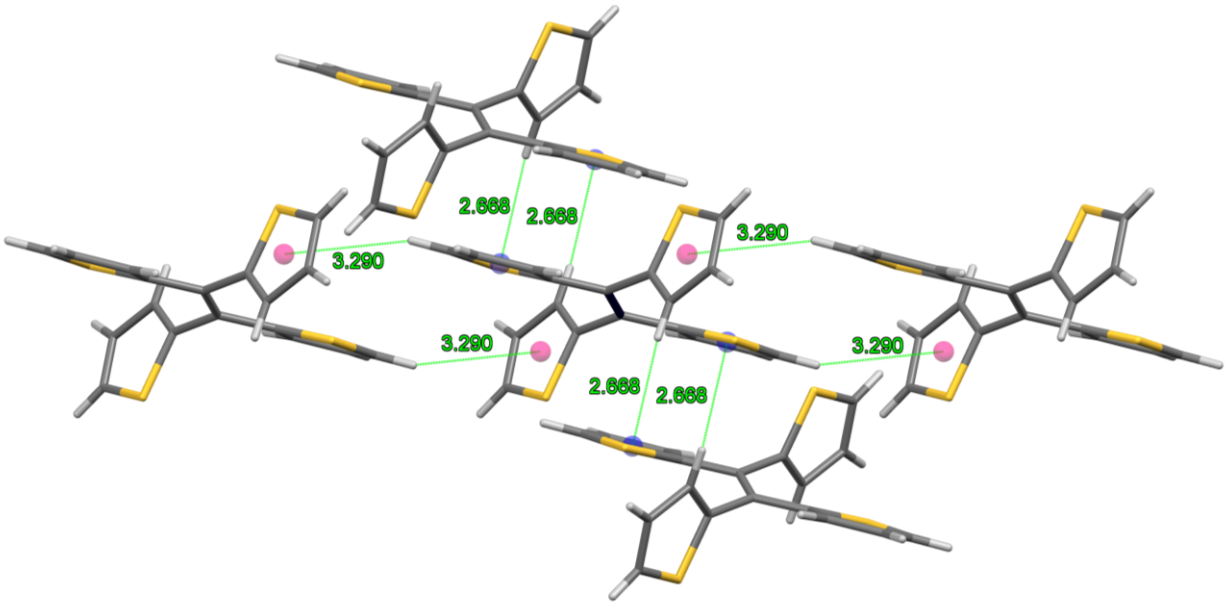

Figure 5.12CH···π interactions in TTE crystal.

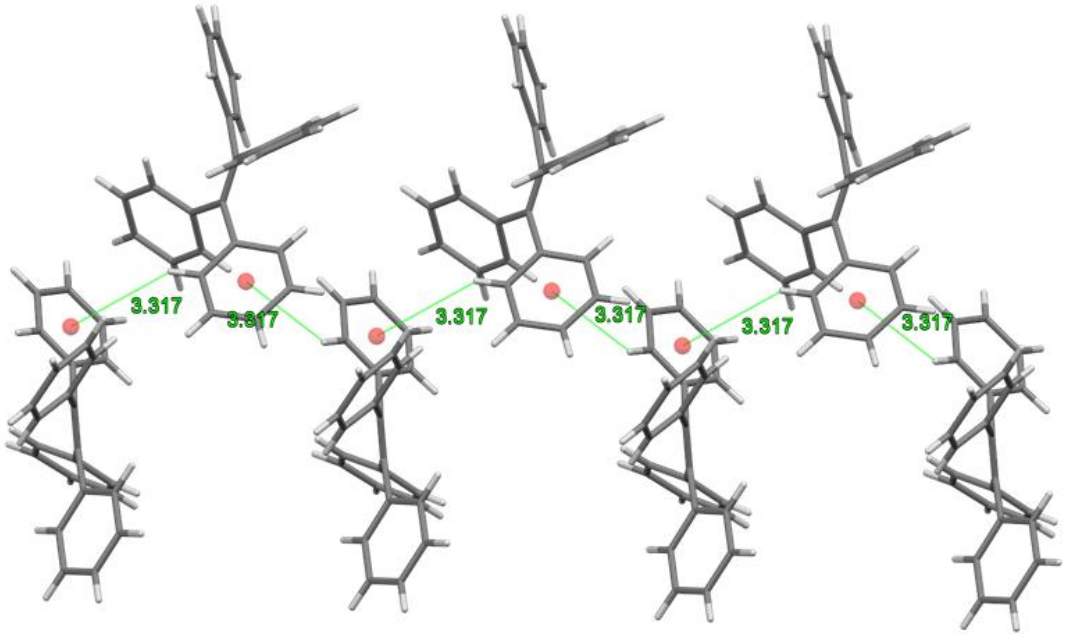

Figure 5.13 CH···π interactions in TPE crystal.

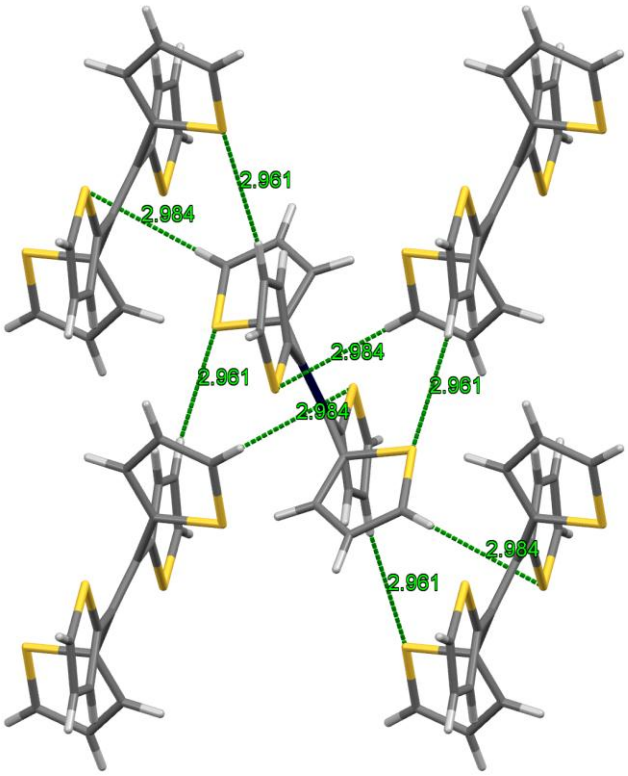

A

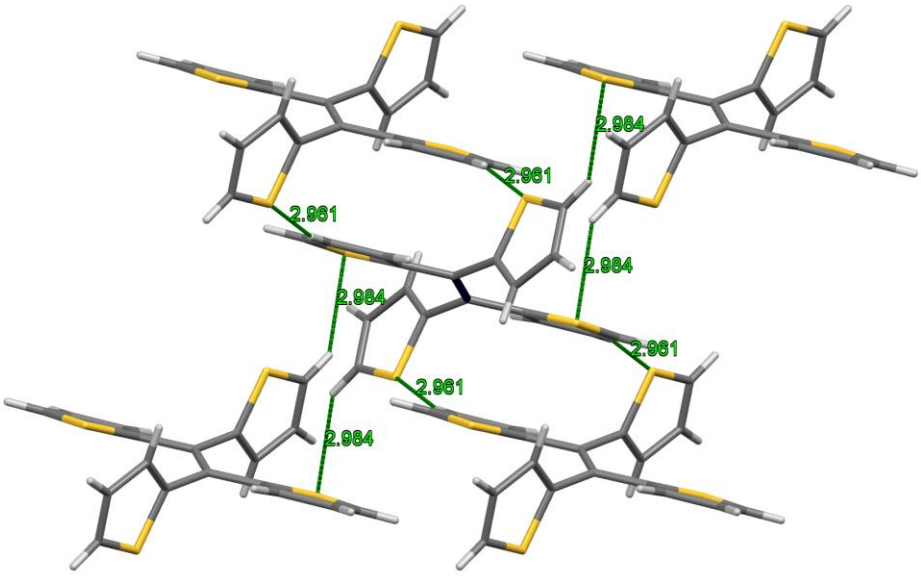

B

Figure 5.14 (A) and (B), Different views of CH···S interactions in TTE crystal.

While in TPE only CH---π interactions exist (in Figure 5.13, we have provided just one type of interaction, since there are four types, one for each ring), and they have an average length of 3.5 Å, in TTE crystal, thanks to the symmetry of the structure, we have found out only two different kind of CH---π contacts. In order to better comment the Figure 5.12, it is useful to label the H atom of the thiophene ring, as reported in Figure 5.15.

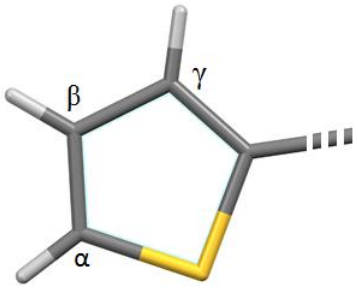

Figure 5.15 One of the thiophene rings in TTE crystal structure.

As it is possible to decipher in Figure 5.12, each "α" H-atom of the "planar" rings (the ones with the blue centroid) points toward the center of the "perpendicular" thiophene ring of the neighbor TTE, and the corresponding distance is equal to 3.290 Å. Similarly each "γ" H-atom of the "perpendicular" rings (those with the pink centroid), points towards the center of the "planar" ring of the neighbor TTE, the distance is equal to 2.668 Å. All these interactions occur intermolecularly.
Similar considerations can be followed to comment the the CH---S interactions, shown in Figure 5.14. Considering again the nomenclature shown above, we can observe that each H-atom in α-position in the "perpendicular" rings, interacts with the Sulfur atom of the "planar" ring of the neighbor molecule (distance = 2.984 Å), and each "β" H-atom of the "planar" rings interacts with Sulfur of the perpendicular thiophenes belonging to the neighbor molecule (distance 2.961 Å); even in this case all these contacts are only intermolecular and this is understandable because of the mutual perpendicularity of the two thiophene ring couples.
The non-covalent interactions just described contribute to the stiffening of the molecule in the crystal state so preventing any movements at molecular level – *e.g.* rotations – (that could allow the occurring of the non-radiative relaxation channel by which the excited state could be deactivated) making possible the light emission in the crystal state possible. Nevertheless these kinds of contacts do not allow to explain why an emission red-shift occurs in TTE going from the aggregation state to the crystal one. Being inspired from a previous work [8] performed in Professor Tang's group according to which, a polymer constituted by no π-conjugated moieties, resulted to be emissive due to the intermolecular interactions between oxygen atoms (belonging to carbonyl units constituting the polymer chain), we have measured the possible interactions between the Sulfur atoms as well. These distances are shown in Figure 5.16 and 5.17.

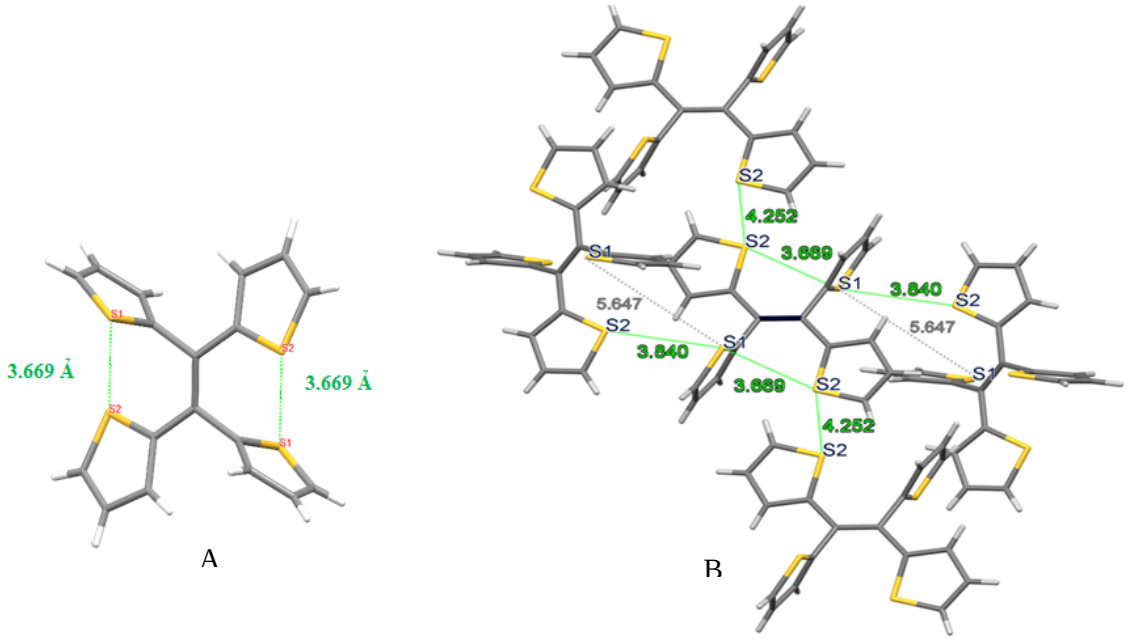

Figure 5.16 (A) Intramolecular S---S interactions; (B) S---S Interactions estended to the nearest neighbours. The most significant are reported in green, and occur between S2-S1 (both *intra*- and *inter*- molecularly) and S2-S2 (intermolecularly).

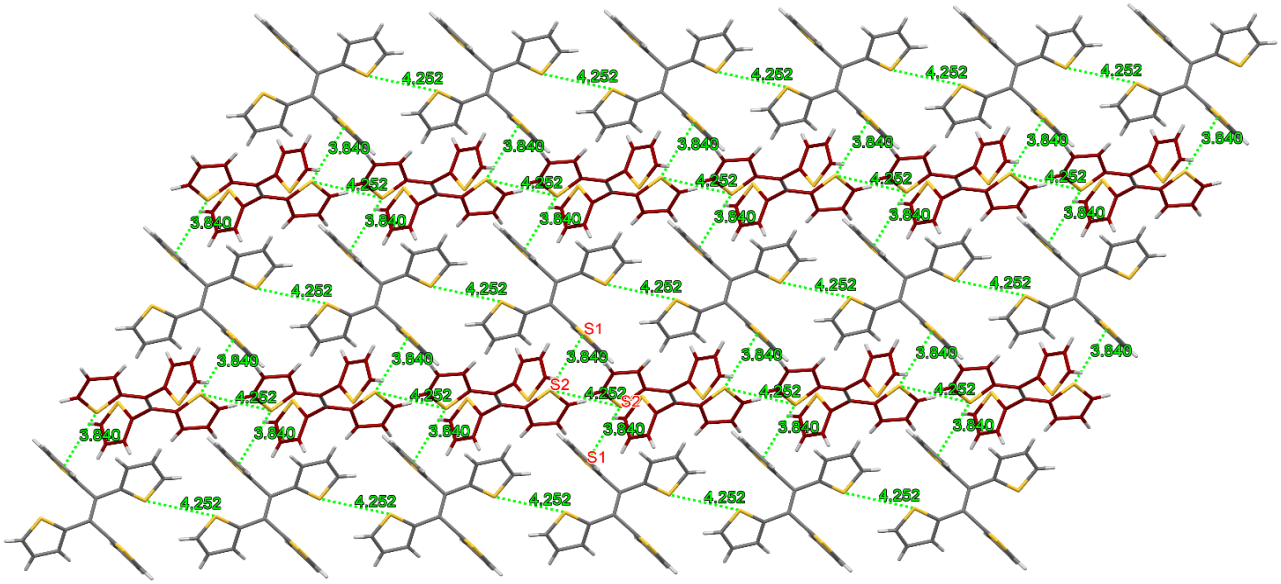

Figura 5.17 Intramolecular S---S interactions network in TTE crystal.

In TTE crystal there are two types of S---S interactions: the intramolecular ones between the sulphur atoms of each ring (S1---S2) in which the distance, 3.669 Å, is the same within each couple (Figure 5.16A), due to the symmetry of the structure; the intermolecular ones between S1 and S2 (3.840 Å), as well as S2 and S2 (4.252 Å) of each ring and that one of the nearest eighbor (Figure 5.16B). Considering to extend this network in space, it is possible to observe in Figure 5.17 that the Sulfur to Sulfur interactions abundantly exist in TTE crystal packing, and they are able to intermolecularly extend the original π-conjugation through space, so allowing the formation of clusters that are electron-richer and the overall π-conjugation is more effective; as a consequence,

they own a lower energy gap. These insights fully explain why there is a red shift emission going from the aggregate to the crystal state in TTE system. With the increasing of the rigidification, or molecular stiffening, that reaches its maximum in the crystal state, the Sulfur atoms tend to acquire the orientation just described, and as a consequence they are more and more oriented towards each other with the increasing of the rigidification degree, the strongest interaction will be experienced once the crystal state will have been formed. In TPE crystal, due to the absence of the heteroatoms, only the CH---π interactions exist, but as discussed before, they mainly contribute to the rigidification of the structure and as proven, they do not provides a better conjugation efficiency as much as the interactions between the sulfur lone pairs. All interactions measured in TTE crystal are reported in Table 3.

Table 3 non-covalent iinteractions in TTE and TPE crystals.

Luminogen	**Interaction**	**Distance / Å**	**Type of interaction**
TPE	CH---π	3.317	intermolecular
TTE	CH---π	2.268; 3.390	intermolecular
	CH---S	2.961; 2.984	intermolecular
	S---S	3.669 3.840 4.252	intramolecular intermolecular intermolecular

As a result of the discussion emerged from the data collected, it is possible to confirm that TTE molecule is a classic AIE luminogen, (classic because his mechanism is due to the RIR phenomenon) owning clusteroluminogenic features too, since the formation of clusters is allowed in the crystal state thanks to the S---S interactions.

5.3.2 TetraFurylEthene TFE

The study on TFE, has been conducted in the same way as the one on TTE. Thus the emission behavior has been investigated in aggregate state, as well as in the solid one. Like TTE, even TFE is soluble in the most common organic solvents but not in water, so we have chosen again the THF/water mixture to study the aggregation behavior, in order to have the same term of comparison with respect to TTE as well. In Figure 5.18 is shown the emission trend of TFE in THF and in THF/water mixtures with increasing amounts of water. In the Figure 5.18A is reported the PL spectra, while Figure 5.18 B shows the emission trend as a function of the water content. Considering the figure A, the tiny peak perceivable at low wavelengths, does not belong to the molecule, but it is a Raman peak (in jargon defined as "ghost peak") that comes from the solvent, indeed it disappears when the amount of water becomes higher than 90%. Unlike TTE, TFE is a little bit emissive in the pure THF, however it really emits only when a large amount of water is added; since in this condition it is not soluble anymore and forms aggregates, (as perceivable even in the photographs inset), its behavior is the typical one of an AIE luminogen.

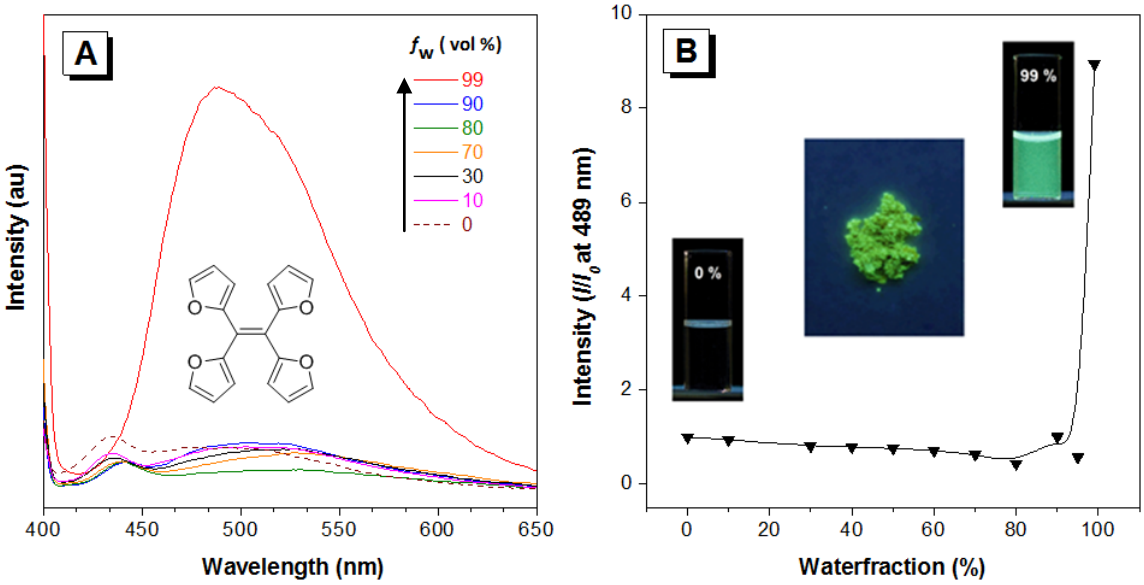

Figure 5.18 (A) The photoluminescence (PL) spectra of TFE in THF and THF/water mixtures with increasing water fractions (*fw*) to 99%. (B) Change in PL intensity of TFE at 489 nm versus water fraction in THF/water mixtures. Excitation at 387 nm.

Like TTE, recording the PL spectra in powder and crystal state, TFE results emissive and the emission peak is even in this case red-shifted going from the aggregate to the crystal state. (Figure 5.19) Before investigating the reason behind this trend, that should be similar to the TTE one, it is firstly necessary to understand the mechanism behind the TFE emission in aggregate state, since TFE is a propeller-shape molecule, the working mechanism behind its AIE phenomenon, should be, the Restriction of Intramolecular Rotation RIR for it too. For this reason the fully-locked TFE by photo-oxidation of TFE, has been synthesized.

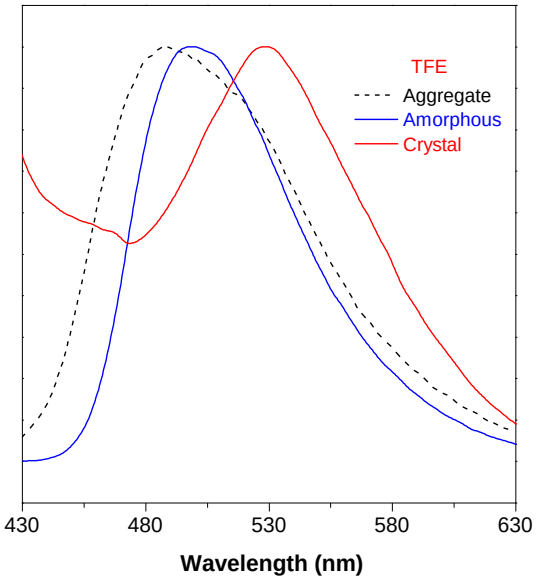

Figure 5.19 The photoluminescence (PL) spectrum of TFE in aggregate, amorphous and crystal state. Excitation at 387 nm.

Fully-locked TetraFurylEthene fl-TFE

TFE is at present a molecule not reported in literature and conceived for the first time during this PhD thesis, this is why even its oxidized form is yet unknown. By exploiting the expertise acquired about the photolysis of TTE, we have reproduced the same pathway also for TFE, obtaining in a low yield the product of interest. Scheme 5.2.

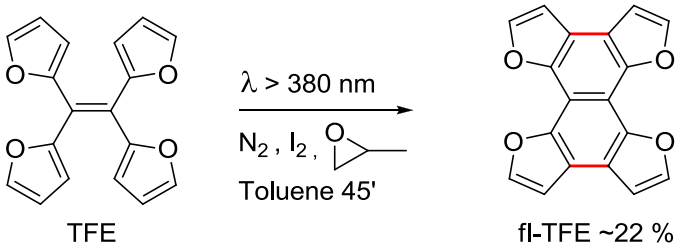

Scheme 5.2 Synthesis of fl-TFE by photo-oxidation of TFE

The procedure needs to be optimized, especially for what concerns the work-up conditions.
Since the furyl rings are locked in this structure, similarly to what happens in fl-TTE case, when the molecule is dissolved in pure organic solvent (*e.g.* THF) upon excitation, it should emits, because the heteroaryl rings are locked and not free to rotate anymore, and the locked molecule is supposed to be flat[iv], like its thiophene-based counter-part; in this condition (solvatation) the molecule is an isolated species only surrounded by the solvent system, hence it cannot effectively interact with the other molecules and the only available relaxation pathway remains the radiative one. In aggregation state (high amount of water) the emission will be quenched due to the effective intermolecular π-π

[iv] When these experiments have been performed the crystal structure were not available yet, this measurments is currently in progress.

interactions. This predictions have resulted to be true, as shown in Figure 5.20 in which the PL spectra of fl-TFE in THF/water mixture (with increasing amount of water) and the emission trend as a function of the water content, are reported.

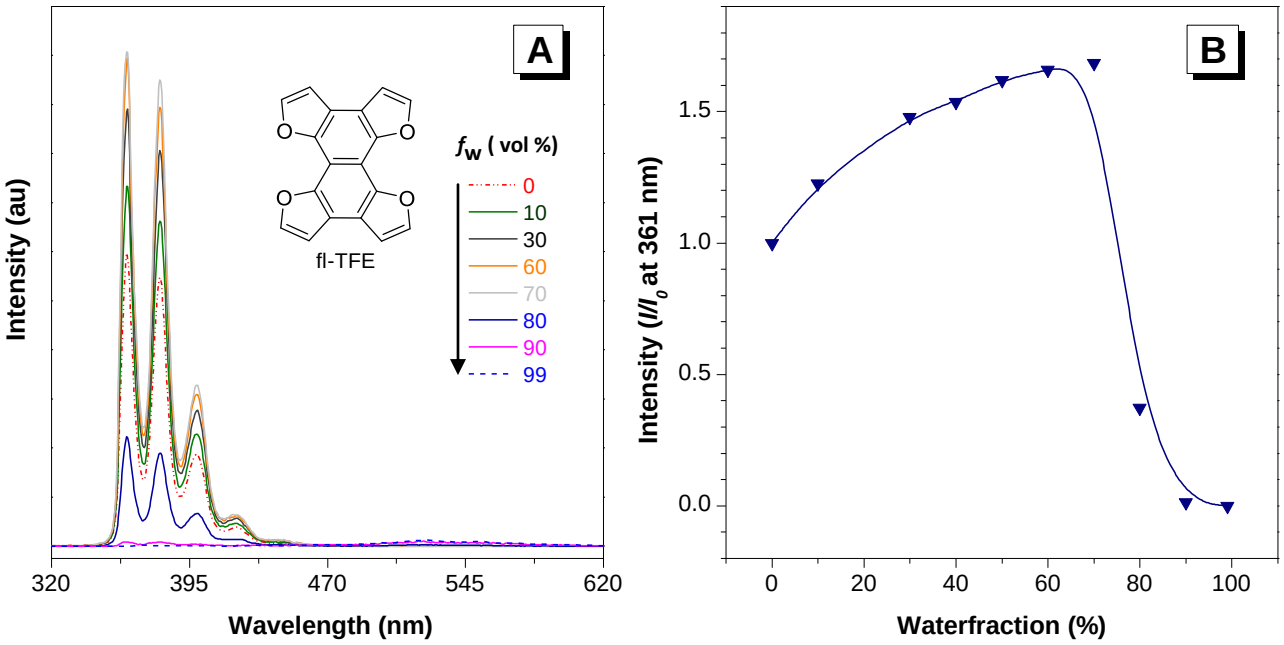

Figure 5.20 (A) The photoluminescence (PL) spectra of fl-TFE in THF and THF/water mixtures with increasing water fractions (*fw*) to 99%. (B) Change in PL intensity of fl-TFE at 361 nm versus water fraction in THF/water mixtures. Excitation at 274 nm.

Therefore, fl-TFE is emissive in solution state with three peaks corresponding to the fine structure, but not in aggregation one, thus it is a typical ACQ molecule. The photophysical features are reported in Table 4, among them unfortunately the quantum yield Φ and the lifetime τ of fl-TFE, are not available yet, and are currently in progress.

Table 4 Photophysical data of the investigated molecules and of TPE indicated as benchmark.

Luminogen	λ_{ab*} /nm	λ_{em} /nm			ΔE /eV	AIE or ACQ	αAIE*	$\Phi_{F,A}$ /%	τ /ns
		Aggregate	Powder	Crystal					
TPE	360	462	447	450	3.45	AIE	344	23[a]	1.29[a]
TFE	439	489	499	532	2.83	AIE	8.9	11[a]	1.58[a]
fl-TFE	382		361[b,c]		3.25	ACQ	$1x10^{-4}$	n.a.[c]	n.a.[c]

[i]Abbreviation: λ_{ab} = absorption maximum in THF; λ_{em} = emission maximum, ΔE, Energy gap calculated by UV-Vis spectrum, $\Phi_{F,A}$ = absolute fluorescent quantum yield measured by a calibrated integrating sphere; *onset value, **αAIE = the ratio between the emission intensity at 99% and 0% of water fraction (i_{99}/i_0),τ = lifetime, [b] solution state, [c] this molecule results a little bit emissive in powder, this aspect is described in a paragraph apart, [d]not available yet.

The quantum yield of TFE is just 11% , and it is higher than TTE (see Table 1) but lower than TPE, this effect even in this case could be ascribable to the presence of the heteroatom. The lifetime value proves that even in TFE case, the PL emission is the fluorescence.

TFE (similarly to TTE) is intrinsically electron-richer than TPE due to the Heterocycles. Its better π-conjugation has been proved by electrochemical approach, and the optical data reported in Table 3 confirm the electrochemical results, since TFE has a higher λ_{ab} and lower optical energy gap respect to TPE. Looking to the emission value in aggregate and solid state, it is possible to observe that contrarily to what happens in TTE case (where the better conjugation is not mirrored in aggregate and solid state due to the tendency of the thiophene rings to acquire a tilted conformation in a more rigid molecular context) TFE owns a redder emission respect to TPE in all of the three aggregation states; this suggests that contrarily to TTE, all furan rings should take part to the overall effective conjugation even in the more rigid molecular environment. Moreover even in TFE case, there is a red-shift of the emission peak going from the aggregate state to the crystal one. The trend is highlighted in Table 5.

Table 5 Main photophisycal value of TFE and TPE (benchmark) in the three aggregation states, the blue and red arrows indicate the blue and red emission shift respectively.

Luminogen	λ_{ab} /nm	λ_{em} /nm		
		Aggregate	Powder	Crystal
TPE	308	462	447	450
TFE	364	409	413	444

The analysis on TFE crystal structure will provides an answer to these experimental evidences.

Crystal structure investigation

In Figure 5.21 are shown the ORTEP picture of TFE and TPE [7] reported as benchmark, in which are highlighted the length of the double and of the adjacent single bonds. As understandable from the pictures and from the value reported in Table 6, both molecules have a propeller shape and TFE, as similarly to TPE but contrarily to TTE, does not show a symmetric structure, since all rings are differently oriented and have their own dihedral angle respect to the double bond plane. The dihedral angles, similarly to TTE and TPE cases, have been calculated measuring the angle between the plane of each ring and the one of the double bond. (An example has been provided in Fig. 5.9).

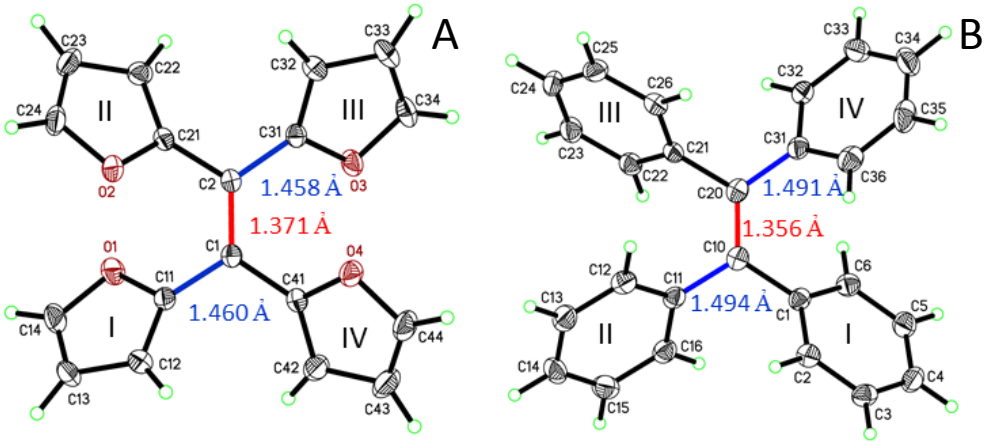

Figure 5.21 ORTEP pictures of (A) TFE and (B) TPE (benchmark) crystal structure, in which are highlighted the double and α–bond lengths.

Table 6 Dihedral Angle of TFE and TPE indicated as benchmark.

Dihedral Angle *		
Molecule / Ring	TFE	TPE
I	37.91	45.50
II	33.97	47.33
III	30.44	44.59
IV	30.50	56.37

* Angle between the plane of each ring and the one of the double bond.

Analyzing the TFE crystal structure we have found out that in the asymmetric unit two different isomers (among which one shows disorder as well) exist, they are shown in Figure 5.22.

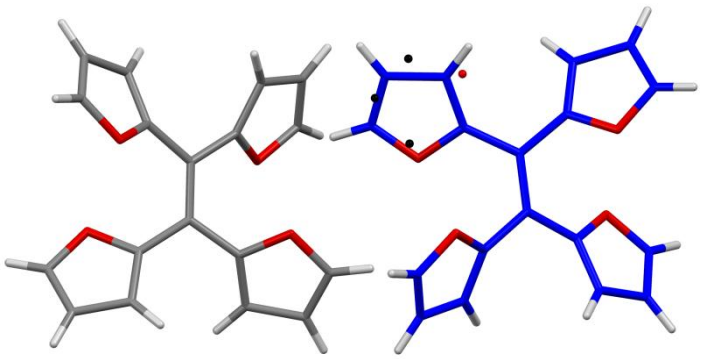

A

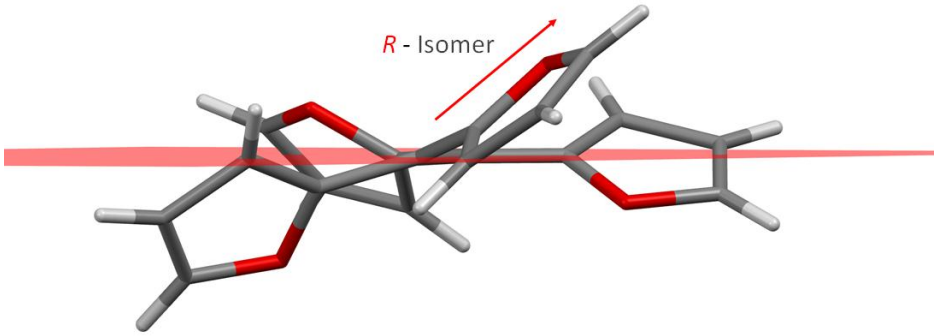

B

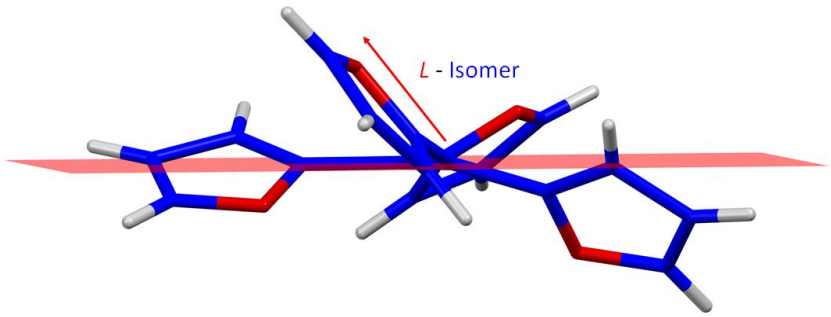

C

Figure 5.22 TFE crystal. (A) The two isomers of TFE in the asymmetric unit. (B) and (C) their stereochemical orientation. In the *Left-Handed* isomer it has been find disorder in correspondence of one of the ring.

With respect to the double bond plane, the two isomers have a different orientation. In one of them, all rings are right-handed (grey isomer) while in the other one all furans are left-handed (blue

isomer). Since the ratio between the two isomers is 1:1, the overall crystal structure does not have chiral property. The *intra*- and *inter*- molecular interactions have been evaluated, and similarly to TTE case, several contacts have been found; they are shown in Figures 5.23 (CH···π interactions) and 5.24-25 (CH···O interactions).

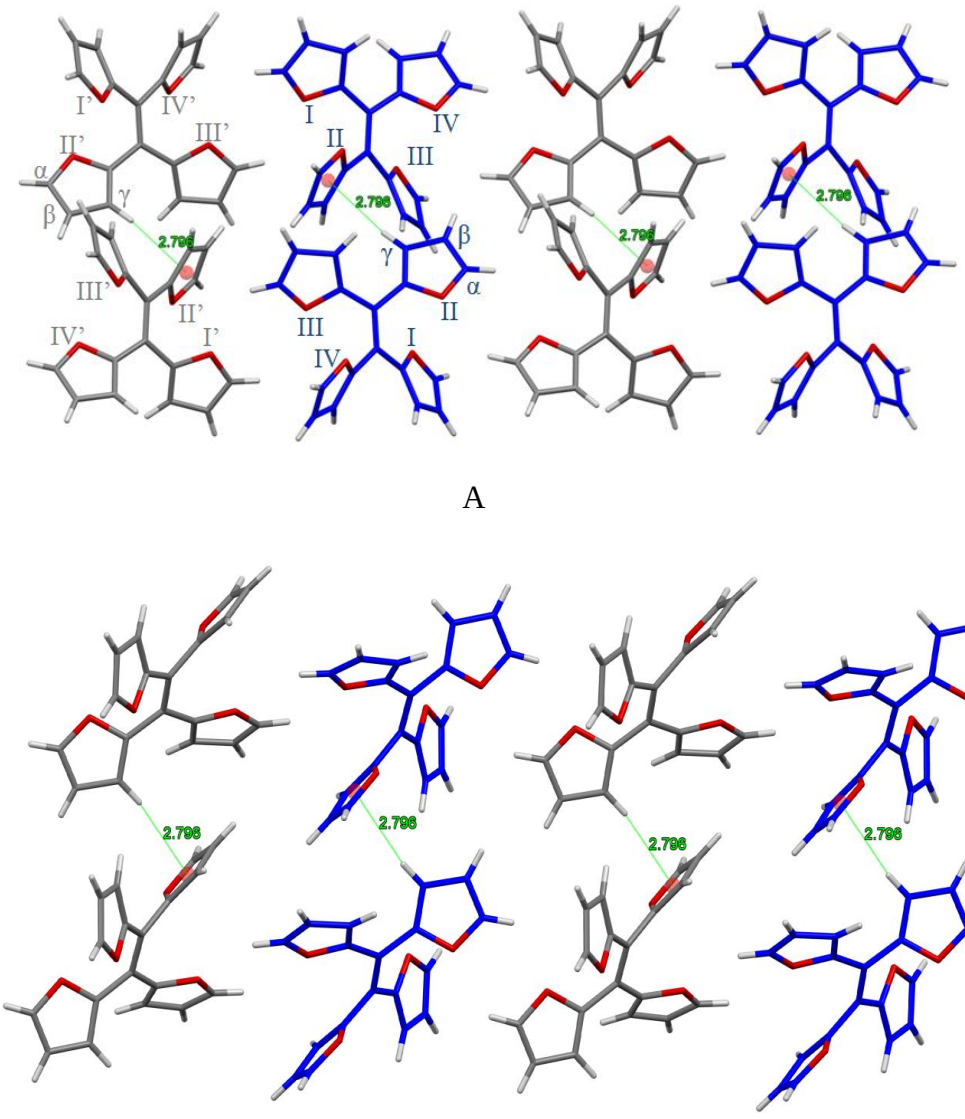

A

B

Figure 5.23 CH···π interactions in TFE crystal (A) top view, (B) side view.

Regarding the CH···π interactions, since the molecule is not symmetric and all rings have their own orientation, several contacts between each ring and the H-atom of the opposite neighbour molecule exist. Here we have chosen to represent the shortest one (2.796 Å), whose interactions occur between the ring II and the H-atom in γ position of the opposite neighbour ring II, within the same type of isomers (both *Right*- or *Left*-handed), the labels are highlighted in Figure 5.23 A. Due to the presence of the heteroatom, similarly to TTE case, H-bond interactions exist, they occur both within the same type of isomers, distance = 2.637 Å, (both *Right*- or *Left*-handed) and between the two different ones, (distances = 2.666 Å and 2.844 Å) as shown in Figure 5.24 and 5.23 respectively.

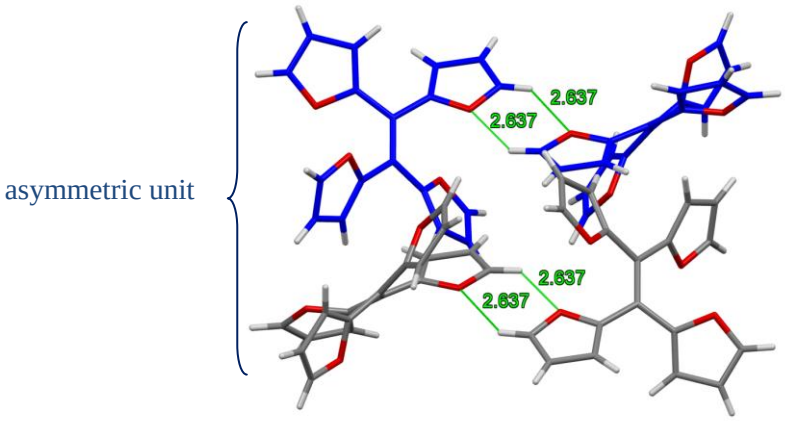

Figure 5.24 CH···O interactions found in the identical TFE isomers.

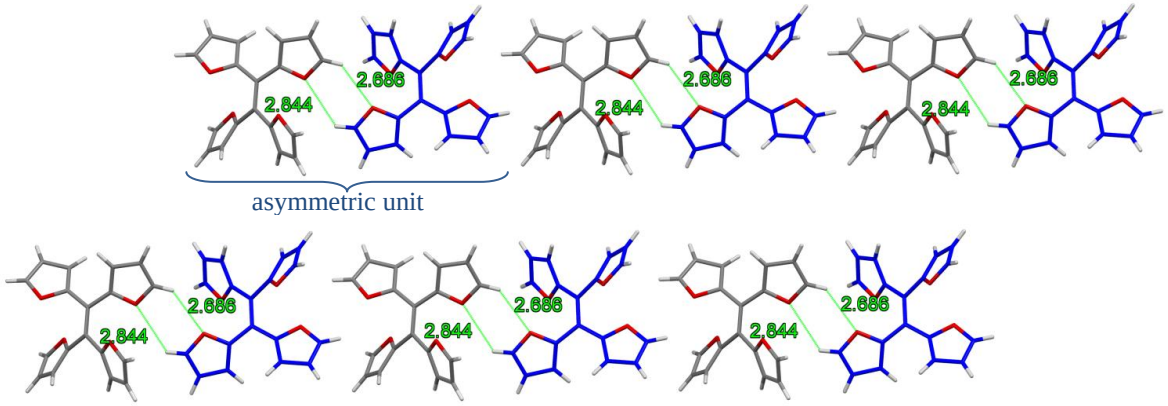

A

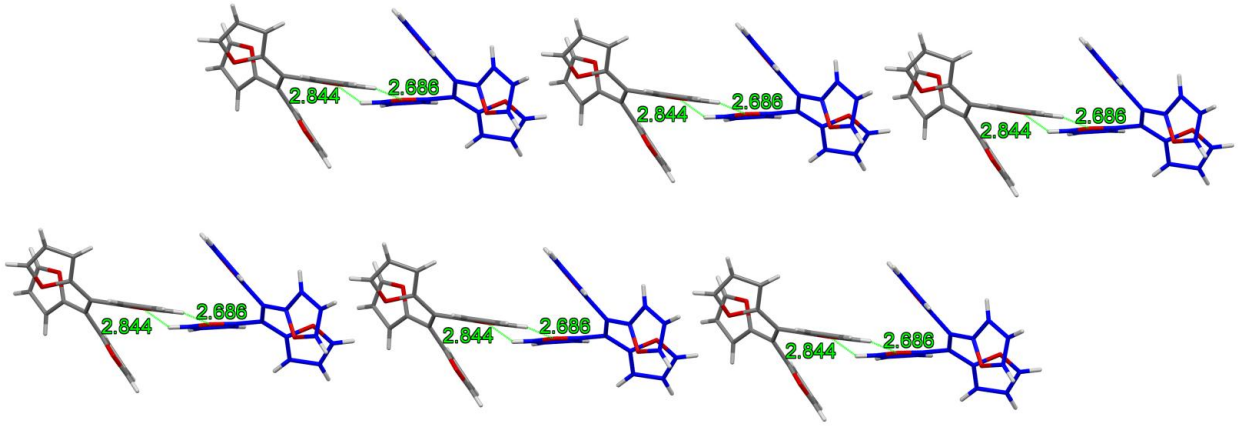

B

Figure 5.25 (A-B) different views of CH···O interactions found in *R*- and *L*- isomers in TFE molecule.

Although the multiple H-bonds and CH···π interactions, contribute to stiffen the molecular conformation in the crystal state providing at the same time a well ordered crystal network with a

certain structural periodicity, they cannot be responsible for the better conjugation of the crystal state that results in its redder emission respect to the aggregation and amorphous conditions. Thus being guided from our previous knowledge about the clusteroluminogenic effect [8] and from the results obtained in TTE case, we have investigated even in TFE crystal structure the distances between the Oxygen atoms. They are shown below in Figure 5.26

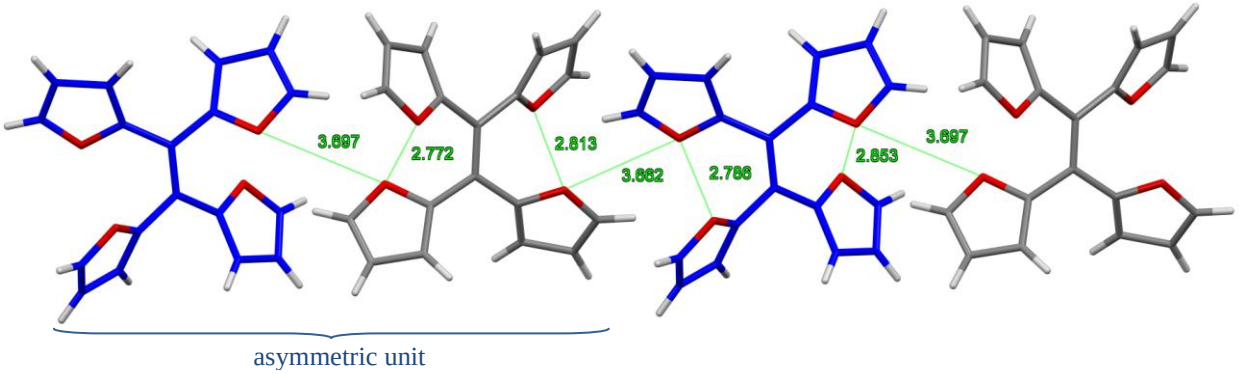

Figure 5.26 O···O interactions in TFE crystal.

The distances between each oxygen atom within each isomer are lower than 3 Å; Oxygen to Oxygen interaction exist between the two isomers both in the same unit cell, and between two different unit cell. Considering that the network shown above (Figure 5.26), is extended to the whole crystal structure, as in TTE case, even in TFE system, the heteroatom to heteroatom contacts are the cause of the emission red-shift that occurs going from the aggregate to the crystal state, since the O···O interactions are able to intermolecularly extend the original π-conjugation through the space, so allowing the formation of clusters that are electron-richer ,more conjugated and as a consequence, owns a lower energy gap. These insights fully explain the observed emission trend and allow to generalize the concept according to a molecule which owns unsaturating atomic system can be subject to this kind of interactions that contributes to enrich its emission properties. All interactions measured in TFE crystal are reported in Table 7, while Figure 5.27 shows a photograph of TFE in powder and crystal state taken at room-light and 365 nm illumination.
As a result of this investigation, it is possible to confirm that TFE molecule is a classic AIE luminogen, fr which in crystal state the formation of clusters is possible thanks to the heteroatom to heteroatom interactions, so that TFE owns clusteroluminogenic features as well.

Table 7 non-covalent interactions in TFE and TPE crystals.

Luminogen	interaction	Distance / Å	Type of interaction
TPE	CH---π	3.317	intermolecular
TFE	CH---π	2.637	intermolecular
	CH---O	2.796	intermolecular
	O---O	2.772;2813(*R*-isomer) 2.786;2.853(*L*-isomer) 3.697;3.662	intramolecular intramolecular intermolecular

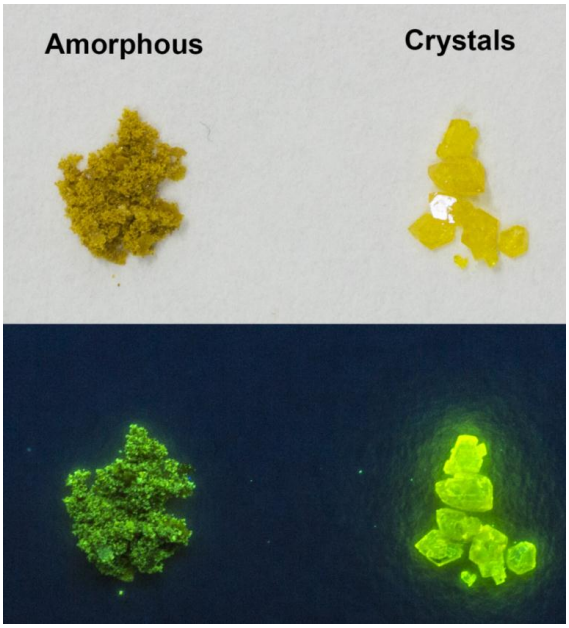

Figure 5.27 Photographs of TFE amorphous (left) and crystal (right) taken under room-light (top) and 365 nm UV-light (bottom) illumination.

5.3.3 fully-locked TTE (fl-TTE) and fully-locked TFE (fl-TFE)

As described in the previous paragraph the fully-locked TTE and TFE have served the aim to prove that the Restriction of Intramolecular Rotation RIR is the working mechanism behind the AIE effect in TTE and in TFE respectively.

In this paragraph dedicated exclusively to the photo-oxidized molecules (shown in Chart 5.3) are highlighted some important features that we have observed during our investigation are highlighted.

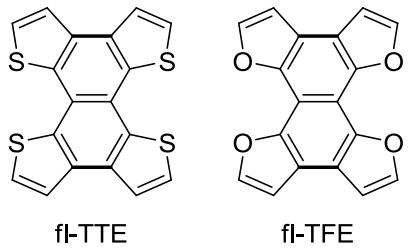

Chart 5.3 Molecular structure of fl-TTE and fl-TFE

Fully-locked TetraThienylEthene (fl-TTE)

The lifetime value reported in Table 1 at page 87 indicates that the molecule should own a certain emission in powder, even if the quantum yield is negligible. This insight has been confirmed recoding the PL spectrum of fl-TTE in powder and it is reported in Figure 5.28, where an emission peak at 450 nm is perceivable.

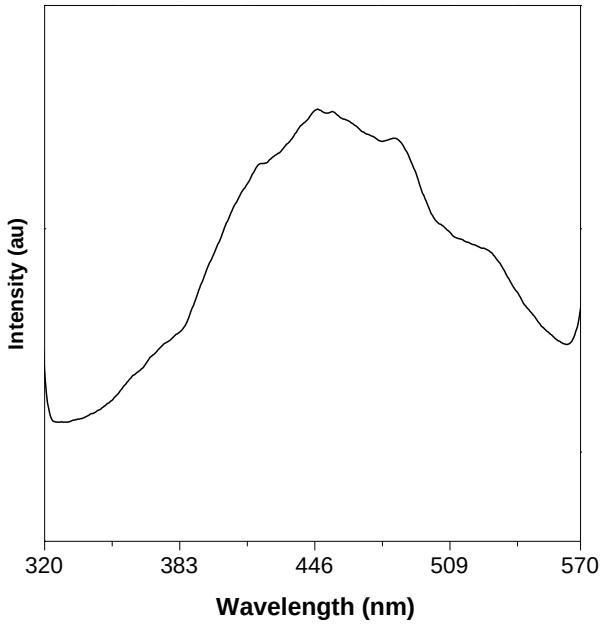

Figure 5.28 Photoluminescence spectrum of fl-TTE in powder.

Comparing the solid state luminescence value of fl-TTE and TTE (Table 8) in powders, and observing the photo shown in Figure 5.29, it is possible to note that fl-TTE has an emission closer to the green than the one TTE has, so its emission is redder than TTE's in powder state. As a consequence in this aggregation state, the locked molecule results more conjugated than the unlocked one.

Table 8, emission value of fl-TTE and TTE in powder state

Molecule	**Emission value in powder /nm**
fl-TTE	450
TTE	413

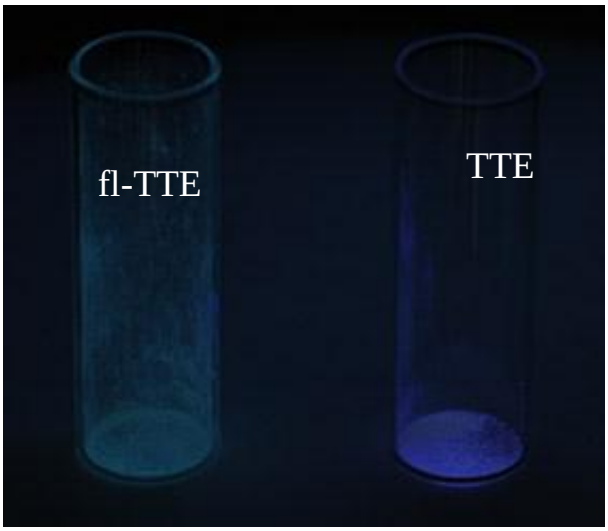

Figure 5.29 Photographs of fl-TTE (left) and TTE (right) taken under 365 nm UV-light illumination.

As we have experimentally proved by our electrochemical study described in Chapter 4, the double bond significantly contributes to the overall π-conjugation efficiency and as a consequence on the energy gap of the molecule; thus when it is lacking, the conjugation and the energy gap are lower. Another aspect that can affect the effective conjugation of the molecule, is the molecular geometry; in Chapter 2 at paragraph 2.1.2.2, (where the electrochemical and optical properties of *linear* and *angular* benzodithiophene –*ang*- and *lin*- BDT- are described in comparison to those of TTE), we have illustrated that despite the angular and linear BDT contain the same number of π-electrons, the linear BDT owns a lower energy gap than the angular one, thus the effective conjugation is lost in the angular structure. Therefore it could be spontaneous to wonder: why should the emission of fl-TTE in powder be redder than TTE if in fl-TTE since there is not the contribution of the double bond anymore (contrarily to TTE)[v] and it owns an angular shape as well? The answer to this

[v] These results have rendered very interesting to measure the experimental energy gap of fl-TTE, by electrochemical approach, our group is currently evaluating the possibility to perform these further measurments.

question can be found considering the results emerged from the crystal structure analysis of TTE, whose evidences can satisfactorily provide an explanation even for this case. So despite TTE is intrinsically more conjugated than fl-TTE the first, owns a bluer emission in solid state probably because of two of the thiophene rings that tend to acquire a perpendicular orientation respect to the double bond, thus resulting excluded from the overall π-conjugation, so what really emits is only the dithienylethene core, which is constituted by only two thiophene rings. On the contrary, in fl-TTE the contribution to the molecular energy gap in solid state comes from four thiophenes instead of two and as a consequence the molecule results able to emit at longer wavelengths. As mentioned before, the crystal structure reported in literature [6] does not belong to the pure molecule but to a complex between fl-TTE and the tetracyano-*p*-quinodimethane, from this, only information about the molecular geometry can be deduced, and not about the interaction or possible orientation that the pure molecule might have, since in the considered crystal environment fl-TTE is not pure because another system exist as well. Thus looking at the crystal structure provided by the Danish researcher in their feature paper, it is clear that the molecule is flat, therefore it is possible to cautiously propose a hypothesis according to, despite the molecular planarity, if the molecule is able to emit in powder even if it owns all requirements (electronics and geometrics) to generate efficient π-π stacking, it could mean that there could not be a sandwich-like arrangements along the molecular network, so that the vertical non covalent interactions (π-π ones) result prevented. An interesting question remains: since fl-TTE owns thiophene rings and hence Sulfur atoms (as it is just the locked counter-part of TTE), could it keep the clusteroluminogenic effect observed in TTE case? The reply to this question can be provided only by analysing the crystal structure of the pure molecule that is unfortunately not available yet.

Fully-locked TetraFurylEthene fl-TFE

Similarly to fl-TTE, even fl-TFE is able to emit in powder state, but before describing this phenomenon, it is noteworthy to show what we have found out during the photo-shooting we have performed for this system. Figure 5.30 shows the solutions of fl-TFE in pure THF and in some THF/water mixtures.

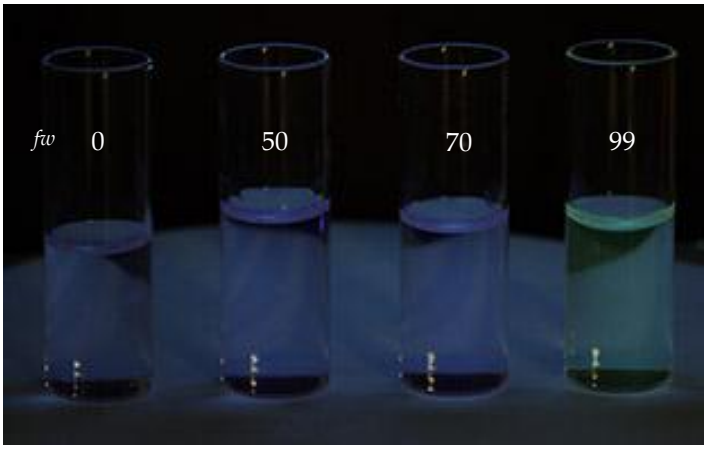

Figure 5.30 Photos of fl-TFE solutions in THF and THF/water mixtures with increasing water fractions (*fw*) to 99% taken under 365 nm UV-light illumination.

It is remarkable to observe that the solution feature significantly changes towards green color, when 99% of water is added. Although in aggregation conditions the molecule does not emit, it seems that in this molecular environment the network constituted by the aggregates is more conjugated, namely with the increasing of the water content, molecules becomes insoluble and tend to aggregate quenching the emission, but at the same time they could acquire a specific orientation that would allow the genesis of a more conjugated system.

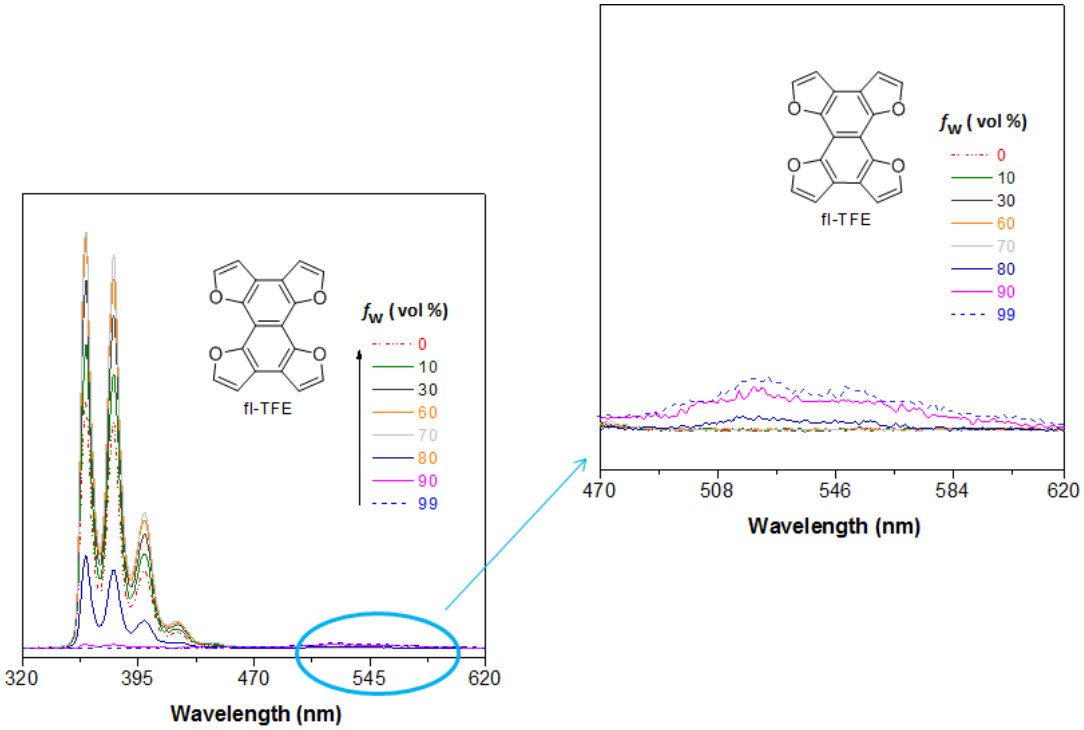

Figure 5.31 PhotoLuminescence (PL) spectra of fl-TFE in pure THF and in THF water mixture with increasing amount of water. a peak in the green region, which appears only in aggregation condition is shown as well.

A comparison between the emission behavior in pure THF, THF/water 1:99 and powder of fl-TFE is provided in Figure 5.32, while Figure 5.33 shows the comparison between the powder emission of TFE and fl-TFE. In Figure 5.34 is reported the PL spectrum of fl-TFE in powder state, while the emission value compared with that one of TFE is reported in Table 9.

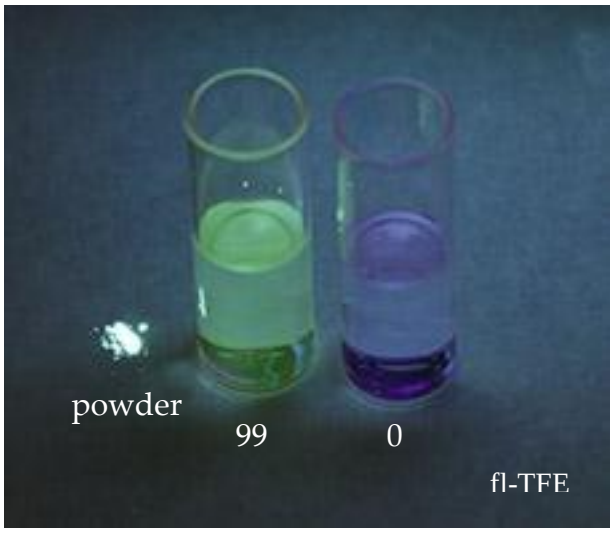

Figure 5.32 Comparison between the powder and the solutions of fl-TFE in THF and THF/water mixture with 99% of water fraction. The photographs have been taken under 365 nm UV-light illumination.

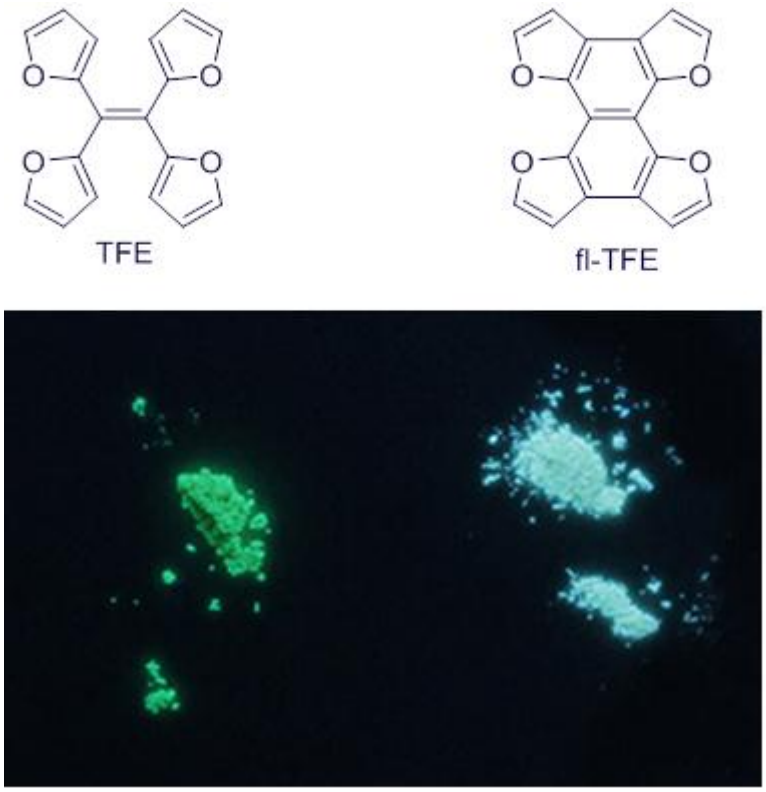

Figure 5.33 Comparison between TFE and fl-TFE powders. The photographs have been taken under 365 nm UV-light illumination.

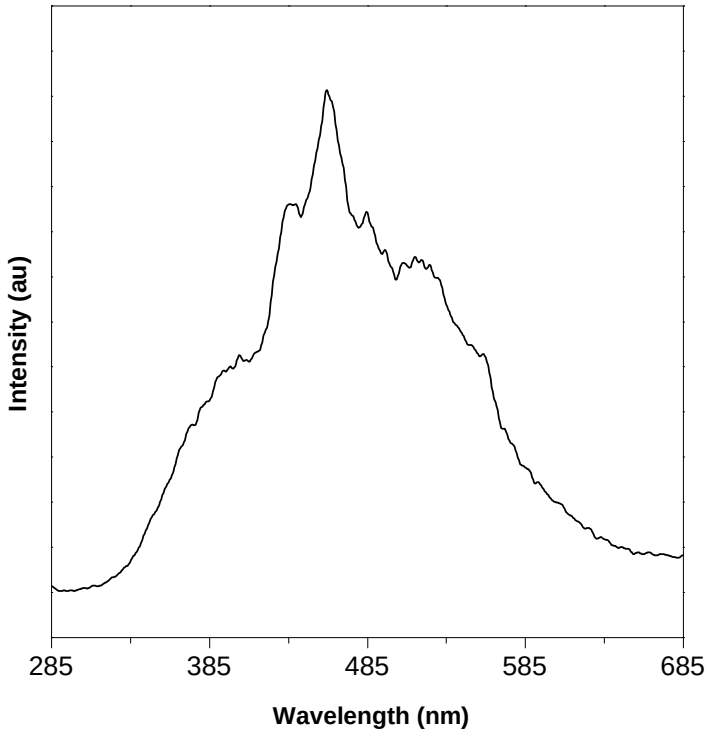

Figure 5.34 Photoluminescence (PL) spectrum of fl-TFE in powder.

Table 9 Emission value of fl-TFE and TFE in powder state

Molecule	**Emission value in powder /nm**
TFE	499
fl-TFE	460

Despite the ACQ trend in aggregation conditions, fl-TFE results emissive in powder, but contrarily to what happened in TTE and fl-TTE cases (discussed above), the emission color is bluer (in terms of wavelengths) than TFE. This perfectly fits what we have determined through the crystal structure analysis, and even if we don't have in our hands yet the fl-TFE crystal, we know that in the TFE one, all rings contribute to the overall π-conjugation efficiency, since (unlike TTE) none of them is perpendicular to the double bond plane. So despite the same number of furan rings, TFE powder has a redder emission than fl-TFE one, since the latter owns a worst π-conjugation efficiency owed to the loss of the central double bond moiety, and to the angular-shape structure. This results further confirm the insights obtained by our electrochemical investigations, that is the double bond and the structural linearity in a molecule play a key role in molecular electronic properties so affecting the photophysical ones as well.

fl-TTE and fl-TFE: a comparison

A direct comparison between the two fully-locked structures, becomes indispensable at this stage. Since we have the lifetime and quantum yield data only for the locked TTE, we can do it only by comparing the emission value and the aspect of the two molecules in powder states. In Table 10 are summarized the data discussed so far. fl-TTE and fl-TFE have a comparable emission since there are just 10 nm difference. Concerning TTE and TFE, even if they show a comparable energy gap both by electrochemical and optical approach[vi] the emission is bluer than the TFE one, due to the tendency of two of the four thiophene rings to acquire a distorted conformation in solid state as widely discussed before. Looking at the photo in Figure 5.35, we can observe that the emission of fl-TFE seems stronger than fl-TTE's. This is reasonable if we consider that the first one contains sulfur atoms, well known as effective fluorescence quenchers while the latter contains oxygenes. Another clue comes from the quantum yield value of TTE and TFE that are 2.6% and 11 % respectively, so we could expected that the fully-locked TTE would result less emissive than the furan-based counter-part (fl-TFE).

Table 10 Emission Value of the indicated molecules in powder states

Molecule	**Emission value in powder /nm**
TTE	413
fl-TTE	450
TFE	499
fl-TFE	460

[vi] Electrochemical approach: (DCM) TTE = 2.88 eV; TFE = 2.87 eV; (ACN) TTE = 2.66 eV; TFE = 2.76 eV, Optical approach (THF) TFE = 2.83, TTE = 3.01.

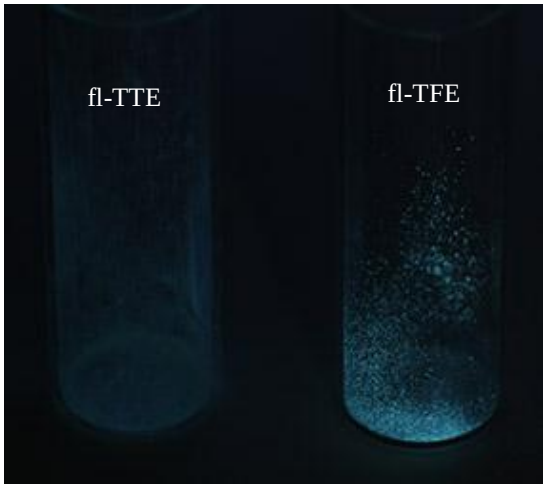

Figure 5.35 Photoluminescence (PL) spectrum of fl-TTE (left) and fl-TFE (right) in powder.

Since we have found out the clusteroluminogenic effect both in TFE and TTE, even for the locked structure fl-TFE, it is spontaneous to wonder if this effect is kept even in the locked structure, but even in this case the crystal structure is necessary to fulfill this question.

Therefore, despite the ACQ behavior proved in the aggregation states, because of their emission in solid state, it could be possible to define fl-TTE and fl-TFE as non-conventional ACQ dyes.

5.4 The study on the Diheteroarylethenes DTE and DFE and on DiPhenylEthene DPE as benchmark.

During our preliminary observations on the photochemical behavior of the HeteroArylEthenes (chart 5.1), we have noticed that the powder of planar molecules: DiThienylEthene (DTE), and DiFurylEthene (DFE), resulted to be emissive. As illustrated in the introduction, there has been the common belief according to which planar molecules bearing aromatic rings (hence being π-electron rich) usually experience effective π-π stacking interactions[4,9] . This is due to the fact they find themselves close to each other, as it occurs in aggregate or solid state. These π-π intermolecular interactions are responsible for the emission quenching since they open a non-radiative relaxation pathway, by which the excited state can be deactivated.The observation of ethylenes luminescence in powder state, surprised us; so we have wondered whether these molecules would have been AIE luminogen or not. In order to clear this doubt, we have performed AIE investigation, according to the AIE protocol. First of all we have studied the emission in solution and aggregation state and hence we have investigated their luminescence behavior in powder and crystal state.The following discussion is organized in a different order with respect to the TetraHeteroArylEthenes, discussed above; indeed the investigated disubstitued molecules and the benchmark (DPE), are firstly described individually, and then a comparison between the heteroaryl- and the phenyl-based molecules is provided.

5.4.1 The DiThienylEthene DTE

The first di-substituted molecule to be investigated, it has been DTE; as similar as TTE, DTE is soluble in most common organic solvents but not in water; thus we have prepared the usual solution set constituted by a solution in pure THF (0% *fw*) and several solutions in THF/water mixture with increasing amount of water for all solutions, concentration was 10^{-5} M. The corresponding PL spectra and the emission trend as a function of the water amount, are shown in Figure 5.36.

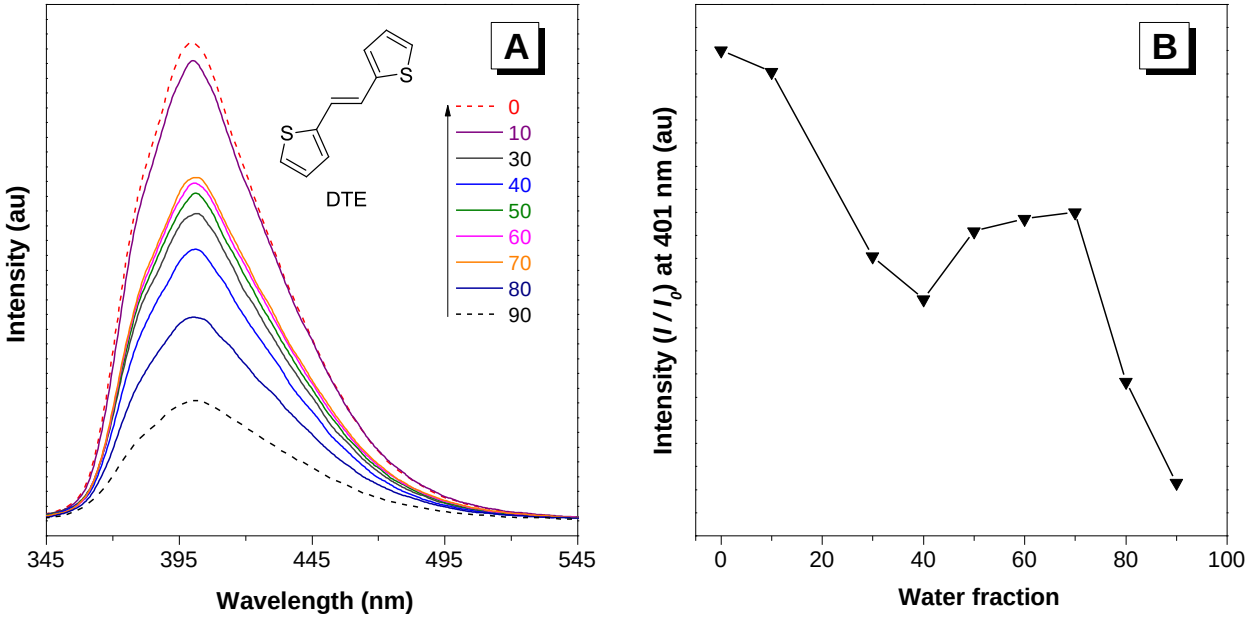

Figure 5.36 (A) The photoluminescence (PL) spectra of DTE in THF and THF/water mixtures with increasing water fractions (*fw*) to 90%. (B) Change in PL intensity of DTE at 401 nm versus water fraction in THF/water mixtures. Excitation at 322 nm.

DTE shows a typical ACQ behavior, since its emission (located at 401 nm) decreases with the increasing of the water content. This trend is not regular, because between 40% and 70% of water fraction there is a slightly increasing of the emission intensity, that turns to go down again with higher amount of water. Despite, the emission peak at 90% of water, (namely in aggregation conditions), is still clearly perceivable, the molecule has to be defined ACQ dye, because the overall trend results in a diminishing of the emission intensity with the increasing of the water content, specifically upon aggregation conditions.

Since we have observed for this molecule luminescence property in powder, we have recorded the PL spectrum in this state as well as in crystal one. The PL spectra in the three aggregation state are reported in Figure 5.37 and the corresponding value are collected in Table 11. As PL spectra shows, DTE is well emissive in powder as well as in crystal state, furthermore even for this molecule there is a red-shift of the emission peak going from the aggregate to the solid state, even if in this case, the emission in powder and in crystal phase are nearly coincident. The deep analysis on its crystal

structure, discussed at the next paragraph, has provided an answer both to the reason of the emission behavior in powder state, and about the red-shift emission property.

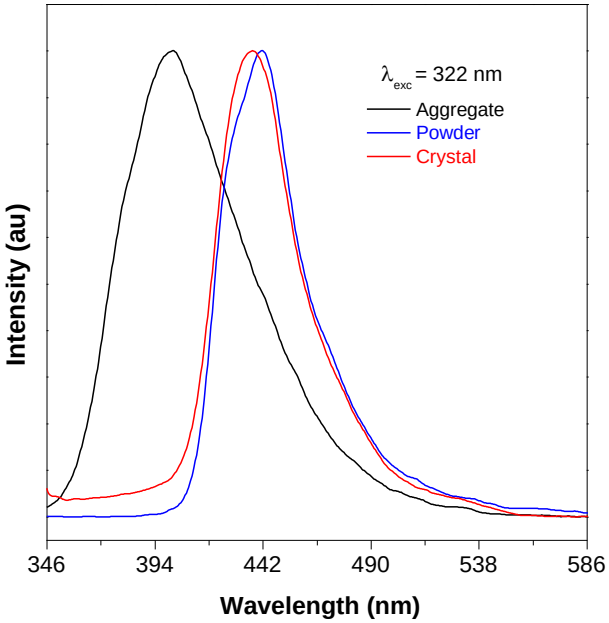

Figure 5.37 The photoluminescence (PL) spectra of DTE in aggregate, amorphous and crystal state. Excitation at 322 nm.

Table 11 Emission peak of DTE in the indicated states

Luminogen	λ_{em} / nm			$\Phi_{F,A}$ / %	τ / ns
	Aggregate	Powder	Crystal	Powder	Powder
DTE	401	442	438	15	0.94

Crystal structure investigation

From the analysis on the crystal structure (ORTEP picture, Figure 5.38), it has emerged that DTE exist in purely *trans*- form and only one single molecule constitutes the asymmetric unit (Figure 5.39).

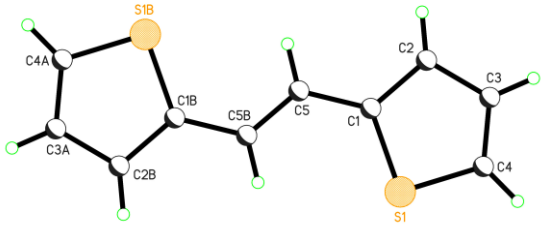

Figure 5.38 ORTEP picture of DTE crystal.

Figure 5.39 Asymmetric unit of DTE crystal.

It is possible to consider the molecule owning a planar structure, since the dihedral angle between, for instance, the Ring 1 and the double bond is just 3.1°, as shown in Figure 5.40.

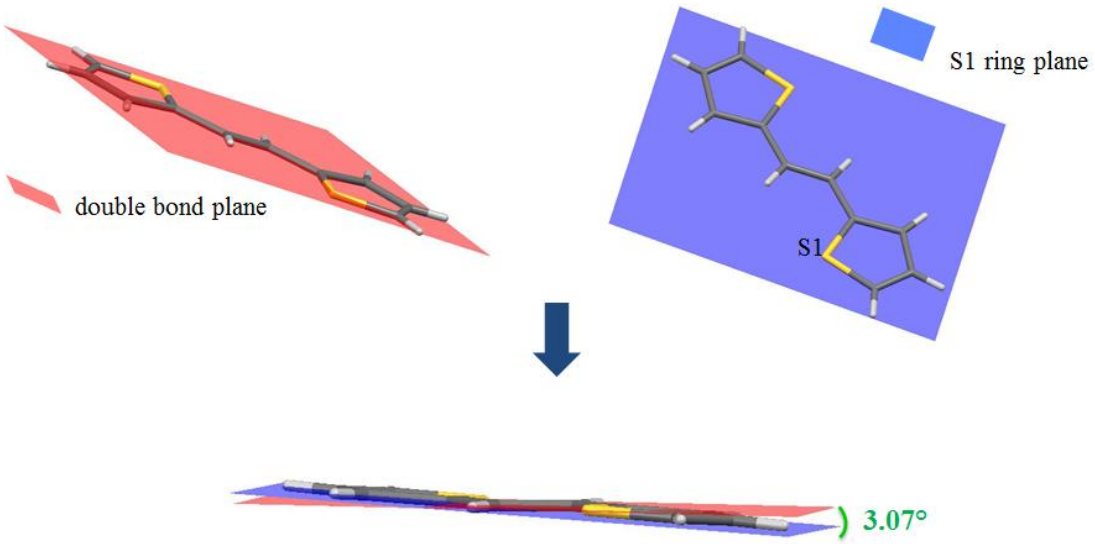

Figure 5.40 Molecular planes of the double bond and one of the thiophene rings, and the related dihedral angle.

Despite its planarity, DTE is a quite good fluorogen emitter in powder state, as proven by the lifetime and quantum yield reported in Table 11. In order to understand why despite its planarity and the possibility to experience π-π interactions (thanks to the presence of heteroaromatic rings), it is able to emit in powder, it is necessary to check how the packing of the molecule is in the crystalline phase. The last is reported in Figure 5.41 and 5.42.

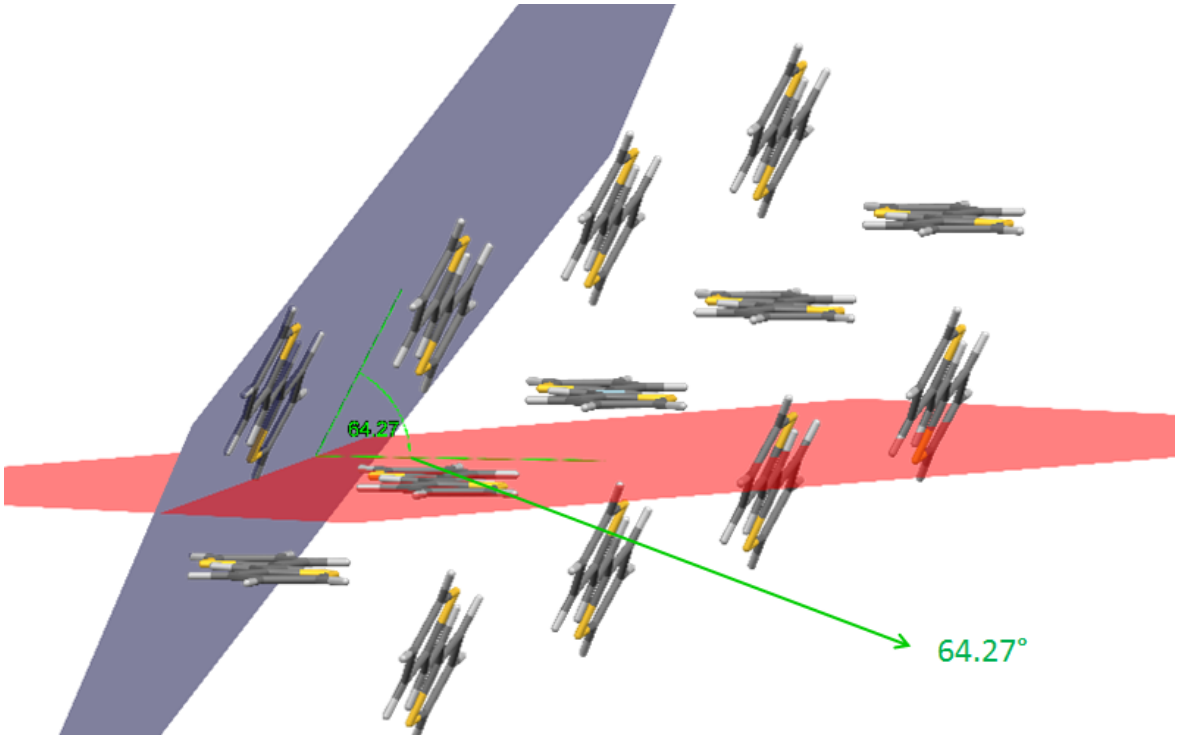

Figure 5.41 Packing in DTE crystal

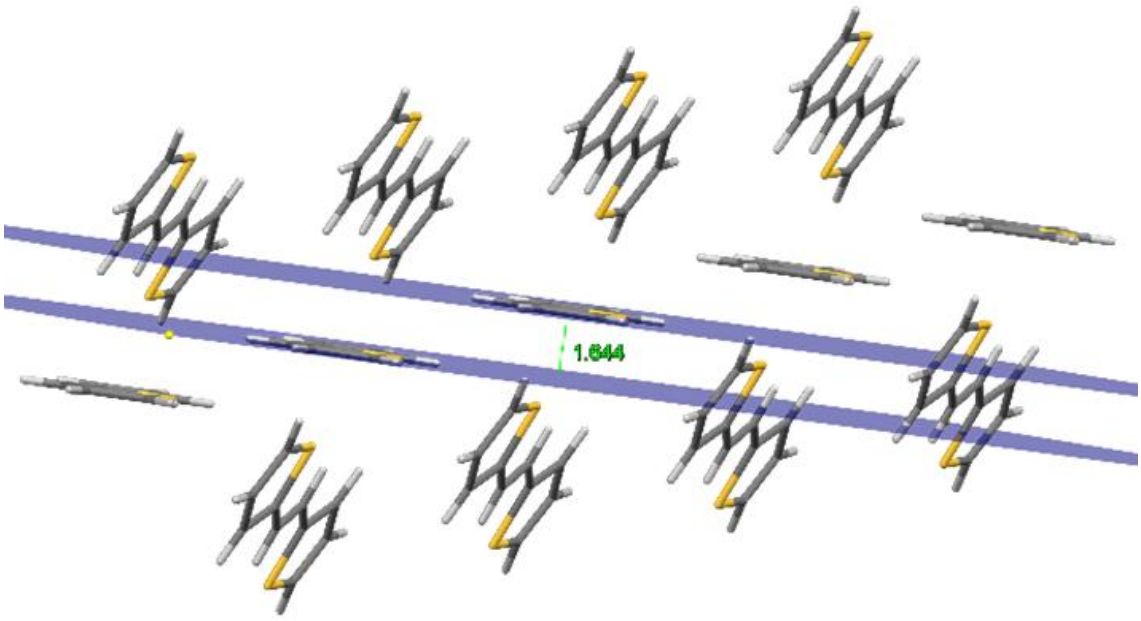

(A)

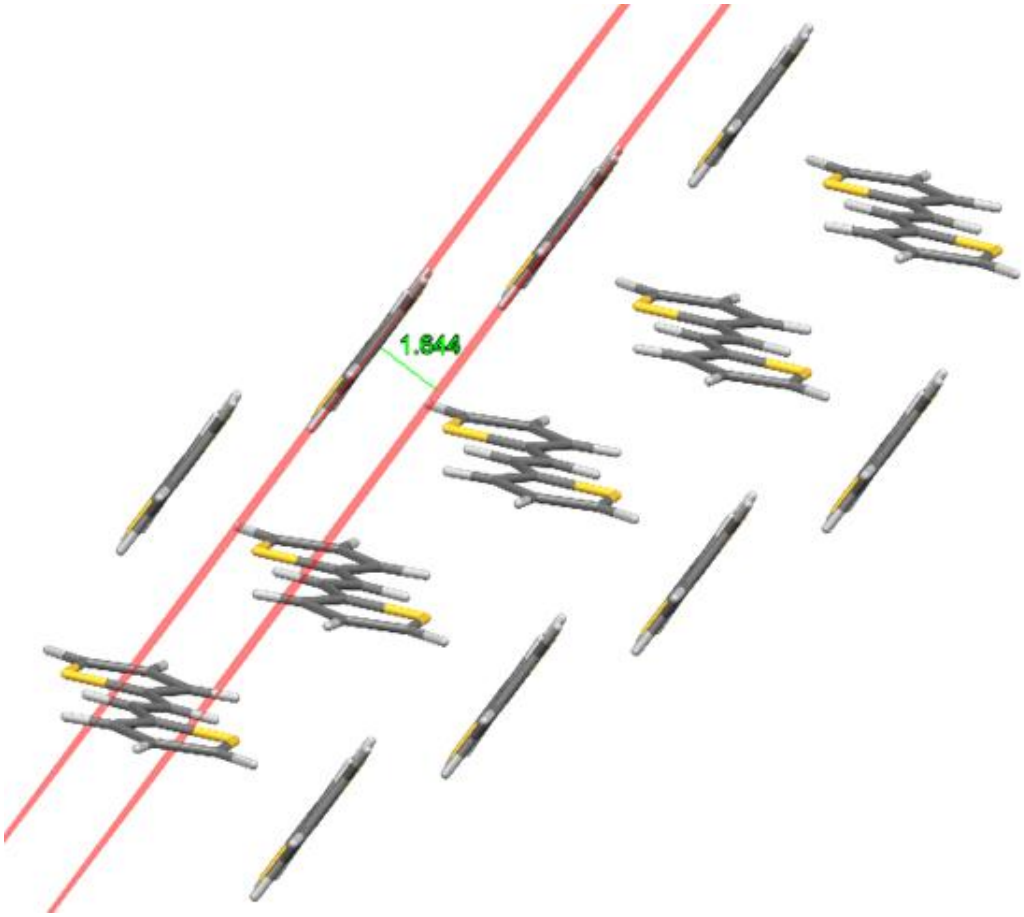

(B)

Figure 5.42 Distance (1.64 Å) between the molecular planes in the crystal packing.

Analyzing the molecular packing it is possible to distinguish two planes: one horizontal and the other one perpendicular but inclined respect to the first one. As a consequence DTE molecules in the crystal are arranged along these two planes, whose angle is 64°. Thus the crystal is constituted by a recurrence of these planes along the 3d space and the distance between each of them (e.g. distance between the horizontal planes and between the vertical ones) is equal and correspond to 1.64 Å. Because of this kind of packing the molecules are not pile-up each other, despite their intrinsic ability in exerting π-interactions, so the π-π does not occur. Therefore, upon excitation in solid state, the molecule results able to deactivate its excited state by the radiative-channel, so resulting emissive, despite its planarity.
Analyzing the possible non-covalent interactions, even in this case, as well as the CH---π and CH---S, we have found the S---S ones. Figures 5.43-45.

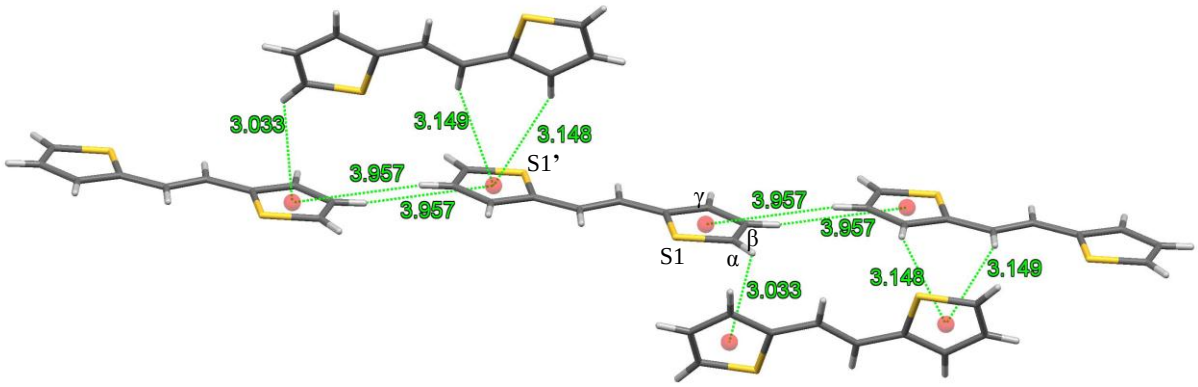

Figure 5.43 CH---π interactions in DTE crystal.

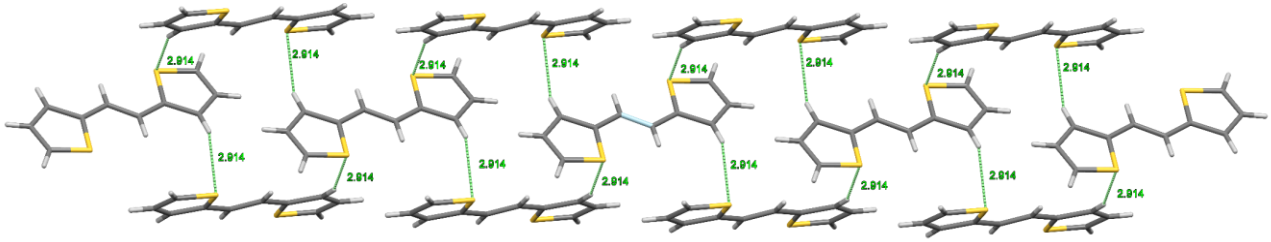

Figure 5.44 CH---S interactions in DTE crystal. The measured distance is 2.914 Å.

The shortest CH---π interaction measures 3.03 Å, and it is even a little bit longer than the CH---S ones, indeed the last own the same length that is equal to 2.915 Å. The S---S contacts are shown below, since they exist and they recur along the whole crystal structure, even in DTE case, it is possible to ascribe the emission red-shift occurring from the aggregation to the solid state, to their contribute; as a result of the through space extended π-electron conjugation.

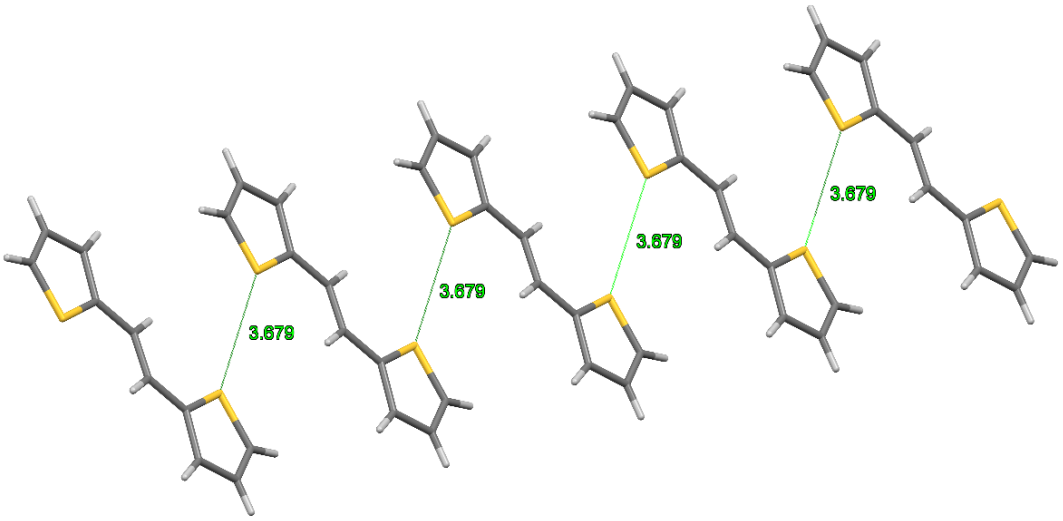

Figure 5.45 S---S interactions in DTE crystal. The measured distance is 3.679 Å.

Since DFE it is also not soluble in water, the study in aggregation condition has been performed by using as solvent system, THF/water mixture just as done for the previous molecules. The PL spectrum of each solution and the related trend is reported below in Figure 5.46.

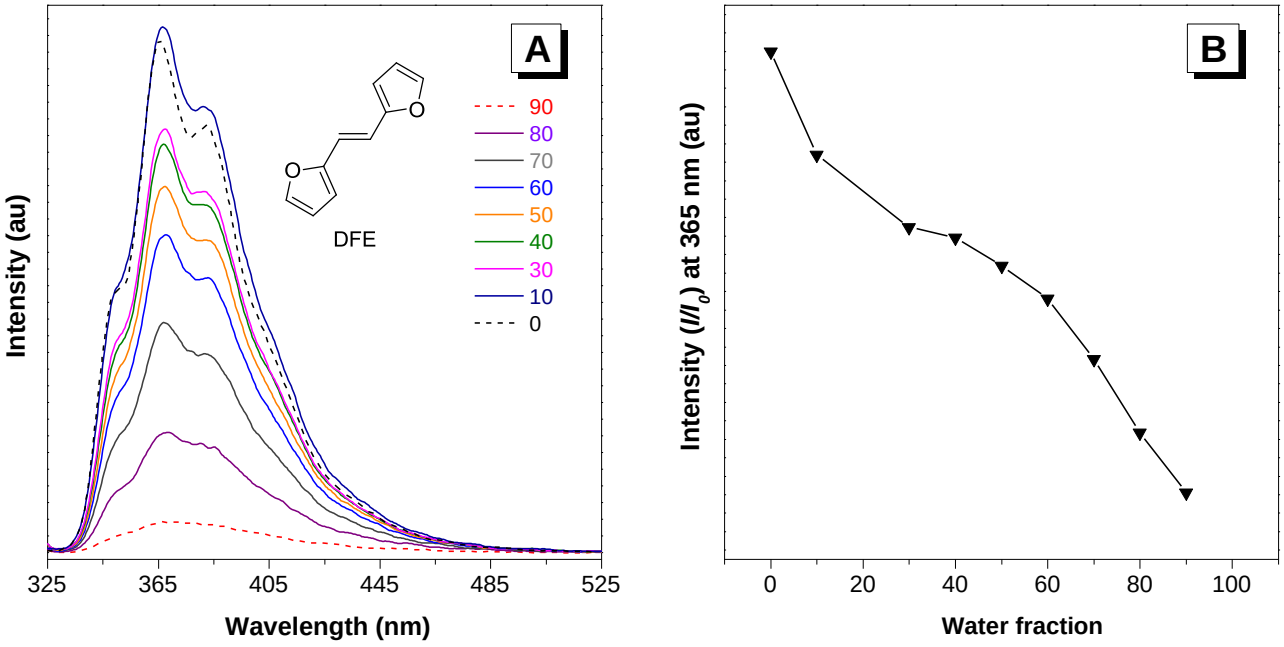

Figure 5.46 (A) The photoluminescence (PL) spectra of DFE in THF and THF/water mixtures with increasing water fractions (*fw*) to 90%. (B) Change in PL intensity of DFE at 365 nm versus water fraction in THF/water mixtures. Excitation at 315 nm.

The PL spectrum of DFE shows a more fine structure respect to DTE's and the related first emission peak is located at 365 nm; even for DFE system the increasing of water content causes a descreasing of the emission intensity, hence the molecule result to be ACQ. Considering our preliminary observation according to which, the molecule resulted to be emissive in powder, we have recorded the PL spectrum for the amorphous as well as for the crystal, the spectra overlaying is shown below. Figure 5.47.

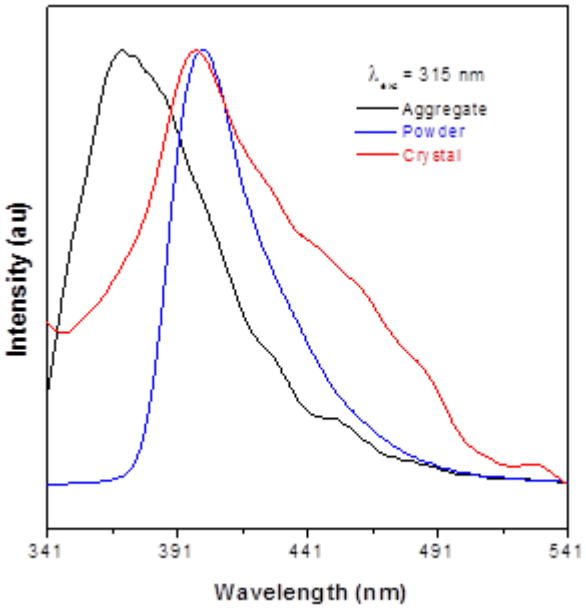

Figure 5.47 The photoluminescence (PL) spectrum of DFE in aggregate, amorphous and crystal state. Excitation at 315 nm.

The PL spectrum of the powder and the crystal, prove the ability of DFE to emit in solid state. As it results from the spectra overlay, even for DFE there is red shift going from the aggregation to the solid, and similarly to DTE the emission peak in amourphous and crystal is located at the same wavelength. The corresponding values are reported in Table 12.

Table 12 Emission peak of DFE in the indicated states

Luminogen	λ_{em} / nm			$\Phi_{F,A}$ / %	τ / ns
	Aggregate	Powder	Crystal	Powder	Powder
DFE	372	401	399	32	1.28

Crystal structure investigation

The ORTEP picture of DFE crystal is shown in Figure 5.48, similarly to DTE, even in DFE case the asymmetric unit is constituted by only one molecule, no-isomers are presents and DFE crystal exist in purely *trans*- form (Figure 5.49).

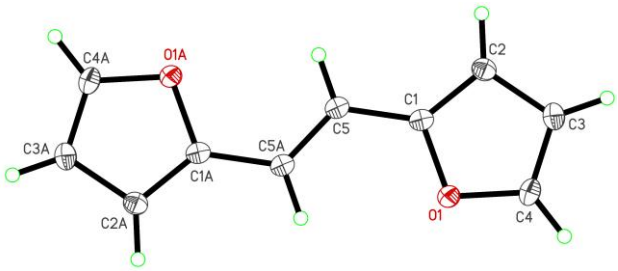

Figure 5.48 ORTEP picture of DFE crystal.

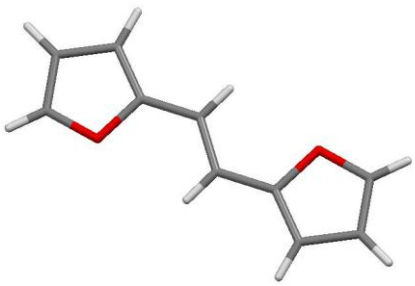

Figure 5.49 Asymmetric unit of DFE crystal.

The angle between the double bond and the ring plane is very small, (even lower than DTE case) so that DFE can be classified as planar molecule.

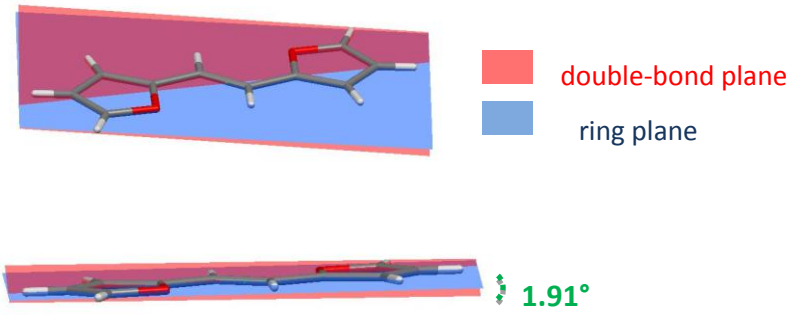

Figure 5.50 Measurement of the dihedral angle between the rings and the double bond plane.

Interactions between the heteroatoms must be looked for in the crystal even in this case, in order to explain the red-shift emission occurring going from the aggregate to the crystal state. They are shown in Figure 5.51. The packing for these molecule is irregular respect to DTE, but observing it along one of the axis, the O---O interactions appears much more clear.

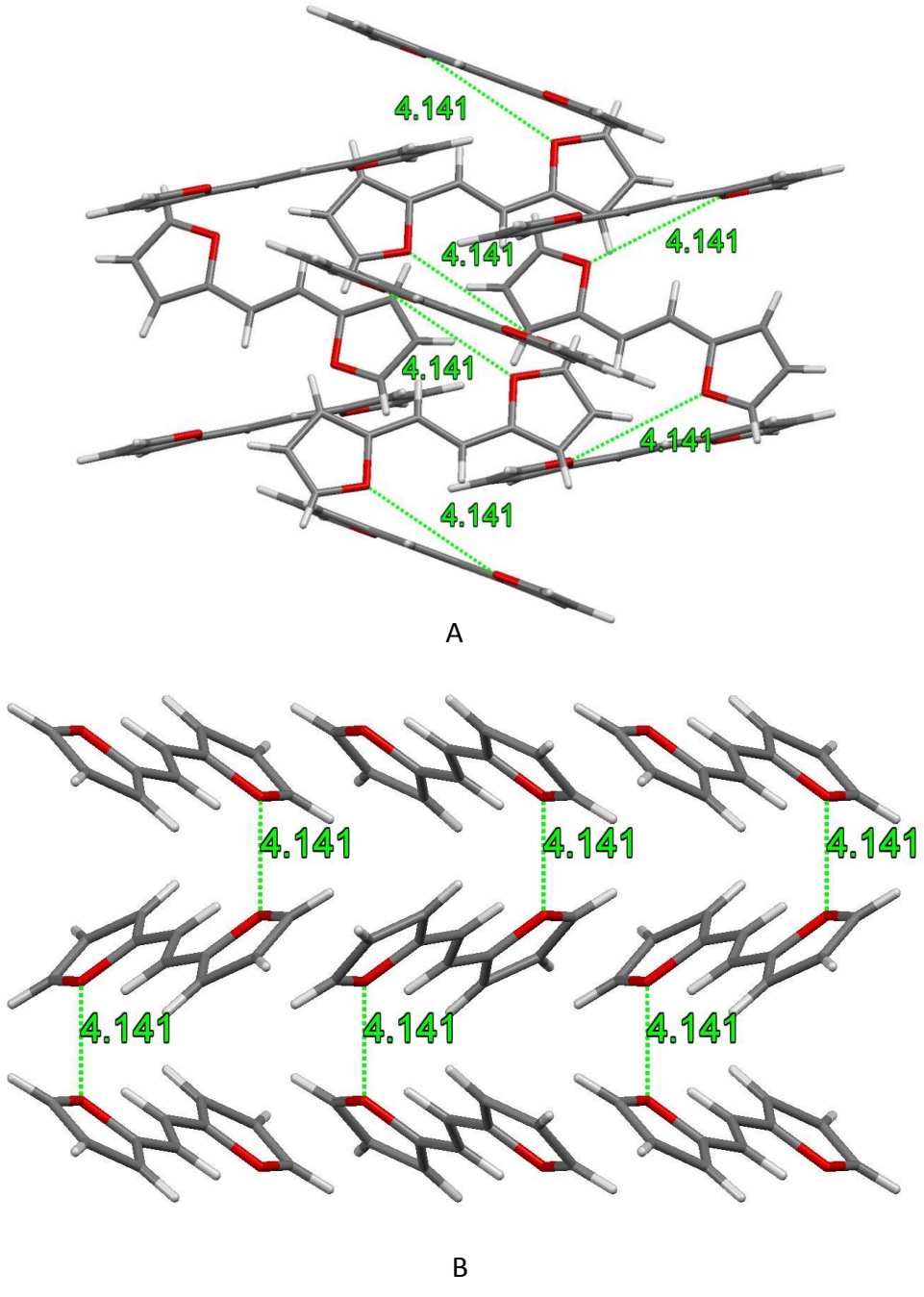

Figure 5.51 O---O interactions in DFE crystal.

Thus even in this case we can ascribe the red-shift emission to the existence of this non-covalent interactions that feature the crystal state rendering it much more conjugated. CH---O and CH---π are present as well. Figure 5.52-53. For the first one, it is interesting to note that both H-atoms (in particular those in β-position) of the ring and of the double bond are involved.

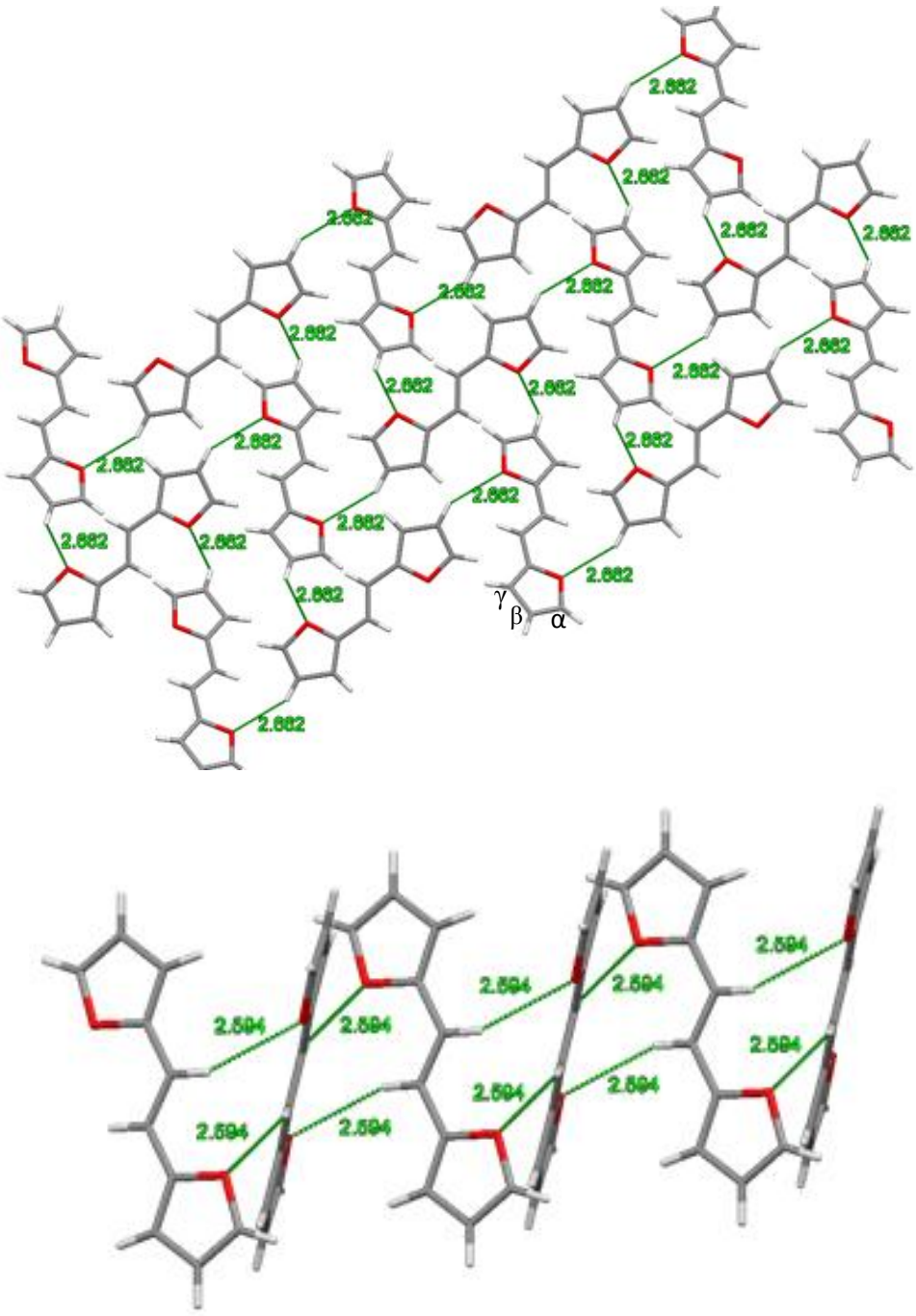

Figure 5.52 CH---O interactions in DFE crystal.

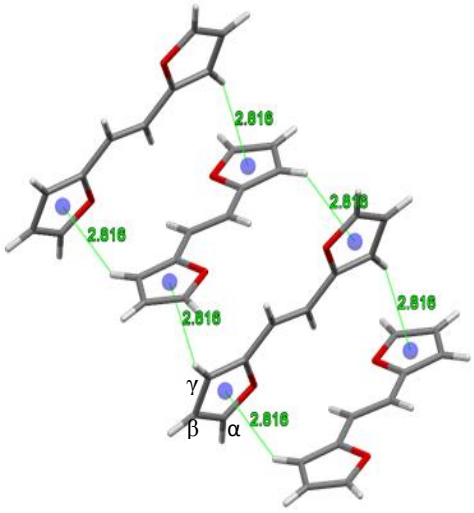

Figure 5.53 CH---π interactions in DFE crystal.

Analyzing the crystal packing, three different types of plane are catchable, Figure 5.54, the shortest distance is equal to 2. 693 Å.

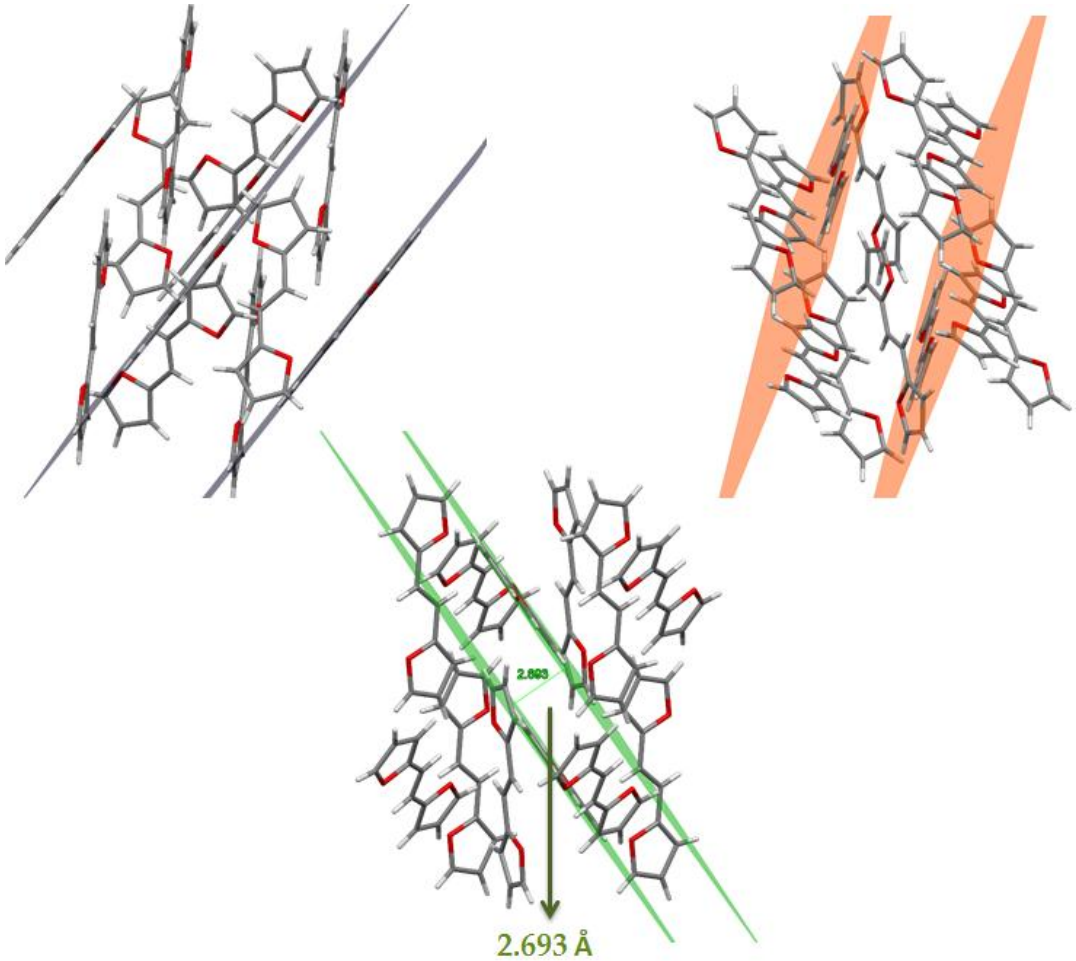

Figure 5.54 Molecular planes in DFE crystal.

5.4.3 The DiPhenylEthene DPE

DPE has been widely investigated over the years [10] in terms of photophisycal properties. In order to have a comparison between the heteroaryl-based molecules and the phenyl-based ones, we have performed a detailed study, investigating, similarly to DTE and DFE, the crystal structure as well. Using the same solvent system constituted by THF and increasing amount of water, the behavior in solution and in aggregation condition, has been investigated. The corresponding PL spectra and the related trend, as a function of the water content, is reported in Figure 5.55.

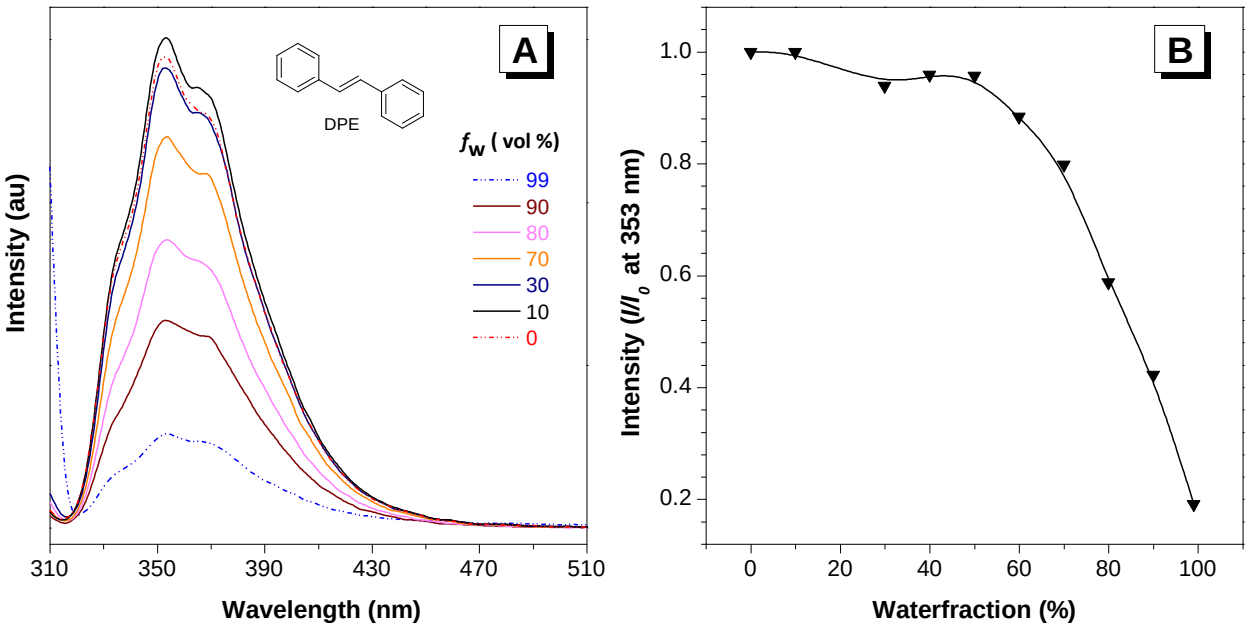

Figure 5.55 (A) The photoluminescence (PL) spectra of DPE in THF and THF/water mixtures with increasing water fractions (*fw*) to 99%. (B) Change in PL intensity of DPE at 353 nm versus water fraction in THF/water mixtures. Excitation at 300 nm.

The emission peak is located at 353 nm, and as expected, DPE owns an ACQ behavior since the emission is quenched upon aggregates formation. However, during our investigation, we have noted that it resulted emissive in powder state, therefore we have wanted to measure the PL spectra for the amorphous and crystal state as well. The comparison is provided in Figure 5.56.
Surprisingly, DPE (also simpler known as stilbene), have resulted to be well emissive in powder and crystal state too. Furthermore, as can be deuced from the spectra overlay and from the value reported in Table 13, there is a red-shift going from the aggregate to the crystal state.
As previously happened for the other molecules, also in this case the crystal structure analysis has revealed to be an effective tool in order to gain a better interpretation of the phenomenon.

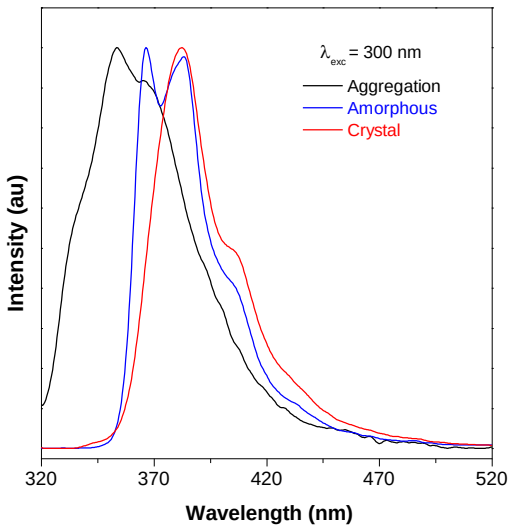

Figure 5.56 The photoluminescence (PL) spectrum of DPE in aggregate, amorphous and crystal state. Excitation at 300 nm.

Table 13 Emission peak of DFE in the indicated states

Luminogen	λ_{em} / nm			$\Phi_{F,A}$ / %	τ / ns
	Aggregate	Powder	Crystal	n.a.	n.a.
DPE	353	367	382		

Crystal structure analysis

Both from the ORTEP picture and from Figure 5.57 that shows the asymmetric unit of the cell, the obtained DPE crystal is purely in its *trans*- form.

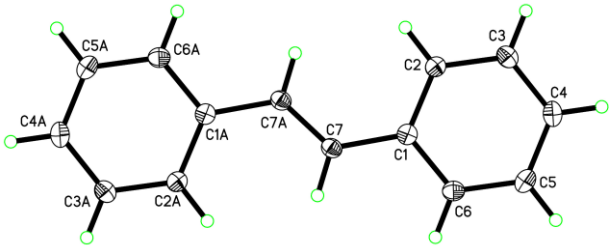

Figure 5.57 ORTEP picture of DPE crystal.

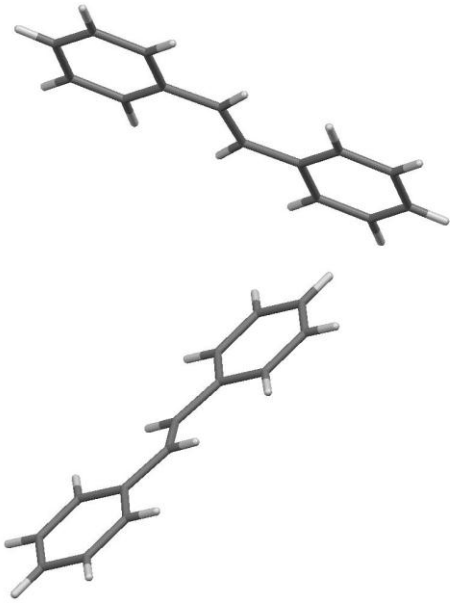

Figure 5.58 Asymmetric unit of DPE crystal.

Contrarily to DTE and DFE, in the asymmetric unit of DPE crystal, it is possible to find two molecules, which are identical, since both of them are in *trans*- form. Due to this arrangement, it is possible to individuate two set of molecular planes that are shown in Figure 5.59. The measured angle between them is 51° while the interplane distance correspond to 2.43 and 2.68 Å.

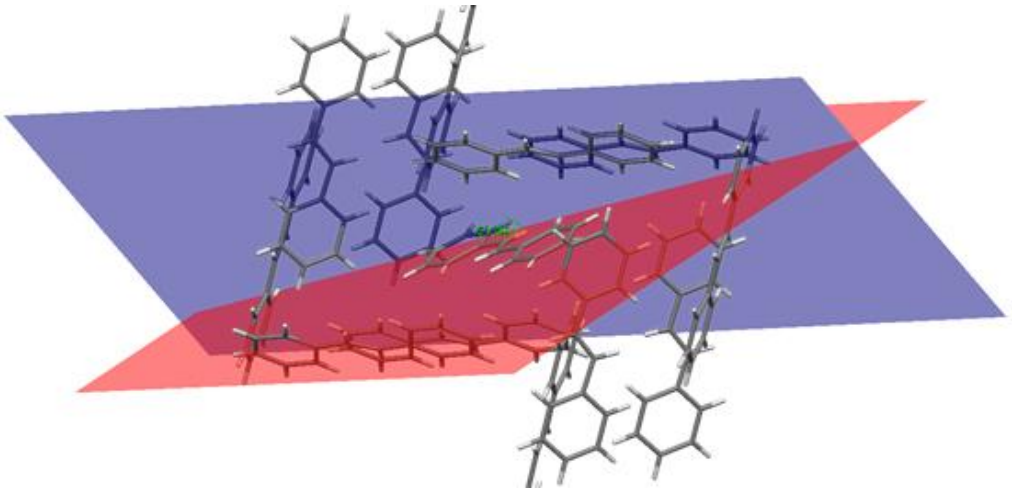

Figure 5.59 Angle (51°) between the two molecular plane catchable in DPE crystal.

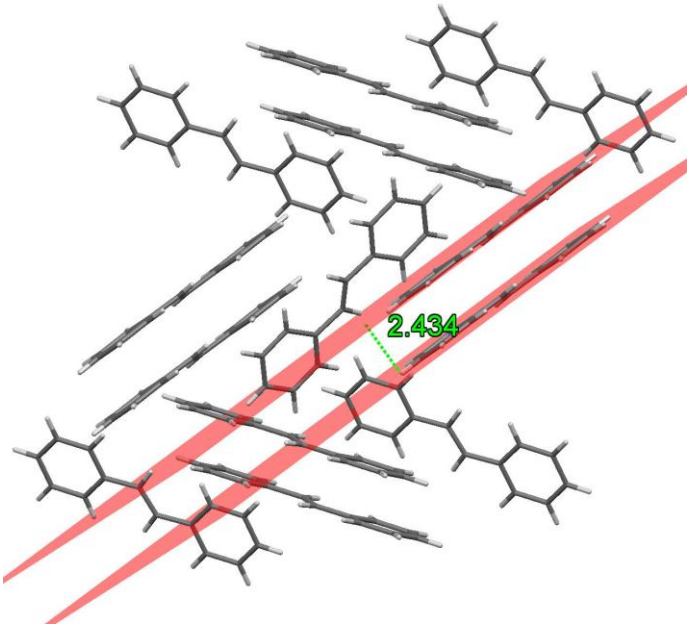

A

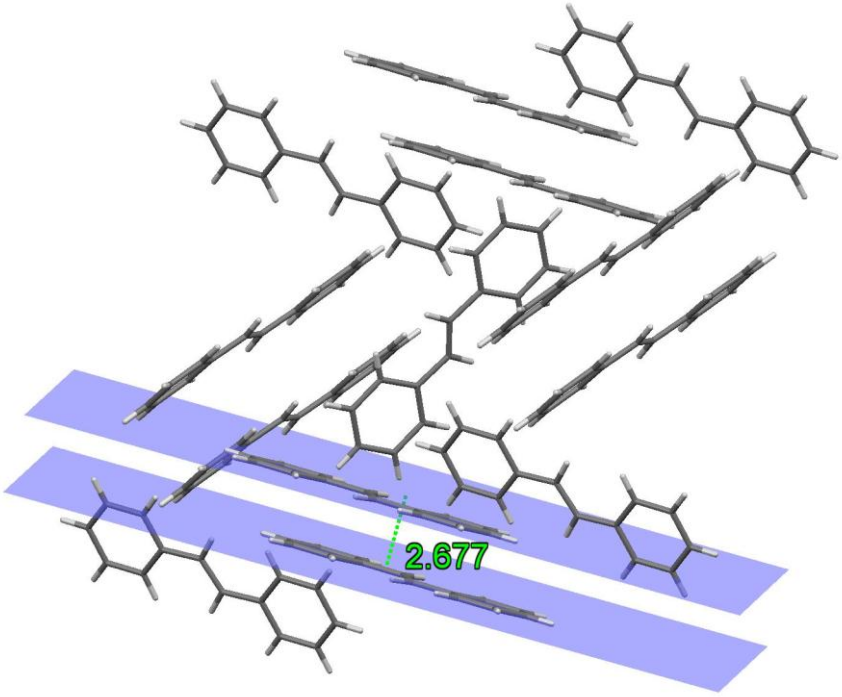

B

Figure 5.60 Distances between the two set molecular plane catchable in DPE crystal.

Looking at the Figure 5.60 and as deducible from the molecular arrangement showed in the previous picture the DPE molecule in the crystal phase, does not have a "pile-up" network that would allow to generate an effective π-π stacking; even if the last can be exerted not necessarily when the molecule lies on parallel planes (arrangement defined *sandwich-shape*), indeed three different kinds of π-π stacking interactions can exist [11] as shown in Figure 5.61, anyway the disposition of DPE molecules in the crystal does not make possible the realization of none of them.

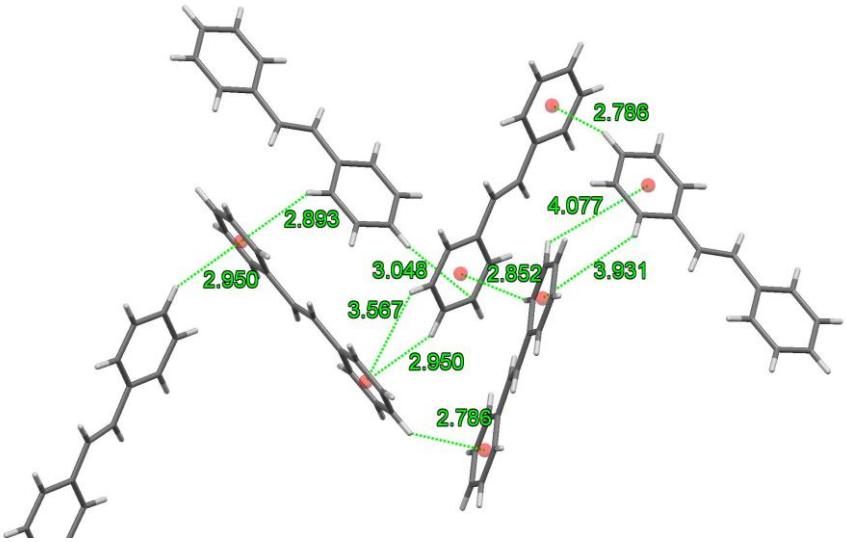

Figure 5.60 CH---π interactions in DPE crystal.

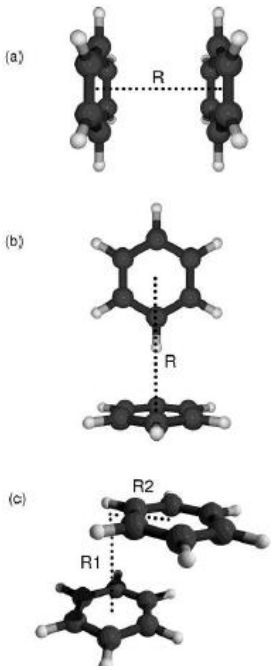

Figure 5.61[11] The different types of π---π stacking, (a) sandwich, (b) T-shaped, (c) parallel displaced.

Therefore the reason according to DPE is emissive in solid state (powder and crystal) is ascribable to the lack of effective π-π stacking interactions. The left question is: why there is an emission red shift going from the aggregate to the crystal, if in DPE there are not heteroatoms? Before trying to provide an answer to this question, it is useful to compare the behaviour of all the planar molecules investigated so far. In Table 13 are collected the emission data of the planar molecules in the three aggregate states.

Table 13 Emission peak of DFE in the indicated states

Luminogen	λ_{em} / nm			$\Delta\lambda^{i}$ /nm	$\Phi_{F,A}$ / %	τ / ns
	Aggregate	Powder	Crystal		Powder	Powder
DTE	401	442	438	36	15	0.94
DFE	372	401	399	27	32	1.28
DPE	353	367	382	29	n.a.	n.a.

[I] difference between the emission wavelength in aggregation and in crystal state.

Table 14 Non-covalent interaction distances in the crystal of DPE, DTE and DFE

Luminogen	interaction	Distance / Å	Type of interaction
DPE	CH---π	2.852	intermolecular
DTE	CH---π	3.033; 3.148; 3.957	intermolecular
	CH---S	2.914	intermolecular
	S---S	3.679	intermolecular
DFE	CH---π	2.816	intermolecular
	CH---O	2.662; 2.584	intermolecular
	O---O	4.414; 4.448; 5.823	intermolecular

Therefore, the three planar molecules investigated, have resulted to be, classic ACQ dye (since their emission decreases with the increasing of the water amount) but luminescent (with a significant quantum yield value) in solid state, because in the latter, as proven by the crystal structure, effective π-π stacking interactions do not exist, and the excited state can be deactivated by radiative-pathway. Since the molecules resulted to be ACQ in aggregation state, we can then deduce that π-π stacking interactions can exist in this molecular environment where probably the arrangement of the molecule is totally different from the solid state, and their disposition allow to generate a π-π stacking so effectively to be able to quench the emission.

5.4.4 DithienylEthene DTE and BenzoDiThiophene BDT: isoelectronic ACQ planar molecules with different solid state luminescent behaviour.

Intriguing by the results emerged with the investigation on the planar molecules: DTE, DFE and DPE; we have wondered how the corresponding photo-oxidized molecules would have behaved, since the latter owning the same number of π-electrons, are isoelectronic with the first ones. Chart 5.4.

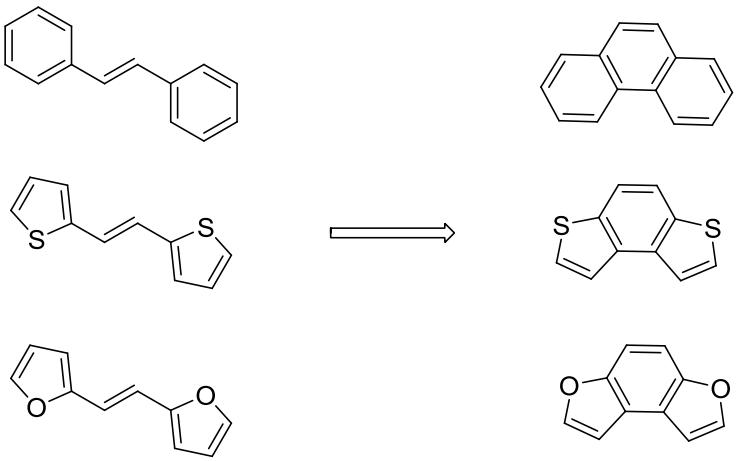

Chart 5.4 DPE, DTE and DFE (left) and the corresponding photo-oxidized products (right).

Among the molecules shown in Chart 5.4 on the right, it has been possible to investigate only the second one: BenzoDiThiophene BDT, product of the phocyclization of DTE. Like DTE, the emission behaviour of BDT has been investigated in solution and in aggregation condition, by preparing the solutions in THF and THF/water mixtures, in which BDT had a concentration of 10^{-5} M. The photoluminescence (PL) spectra are shown in Figure 5.62, where it is possible to note that BDT is an ACQ dye, since the emission (located at 332 nm) decreases with the increasing of the water content.

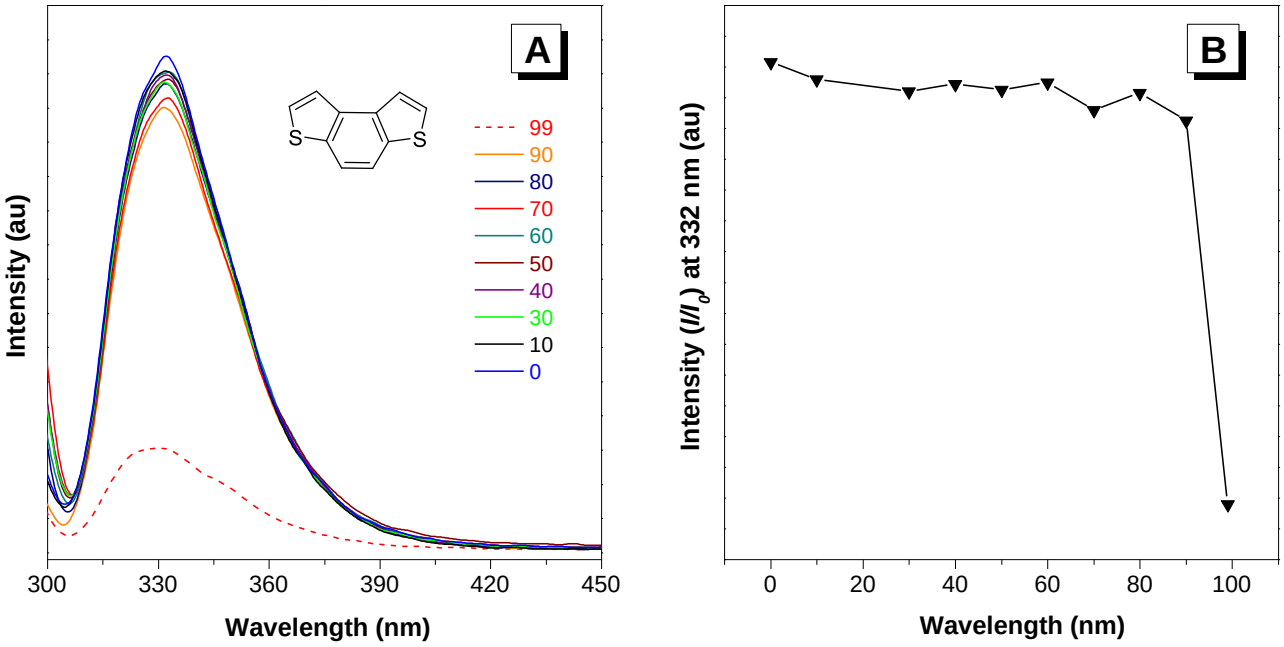

Figure 5.62 (A) The photoluminescence (PL) spectra of BDT in THF and THF/water mixtures with increasing water fractions (*fw*) to 99%. (B) Change in PL intensity of BDT at 332 nm versus water fraction in THF/water mixtures. Excitation at 288 nm.

The BDT emission has been also measured in powder and crystal state (Figure 5.63), where the molecule results not emissive, indeed the spectra in solid state have the same intensity of the Aggregate one (in which the molecule is a little bit emissive) only because of the normalization. For a better understanding, a further comparison between the overlay spectra of DTE and BDT is provided in Figure 5.64.

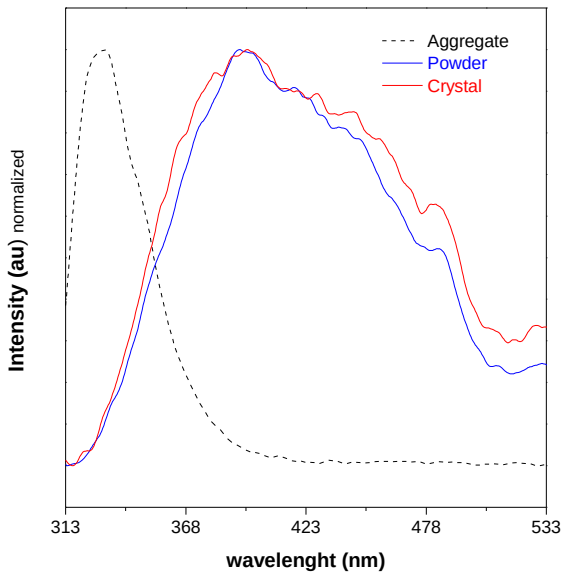

Figure 5.63 Photoluminescence (PL) spectra of BDT in Aggregate (black), Powder (blue) and Crystal (Red) state.

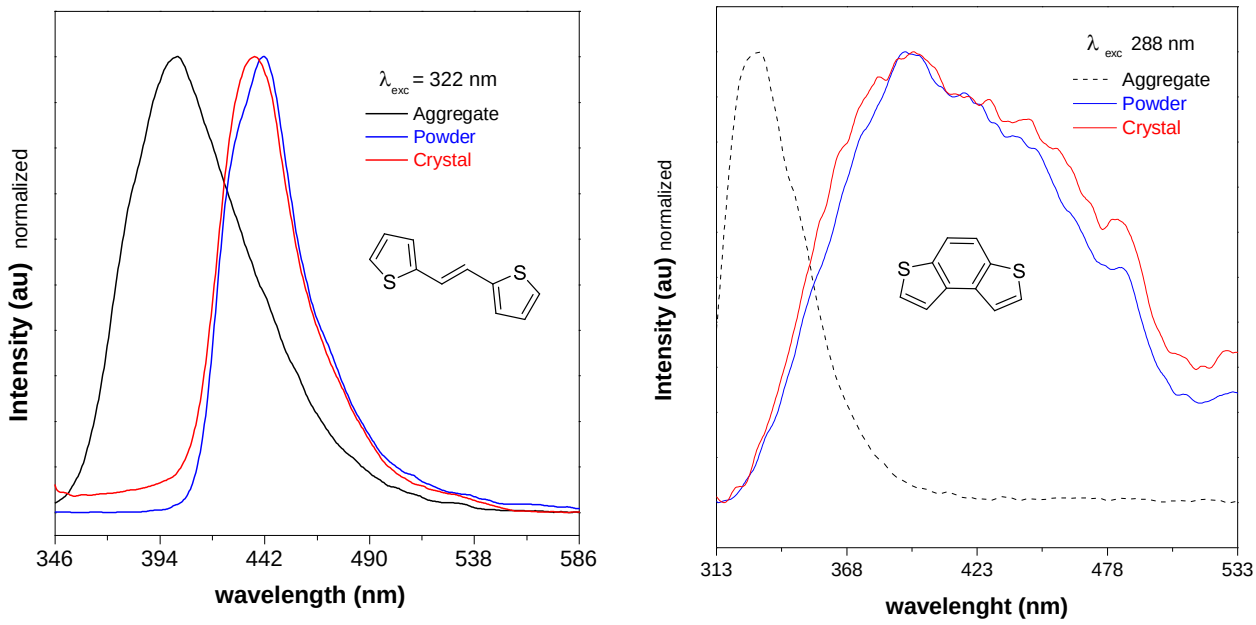

Figure 5.64 Photoluminescence (PL) spectra of DTE (left) and BDT (right) in Aggregate (black), Powder (blue) and Crystal (Red) state.

Therefore BDT and DTE, isoelectronic planar molecules both having an ACQ behaviour in aggregate state, show different performance in solid one, since the first does not result emissive like the second. In order to understand which could be the reason behind this phenomenon, a deep investigation on the crystal structure of BDT has been necessary.

Crystal structure investigation

In Figure 5.65 is shown the asymmetric unit of BDT crystal, like in DTE case, it is constituted by only one molecule.

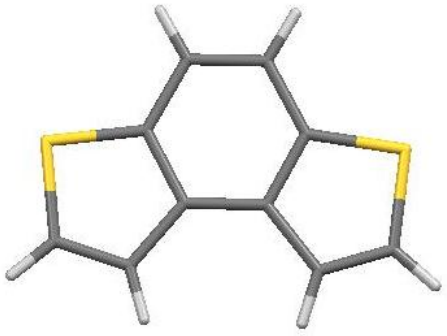

Figure 5.65 Asymmetric unit in BDT crystal.

In Figure 5.66 is reported the packing of the molecule, in the crystal, as it can be seen, the molecules lie on two different planes that are inclined each other, and whose angle correspond to 59°, a little bit lower compared to DTE one (see Figure 5.41 page 127) that is 64°. So in BDT crystal, each molecule is a little bit more inclined one towards each other. This arrangement consents to the molecules to experience the π-π stacking interaction in the "parallel displacement" mode, as shown in Figure 5.67, where 2.896 Å is the distance between the two parallel plane on which the interacting molecules lie, 5.866 Å is the distance between the two molecular centroid, considering the first distance as the cathetus and the second one as the hypotenuse of the righ-angled triangle that the interacting molecules form, applying the Pitagora's theorem, it is possible to calculate the displacement of the interacting molecules.

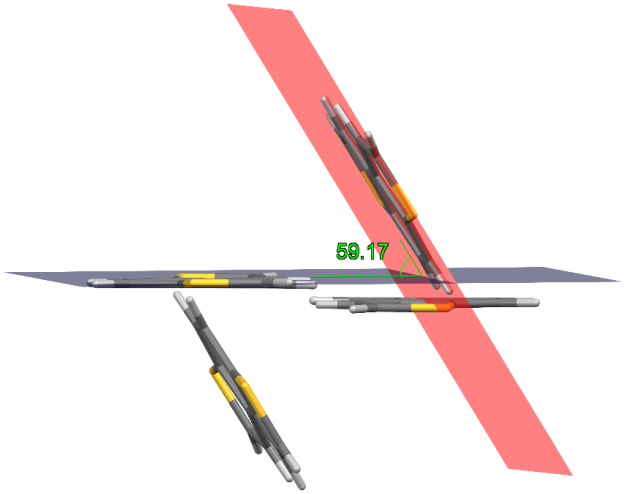

Figure 5.66 Asymmetric unit in BDT crystal.

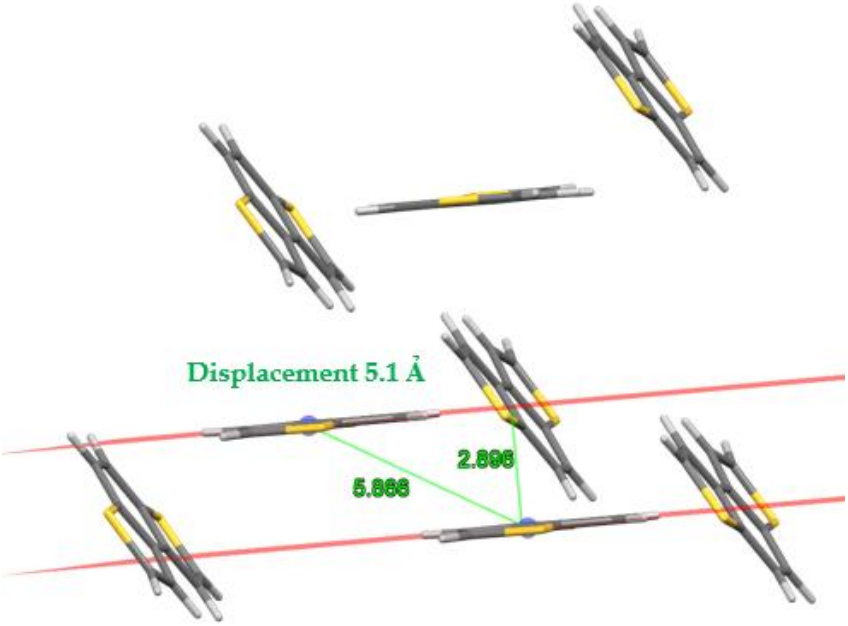

Figure 5.67 *Parallel displacement* π-π stacking in BDT crystal.

Analysing the short contact it has been possible to find even in this case, the CH---π interactions, mainly responsible of the molecular stiffening. Figure 5.68.

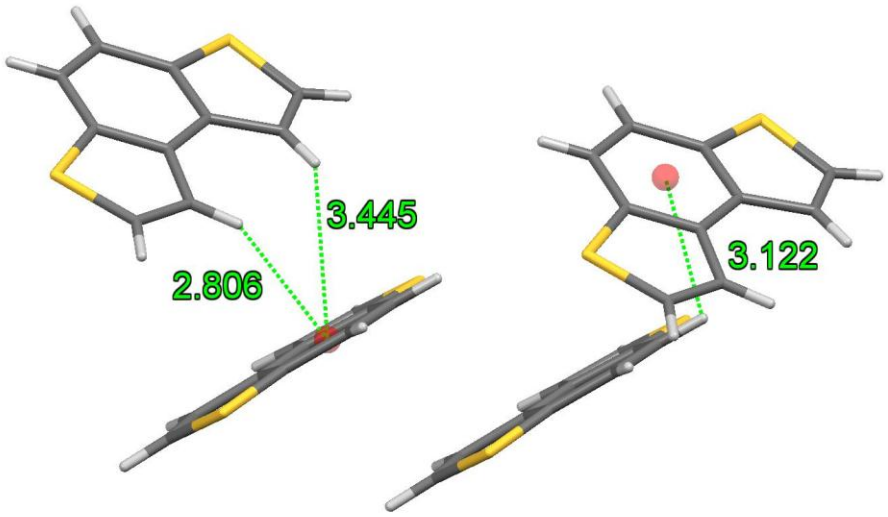

Figure 5.68 CH---π interaction in BDT crystal.

Therefore BDT does not result emissive in solid state since an effective π-π stacking occur in this molecular environment, so allowing the deactivation of the excited state through a non-radiative relaxation pathway.

5.5 TriThienylEthene TrTE

As shown in Figure 5.2 at page 86, TrTE resulted to be emissive in solid state, so that we have investigated its luminescent behaviour by using the AIE protocol like we have done for the other molecules investigated so far; in order to check whether the emission could also have verified in aggregation state. Contrarily to the previous molecule (tetra- and di- substituted ones) and to the study performed by electrochemistry (Chapter 4), for TrTE it has not been possible to have a comparison with respect to the phenyl-based counterpart TriPhenylEthene TrPE, since the purity of the available sample, sufficient for the electrochemical measurments, has revealed to be not proper for photophysical ones. Furthermore, crystal it has not been obtained for TrTE, so that the investigation have been performed only in solution, aggregation and powder state.

As usual we have prepared the solution set, by using THF as organic solvent and water as co-solvent, since TrTE is not soluble in this medium. As shown in Figure 5.69 the emission almost faint until 80% of water content, rapidly increases when *fw* reaches the 90%. The emission peak is located at 396 nm.

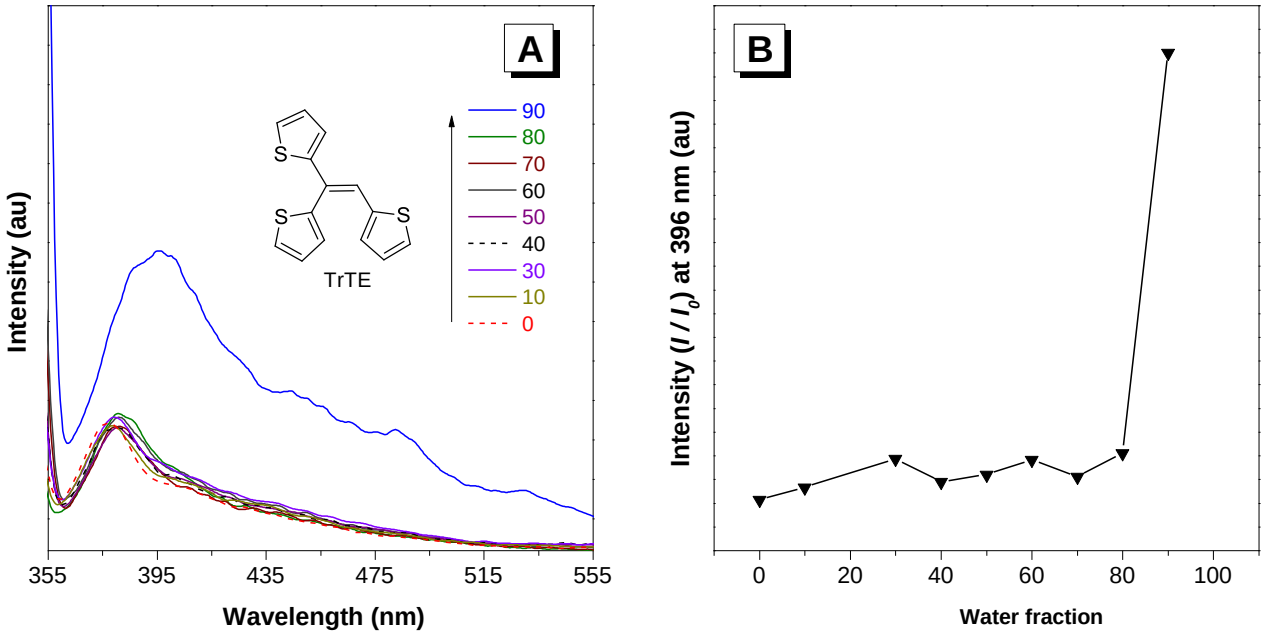

Figure 5.69 (A) The photoluminescence (PL) spectra of TrTE in THF and THF/water mixtures with increasing water fractions (*fw*) to 99%. (B) Change in PL intensity of TrTE at 396 nm versus water fraction in THF/water mixtures. Excitation at 338 nm.

Recording the PL spectrum in powder and comparing it with respect to the one recorded in aggregation condition, we can observe (Figure 5.70), that even in this case, there is red-shift going from the aggregation to the powder. Although for this molecule the crystal structure is not available, from the experimental results, obtained for the other molecules, we can suppose that even in this case, the significant red shift (34 nm) is ascribable to the clusteroluminogenic effect, generated due to the S---S interactions.

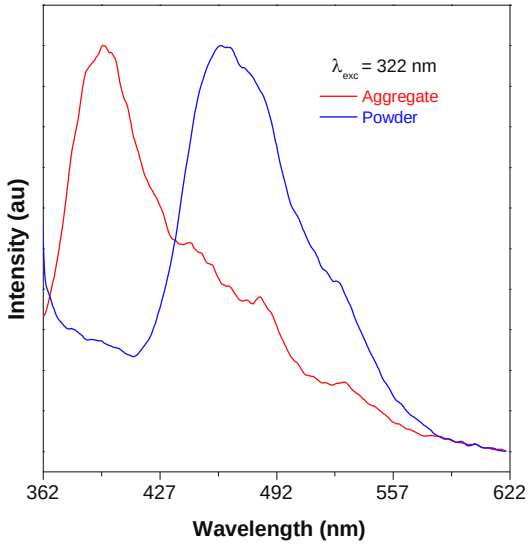

Figure 5.70 Photoluminescence (PL) spectra of TrTE in aggregate (red) and powder (blue) state.

5.7 Summarizing…

In Table 15, are collected all the data obtained during the investigation, both the photophysical and the crystal one. Summarizing the concepts came into the light during this pioneering work, it is remarkable to note that:

- TTE and TFE have revealed to be AIE luminogen whose emission work mechanism is the restriction of intramolecular rotation RIR, as it has been proved by synthesizing and investigating the emission of the locked counterparts fl-TTE and fl-TFE respectively.
  TTE and TFE are also good emitter in powder and crystal state and a red-shift emission has been observed going from the aggregate to the crystal. Thanks to a very deep investigation on the crystal structure of TTE and TFE, it has been found out that the crystal network is much more conjugated than the aggregate one due to the presence of heteroatom to heteroatom interactions that allow to extend the π-conjugation efficiency through the space, so allowing cluster formation in the crystal state. This effect is known as clusteroluminogenic effect.
- fl-TTE and fl-TFE as well as to be classic ACQ molecule, they resulted to be emissive in solid state, even if no crystal date were available for this molecule, a combination of no effective π-π stacking and clusteroluminogenic effect can be the cause of the solid state luminescent property;

- DTE and DFE are ACQ dye since the emission is quenched in aggregation condition; however they are good emitter both in powder and crystal and even in their case an emission red-shift occurs going from the aggregate to the crystal. Also DPE (stilbene) resulted to be emissive ACQ but emissive in solid state. The reason behind this behaviour is due to the lack of effective π-π stacking interactions in solid that would lead to the emission quenching that contrarily to the solid state occurs for all of them in aggregation condition;

- The comparison between DTE and the oxidized counter-part BDT which have resulted not-emissive in all three aggregate states (aggregation, powder and crystal); have proved that locking the molecule and so creating a central benzene ring to which the side thiophenes are condensed effective π-π stacking can be generated in the crystal, so preventing the realization of a radiative relaxation pathway that would lead to the light emission;

- TrTE have resulted to be an AIE luminogen whose working mechanism supposed to be the RIR like occurs for TTE, will be investigated by synthesizing the corresponding locked structure. Similarly to TTE, TrTE also emits in powder and the related emission is red-shifted compared to the Aggregation one.

It is remarkable to note that the crystal state analysis has revealed to be an indispensable tool to understand and correctly decipher the emission trend for this class of molecules.

Table 15 Photophysical data of the investigated molecules

Luminogen	λ_{ab} /nm	ΔE /eV	λ_{em} /nm			$\Delta\lambda^a$ /nm	AIE or ACQ	α AIE[b]	$\Phi_{F,A}$ / %	τ / ns
			Aggregate	Powder	Crystal					
TPE	360	3.45	462	447	450	-12	AIE	344	23[c]	1.29[c]
TTE	413	3.01	409	413	444	35	AIE	20	2.6[c]	0.47[c]
sl-TTE	359	3.46	380[c], 389[c], 489[d]			/	AIE and ACQ	1.47	N.A.	N.A.
fl-TTE	382	3.25	381[d]; 450[e]			/	ACQ	0.1	0.1	0.94
TFE	439	2.83	489	499	532	43	AIE	8.9	11[c]	1.58[c]
fl-TFE	363	3.42	361[d]; 460[e]			/	ACQ	0.0001	N.A.	N.A.
DPE	334	3.72	353	367	382	29	ACQ	0.2	N.A.	N.A.
DTE	377	3.29	402	442	438	36	ACQ	0.25	15	0.85
DFE	352	3.53	372	401	399	27	ACQ	0.058	32	1.28
BDT	322	3.86	330	not emissive	not emissive	/	ACQ	0.21	N.A.	N.A.
TrTE	385	3.22	363	497	/	/	AIE	4.00	2.6	0.44

λab = longest absorption in THF, onset value; λem = emission maximum, ΔE, Optical Energy gap calculated by UV-Vis spectrum, ΦF,A = absolute fluorescent quantum yield measured by a calibrated integrating sphere, τ = lifetime, [a] difference between the emission wavelength in crystal and in aggregate state, [b] the ratio between the emission intensity at 99% and 0% of water fraction (i99/i0), [c] aggregation state, [d] solution state, [e] powder stat.,

5.8 Applications of the investigated molecules

5.8.1 Bioimaging applications

Since the advent of AIE, a plenty of AIEgen has been successfully used in bioimaging [12] a field in which luminescent materials are used to visualize and track cellular events, by exploiting the fluorescence emission of the molecule used as probe. In order to unearth a possible application for the investigated molecules, that have revealed to be good AIE gen all of them (with the exception of TrTE) have been tested in this field; but among DTE, DFE, TTE and TFE, only TTE has been able to enter inside the cells. Two different kind of human cancer cells have been tested: Hela cells and lung cancer cells. TTE has been able to go inside both of them just after 15', selectively marking the lipid droplets, in Figure 5.71 are shown the images after an incubation time of 30'.

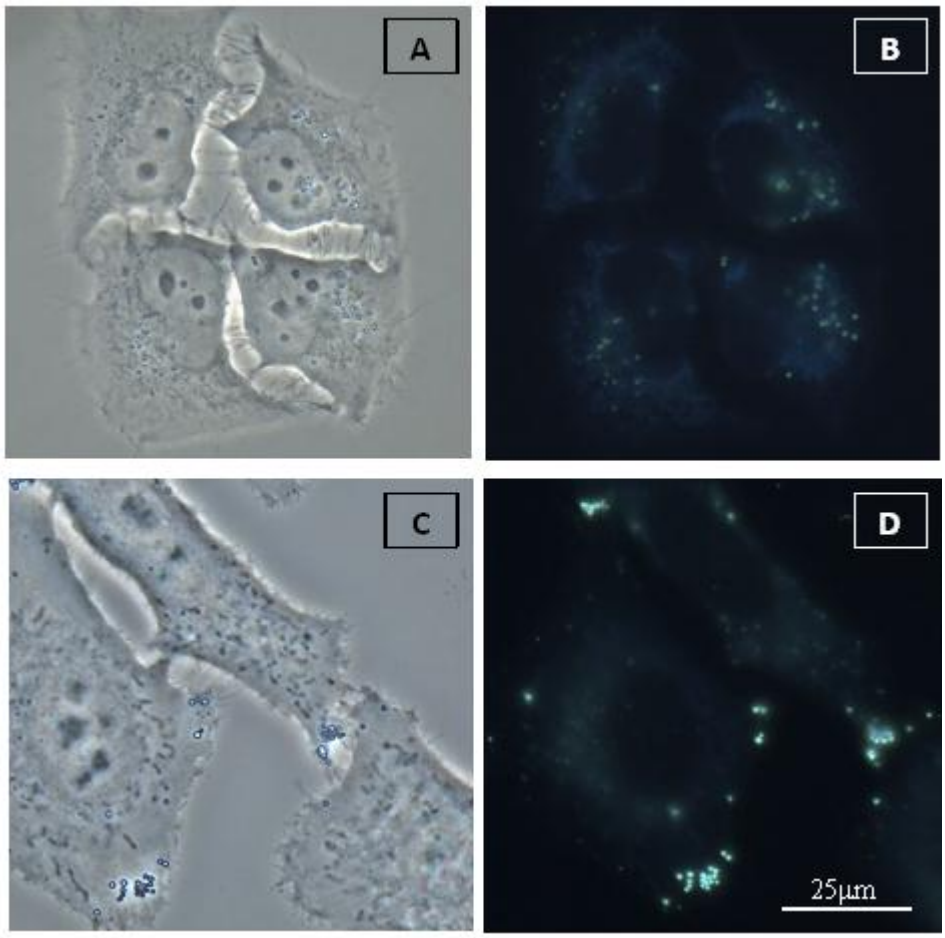

Figure 5.71 Images of lipid droplets selectively targeted by TTE. (A) Bright field and (B) fluorescent images of the HeLa cells; (C) bright field and (D) fluorescent images of the lung cancer cells A549. Incubation time 30'; excitation wavelength 330-385 nm.

In order to prove that TTE really select the lipid droplets, a co-staining experiment has been performed by using the commercial dye BODIPY, that is well known to selectively marked these organelles. This experiment has been carried out both in HeLa and in lung cancer cell, co-staining the cells with both dyes, TTE and BODIPY. In Figure 5.72 is reported the result obtained for the HeLa cells, that have been incubated with oleic acid before the staining. In HeLa cells the amount of the lipid droplets is typically low (contrarily to the lung cancer cells),

since these kind of organelles were monitored, before performing this experiment, the cell has been incubated with oleic acid, in order to promote the production of the lipid droplets inside, so having the possibility to have a better tracking of the phenomenon. This procedure, have not been followed for the lung cancer cells, since they intrinsically own a higher amount of lipid droplets. As it is possible to observe in Figure 5.72, TTE and BODIPY stain the same area of the cellular environment, since BODIPY is used as lipid droplets marker, it is possible to deduce that TTE definitely stain these organelles.

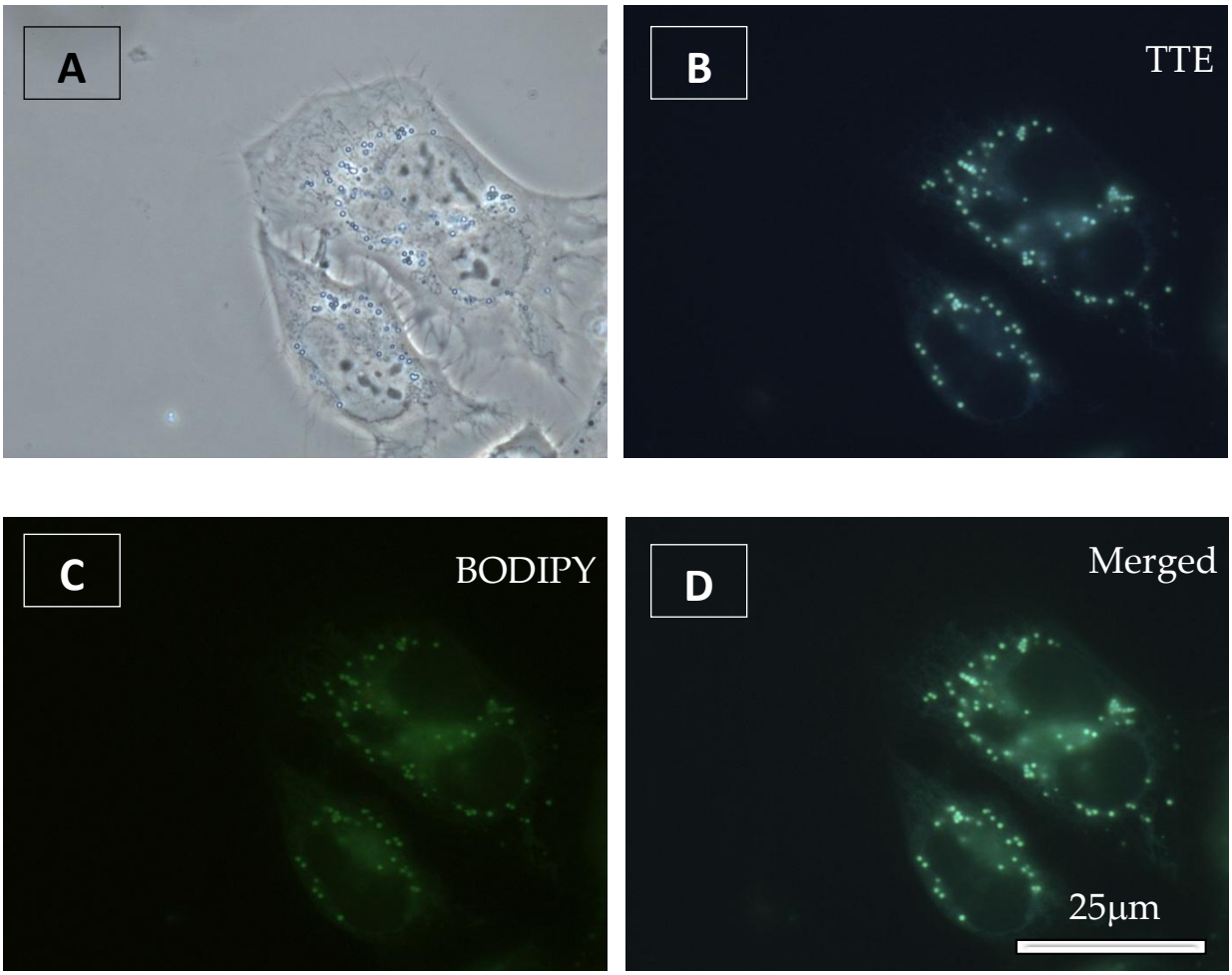

Figure 5.72 HeLa cells incubated with oleic acid for 6h and then stained by TTE (10µM) and BODIPY(1 µ g/mL) for 15'. (A) bright field, (B-D) fluorescent images. Excitation wavelength 330-385 nm.

The same experiment, the co-staining of the cell by BODIPY and TTE, has been performed for lung cancer cell, (without the previous incubation with oleic acid) the results is reported in Figure 5.73. Even in this case the experiment prove that TTE really stain the lipid droplets, since the same cellular organelles is marked also by BODIPY.

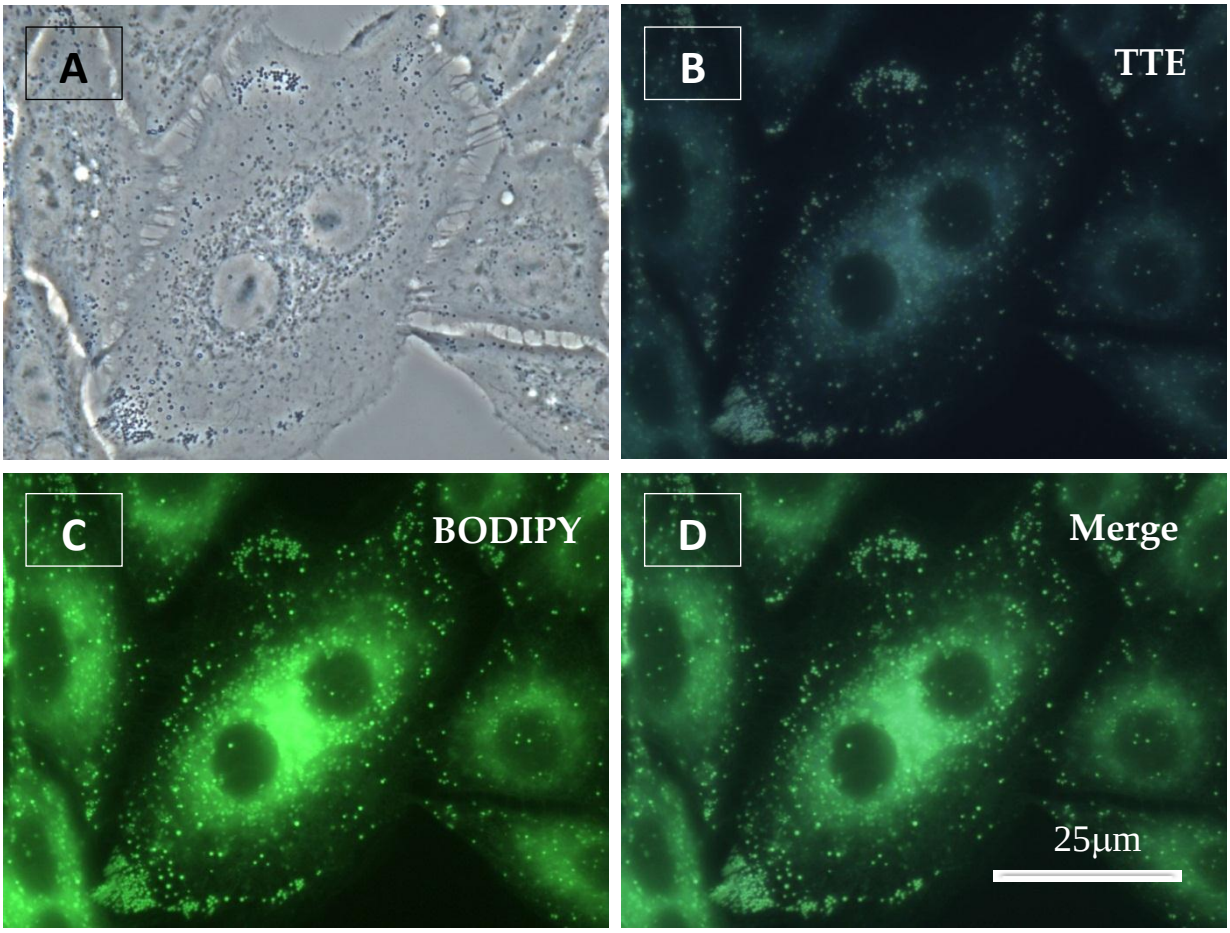

Figure 5.73 Lung cancer cell A549 stained by TTE (10μM) and BODIPY(1 μ g/mL) for 15'. (A) Bright field, (B-D) fluorescent images. Excitation wavelength 330-385 nm.

Comparing the two set of images (Figure 5.72 and 5.73), we can note that in HeLa case, TTE provides a shinier images respect to BODIPY, while the opposite effect occur in lung cell (figure above) where BODIPY is more emissive than TTE. BODIPY should be a better an greener emitter than TTE (like occurs in lung cancer cell experiment), therefore the results emerged in HeLa cell case it has been a little bit abnormal. Since the difference between the two experiments has been just the use of the oleic acid before the staining, we have repeated the experiment in HeLa cell without the previous incubation with the oleic acid. The results, reported in Figure 5.74, has been in this case equal to the lung cancer cell experiment, as TTE have resulted to be less emissive than BODIPY. Therefore we can deduce that a specific interaction with the organelles, occurs when the cell are previously incubated with oleic acid.

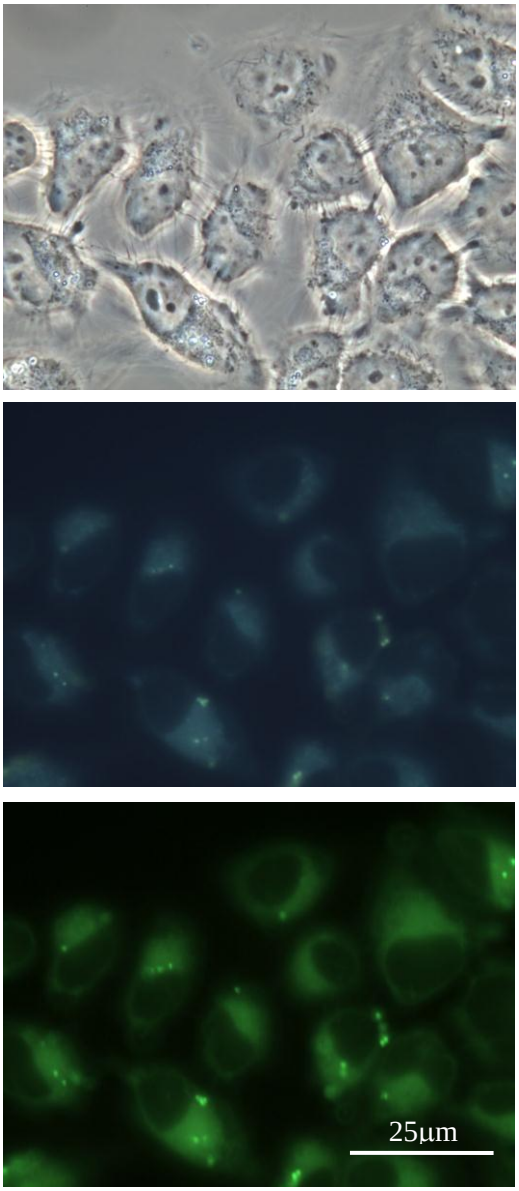

Figure 5.74. HeLa stained by TTE (10μM) and BODIPY(1 μg/mL) for 15'.

The photostability of TTE has been tested both in HeLa and in lung cancer cell, they are reported in Figure 5.75-76.

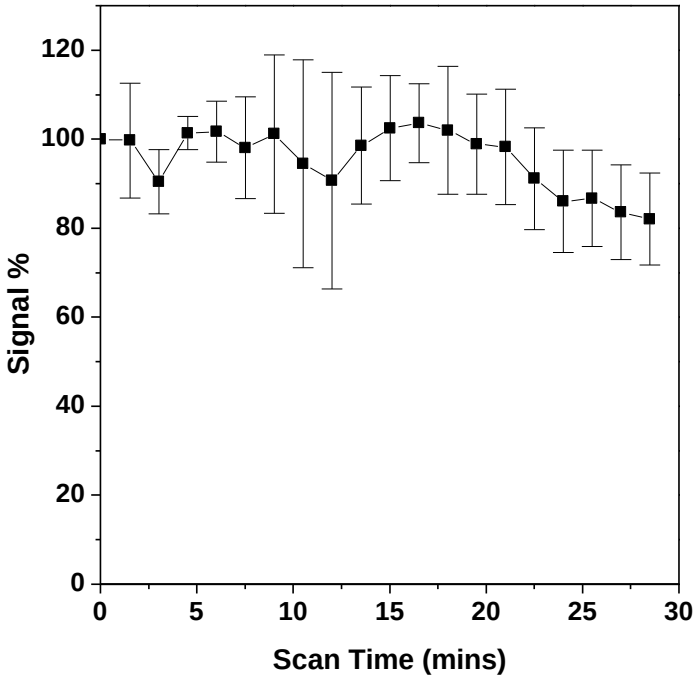

Figure 5.75 Photostability of TTE in HeLa cell.

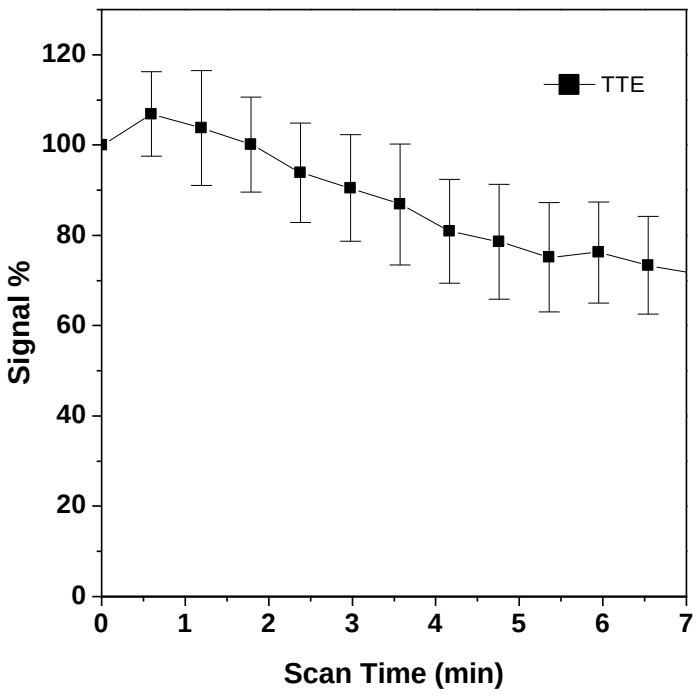

Figure 5.76 Photostability of TTE in lung cancer cell A549.

In Figure 5.77 is reported the cytotoxicity of TTE in HeLa cells, from which it emerges that TTE is biocompatible since cell viability has only a slight decrease with the increasing of the dye concentration.

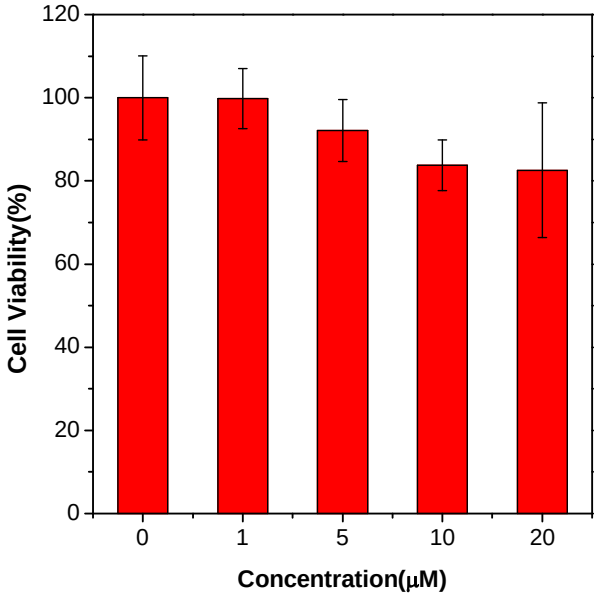

Figure 5.77 Cell viability tested by MTT assay: Hela cells were incubated with different concentrations of TTE in culture medium for 24 hours.

Therefore TTE, has revealed to be a promising scaffold for bioimaging, since without owning any functional groups it has been able to enter inside the cell and selectively marked the lipid droplets.

5.8.2 Potential Photochromic applications

During the study performed for TTE molecules, we have taken picture of TTE, sl-TTE and fl-TTE in powder state irradiating the samples by the handle UV-lamp at 365 nm, we have noted that, while TTE and fl-TTE do not change their color after the irradiation, the sl-TTE, that is a white powder, becomes ligh pink after absorbing light (Figure 5.75 C). The effect take place after just 30'', and it is reversible since irradiating the sample by visible light, the color turn to be white. This phenomenon can pave the way in developing new TTE-based molecules with photochromic features.

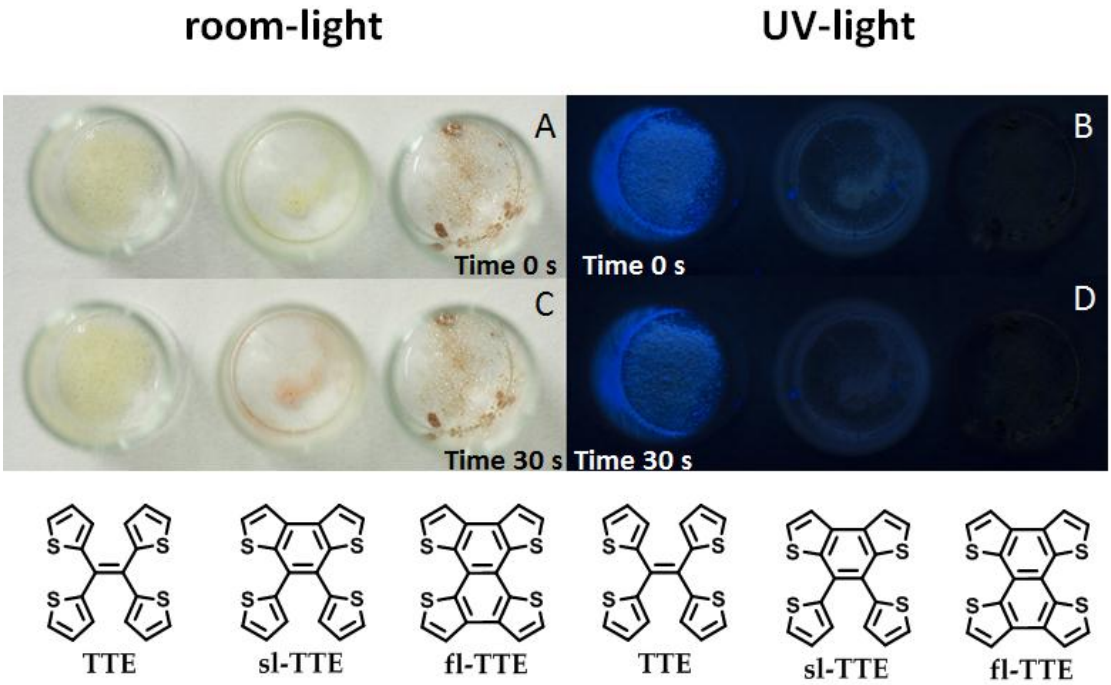

Figure 5.75. Photochromism phenomenon in sl-TTE. (The other indicated molecules are reported for sake of comparison).

Bibliography Chapter 5

[1] *Acta Crystallographica section B: Structural Crystallography and Crystal Chemistry* **1975**, *31*, 2633;
[2] (a) A. Bolzoni, L. Viglianti, C. Baldoli, E. Licandro *et al*, *Eur JOC*, **2013**, *33*, 7489; (b) F. Martinez *et al*. Structural Chemistry **2012**, *23*, 1751; (c) S. C. Capelli, S. V. Meille, C. Bertarelli, *Journal of the Chemical Society*, *Perkin Transactions* 2, **2002**, *10*, 1752; (d) I. Hiraku et al, *Heterocycles*, **1986**, *24*, 1291; (e) Kellog et al, *JOC*, **1967**, *32*, 3093;
[3] J. W. Y. Lam, Y. Dong B. Z. Tang *et al*., *Chem. Mater*., **2003**, *15*, 1535;
[4] J. W. Y. Lam, Y. Dong B. Z. Tang *et al*., *Chem. Commun.*, **2009**, 4332;
[5] R. Hu, H. deng, J. W. Y. Lam, B. Z. Tang *et al*., *J. Mater. Chem. C.*, **2014**, 6326;
[6] N. Harrit *et al*., *JOC*, ***1996***, *61*, 6997;
[7] Dr. Ni Xie PhD Thesis in Chemistry, 2013, The Hong Kong University of Science and Technology;
[8] E. Zhao, J. W. Y. Lam, B. Z. Tang *et al*, Macromolecules, **2015**, *48*, 64;
[9] S. Grimme, *Angew. Chem. Int. Ed*., **2008**, *47*, 3430;
[10] (a) F. D. Lewis *JACS*, **1977**, *99*, 7991; (b) P. Vladimir et al., *Inorganica Chimica Acta*, **2014**, *409*,342; (c) Aloisi, Sanderson et al., *Chemical Physics letters*, **1997**, *266*, 309;
[11] D. Sherrill *et al*., *JACS*, **2002**, *124*, 10887;
[12] (a) E. Wang, E. Zhao, Y. Hong, J. W. Y. Lam, B. Z. Tang et al, *J. Mater. Chem. B.* **2014**, *2*, 2013; (b) J. W. Y. Lam, B. Z. Tang *et al*, *Adv. Funct. Mater.* **2011**, *21*, 1733; (c) J. W. Y. Lam, B. Z. Tang *et al*, *Chem. Eur. J*. **2010**, *16*, 4266.

UV-vis characterization of the investigated molecules

Table I Key absorption features of the investigated molecules.

Molecule	$\lambda_{ab\,/nm}$ [i]	$\varepsilon / M^{-1} cm^{-1}$ [ii]	***Energy Gap /eV***
TPE	360	$0.725x10^4$	3.45
TTE	413	$1.35x10^4$	3.01
sl-TTE	359	$0.77x10^4$	3.46
fl-TTE	382	$0.86x10^4$	3.25
TFE	439	$2.28x10^4$	2.83
fl-TFE	363	$0.49x10^4$	3.42
DPE	334	$1.25x10^4$	3.72
DTE	377	$2.09x10^4$	3.29
DFE	352	$2.72x10^4$	3.53
BDT	322	$0.14x10^4$	3.86
TrTE	385	$5.24x10^4$	3.22
TrFE[iii]	*386*	*$9.9x10^4$*	*3.22*

© onset value, [ii] value at λ_{max}, [iii] recorded in DCM

All the apsorption spectra have been recorded in THF except the one for TrFE that has been performed in DCM, in a precedent work. According to the values reported in the table above, we can observe that energy gaps decrease within each series, with the increasing ring number linked to the ethene core. (Di > Tri > Tetra). The locked molecules have less freedom degrees with respect to the unlocked counterpart, so that their absorption spectrum is featured by sharper and narrower peaks and higher molar absorptivity values; in addition these molecules have a higher energy gap respect to the unlocked ones so proving that the conjugation efficiency is more effective in the unlocked counterparts.

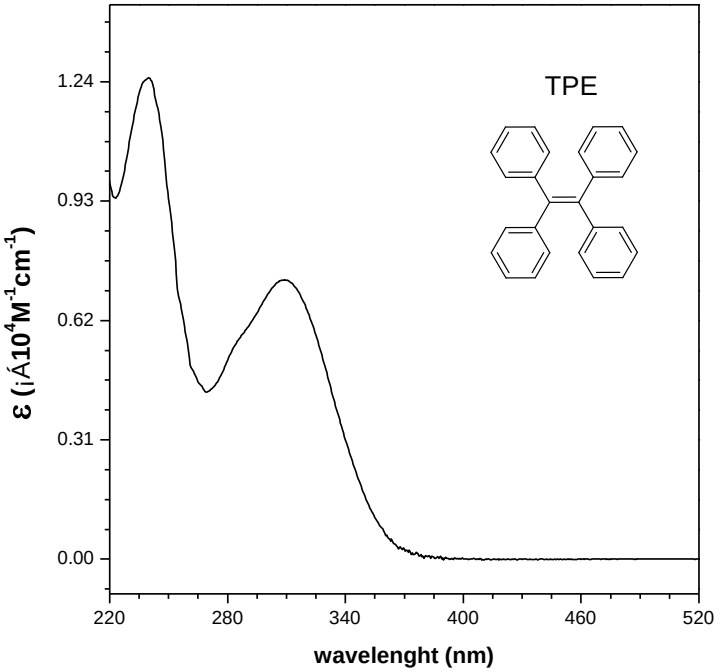

Figure I Molar absorptivity of TPE

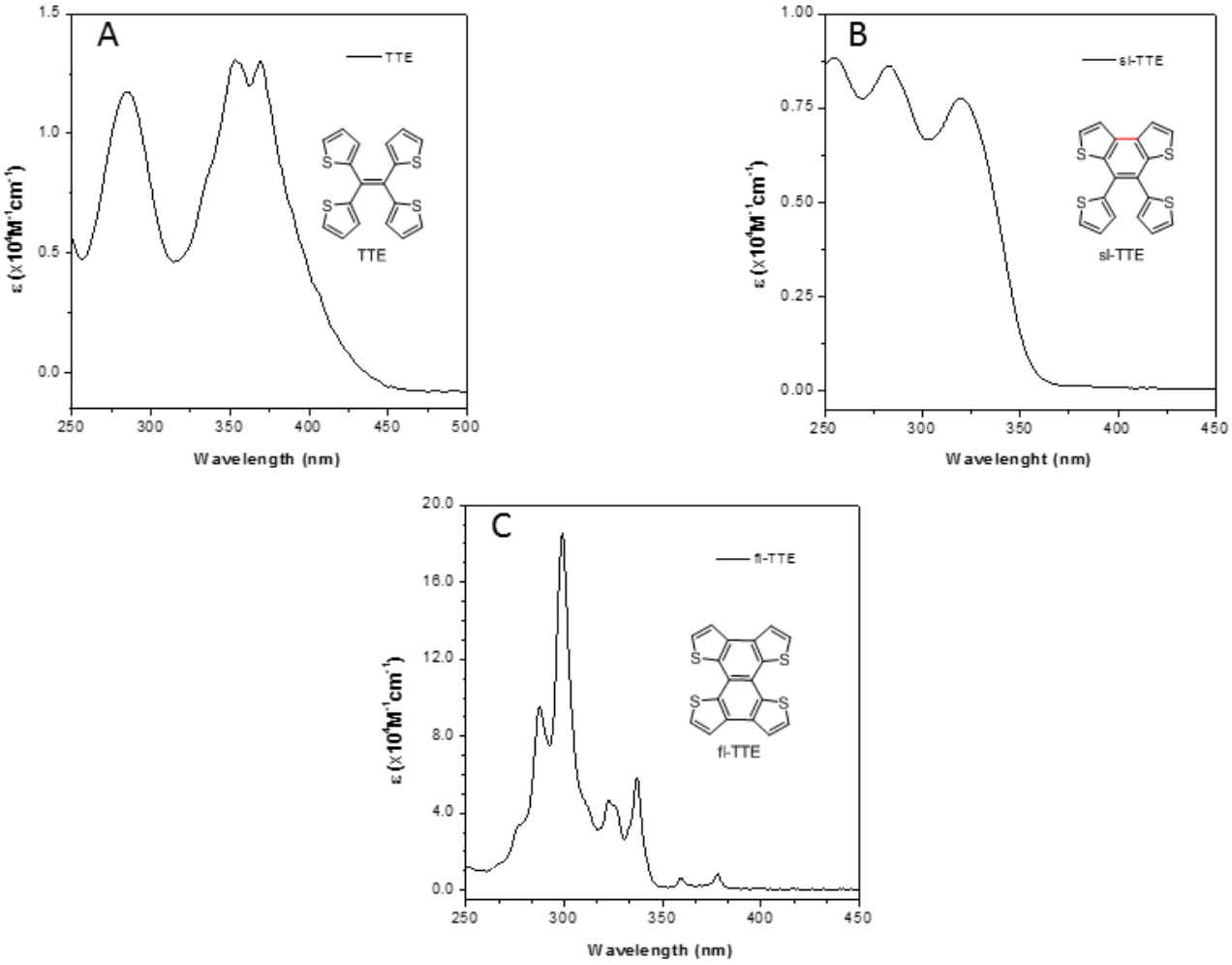

Figure II Molar absorptivity of (A) TTE, (B) sl-TTE, (C) fl-TTE. With the increasing of the rigidity of the molecule absorption becomes narrower and sharper.

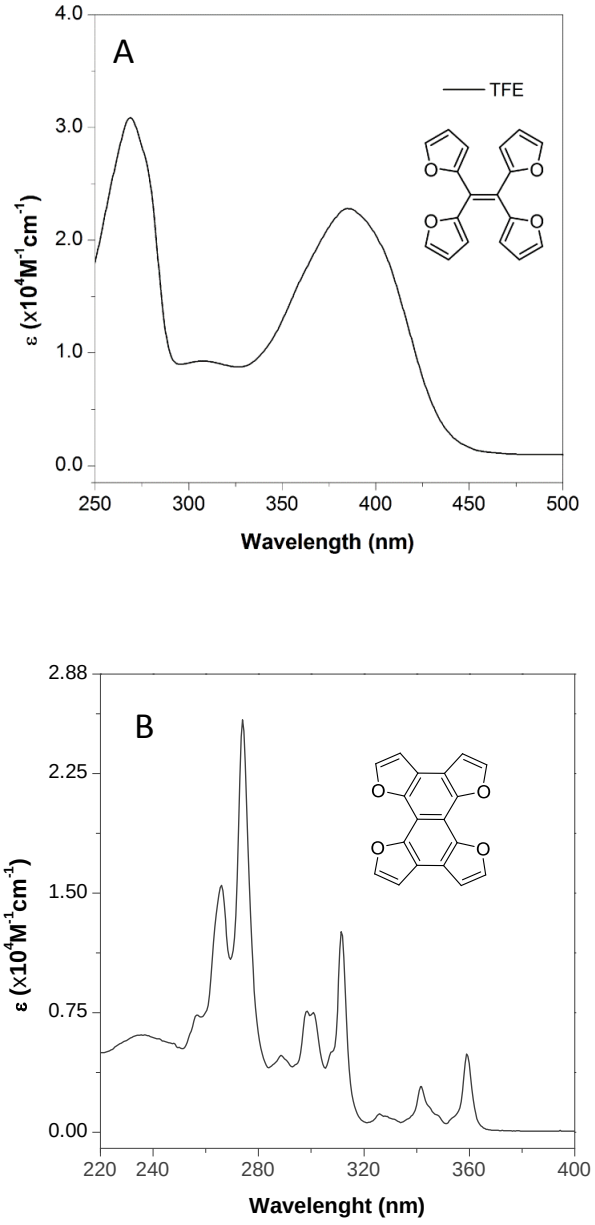

Figure III Molar absorptivity of (A) TFE and (B) fl-TFE.

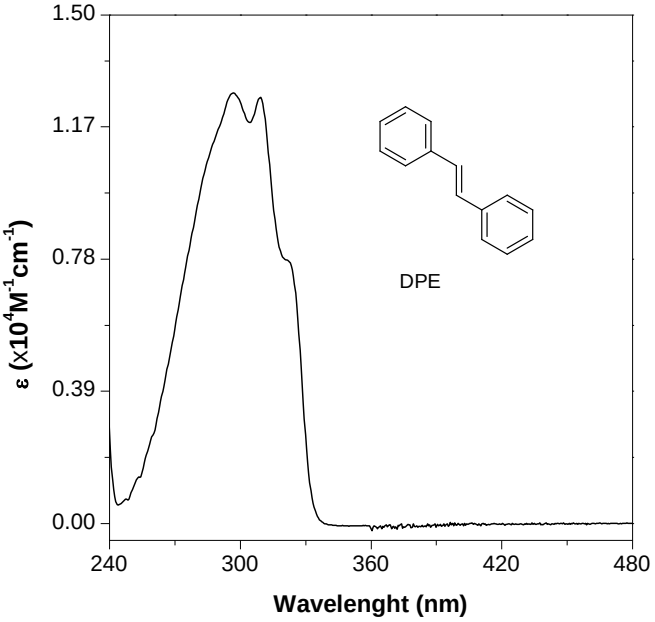

Figure IV Molar absorptivity of DPE

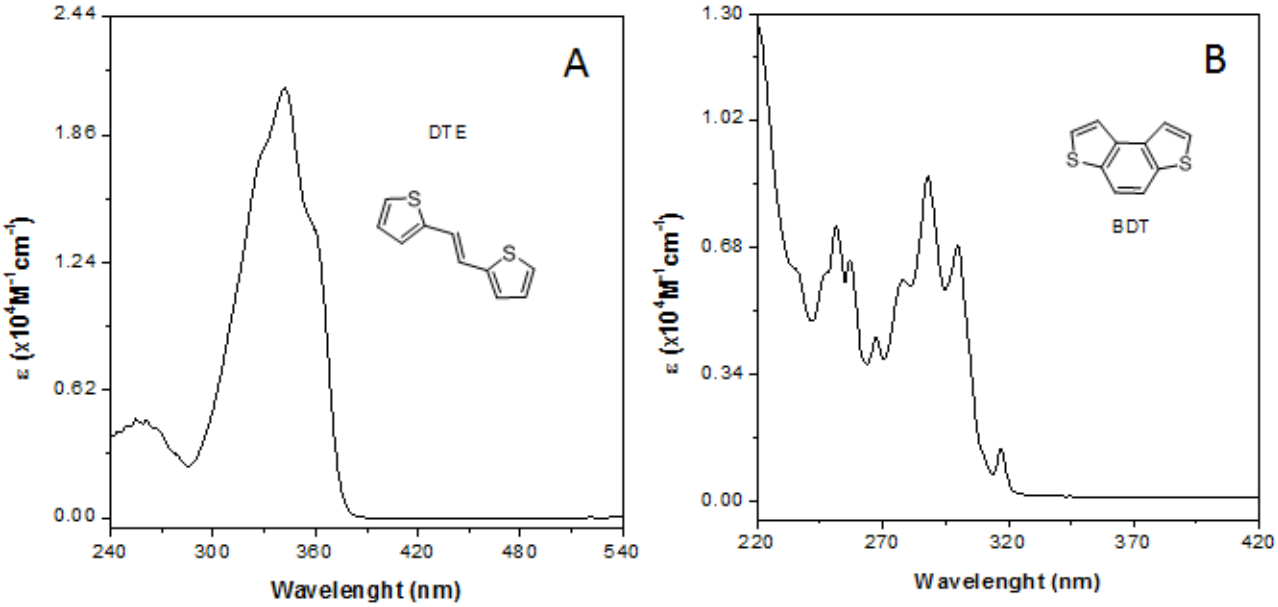

Figure V Molar absorptivity of (A) DTE and (B) BDT

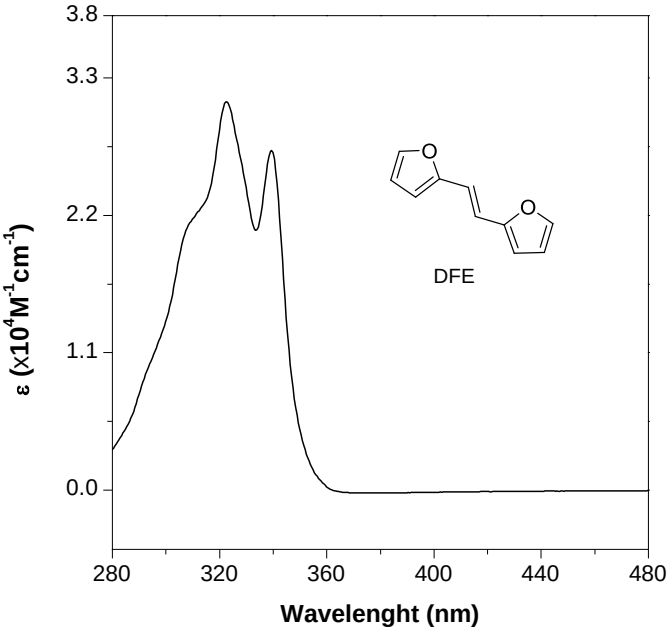

Figure VI Molar absorptivity of DFE

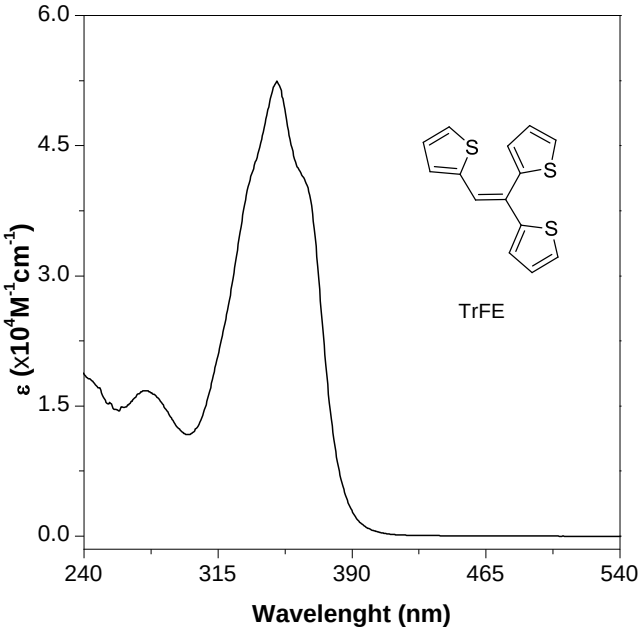

Figure VII Molar absorptivity of TrTE

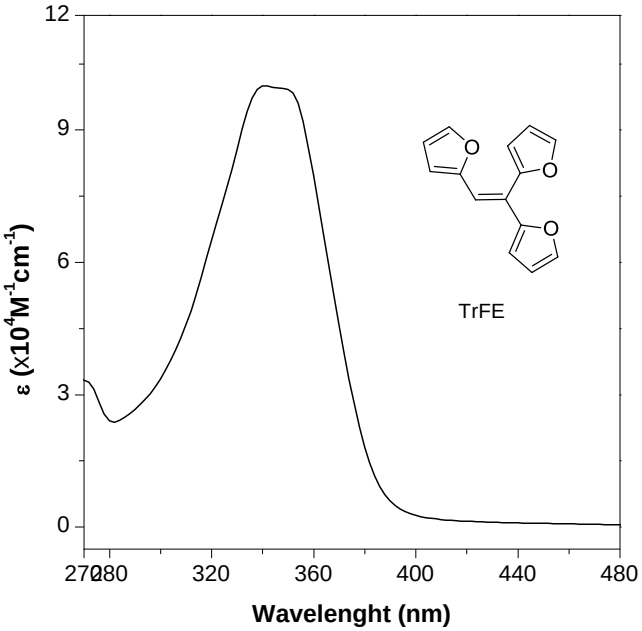

Figure VIII Molar absorptivity of TrFE

Preliminary Theoretical Calculations

Here below are reported some preliminary theoretic results regarding TTE and TFE, that have been performed in collaboration with Prof. Emanuele Ortoleva (UNIMI). From the data described below that have been obtained by using both Hartree-Fock and density functional theory, it has emerged that both TTE and TFE can exist in several conformers and they differ from one another by 10 Kcal/mol, so that all of them are accessible from the energetic point of view. The HOMO-LUMO gap have also been calculated.

Hartree-Fock (HF) and density functional theory (DFT) computations had been done using GAUSSIAN 09 suite of programs. Meta-hybrid GGA functional M06 had been chosen as it can take account of long range dispersion interaction, that is important in assessing rings orientation, and gives energy barriers enough accurate.

In HF computations valence double zeta plus polarization on all atoms basis set, 6-31g(d,p), had been used and in DFT valence triple zeta plus polarization on all atoms plus diffused on heavy atoms basis set 6-311+g(d,p).

Seven distinct structures had been identified for both TFE and TTE, they are hereafter indicated by the form **c+t-c+t-** where **c** and **t** are in place of *cis* and *trans* and indicate the orientation of the heteroatom respect to the ethene double bond and + and – indicate the position of the heteroatom below or over the mean plane of the molecule. The order is indicated by the subscript of torsion angles in the following scheme.

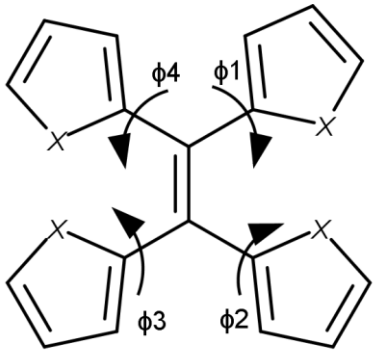

As each structure presents two enantiomers the are fourteen conformers. Each structure have been fully optimized and vibrational frequencies have been computed to confirm the stationary point type. Both Tetra(2-furyl)ethene TFE and Tetra(2-thienyl)ethene TTE have rings tilted out of plane as it happens in Tetraphenylethylene TPE because of the steric hindrance of the rings. The ethene bond, also, is rather twisted featuring an angle between 10° and 20°. The relevant geometrical data are reported in Table I.

Table I: relevant geometrical parameters of TFE (Tetra(2-furyl)ethylene), TTE (Tetra(2-thienyl)ethylene) and TPE (Tetraphenylethylene) computed at HF and DFT level. $\theta_{C=C}$ is the torsion of the ethylene bond, ϕ_1, ϕ_2, ϕ_3 and ϕ_4 are the torsions X-C-C=C as indicated in the preceding scheme. For comparison sake the C=C distance in ethylene is: 1.3223 Å with HF and 1.3230 with DFT.

TFE													
		HF/6-31g(d,p)						**M06/6-311+g(d,p)**					
	Sym	$R_{C=C}$ (Å)	$\vartheta_{C=C}$	φ_1	φ_2	φ_3	φ_4	$R_{C=C}$ (Å)	$\vartheta_{C=C}$	φ_1	φ_2	φ_3	φ_4
c+t+c+c-		1.3462	-14.1	-38	130	-37	-33	1.3715	-20.4	-32	146	-33	-37
t+t-c-t-		1.3432	-13.9	135	140	-38	124	1.3678	-16.9	127	156	-40	146
t-t+c+c-	C_2	1.3440	-12.9	127	127	-35	-35	1.3699	-19.2	-34	144	129	-28
c+t+c+t+	C_2	1.3443	-14.5	-37	132	-37	132	1.3703	-17.8	-41	153	-41	153
c+t+t-c-	C_2	1.3456	-15.5	-39	138	138	-39	1.3714	-20.5	-36	146	146	-36
t-t+t-t+	D_2	1.3425	-15.4	135	135	135	135	1.3643	-18.5	128	150	128	150
c+c-c+c-	D_2	1.3483	-14.7	-36	-36	-36	-36	1.3719	-20.1	-33	-33	-33	-33
TTE													
c+c-t-c-		1.3434	-10.3	-55	-54	128	-56	1.3667	-15.3	-41	-54	128	-35
t+t-c-t+		1.3421	-11.2	123	122	-56	128	1.3657	-15.4	129	134	-39	127
c+c-t-t+	C_2	1.3424	-10.2	-54	-54	123	123	1.3672	-17.7	-46	-46	135	135
c+t+c+t+	C_2	1.3434	-10.9	-56	128	-56	128	1.3659	-14.1	-35	123	-35	123
c+t+t-c-	C_2	1.3426	-10.1	-58	126	-58	126	1.3662	-16.1	-44	132	132	-44
t-t+t-t+	D_2	1.3413	-10.7	124	124	124	124	1.3630	-13.5	131	131	131	131
c+c-c+c-	D_2	1.3437	-10.8	-54	-54	-54	-54	1.3671	-16.3	-46	-46	-46	-46
TPE													
	D_2	1.3394	7.9	-126	56	-126	56	1.3537	9.4	-130	51	-130	51

As can be deduced from the table the CC double bond is more twisted in TFE than in TTE with a consequent elongation of the CC distance while TPE show only a slight torsion. As a consequence of the reduced torsion in TTE the thiophene rings are more out of plane.

The M06 results are in agreement with the HF ones; as this DFT functional contains a certain degree of correlation error correction it gives a C=C distance longer than the one computed with HF: therefore there is a reduction of hindrance which produces a lesser twisting of both the C=C bond and of the rings.

Energies of different conformers are reported in Table II in any case all the conformers lay in a range of maximum 3 kcal/mol. A complete analysis of the reaction pathway among such a number of conformers is outside the aim of this work, relaxed scans, with both methods, of the complete rotation of a single ring either in TFE or in TTE showed barriers of few kcal/mol and anyway less

than 10 kcal/mol. As a consequence, in experimental condition, all the conformers should be present with a rather uniform distribution both in gas and diluted solution phases.

Table II. Energies and relative energies of TFE and TTE. a) E_{tot} is sum of the electronic energy and the zero point vibrational energy computed in harmonic approximation. b) relative energy in kcal/mol.

	TFE				**TTE**			
	HF/6-31g(d,p)		**M06/6-311+g(d,p)**		**HF/6-31g(d,p)**		**M06/6-311+g(d,p)**	
	E_{tot} (a.u.)[a]	ΔE[b]	E_{tot} (a.u.)[a]	ΔE[b]	E_{tot} (a.u.)[a]	ΔE[b]	E_{tot} (a.u.)[a]	ΔE[b]
c+t+c+c-	-987.679483	0.80	-993.259444	0.82	-2278.334534	1.97	-2285.200264	0.31
t+t-c-t-	-987.678242	1.57	-993.257334	2.15	-2278.336528	0.72	-2285.200234	0.33
t-t+c+c-	-987.679091	1.04	-993.257772	1.87	-2278.335672	1.26	-2285.200031	0.46
c+t+c+t+	-987.678133	1.64	-993.258392	1.48	-2278.335277	1.50	-2285.200711	0.03
c+t+t-c-	-987.678748	1.26	-993.258728	1.27	-2278.335450	1.40	-2285.200757	0.00
t-t+t-t+	-987.677909	1.78	-993.255831	3.09	-2278.337675	0.00	-2285.199805	0.60
c+c-c+c-	-987.680750	0.00	-993.260758	0.00	-2278.333693	2.50	-2285.200020	0.46

In Table III are reported the gaps between the highest occupied (HOMO) and lowest unoccupied (LUMO) orbitals. It should be noted that HF eigenvalues are true energies of the orbitals and, in the scheme of Koopmans theorem, the eigenvalue of HOMO is the opposite of the energy to extract an electron and that of LUMO is the energy to add an electron so the difference between LUMO and HOMO is an adiabatic approximation of excitation energy to the first excited electronic state. Otherwise the DFT eigenvalues are the derivate of energy respect the occupation number of pseudo-orbitals: in fact in Kohn-Sham method the "orbitals" are not true wave functions but only a tool to get the correct electron density.

With a heavy approximation we can obtain the energy, ΔE , to extract an electron from *i-th* pseudo-orbital:

$\Delta E = -\int_{2}^{1} \frac{\partial E(n)}{\partial n_i} dn_i$, if we assume that $\frac{\partial E(n)}{\partial n_i}$ is constant from n_i =2 to n_i =1, which is a rough approximation then: $\Delta E = -\frac{\partial E(n)}{\partial n_i} = -\varepsilon_i^{(DFT)}$.

Anyway is known that LUMO energies, as computed by DFT methods, are generally unrealistically low, so, while HF gaps are expected to be too high, the DFT gap are definitely too low.

Table III. Highest occupied (HOMO) and lowest unoccupied (LUMO) orbitals energies of TFE,TTE and TPE along with HOMO-LUMO gap, Δε. The LUMO HOMO gap in Ethylene is 15.01 eV (HF) and 7.76 eV (DFT).

	HF/6-31g(d,p)			**M06/6-311+g(d,p)**		
	HOMO (a.u.)	LUMO (a.u.)	Δε (eV)	HOMO (a.u.)	LUMO (a.u.)	Δε (eV)
	TFE					
c+t+c+c-	-0.25441	0.08036	9.11	-0.19791	-0.06801	3.53
t+t-c-t-	-0.26192	0.08619	9.47	-0.20238	-0.06727	3.68
t-t+c+c-	-0.26022	0.08467	9.39	-0.20088	-0.06776	3.62
c+t+c+t+	-0.25963	0.08356	9.34	-0.20021	-0.06793	3.60
c+t+t-c-	-0.25647	0.08173	9.20	-0.19912	-0.06816	3.56
t-t+t-t+	-0.26158	0.08788	9.51	-0.20343	-0.06654	3.72
c+c-c+c-	-0.24878	0.07710	8.87	-0.19608	-0.06812	3.48
	TTE					
c+c-t-c-	*-0.27141*	0.07746	9.49	-0.20608	-0.06978	3.71
t+t-c-t+	-0.27596	0.08285	9.76	-0.20774	-0.06820	3.80
c+c-t-t+	-0.27441	0.08035	9.65	-0.20621	-0.06988	3.71
c+t+c+t+	-0.27276	0.07919	9.58	-0.20736	-0.06827	3.78
c+t+t-c-	-0.27382	0.08082	9.65	-0.20659	-0.06908	3.74
t-t+t-t+	-0.27813	0.08587	9.91	-0.20976	-0.06610	3.91
c+c-c+c-	-0.26951	0.07519	9.38	-0.20513	-0.07073	3.66
c+t+c+c-	-0.27141	0.07746	9.49	-0.20608	-0.06978	3.71
	TPE					
	-0.27277	0.10171	10.19	-0.21924	-0.05175	4.56

Range gap HF : TFE .64 TTE .53 – DFT: TFE .24 TTE .25
Range C=C HF: TFW .0058 TTE .0041 - DFT: TFE .0024 TTE .0041

Bibliography

Gaussian 09, Revision A.02, M. J. Frisch, G. W. Trucks, H. B. Schlegel, G. E. Scuseria, M. A. Robb, J. R. Cheeseman, G. Scalmani, V. Barone, B. Mennucci, G. A. Petersson, H. Nakatsuji, M. Caricato, X. Li, H. P. Hratchian, A. F. Izmaylov, J. Bloino, G. Zheng, J. L. Sonnenberg, M. Hada, M. Ehara, K. Toyota, R. Fukuda, J. Hasegawa, M. Ishida, T. Nakajima, Y. Honda, O. Kitao, H. Nakai, T. Vreven, J. A. Montgomery, Jr., J. E. Peralta, F. Ogliaro, M. Bearpark, J. J. Heyd, E. Brothers, K. N. Kudin, V. N. Staroverov, R. Kobayashi, J. Normand, K. Raghavachari, A. Rendell, J. C. Burant, S. S. Iyengar, J. Tomasi, M. Cossi, N. Rega, J. M. Millam, M. Klene, J. E. Knox, J. B. Cross, V. Bakken, C. Adamo, J. Jaramillo, R. Gomperts, R. E. Stratmann, O. Yazyev, A. J. Austin, R. Cammi, C. Pomelli, J. W. Ochterski, R. L. Martin, K. Morokuma, V. G. Zakrzewski, G. A. Voth, P. Salvador, J. J. Dannenberg, S. Dapprich, A. D. Daniels, Ö. Farkas, J. B. Foresman, J. V. Ortiz, J. Cioslowski, and D. J. Fox, Gaussian, Inc., Wallingford CT, 2009.

Zhao, Y.; Truhlar, D.G. *Theor. Chem. Accoun*, **2008**,120, 215
R.Ditchfield, W.J.Hehre, J.A.Pople, *J.Chem.Phys*. **1971**,54, 724
R.Krishnan, J.S.Binkley, R.Seeger, J.A.Pople, *J.Chem.Phys*., **1980**,72, 650
John P. Perdew, Mel Levy, Phys*. Rev. Lett.*, **1983**,51, 1884
G. Zhang, C. B. Musgrave, *J. Phys. Chem. A,* **2007**, 111, 1554;

6
Concluding Remarks

Thanks to the work performed in this PhD thesis, several featured properties of the investigated Heteroarylethenes (thiophene and furan- based ones) came to the light. The investigated systems were known in literature for many years, but mostly from the synthetic point of view, since most of the molecules (*e.g.* TTE, DTE, DFE) have been simply used as intermediate scaffolds with the aim of synthesizing more complex structures. Therefore the highly interesting electrochemical and photoluminescence characteristics remained concealed until the study performed in this research work. Known synthetic procedure have been optimized and a new synthetic pathway has been performed in order to synthesize the Tri-substituted ethenes.

The electrochemical investigation, performed by cyclic voltammetry, allowed to rationalize the redox properties and the HOMO-LUMO energy gaps, as a function of the ring number and of type of heterocycle. The Heteroarylethenes own a lower energy gap than phenyl-based ones, due to the intrinsic higher electron-richness of the heterocycle. The further comparison between the energy gaps of the investigated molecules and α-α linked oligoarylenes and heteroarylenes proved that the double bond can significantly contribute to the overall π-conjugation efficiency of the molecule. With respect to the phenyl-based counter-parts the heteroarylethenes own electro-oligomerization ability that decreases with the increasing of the ring number linked to the ethene core. All electrodeposited films have resulted to be electrochromic, and the change of color is perceivable when the film grows on ITO, used as working electrode.

By the photoluminescence study performed at *The Hong Kong University of Science and Technology* in Prof. Tang's group, the luminescent behavior of the investigated molecules has been decipher and quantitative proofs of the working mechanism behind, have been provided as well.
Thanks to the research work, performed in his group, it has been possible to confirm the that both TTE and TFE are AIE luminogen whose working mechanism accounted for the restriction of intramolecular rotations RIR. The detailed investigation on their crystal structure allowed to unearth another important phenomenon: the clusteroluminogenic effect; according to, thanks to the Heteroatom to Heteroatom interactions occurring in crystal state, the formation of cluster is realized, as a consequence the molecular network results to be electron-richer and owning a lower energy gap, so that the emission is red-shifted going from the aggregation to the crystal state. The same effect has been observed even in TrTE and in the planar molecules DTE and DFE. The last, on the contrary of TTE, TrTE and TFE, have resulted to be ACQ dyes, since the emission is quenched upon aggregation formation; however DTE and DFE have resulted to be emissive in powder and crystal state too; analyzing their crystal structure it has come out that, despite their planarity and their effective π-conjugation, no π- π stacking interactions occur so that the the excited state, can be deactivated in solid state through the radiative relaxation channel. The molecules have been tested in bioimaging applications. Only TTE has been able to enter inside the cell, selectively staining the lipid droplets both in HeLa and in lung cancer human cells. This results make TTE an extremely promising molecules, since without any functional groups it can go inside the cellular environment selectively marking one of the organelles (*e.g. lipid droplets*).
As described in the introduction, the molecules that show AIE effect are in extremely large number so far, TetraThienylEthene TTE, TetraFurylEthene TFE and TriThienylEthene TrTE are the first example of fully-heterocycle based AIE luminogen. Thus in 2015, international year of the light the AIE luminogenes shine a new light, the light of Heterocycles.

7
Experimental Section

Synthesis of 2-thienylcarbonyl chloride

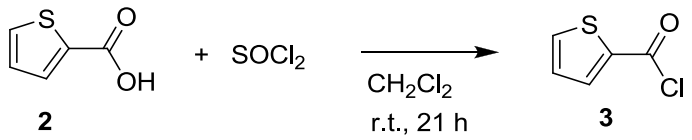

2 **3**

Reference: "*Journal of Medicinal Chemistry"*, (**1989**), 2322

Experimental Procedure:
In a three necked flask (100 mL) equipped with termometer and $CaCl_2$ valve; 2-thiophencarboxylic acid (3.99 g, 31.1 mmol, 1.0 eq.) was dissolved in 50 mL of CH_2Cl_2. $SOCl_2$ (8 mL, 109.7 mmol, 3.5 eq.) was added carefully to the acid solution with a dry glass pipette. The reaction mixture thus obtained did not show any change in temperature, so neither exo- nor endothermic effect were detected. It was observed that reaction mixture aspect changed: from milky to a colorless/yellowish solution just after 40 minutes.

The isolation of acyl chloride was performed by vacuum distillation. In order to distill off all unreacted $SOCl_2$ the following procedure was adopted:

a) a first distillation was carried out (40°C) until 10 mL of reaction mixture were left in the reactor

b) the reactor was cooled to room temperature and vacuum removed

c) 25 mL of CH_2Cl_2 were added to the reaction mixture

d) and distillation was again performed

This procedure (a-d) was repeated three times (Teb(miscela) = 10°C).

Finally temperature was raised to 100°C to distill off eaven the last traces of $SOCl_2$ e CH_2Cl_2.

Acyl chloride was isolated as an orange-brown liquid which was used as such in the subsequent reaction of acylation of Friedel-Craft.

Reaction yield is quantitative.

Synthesis of bis-2-thienyl-ketone

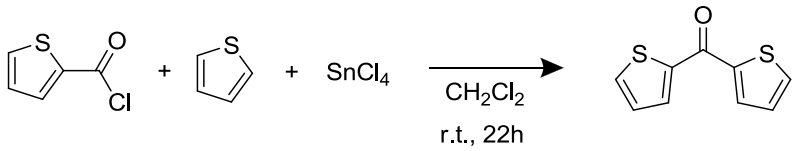

Reference: *"Russian Chemical Bulletin", International Edition*, (**2005**), 54 (5), 1212

Experimental Procedure:
In a three necked flask (100 ml) equipped with termometer, $CaCl_2$ valve and a dropping funnel; acyl chloride was weighted (1.0 g, 6.82 mmol, 1.00 equiv.). Then thiophene (0.6 ml, 7.78 mmol, 1.14 equiv.) was added and the mixture dissolved in CH_2Cl_2 (20 ml), obtaining an orange clear solution.

$SnCl_4$ (2.00 g, 7.64 mmol, 1.12 equiv.) was added dropwise to the reaction mixture. Reaction temperature was kept below 26°C. The starting orange solution turned into a red suspension.

Reaction was monitored by TLC. After 10h only the desired ketone (Rf = 0.730 (AcOEt : MeOH = 1 : 1)) was present.

Reaction mixture was poured into 50 ml of iced water to allow decomplexation at the carbonylic oxygen. A two phases system was formed:

- a red organic layer containing the product

- a green acqueous layer containing all inorganic salts

A filtration trough a celite pad was needed in order to clarify the two phases which were subsequently separated. The acqueous layer was washed repetedly with . All organic phases were collected together, dried over $NaSO_4$, filtered and the solvent distilled off.

The crude obtained was recrystallized from ethanol (6 ml of ethanol for each gram of crude). The product was filtered on Buchner. The product was isolated as white needles in 95% yield

Characterization:
m.p. = 88.0-89.3°C reference (p.f. = 88.0-89.3°C)
^{1}H-NMR (300 MHz, $CDCl_3$): δ, ppm = 7.95 (d, 2H, H(5), ^3J = 3.8 Hz, ^4J = 0.8 Hz); 7.74 (d, 2H, H(3), ^3J = 5.0 Hz, ^4J = 0.8 Hz); 7.23 (q, 2H, H(4), ^3J = 5.0 Hz, ^3J = 3.8 Hz)
^{13}C-NMR: (75 MHz, $CDCl_3$): δ, ppm = 181.24 (C(C=O)); 145.44(C(2)); 135.98 (C(3)); 135.65 (C(4)); 130.50 (C(5))
IR: (CCl_4 solution) 3108.69; 3081.69 cm^{-1} ν stretching C-C aromatic, 1627.63 cm^{-1} ν stretching C=O conjugated with aromatic C=C
UV: (CH_2Cl_2) λ max = 269, 309 nm
MS: m/z 195.1 (M^+,100)
MS-EI (m/z): 195 ([M^+], 100%).

Synthesis of Tetrakis(2-furyl)ethene

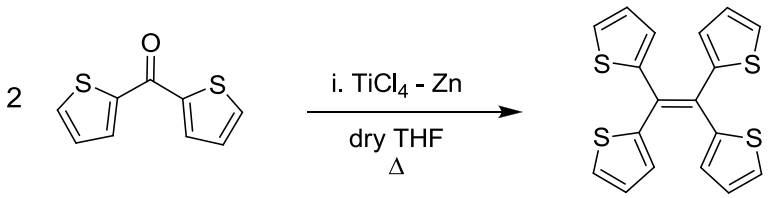

Reference: T. Suzuki, et al., *Angew. Chem . Int. Ed. Engl.*, 1992, 31 *(4)*, 455-458

Experimental Procedure:
In a four necked flask (100 mL) equipped with nitrogen inlet, thermometer and condenser, was introduced deareated, dry THF (15 mL). Then the solvent was cooled to -10°C and $TiCl_4$ (0.31 mL, 2.8 mmol) was added under inert atmosphere. The temperature raised up to -7°C and the reaction mixture became yellow. Then zinc (0.42 g, 6.0 mmol) was added in two portions, temperature raised up to -5°C. The reaction mixture was allowed to stir for 30 minutes at room temperature. At the end of formation of Ti(0) the reaction mixture looked like a green suspension. A solution of di-2-furylketone (0.52 g, 2.7 mmol) in 5 mL of dry THF was added dropwise to the reaction mixture. Then the reaction was refluxed for 10h. The reaction was monitored by TLC (*n*-Hexane/AcOEt : 8/2) till the complete consumption of the ketone. Then the reaction mixture was poured into 20 mL of CH_2Cl_2 and treated with saturated $NaHCO_3$ solution till slightly basic pH. This mixture was allowed to stir for 10 minutes and then filtered through a Celite pad. The organic layer (orange) was separated from the aqueous phase. The aqueous phase was extracted repeatedly with CH_2Cl_2. The organic phases were collected together and dried over Na_2SO_4. Sodium sulfate was filtered off and the solvent distilled off leaving 362 mg of crude. The crude was purified by column chromatography (Hexane/DCM : 8/2) affording 144 mg of desired product (38% yield).

Characterization:

m.p. = 197.5-198.3°C
^{1}H-NMR: δ, ppm = 7.30 (d, 4H, H(5), ^{3}J = 5.0 Hz), 6.94 (q, 4H, H(4), ^{3}J = 5.0 Hz, ^{3}J = 3.7 Hz), 6.87 (d, 4H, H(3), ^{3}J = 3.7 Hz)
IR: (CCl_4 solution) 3077.83 ν aromatic stretching C-C ~ 1620 ν aromatic stretching C=C
UV: (CH_2Cl_2) λ max (ε) = 234 (12490), 285 (12140) , 354 (12160), 370 (12450) nm
MS: m/z 356 (M^+,100), 290 (32), 272 (9), 179 (28)

Synthesis of 4,5-Bis(thiophene-2-yl)thieno[3,2-*e*]benzo[*b*]thiophene (sl-TTE) and Tetrathieno[2,3-*a*:3',2'-*c*:2'',3''-*f*:3''',2'''-*h*]- naphthalene (fl-TTE)

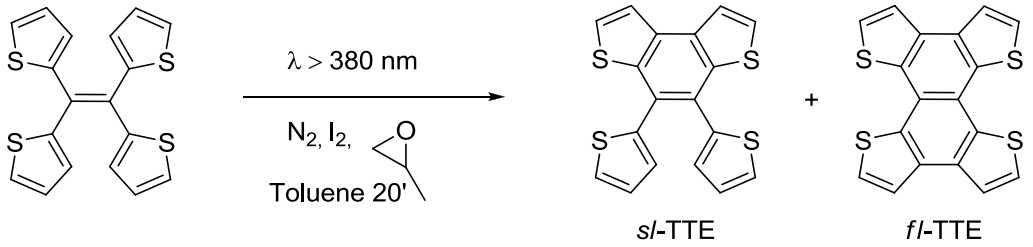

Reference: E. Fischer et al., *J. Org. Chem.*, 1996, 61, 6997-7005

Experimental Procedure:
In a typical run for photochemical reactions, 80 mg (0.217 mmol, 1 eq) of Tetrakis(2-thienyl)ethene (TTE) were dissolved in 200 mL of Toluene (solution color: yellow) and the solution was deaerated under N_2 atmosphere for 30'. After this time, 116 mg (0.457 mmol, 2 eq) of I_2 were added to the solution (which turned its color from yellow to red) and it was deaerated again for other 30'. Then 50 mL (714 mmol, *d*=0.83 g mL^{-1}) of 2-methyl oxirane (propylene oxide) were added in the reaction mixture and the solution was deaerated for 30' more. The resulting mixture was irradiated with UV-light from a 500 W high pressure Hg vapor lamp placed in the immersion quartz well under N_2 flow. The reaction was monitored by TLC (eluent: Hexane/DCM 8/2) and it was carried on till the consumption of the starting material and the appearance of the final product. The overall reaction time was 20'. The reaction product precipitated during the photolysis due to its insolubility in the reaction solvent. The crude was washed with DCM and Ethanol to remove the alcohol (1-idroxy, 2-Iodo, 2-MethylEthane) byproduct of this reaction, which is soluble in this medium, contrarily to the reaction products which are insoluble both in DCM and in EtOH. By washing the residual crude with Hexane, it was possible to isolate the intermediate product (4,5-Bis(thiophene-2-yl)thieno[3,2-*e*]benzo[*b*]thiophene (sl-TTE). By recrystallizing once the remaining crude, from *Ortho*-Xylene it was obtained the final desired product Tetrathieno[2,3-*a*:3',2'-*c*:2'',3''-*f*:3'',2''-*h*]-naphtalene (fl-TTE) (50 mg 64% yield) as pink micro-crystalline powder.

Characterization (fl-TTE):
^{1}H-NMR (400 MHz, CS_2 + Acetone *d*6): δ, ppm = 8.09 (d, 1H, *J*= 4.8 Hz), 7.94 (d, 1H, *J*= 5.2 Hz),
UV/Vis (THF), λ/nm (ε, M^{-1} cm^{-1}): 338 (1.86 10^5)
MS: 352.96 [M+];
Characterization (sl-TTE):
^{1}H-NMR (400 MHz, CS_2 + Acetone *d*6): δ, ppm = 7.99 (d, 1H, *J*= 4.8 Hz), 7.86 (d, 1H, *J*= 4.8 Hz), 7.54 (d, 1H, *J*= 4.8 Hz), 7.25 (bs, 1H), 7.11 (bs, 1H)
UV/Vis (THF), λ/nm (ε, M^{-1} cm^{-1}): 320 (7.73 10^3)
MS: 353.97 [M+]

Synthesis of benzodithiophene BDT

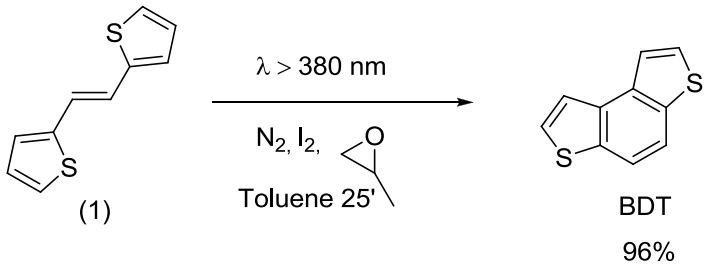

Reference: E. Fischer et al., *J. Org. Chem.*, 1996, 61, 6997-7005

Experimental Procedure:

In a typical run for photochemical reactions, 45 mg (0.23 mmol, 1 eq) of 2-thienyl-ethene was dissolved in 200 mL of Toluene and 94 mg (0.370 mmol 1.6 eq) of I_2 (solution color deep magenta) the solution mixture was deareated for 30' under N_2 flux. Then 22 mL (314 mmol, d=0.83 g mL^{-1}) of 2-methyl oxirane (propylene oxide) were added and the solution was deareated again for 15' more. The mixture was then irradiated with UV-light from a 500 W high pressure Hg vapor lamp placed in the immersion quartz well under N_2 flow. The reaction was monitored by TLC (Hexane:DCM 8:2) and it was carried on till the consumption of the starting material and the appearance of the final product. The overall reaction time was 25'. The crude was washed twice with saturated aqueous solution of $Na_2S_2O_5$. The aqueous was extracted with DCM. After anhydrification by Na_2SO_4 the crude was purified by column chromatography in pure hexane.

Characterization:

^{1}H-NMR (400 MHz, CS_2 + Acetone d_6): δ, ppm = 8.09 (d, 1H, *J*= 4.8 Hz), 7.94 (d, 1H, *J*= 5.2 Hz)
MS : 190.0 [M^+]

Synthesis of 2-(2,2-dibromovinyl)thiophene

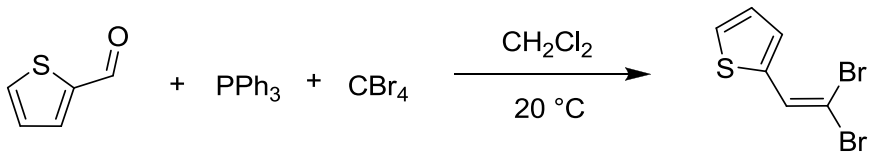

Reference: Mori A., et al.; *Tetrahedron Letters*, **2008**, 49, 1000-1003

Experimental Procedure:
In a three necked flask (100 mL) equipped with termometer, 2-thiophenecarboxyaldehyde (584 mg, 5.2 mmol, 1.0 eq.) was dissolved in CH_2Cl_2 (50 mL). PPh_3 (3.28 g, 12.5 mmol, 2.5 eq.) was added at room temperature CBr_4 (2.08 g, 6.28 mmol, 1.2 eq.). The reaction is slightly exothermic: temperature raised from 21 to 28°C. The mixture become initially red and after 2h a white precipitate (phosphine oxide) was visible. The reaction progress was monitored by TLC (Hexane/AcOEt, 9:1) controlling the consumption of the reagent and the formation of the product (R.f. = 0.57). After 3h reaction was complete.

Reaction mixture was fitered and the solvent evaporated affording 5 mL of a red crude wich was purified by column chromatography (Hexane). The desired product was isolated as a white solid in 81% yield (1,14 g).

Characterization:
m.p.: 54,1-55,6 °C (ref: 56-57 °C)
^{1}H-NMR (300 MHz, $CDCl_3$): δ,ppm= 7,65 (s,1 H,CH=); 7,38 (d, *J* = 5,1 Hz, 1 H) ; 7,25 (d, *J* = 3,33 Hz, 1 H); 7,03 (t, *J* = 4,08 Hz, *J* = 4,72 Hz, 1 H)

Synthesis of 4,4,5,5-tetramethyl-2-(thienyl)-1,3,2-dioxaborolane

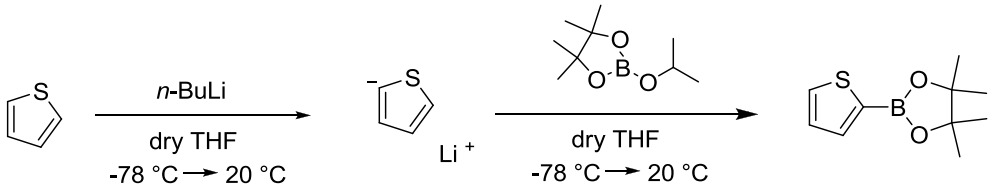

Reference: Dienes, Toni, Thomas; *Chem. Eur. JOC.*, **2007**, 7487

Experimental Procedure:
In a three necked flask (100 mL) equipped with termometer, nitrogen inlet and dropping funnel, thiophene (4.21 g, 50 mmol, 1.0 eq.) was dissolved in dry THF (10 mL). The solution was cooled to -78°C and *n*-BuLi 1.6M (37.5 mL, 1.2 eq.) was added dropwise. Temperature was kept below -70°C during the addition and then allowed to reach room temperature for 30 minutes. Reaction mixture was cooled again to -78°C and a solution of 4,4,5,5-tetramethyl-1,3,2-dioxaborolane (9.3 g, 50 mmol, 1.0 eq.) in dry THF (15 mL) was added dropwise. The solution aspect changes from colorless to deep yellow. At the end of the addition, temperature was allow to reach spontaneously room temperature and was kept under stirring for further 30 minutes.

Finally a solution of HCl 6M (10 mL) was added and the water phase was extracted with CH_2Cl_2 (3x20 mL). The organic phases were collected together, dried over Na_2SO_4, filtered and the solvent distilled off. The desired product (871 mg) was isolated as a withish solid in 83% yield.

Characterization:

^{1}H-NMR (300 MHz, $CDCl_3$): δ,ppm= 1,33 (s, 12 H); 7,57 (m, 2H); 7,23 (t, J_1=4,30 Hz , J_2= 3,88 Hz, 1 H)

Synthesis of 1,1,2-tris(2'-thienyl)ethylene

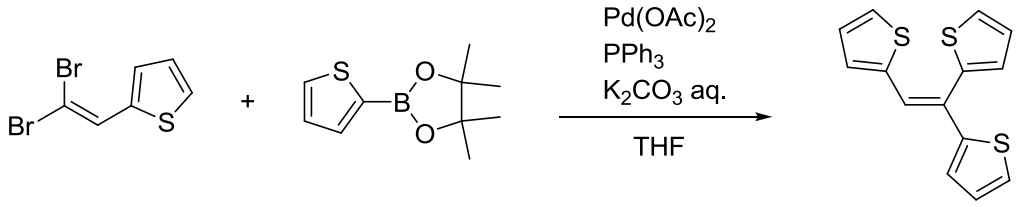

Reference: Mori A., et al.; *Tetrahedron Letters*, **2008**, 49, (1000-1003)

Experimental Procedure:
In a three necked flask (50 mL) equipped with termometer, nitrogen inlet and condenser; 2-(2,2-dibromovinyl)thiophene (100 mg, 0.37 mmol, 1.0 eq.) and 2-thienyl-pinacolboronic ester (156 mg, 0.74 mmol, 2.0 eq.) were dissolved in dry THF under nitrogen atmosphere. To the clear yellow solution thus obtained, K_2CO_3 1M in water (3 mL), $Pd(Oac)_2$ (4.20 mg, 0.018 mmol, 0.05 eq.) and PPh_3 (19.6 mg, 0.072 mmol, 0.20 eq.) were added in this order. After the addition of $Pd(Oac)_2$ the reaction mixture become black.

The reaction mixture was then refluxed (68°C) for 8h and monitored by TLC (Hexane/AcOEt, 9:1) and HPLC. While boronic ester got completely consumed, dibromo reagent was still present. So further additions of boronic ester were made in order to react it completely. The total quantity of boronic ester added was 235 mg (1,12 mmol, 4.5 eq.). Its stepwise (or better dropwise) addition is fundamental in order to limit the self coupling product (2,2'-bithiophene).

The reaction mixture was filtered trough a celite pad and the solvent evaporated. Water was added to the oily crude and the water phase extracted with CH_2Cl_2 (3x20 mL). The organic phases were collected together, dried over Na_2SO_4, filtered and the solvent distilled off. The orange oily crude was the purified by column chromatography (hexane), affording 69 mg (yield 70%) of the desired product.Along with desired product, two others byproducts were isolated: 2,2'-bithipohene and *E*/*Z* 2-(2-bromo-2-(thienyl)vinyl)thiophene.

Characterization:
m.p.: 58,1-58,9 °C
^{1}H-NMR (300 MHz, $CDCl_3$): δ,ppm= 7,54 (d, *J*=5,082 ,1H); 7,38 (s, 1 H); 7,214-7,170 (m, 2H); 7,14 (d, *J*=5,112, 1H); 7,08 (d, *J*=3,391, 1H); 7,01 (d, *J*=3,549, 1H); 6,967-6,904 (qu, J_1=3,997 Hz , J_2=5,913 Hz, J_3= 5,127 Hz , J_4= 3,831 Hz, 2H); 6,83 (d, J_1=3,618 Hz, 1H)

^{13}C-NMR (300 MHz, $CDCl_3$): δ,ppm= 122,98; 124,86; 125,89; 126,42; 127,63; 127,75; 127,81; 129,01; 129,70; 140,32

HRMS-EI(m/z): calculated for $C_{14}H_{10}S_3$: 273,99446, found 273,993160

Synthesis of difuryl ketone

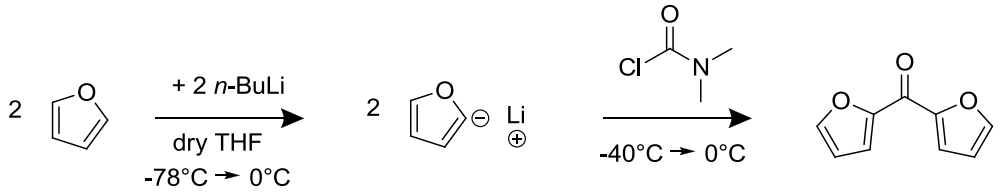

Reference: P. Lucas, et al.; *Synthesis*, **2000**, 9, 1253-1258

Experimental Procedure:
In a three necked flask (100 ml) equipped with termometer and nitrogen inlet, furan (1.0 g, 14.6 mmol, 1.0 eq.) was dissolved in dry THF (20 ml) and the solution cooled to -78°C. Then n-BuLi 1.6M (10 ml, 16 mmol, 1.1 eq.) was added dropwise and the reaction allowed to reach spontaneously 0°C. The temperature was kept for 3h at 0°C to promote furan deprotonation.

After that the furan lithium salt was cooled to -50°C and pure N,N-dimethylcarbamyl chloride (584 mg, 5.4 mmol, 0.38 eq.) was added in three steps to favor the consuption of the intermediate and enhance ketone formation. After the last addition step, temperature was allowed to reach 0°C and was mantained for 2h. The reaction mixture was controlled by TLC and, since some traces of carbamoyl chloride were still present, the reaction was stirred overnight. Finally to the reaction mixture were added 25ml of a saturated NH4Cl solution. The clear solution obtained was stirred for 30 minutes and extracted with Et2O. The aqueous layer was separated and extracted repeatedly with

CH_2Cl_2. All organic phases were collected together, dried over $NaSO_4$, filtered and the solvent distilled off.

The crude obtained was purified by column chromatography (starting with hexane/AcOEt 1:2 ending with hexane/AcOEt 6:4). The product was isolated as a white solid in quantitative yield.

Characterization:

^{1}H-NMR (300 MHz, $CDCl_3$): δ, ppm = 7.72 (s, 2H); 7.59 (d, 2H, H(3), ^3J = 3.0 Hz); 6.64 (dd, 2H, ^4J = 1.8 Hz)

IR (neat): 3139.54 cm^{-1} ν stretching C-C aromatic, 1631.63 cm^{-1} ν stretching C=O conjugated with aromatic C=C

MS-EI (m/z): 162 ([M^+], 100%).

Synthesis of Tetrakis(2-furyl)ethene

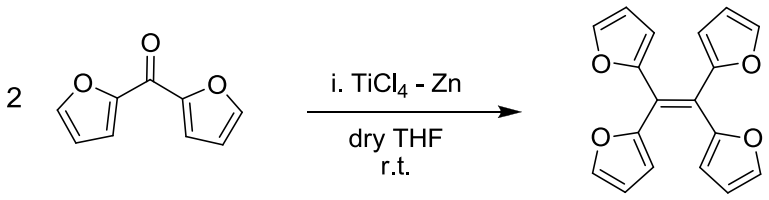

Reference: T. Suzuki, et al., *Angew. Chem . Int. Ed. Engl.*, 1992, 31 *(4)*, 455-458

Experimental Procedure:
In a four necked flask (100 mL) equipped with nitrogen inlet, thermometer and condenser, was introduced deareated, dry THF (17 mL). Then the solvent was cooled to -10°C and $TiCl_4$ (0.31 mL, 2.8 mmol) was added under inert atmosphere. The temperature raised up to -7°C and the reaction mixture became yellow. Then zinc (0.42 g, 6.0 mmol) was added in two portions, temperature raised up to -5°C. The reaction mixture was allowed to stir for 30 minutes between -7/-9°C. At the end of formation of Ti(0) the reaction mixture looked like a green suspension. A solution of di-2-furylketone (0.43 g, 2.7 mmol) in 3 mL of dry THF was added dropwise to the reaction mixture at 0°C. Then the reaction was allowed to reach room temperature within 1,5 h and left stirring overnight. The reaction was monitored by TLC (*n*-Hexane/AcOEt : 8/2) till the complete consumption of the ketone. Then the reaction mixture was poured into 20 mL of Et_2O and treated with saturated $NaHCO_3$ solution till slightly basic pH. This mixture was allowed to stir for 10 minutes and then filtered through a Celite pad. The organic layer (orange) was separated from the aqueous phase. The aqueous phase was extracted repeatedly with DCM (dichloromethane) which seemed a better solvent than Et_2O. The organic phases were collected together and dried over Na_2SO_4. Sodium sulfate was filtered off and the solvent distilled off leaving 300 mg of crude. The crude was purified by column chromatography (Hexane/DCM : 1/1) affording 191 mg of desired product (49% yield).

Notes: It is important to store the product in the dark, under N_2 atmosphere, otherwise it becomes dark; in this case it is enough to purify it by filtration on silica pad using Hexane:DCM 8:2 as eluent.

Characterization:
m.p. = 163-164 °C
^{1}H-NMR (300 MHz, $CDCl_3$): δ, ppm = 7.35 (*d*, 1H, *J*=1.6 Hz), 6.44 (*dd*, 1H, *J*=3.36 Hz, *J*=1.6 Hz), 6.30 (*d*, 1H, *J* = 3.33 Hz)
^{13}C-NMR (75 MHz, $CDCl_3$): δ, ppm = 152.96 (Cq), 142.65 (Cp), 112.24 (Cp), 111.39 (Cp).
UV/Vis (CH_2Cl_2): λ_{max} nm = 400

Synthesis of Tetrafuro[2,3-*a*:3',2'-*c*:2'',3''-*f*:3''',2'''-*h*]-naphthalene-(fl-TFE)

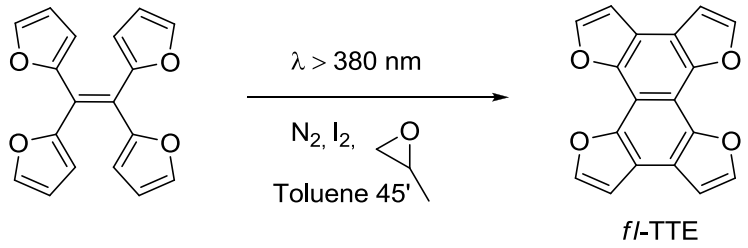

Reference: E. Fischer et al., *J. Org. Chem.*, 1996, 61, 6997-7005

Experimental Procedure:
In a typical run for photochemical reactions, 110 mg (0. 38 mmol, 1 eq) of Tetrakis(2-furyl)ethene (TFE) were dissolved in 200 mL of Toluene (solution color: yellow) and the solution was deaerated under N_2 atmosphere for 30'. After this time, 193 mg (0.76 mmol, 2 eq) of I_2 were added to the solution (which turned its color from yellow to red) and it was deaerated again for other 30'. Then 40 mL (572 mmol, d=0.83 g mL^{-1}) of 2-methyl oxirane (propylene oxide) were added in the reaction mixture and the solution was deaerated for 30' more. The resulting mixture was irradiated with UV-light from a 500 W high pressure Hg vapor lamp placed in the immersion quartz well under N_2 flow. The reaction was monitored by TLC (eluent: Hexane/DCM 8/2) and it was carried on till the consumption of the starting material and the appearance of the final product. The overall reaction time was 45'. The crude was washed with saturated acquous solution of Sodium metabisulphite and extracted with DCM. The crude was washed with Ethanol to remove the alcohol (1-idroxy, 2-Iodo, 2-MethylEthane) byproduct of this reaction. The residual crude has been recrystallizing once, from *Ortho*-Xylene so obtaining the final desired product Tetrafuro[2,3-*a*:3',2'-*c*:2'',3''-*f*:3'',2''-*h*]-naphtalene (fl-TTE) (~22% yield) as yellow microcrystalline powder. (fl-TFE).

Characterization:

^{1}H-NMR (400 MHz, THF d_8): δ, ppm = 8.09 (d, 1H, J= 2.0 Hz), 7.32 (d, 1H, J= 2.0 Hz)
UV/Vis (THF): λ_{max}/nm = 360 ($4.9x10^3$);
MS: 288.04 [M+];

Synthesis of 1,1,2-tris(2'-furyl)ethylene

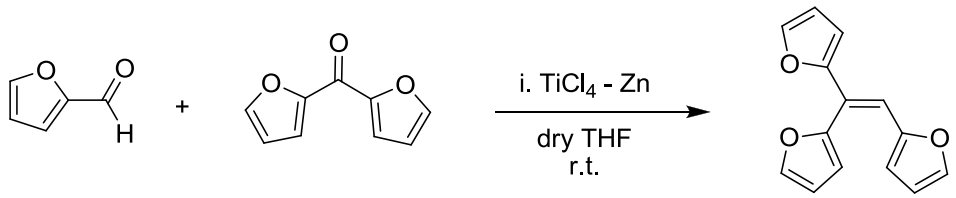

Reference: Castagnino E. *Tetrahedron Letters.* **1985**, *26*, 6399

Experimental Procedure:
In a three necked flask (100 mL) equipped with nitrogen inlet, thermometer and condenser, was introduced and deareated, dry THF (20 mL). Then the solvent was cooled to -10°C and $TiCl_4$ (0.73 mL, 6.7 mmol) was added under inert atmosphere. The reaction mixture became yellow. After 10 minutes zinc (0.87 g, 13.3 mmol) was added in two portions, temperature raised up to -2°C. The reaction mixture was allowed to stir for 30 minutes at -10°C and then warmed to 0°C. At the end of formation of Ti(0) the reaction mixture looked like a green suspension. In the meantime in a small round bottom flask furfural (0.34 g, 3.7 mmol) and bis(2-furyl)ketone (0.30 g, 1.9 mmol) were dissolved together in dry THF (5 ml). This solution was added to the reaction mixture. The temperature raised up to 13°C and then the reaction was cooled to 0°C for 40 minutes. After that the mixture was warmed to room temperature and monitored by TLC (*n*-Hexane/AcOEt : ½) till the complete consumption of the ketone. Then the reaction mixture was poured into 20 mL of Et_2O and treated with saturated $NaHCO_3$ solution till slightly basic pH. This mixture was allowed to stir for 10 minutes and then filtered through a Celite pad. The organic layer was separated from the aqueous phase. The aqueous phase was extracted repeatedly with DCM (dichloromethane). The organic phases were collected together and dried over Na_2SO_4. Sodium sulfate was filtered off and the solvent distilled off leaving 561 mg of crude. The crude, was purified by column chromatography (Hexane/DCM : 8/2) affording 82 mg of desired product (21% yield). Aside 46 mg of di-(2-furyl)ethene and 14 mg of tetrakis(2-thienyl)ethene were obtained.

Characterization:

^{1}H-NMR (300 MHz, CD_2Cl_2): δ, ppm = 7.59 (s, 1H), 7.51 (s, 1H), 7.09 (s, 1H), 7.59 (s, 1H), 6.61-6.58 (m, 2H), 6.48 (*s*, 1H), 6.43 (*d*, 1H, *J*=1.2), 6.30 (*d*, 1H, *J*=3.0), 6.05 (*d*, 1H, *J*=3.0)
^{13}C-NMR (75 MHz, $CDCl_3$): δ, ppm = 153.87, 152.16, 149.51, 142.70, 142.63, 142.55, 142.12, 118.20, 111.94, 111.83, 111.19, 110.69, 109.29.
MS-E.I.(m/z) = 226 [M^+]

Synthesis of 2-(2',2'-dibromovinyl)furan

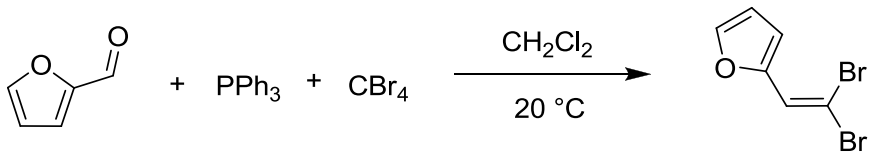

Reference: Mori A., et al.; *Tetrahedron Letters*, **2008**, 49, (1000-1003)

Experimental Procedure:
In a three necked flask (100 mL) equipped with termometer, furfural (500 mg, 5.4 mmol, 1.0 eq.) was dissolved in CH_2Cl_2 (20 mL). CBr_4 (2.08 g, 6.28 mmol, 1.2 eq.) and PPh_3 (3.28 g, 12.5 mmol, 2.5 eq.) were added at room temperature. The reaction is slightly exothermic: temperature raised from 21 to 28°C. The mixture become initially red and after 2h a white precipitate (phosphine oxide) was visible. The reaction progress was monitored by TLC (Hexane/AcOEt, 9:1) controlling the consumption of the reagent and the formation of the product (R.f. = 0.57). After 3h reaction was complete.

Reaction mixture was fitered and the solvent evaporated affording 5 mL of a red crude wich was purified by column chromatography (Hexane). The desired product was isolated as a red-oil in 81% yield (1,14 g).

Characterization:

^{1}H-NMR (300 MHz, $CDCl_3$): δ, ppm = 7.47 (d, 1H, *J = 3.0*), 7.43 (s, 1H), 7.09 (s, 1H), 6.98 (d, 1H *J = 6.0*), 6.50 (*dd*, 1H, *J*=3.0, *J = 3.0*).

Synthesis of 4,4,5,5-tetramethyl-2-(furyl)-1,3,2-dioxaborolane

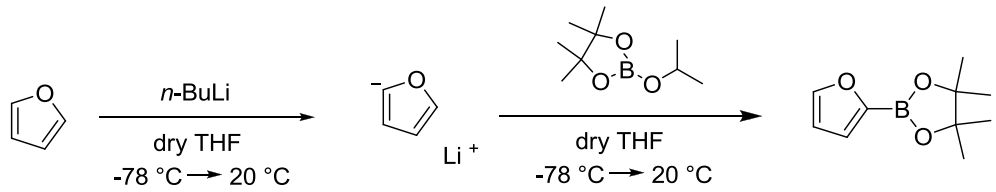

Reference: Ebner D., et al.; *Chemistry a European Journal*, **2009**, 15, 12978

Experimental Procedure:

In a three necked flask (100 mL) equipped with termometer, nitrogen inlet and dropping funnel, furan (2.0 g, 2.9 mmol, 1.0 eq.) was dissolved in dry THF (10 mL). The solution was cooled to -78°C and *n*-BuLi 1.6M (18.4 ml, 1.01 eq.) was added dropwise. Reaction was exothermic and temperature arose till -59°C. The starting solution turned into a milky suspension. At the end of the addition, temperature was kept below -70°C for 20 min and then allowed to reach room temperature for 30 minutes. Reaction mixture was first cooled to -30°C for 20 minutes and then again to -78°C. 4,4,5,5-tetramethyl-1,3,2-dioxaborolane (5.47 g, 29.4 mmol, 1.0 eq.) was added dropwise (10 minutes). The solution temperature increased till -55°C. At the end of the addition, temperature was initially kept at -71°C for 20 minutes and then allow to reach spontaneously room temperature. Reaction mixture was kept under stirring for further 30 minutes resulting in a viscous white suspension.

Finally Et_2O 10 mL and a saturated solution of NH_4Cl (10 mL) was added, but a very viscous, gel-like system was obtained. So HCl 37% 8 mL was added resulting in a clear two phase system. The water phase was extracted with Et_2O (5x10 mL). The organic phases were collected together, dried over Na_2SO_4, filtered and the solvent distilled off. The desired product (871 mg) was isolated as a yellow-green oil in 98% yield.

Characterization:

^{1}H-NMR (300 MHz, $CDCl_3$): δ,ppm= 7,49 (d, 2H, *J*=1,50 Hz); 6,92 (d, 2H, *J*=3,60 Hz), 6,26 (dd, *J*=3,60 Hz , *J*= 1,50 Hz, 1 H); 1,17 (s, 12 H)

Synthesis of 1,1,2-tris(2'-furyl)ethylene

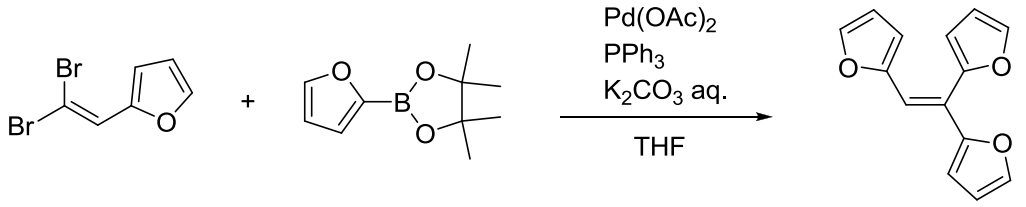

Reference: Mori A., et al.; *Tetrahedron Letters*, **2008**, 49, 1000-1003

Castagnino A.; *Tetrahedron Letters*, **1985**, 51, 6399-6402

Experimental Procedure:
In a three necked flask (50 mL) equipped with termometer, nitrogen inlet and condenser; 2-(2,2-dibromovinyl)furan (300 mg, 1.19 mmol, 1.0 eq.) and 2-furyl-pinacolboronic ester (1.04 g, 5.36 mmol, 4.5 eq.) were dissolved in dry THF (10 mL) under nitrogen atmosphere. To the clear yellow solution thus obtained, K_2CO_3 1M in water (6.8 mL), $Pd(Oac)_2$ (13.4 mg, 0.06 mmol, 0.05 eq.) and PPh_3 (62.5 mg, 0.26 mmol, 0.20 eq.) were added in this order. After the addition of $Pd(Oac)_2$ the reaction mixture become black.

The reaction mixture was then refluxed (68°C) for 8h and monitored by TLC (Hexane/ CH_2Cl_2, 7:3) and HPLC. While boronic ester got completely consumed, dibromo reagent was still present. So further additions of boronic ester and reagents were made in order to react it completely. Total quantity of boronic ester 1.76 g (9.06 mmol, 7.6 eq.), $Pd(Oac)_2$ 33.4 mg (0.14 mmol, 0.12 eq.) and PPh_3 239 mg (0.90 mmol, 0.76 eq.) are reported. The dropwise addition of 2-furyl-pinacolboronic ester is fundamental in order to avoid its self coupling product (2,2'-bifuran). The reaction solvent was evaporated, water was added to the oily crude and the water phase extracted with CH_2Cl_2 (7x6 mL). The organic phases were collected together, dried over Na_2SO_4, filtered and the solvent distilled off. The crude was the purified by column chromatography (Hexane/ CH_2Cl_2, 7:3), affording 60 mg (yield 22%) of the desired product.

Characterization:

^{1}H-NMR (300 MHz, CD_2Cl_2): □, ppm = 7.59 (s, 1H), 7.51 (s, 1H), 7.09 (s, 1H), 7.59 (s, 1H), 6.61-6.58 (m, 2H), 6.48 (*s*, 1H), 6.43 (*d*, 1H, *J*=1.2), 6.30 (*d*, 1H, *J*=3.0), 6.05 (*d*, 1H, *J*=3.0)

^{13}C-NMR (75 MHz, $CDCl_3$): δ, ppm = 153.87, 152.16, 149.51, 142.70, 142.63, 142.55, 142.12, 118.20, 111.94, 111.83, 111.19, 110.69, 109.29.

MS-E.I.(m/z) = 226 [M^+]

Synthesis of di(2-furyl)ethene

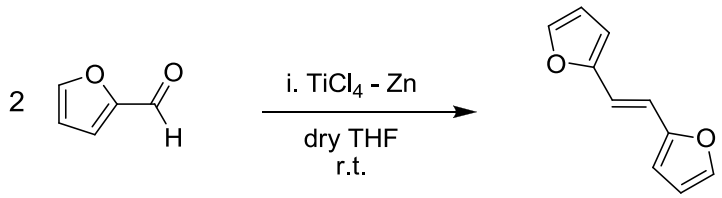

References: G. Radivoy, et al., *Organic Chemistry in Argentina* **2011**, 312-326;

Experimental Procedure:
In a three necked flask (100 mL) equipped with nitrogen inlet, thermometer and condenser, was introduced furfural (2.00 g, 1.72 mL, 21.5 mmol). Then dry THF was added (40 mL) and the solution cooled to -20°C and $TiCl_4$ (2.83 mL, 25.8 mmol) was added under inert atmosphere. The reaction mixture was allowed to stir 20 minutes at -20°C. Zinc (2.83 g, 25.0 mmol) was added in two portions, temperature raised up to -5°C. The reaction mixture was allowed to stir for 10 minutes below 0°C and then refluxed for 3,5h. The reaction was monitored by TLC (*n*-Hexane/AcOEt : 8/2) till the complete consumption of the ketone. Then the reaction solvent was distilled off affording the crude product. The crude was treated with HCl 2M and dissolved in DCM. The organic layer (orange) was separated from the aqueous phase. The aqueous phase was extracted repeatedly with DCM (3x15 mL). The organic phases were collected together and dried over Na_2SO_4. Sodium sulfate was filtered off and the solvent distilled off leaving 1,7 g of crude. The crude was purified by column chromatography (Hexane/DCM : 9/1) affording 1.14 g of a white solid (66% yield).

Notes: It is important to store the product in the dark, under N_2 atmosphere, otherwise it becomes dark; in this case it is enough to purify it by filtration on silica pad using Hexane:DCM 9:1 as eluent.

Characterization:
m.p. = 99-100 °C
^{1}H-NMR (300 MHz, $CDCl_3$): δ, ppm = 7.40 (*d*, 1H, *J*=2.1 Hz), 6.83 (*s*, 1H), 6.43 (*dd*, 1H, *J*=3.3 Hz, *J*= 1.8 Hz), 6.34 (*d*, 1H, *J* = 3.3 Hz)
^{13}C-NMR* (75 MHz, $CDCl_3$): δ, ppm = 144.17 (Cq), 131.17 (Cq), 129.94 (Cp), 127.58 (Cp), 126.58 (Cp).

UV/Vis (CH_2Cl_2): λ_{max} nm = 359

General Information

Unless otherwise specified, all the reactions were performed under nitrogen atmosphere using standard techniques using flask equipped with a magnetic stirring bar, septum inlet, and reflux condenser. All reagents and solvents were obtained from highest grade commercial sources and used without further purification unless otherwise stated. Anhydrous solvents were purged with nitrogen before use or fresh distilled (THF) before use. The reaction outcome was monitored by TLC silica gel plates and HPLC. All chromatographic separations were carried out on Merck silica gel (60μ, 230–400 mesh). Melting points were obtained with a Büchi B-540 melting point apparatus and are uncorrected.
UNIMI reaction: 1H NMR and 13C NMR spectra were recorded on a Bruker AVANCE DRX-400, Bruker AC300 and AMX at 300 MHz spectrometers;
HKUST reaction (photo-cyclization reactions) : 1H-NMR spectra were recorded on a Bruker ARX 400 NMR spectrometer. Mass spectra were recorded on a GCT premier CAB048 mass spectrophotometer operating in a MALDI-TOF mode.

HPLC chromatograms were recorded in reverse phase, isocratic conditions, by using as eluent the mixture CH_3CN:H_2O 6:4 or 8:2, or 7:3 (1mL / min). Column: Zorbax eclipse XBD-C18, 4.6×150 mm, 5μm particle size (UNIMI), and on an Agilent 1260 Infinity equipped with a PDA detector and the reverse phase Zorbax SB-C18 4.6 X 150 mm, 5 μm particle size (HKUST).

Electrochemistry

The cyclovoltammetric study of the investigated molecules has been performed at scan rates typically ranging 0.05–2 V s^{-1}. The concentration of analytes was tipically 0.0005 M in CH_2Cl_2 and in CH_3CN with tetrabuthylammoniumhexafluorophosphate $TBAPF_6$ 0.1M as the supporting electrolyte. The solutions were deaerated by N_2 bubbling. The ohmic drop has been compensated by the positive feedback technique.
The experiments were carried out using an AUTOLAB PGSTAT potentiostat (EcoChemie,The Netherlands) run by a PC with GPES software. The working electrode was a glassy carbon GC one (AMEL, diameter = 1.5 mm) cleaned by diamond powder (Aldrich, diameter = 1 mm) on a wet cloth (Struers DP-Nap). The counter electrode was a platinum wire while the reference electrode was an aqueous saturated calomel electrode (SCE), having *vs* the Fc^+|Fc couple (the intersolvental redox potential reference currently recommended by IUPAC) a difference of –0.495 V in CH_2Cl_2 and of -0.391 V in CH_3CN.
The electropolymerization has been carried out on GC and ITO electrodes by repeated cycling around the first oxidation peak at 0.2Vs^{-1} scan rate, after which the electrochemical activity of the resulting conducting film was tested by extracting the electrode from the working solution and inserting it into a monomer free solution.

Aggregation- Induced emission study

The solutions in THF and in THF-water mixtures have been prepared by using distilled water and THF previously distilled under normal pressure from sodium benzophenone ketyl under nitrogen. A stock solution of the investigated molecule dissolved in THF having a concentration of 10^{-4} M is prepared and from it more dilute solutions owning a concentration of 10^{-5} M in THF and water (fraction in volume from 0 to 90 or 99%) are made.

Crystals

All crystals (except TTE one) investigated in this thesis have been obtained by dissolving the molecule of interest in THF and by slowly adding MetOH as co-solvent in order to create a second layer, that slowly diffuse into the first one. The vial containing this mixture is than capped and stored for one week (more or less) after that, the crystal is obtained. Concerning TTE crystal, it can be similarly obtained by dissolving the sample in DCM and using the Hexane as co-solvent to create the second layer.
Reagarding the measurments, a suitable crystal was selected and it was anlyzed on a SuperNova, Dual, Cu at zero, Atlas diffractometer. The crystal was kept at 100.0 K during data collection. Using Olex2[vii] the structure was solved with the ShelXS[viii] structure solution program using Direct Methods and refined with the XL refinement package using Least Squares minimization.

Cell Culture

HeLa cells were cultured in MEM containing 10% FBS and antibiotics (100 units/mL penicillin and 100 g/mL streptomycin) in a 5% CO_2 humidity incubator at 37 °C. Cell Imaging. Lung cancer cell A549 were cultured in DMEM containing 10% FBS and antibiotics (100 units/mL penicillin and 100 g/mL streptomycin) in a 5% CO2 humidity incubator at 37 °C. Two different kind of cells were grown overnight on a 35 mm petri dish with a cover slip. The live cells were incubated with 10 μM of TTE for 15/30 mins. In a typical experiment, 2 μL of a 10 mM stock solution of TTE in DMSO were diluted to 1 mL with cell culture medium, followed by further dilution to desired concentration. The cells were imaged under a fluorescent microscope (BX41 Microscope) using same excitation and emission filters: excitation filter = 330–385 nm, dichroic mirror = 420 nm, and emission filter = 400 nm long pass.

[vii] O.V Dolomanov, L.J. Bourhis, R.J Gildea, J.A.K. Howard, & H. Puschmann, *J. Appl. Cryst.*, 2009, **42**, 339.

[viii] G.M. Sheldrick, *Acta Cryst.*, 2008, **A64**, 112-122.

Cancer cell discrimination

HeLa Cells

The HeLa cells were grown overnight on a 35 mm petri dish with a cover slip. The live cells were incubated with 10 μM of TTE for 30 mins. The HeLa cells were incubated with 50 μM oleic acid for 6 h (only in one case, since the cancer cell discrimination has been performed even without incubating the cell with the oleic acid) and then were co-stained by 10 μM TTE and 1μg/mL BODIPY for 15 mins, The good overlap between Images of TTE and BODIPY indicated that TTE can selectively target lipid droplets.

Lung Cancer Cells

The A549 cells were grown overnight on a 35 mm petri dish with a cover slip. The live cells were incubated with 10 μM of TTE for 30 mins. The A549 cells were incubated with 10 μM TTE and 1μg/mL BODIPY for 15 mins. The good overlap between Images of TTE and BODIPY indicated that TTE can selectively target lipid droplets.

Appendix
Side work

Side works: Electrochemical Investigation on Helicene-based Phosphanes and Benzodithiophene-based push-pull systems.

Thanks to my electrochemical background, during my PhD I have also performed a cyclic voltammetry investigation on two important class of molecules: Helicene-Based Phosphanes and Benzodithiophene-based *Push-Pull* systems, that have been employed in asymmetric catalysis and in dye sensitized solar cells (DSSCs), respectively. Here only a brief description is provided. The research work concerning the *push-pull* system has been already published [I]; the other one regarding the Helicene-based phosphines is ready to be submitted [II].

1 Helicene-based Phosphanes

The tetrathiahelicene scaffold, shown in Chart 1, of a peculiar helical shape endowing it with intrinsic chirality, have been investigated in our group for many years, [III] at the beginning mainly in view of possible applications in non-linear optics; more recently, also in view of its use in asymmetric catalysis, by functionalizing one or both of the terminal *alpha* positions by phosphane groups. A new family of Helicene Phosphanes became thus available, together with their Phosphane-Borane , Phosphinoxides and Phosphane-selenide analogues, as shown in Chart 2.
For the catalytic applications, the knowledge of the phosphane oxidation potential was indispensable to estimate the donor ability of the Phosphor atom, as it is the latter to be directly involved in the catalytic action when the molecule to which it belongs is chosen as catalyst. Moreover, the availability of four systematic families of phosphorous-based helicene derivatives, quite new and interesting from an electrochemical perspective, suggested the opportunity to carry out a complete characterization work.

A detailed electrochemical investigation of these four families has been therefore carried out, focusing on the localization of the redox centres and on the rationalization of the redox properties of the molecules in terms of number and nature of the terminal substituent groups.

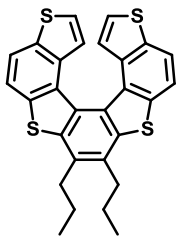

Chart 1 Molecular structure of the TetraThienylhelicene

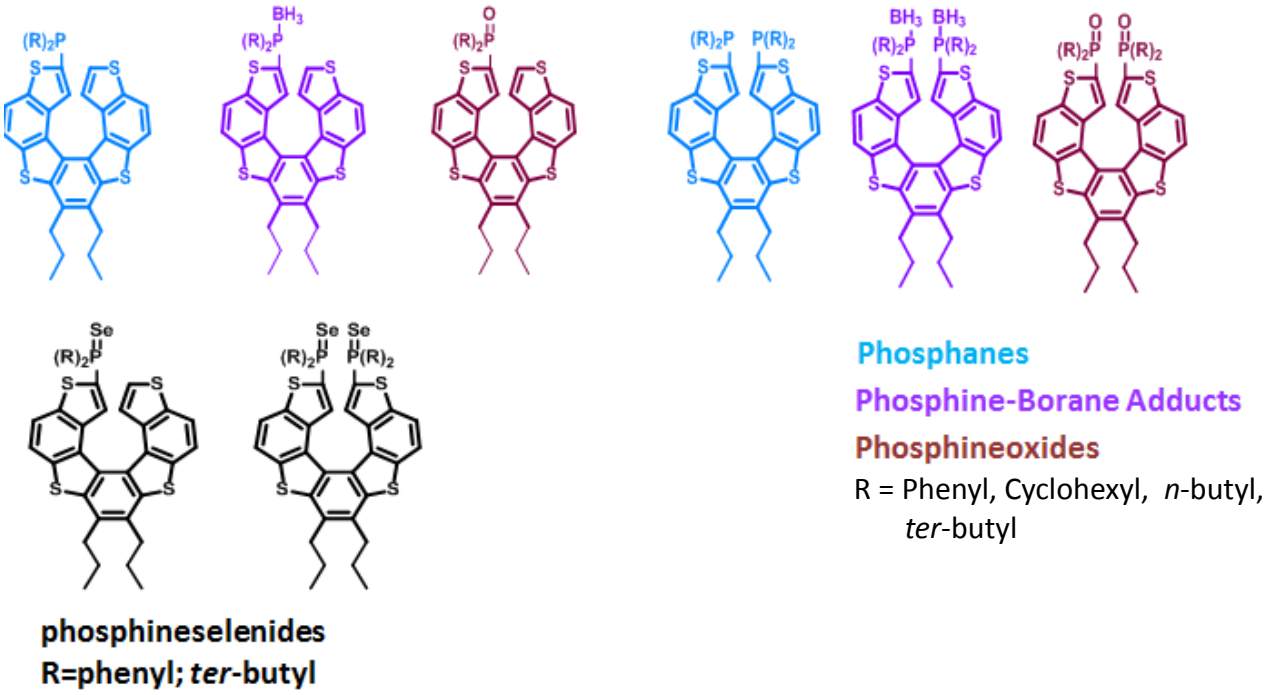

Chart 2 Molecular structures of the thiahelicene-based phosphorous derivatives.

From this investigation, it has emerged that concerning the phosphanes a comparison between aryl and alkyl cases reveals that the overall reactivity stems from a combination of inductive effects, sterical hindrance and conjugation effects. Regarding the Phosphine-Borane Adducts, the Phosphineoxides and the Phosphineselenides the most conspicuous effect is the disappearance of the free phosphines signal and the positive shift of the CV signals on account of the electronwithdrawing power of BH_3, P=O and P=S groups.

2 Benzodithiophene-based *push-pull* systems for application in DSSCs

As mentioned above, another important scaffold investigated in our group has been the benzodithiophene one, both angular and linear one. The structures have been shown in Chart 2.3.
Both have been used as spacer in metal free *push-pull* dyes to be employed in Dye Sensitizer Solar Cells, DSSC. The general design of these systems is shown in Figure 1. The most employed *metal-free* dye, are constituted by a donor unity, usually an amino moiety, a suitable π-spacer and an acceptor unit, usually a cyano-acrylic moiety which also acts as anchoring group onto the TiO_2 surface.The π-spacer plays an important role for the dye efficiency, as it is responsible of the overall effective conjugation of the system, and can influence the absorption range of the dye; in addition, the charge injection from the dye to the TiO_2 after light absorption is significantly affected by the spacer geometry that should be planar. In a previous work performed during 2012, our group proved that the best performances are obtained if the *push-pull* systems is builded by using the *lin*-BDT as spacer instead of the angular one. [IV]

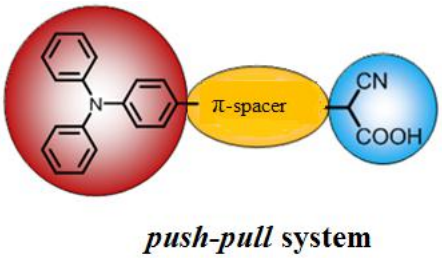

Figura 1 General scheme of a metal-free *push-pull* dye.

Despite promising results have been obtained, the investigated dyes suffered from an aggregation phenomenon occurring perpendicularly to the dye layers when they were anchored to the Titania surface. Figure 2. In order to prevent such π-π stacking, it has been decided to link long alkyl chains to the phenyl core of the BDT unit, to increase the distance between the dye layers thus preventing the above intermolecular interactions, ensuring an efficient charge injection into the Titania layer. Thus a new series of BDT-based *push-pull* systems have been created. (Chart 3). The most important requirements that a dye must have in order to be employed as photosensitizer is that its LUMO and HOMO levels must be above the TiO_2 conduction band and below the chosen mediator redox couple, respectively; moreover, the width of the HOMO-LUMO gap is determining for the portion of absorbable solar light spectrum (the narrower the gap, the larger the absorbed wavelength range). Thus we have applied electrochemistry (in particular, cyclic voltammetry) to the experimental determine HOMO and LUMO levels and gaps, as well as redox center localization, to predict the suitability of these systems for DSSC application and possibly achieve rationalization guidelines concerning the relationship between molecular design, electronic properties and operating efficiency in preapplicative device testing.

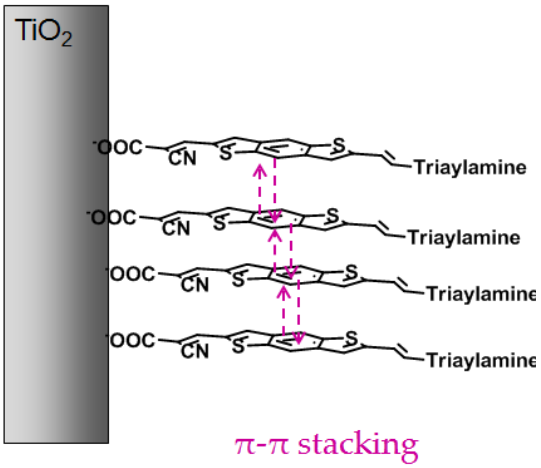

Figure 2. Exemplification of the aggregation phenomenon in a typical DSSC device.

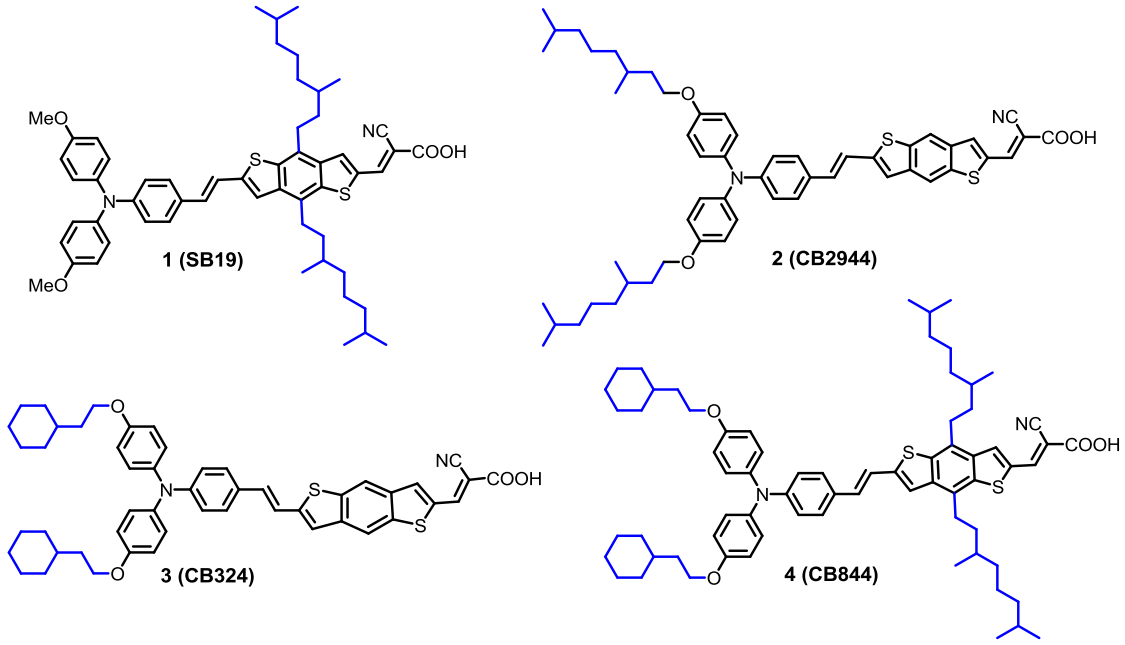

Chart 3 Molecular structure of the investigated push-pull systems tested in liquid DSSCs

All of the dye reported above, have resulted to be suitable for application in DSSCs since their HOMO is lower than the energetic level of the redox couple, and LUMO is higher then TiO_2 conduction band. (Figure 3). All of them have been tested in liquid DSSCs, the best results have been obtained by using SB19 that has provided 6.4 % as efficiency.

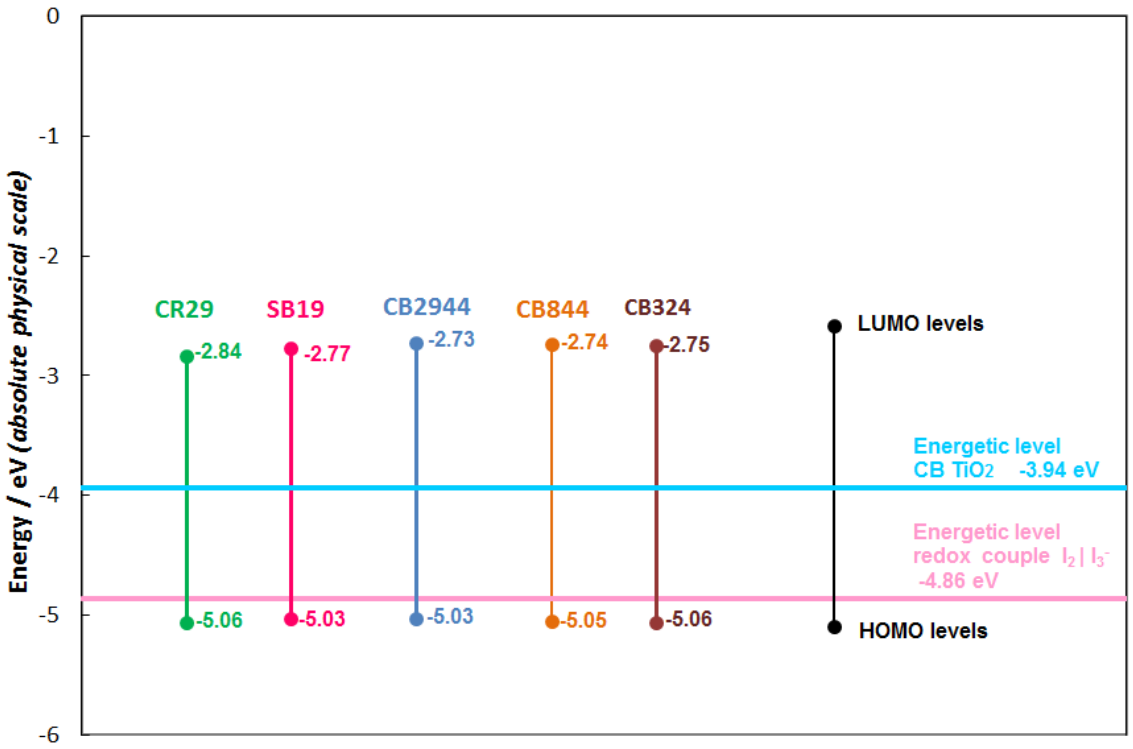

Figure 3 HOMO and LUMO levels if the investigated dyes, compared to the energetic levels of the redox mediator and TiO_2

Bibliography

[I] C. Baldoli, S. Bertuolo, E. Licandro, L. Viglianti, P.R. Mussini *et al Dyes and Pigments,* **2015,** *121,* 351;

[II] D. Dova, L. Viglianti, S. Cauteruccio, P.R. Mussini, E. Licandro *et al* paper ready to submit;

[III] B. champagne, A. Bossi, S. Maiorana, E. Licandro, *ChemPhysChem,* **2004,** *5,* 1438;

[IV] E. Longhi, C. Baldoli, E. Licandro *et al*, *Eur JOC*, **2013**, *1*, 84.

Acknowledgments

Università degli Studi di Milano (UNIMI)

Prof. Emanuela Licandro, Prof. Patrizia. R. Mussini, Prof. Stefano Maiorana, Dr. Clara Baldoli, Prof. Emanuele Ortoleva, Alessandro Bolzoni, Dr. Alberto Bossi, Dr. Davide Dova, Dr. Silvia Cauteruccio.

The Hong Kong University of Science and Technology (HKUST)

Prof. Ben Zhong Tang, Dr. Ni Xie, Chen Gui, Dr. Xingui Gu, Dr. Jacky Lam, Nelson Leung, Dr. Ryan Kwok, Dr. Engui Zhao, Chun Sing Leung, Dr. Laura Cao, Dr. Eunice Wang, Dr. Herman Sung.

South China University of Technology (SCUT)

Prof. Anjun Qin and Prof. Rongrong Hu.

The Chinese University of Hong Kong (CUHK)

Prof. Qian Miao

Consiglio Nazionale delle Ricerche - Istituto per lo Studio delle Macromolecole (CNR-ISMAC)

Dr. Chiara Botta, Dr. Francesca Villafiorita Monteleone.

Special Acknowledgements

In this special section of acknowledgements, I want to express my heartfelt gratitude to all the people I have met in the last years, who supported and believed in me and that accompanied me during my journey towards the accomplishment of this important goal.

To my family for the GREAT support and encouragement they have provided me over the years and to my cousin Tiziana for her special help.

To my best friends Angela, Mariagrazia, Matteo and to two special colleagues who are special friends too: Serena and Mirko.

To Alessandro for his special support and for believing in me and in this work as much as me, despite his distance from the university network; for his constant believing in this project and for the enthusiasm that he never lost about these wonderful luminescent molecules.

To Leo, an extraordinary scientist and person I have the honour to have met and worked with. I thanks him very much for teaching me all experimental protocols, data processing, and the authentic AIE philosophy, but especially for having believed in me and for transferring to me his highly accurate and precise scientific approach which has contributed to improving the essence of my being researcher.

To Professor Emanuela and Professor Patrizia for giving me the possibility of doing my PhD in their group and for trusting me; to Dr. Clara for teaching me the best in organic synthesis and to Professor Maiorana for his support.
To Professor Tang for having believed in me so much, for his support during my period in Hong Kong and for giving me the GREAT possibility to join his group.

To you who are so special for me, and to You, Light of the word, for enlightening my path so far, and for giving me all this…

heartfelt…GRAZIE